RĪGAS TEHNISKĀ UNIVERSITĀTE

Aleksejs Burcevs

JAUNU FUNKCIONALIZĒTU PURĪNU SINTĒZE, FOTOFIZIKĀLIE PĒTĪJUMI UN PIELIETOJUMS

Promocijas darbs

SYNTHESIS OF NEW FUNCTIONALIZED PURINES, PHOTOPHYSICAL RESEARCH AND APPLICATION

Doctoral Thesis

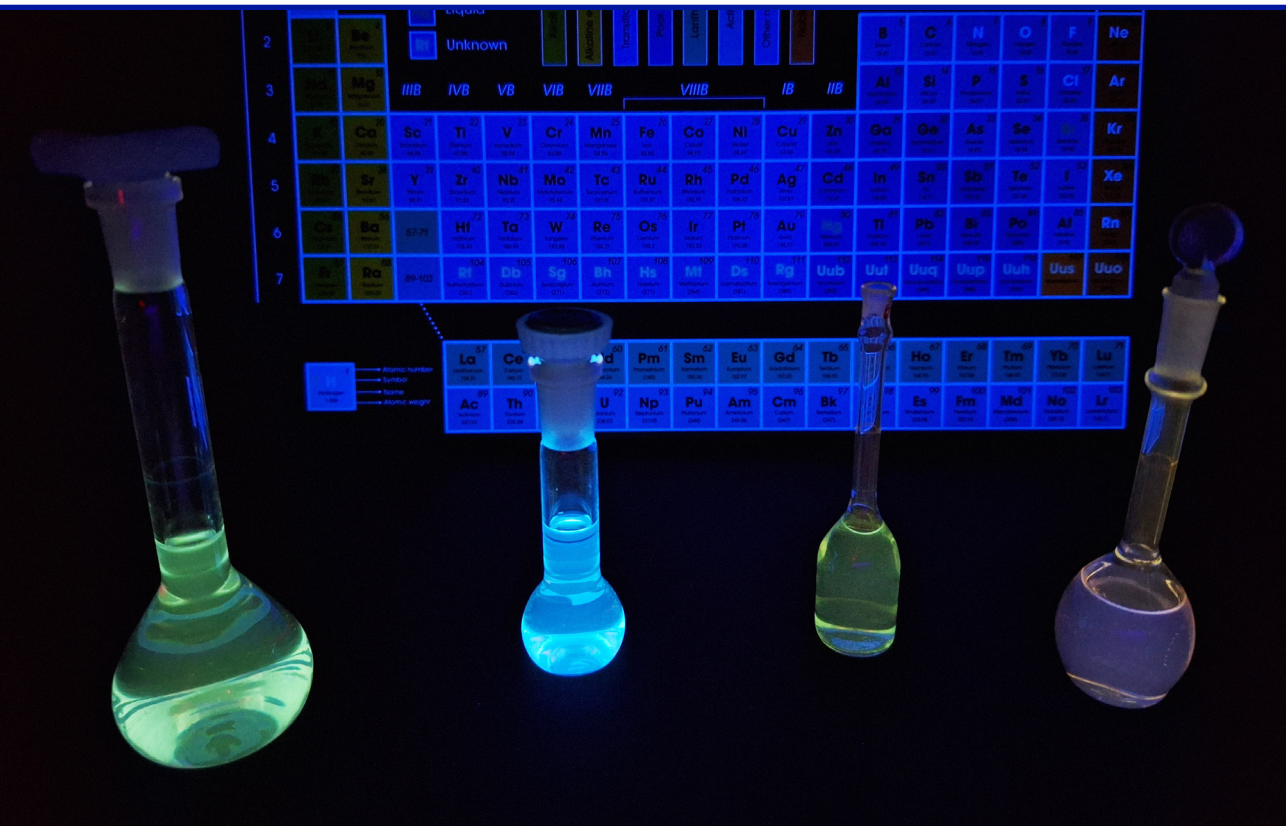

RTU Izdevniecība
RTU Press
Rīga 2025

RĪGAS TEHNISKĀ UNIVERSITĀTE
Dabaszinātņu un tehnoloģiju fakultāte
Ķīmijas un ķīmijas tehnoloģijas institūts

RIGA TECHNICAL UNIVERSITY
Faculty of Natural Sciences and Technology
Institute of Chemistry and Chemical Technology

Aleksejs Burcevs
Doktora studiju programmas "Ķīmija, materiālzinātne un tehnoloģijas" doktorants
Doctoral Student of the Study Program "Chemistry, Materials Science and Engineering"

JAUNU FUNKCIONALIZĒTU PURĪNU SINTĒZE, FOTOFIZIKĀLIE PĒTĪJUMI UN PIELIETOJUMS

Promocijas darbs

SYNTHESIS OF NEW FUNCTIONALIZED PURINES, PHOTOPHYSICAL RESEARCH AND APPLICATION

Doctoral Thesis

Zinātniskā vadītāja / Supervisor
Asociētā profesore *Dr. chem.* / Associate Professor Dr. chem. IRINA NOVOSJOLOVA

RTU Izdevniecība
Rīga 2025
RTU Press
Riga 2025

Burcevs A. Jaunu funkcionalizētu purīnu sintēze, fotofizikālie pētījumi un pielietojums. Promocijas darba kopsavilkums. Rīga: RTU Izdevniecība, 2025. – 190 lpp.

Burcevs, A. Synthesis of New Functionalized Purines, Photophysical Research and Application. Summary of the Doctoral Thesis. Riga: RTU Press, 2025. – 190 p.

Publicēts saskaņā ar promocijas padomes "RTU P-01" 2025. gada 3. aprīļa lēmumu, protokols Nr. 04030-9.1/68.

Published in accordance with the decision of the Promotion Council "RTU P-01" of April 3, 2025, Minutes No. 04030-9.1/68.

PATEICĪBAS

- Eiropas Sociālā fonda projektam Nr. 8.2.2.0/20/I/008 “Rīgas Tehniskās universitātes un Banku augstskolas doktorantu un akadēmiskā personāla stiprināšana stratēģiskās specializācijas jomās” no 2021. līdz 2023. gadam.
- Latvijas-Lietuvas-Taivānas sadarbības grantam LV-LT-TW “Funkcionalizēto purīnu molekulārā elektronika: fundamentālie pētījumi un pielietojums (MEPS)” no 2022. līdz 2024. gadam.
- Rīgas Tehniskās universitātes 2024. gada Doktorantūras grantu programmai.
- *Dr. chem.* K. Traskovskim un *Ph. D.* A. Rudušam par fotofizikāliem mērījumiem.
- *Dr. phys.* A. Mišņevam par kristālu rentgenstruktūranalīžu veikšanu.

ACKNOWLEDGMENTS

- European Social Fund project No. 8.2.2.0/20/I/008 “Strengthening of PhD students and academic personnel of Riga Technical University and BA School of Business and Finance in the strategic fields of specialization”, 2021–2023.
- Latvian-Lithuanian-Taiwan joint grant “Molecular Electronics in Functionalized Purines: Fundamental Study and Applications (MEPS)”, 2022–2024.
- 2024 Riga Technical University's Doctoral Grant programme.
- Dr. chem. K. Traskovskis and Ph. D. A. Rudušs for photophysical measurements.
- Dr. phys. A. Mishnev for X-Ray analysis.

PROMOCIJAS DARBS IZVIRZĪTS ZINĀTNES DOKTORA GRĀDA IEGŪŠANAI RĪGAS TEHNISKAJĀ UNIVERSITĀTĒ

Promocijas darbs zinātnes doktora (*Ph. D.*) grāda iegūšanai tiek publiski aizstāvēts 2025. gada 17. jūnijā Rīgas Tehniskās universitātes Dabaszinātņu un tehnoloģiju fakultātē, Rīgā, Paula Valdena ielā 3, 272. auditorijā.

OFICIĀLIE RECENZENTI

Vadošā pētniece *Dr. chem.* Aiva Plotniece,
Latvijas Organiskās sintēzes institūts, Latvija

Dr. chem. Māra Jure,
Latvijas Zinātņu akadēmijas korespondētājlocekle, Latvija

Docente *Dr. chem.* Jeļena Kirilova,
Daugavpils Universitāte, Latvija

APSTIPRINĀJUMS

Apstiprinu, ka esmu izstrādājis šo promocijas darbu, kas iesniegts izskatīšanai Rīgas Tehniskajā universitātē zinātnes doktora (*Ph. D.*) grāda iegūšanai. Promocijas darbs zinātniskā grāda iegūšanai nav iesniegts nevienā citā universitātē.

Aleksejs Burcevs ……..….
(*paraksts*)

Datums …..……...….

Promocijas darbs sagatavots kā tematiski vienotu zinātnisko publikāciju kopa ar kopsavilkumu latviešu un angļu valodā. Promocijas darbs apkopo četras oriģinālpublikācijas *SCI* žurnālos, vienu apskatrakstu, divus patentus un nepublicētus rezultātus. Publikācijas zinātniskajos žurnālos uzrakstītas angļu valodā, to kopējais apjoms, neieskaitot pielikumus, ir 60 lappuses. Publikācijas manuskripts ir uzrakstīts angļu valodā, to kopējais apjoms, neieskaitot pielikumus, ir 29 lappuses.

SATURS

switching for Intracellular Detection of Mercury Ions. Manuskripts iesniegts *Scientific Reports* 11.03.2025.

Pielikums V: Novosjolova, I.; Burcevs, A.; Tulaite, K.; Kapilinskis, Z.; Jovasaite, J.; Jursenas, S.; Turks, M. 2-Amino-6-triazolilpurīna atvasinājumu izmantošanas paņēmiens par metālu jonu sensoriem. LVP2024000072, 29.11.2024.

Pielikums VI: Kapilinskis, Z.; Burcevs, A.; Novosjolova, I.; Turks, M. Ūdenī šķīstoši 2-amino-6-triazolilpurīni un to sintēzes paņēmiens. LV15925A, 20.03.2025.

Pielikums VII: Burcevs, A.; Jonusauskas, G.; Turks, M.; Novosjolova, I. Synthesis of purine-1,4,7,10-tetraazacyclododecane conjugate and its complexation modes with copper(II). *Molecules*, **2025**, 30, 1612.

Pielikums VIII: Burcevs, A.; Sebris, A.; Novosjolova, I.; Mishnev, A.; Turks, M. Synthesis of Indole Derivatives via Aryl Triazole Ring-Opening and Subsequent Cyclization. *Molecules*, **2025**, 30, 337.

SAĪSINĀJUMI

AcOH	etiķskābe
Ar	aril-
Bn	benzil-
Bu	butil-
CuAAC	vara katalizēta azīda-alkīna ciklopievienošana
Cy	cikloheksil-
CyHex	cikloheksāns
DBU	diazabicikloundecēns
DCM	dihlormetāns
DEE	dietilēteris
DIAD	diizopropilazodikarboksilāts
DMAP	4-dimetilaminopiridīns
DME	dimetoksietāns
DMF	*N*,*N*-dimetilformamīds
DMSO	dimetilsulfoksīds
DNS	dezoksiribonukleīnskābe
E2	bimolekulārā eliminēšanas reakcija
EA	etilacetāts
EAG	elektronatvelkošā grupa
EDG	elektrondonorā grupa
ekv.	ekvivalents
Et	etil-
h	stunda
HIV	cilvēka imūndeficīta vīruss
HOMO	augstākā aizņemtā molekulārā orbitāle
KMR	kodolu magnētiskās rezonanses spektroskopija
kat.	katalizators
LDA	litija diizopropilamīds
LUMO	zemākā neaizņemtā molekulārā orbitāle
Me	metil-
MeCN	acetonitrils
MeCN-d_3	deiteroacetonitrils
MeOH	metanols
Ms	mezil-
MTBE	metil-*terc*-butilēteris
NBS	*N*-bromsukcinimīds
OLED	organiskā gaismu emitējošā diode
Ph	fenil-
ppm	miljonās daļas
RNS	ribonukleīnskābe
S_N2	nukleofīlās aizvietošanās reakcija
S_NAr	nukleofīlās aromātiskās aizvietošanās reakcija
t-Bu	*terc*-butil-
TADF	termiski aktivētā aizturētā fluorescence
TBHP	*terc*-butilhidroperoksīds
TBS	*terc*-butildimetilsilil-
TEG	tetraetilēnglikols
TFA	trifluoretiķskābe
THF	tetrahidrofurāns
THP	tetrahidropiranil-
TMS	trimetilsilil-
Tol	toluols
Ts	tozil-
UV	ultravioletais starojums
UV-Vis	ultravioletais starojums un redzama gaisma
$\lambda_{abs\ max}$	absorbcijas viļņa maksimums
$\lambda_{em\ max}$	emisijas viļņa maksimums
τ_{rad}	starojuma pārejas varbūtības laiks
τ_{nonrad}	bezizstarojuma pārejas varbūtības laiks
QY	kvantu iznākums

PROMOCIJAS DARBA VISPĀRĒJS RAKSTUROJUMS

Tēmas aktualitāte

Purīns kā viens no DNS un RNS būvblokiem ir dabā visbiežāk sastopamais heterocikls ar lielu nozīmi ģenētiskās informācijas pārnesē.[1] Purīna atvasinājumi ir svarīgi arī dažādos metabolisma procesos, tādos kā enerģijas pārnese un intracelulārā signālu pārraide, un tāpēc par tiem ir liela bioķīmiķu interese.[2] Dažas purīna atvasinājumu klases, piemēram, citokinīni un sinefungīni, bija atrastas un izdalītas no baktērijām, un savienojumiem piemīt augšanu stimulējoša iedarbība, kā arī pretvīrusu un pretvēža aktivitātes.[3] Kopumā purīna gredzens nodrošina lielisku molekulāro kodolu jaunu savienojumu, kuriem piemīt bioloģiskā aktivitāte un ir potenciāls izmantošanai farmācijā, sintēzei. Lielākajai daļai purīna atvasinājumu piemīt arī luminiscējošas īpašības, ko var izmantot šūnu attēlveidošanā un bioloģisko procesu pētīšanā.

Daudzi literatūras avoti apraksta fluorescentu purīna atvasinājumu izmantošanu. Purīna atvasinājumus izmanto kā organiskās gaismu emitējošas diodes (*OLED*),[4, 5] termiski aktivētas aizturētas fluorescences (*TADF*) emiterus,[6] pH sensorus,[7] metālu jonu detektorus, kā arī šūnu attēlveidošanā.[8–12] Pēdējos gados arvien vairāk tiek sintezēti fluorescenti purīna atvasinājumi ar jauniem strukturāliem elementiem, kas ietekmē fotofizikālās īpašības. Tomēr joprojām ir nepieciešamība sintezēt jaunus savienojumus, jo pastāv vairāki esošo struktūru ierobežojumi – tādi kā nepietiekama šķīdība ūdens vidē un zema receptoru selektivitāte vai reakcijas spēja. Daudzi vienkārši purīna atvasinājumi, tādi kā 6-metilpurīns, 6-aminopurīns un 6-merkaptopurīns, uzrāda fosforescenci.[13–15] Purīnus var modificēt pie oglekļa un slāpekļa atomiem – attiecīgi *C*2, *C*6, *C*8 un *N*7, *N*9 pozīcijās.[16] Literatūrā ir aprakstītas daudzas augsti selektīvas metodes modificēšanai izvēlētajās pozīcijās, purīna *C*2, *C*6 un *C*8 pozīciju funkcionalizēšanai visbiežāk izmanto nukleofīlās aromātiskās aizvietošanas (S_NAr)[17–19] un šķērssametināšanas reakcijas.[20–25] *N*9 pozīcijas modificēšanai izmanto tiešo alkilēšanu, Micunobu (*Mitsunobu*) vai Čana-Lama (*Chan-Lam*) reakcijas.[19, 26] Savukārt panākt selektīvu purīna *N*7 pozīcijas modificēšanu ir daudz grūtāk, bieži ir nepieciešams izveidot purīna gredzenu, izmantojot *de novo* sintēzi[27] no atbilstoša imidazola vai pirimidīna atvasinājuma.

Purīna atvasinājumi veido metālu kompleksus ar noteiktu metālu joniem (piemēram, Ca^{2+}, Fe^{2+}, Cu^{2+}, Pd^{2+}, un Zn^{2+}), un ar šo kompleksu veidošanos mainās to fotofizikālās īpašības.[28, 29] Parasti kompleksu veidošanās izraisa emisijas viļņa maksimuma nobīdi un fluorescences dzēšanu, bet iespējami arī gadījumi, kad savienojuma fluorescentās īpašības uzlabojas pēc kompleksa izveidošanās.[9] Šādu savienojumu šķīdināšana un fluorescences izmaiņu novērošana ir metālu jonu analīzes principu pamatā šķīdumos, izmantojot ultravioletā starojuma un redzamās gaismas (UV-Vis) spektroskopiju. Savienojuma-metāla kompleksu veidošanos var novērot arī gadījumos, kad tiek izmantota ^{1}H-KMR titrēšana.

Triazolilpurīni ir ievērojamas fluorescējošo purīna atvasinājumu struktūras, kas pieder pie iekšmolekulāro lādiņu pārneses ("*push-pull*") hromoforu kategorijas.[17] Šādiem savienojumiem ir labas fotofizikālās īpašības, sasniedzot kvantu iznākumus līdz pat 91 %,[30, 31], un potenciāli tos var lietot šūnu attēlveidošanā, optoelektronikā vai par sensoriem.

Otrs heterocikls, kas, līdzīgi purīnam, ir plaši izplatīts dabā un kam ir plašs bioloģisko aktivitāšu klāsts, ir indols. Tā atvasinājumiem, piemēram, serotonīnam, ir liela nozīme cilvēka bioloģijā, tas darbojas kā neirotransmiters, savukārt mitomicīns C ir zināms savu pretvēža īpašību dēļ.[32] Ir literatūras dati par indola atvasinājumiem, kas ir jauni daudzsološi pretvīrusu medikamenti pret tādiem vīrusiem kā hepatīts C, cilvēka imūndeficīta vīruss (*HIV*) un gripa.[33] Kopš pirmā Fišera (*Fischer*) ziņojuma par indola sintēzi 1883. gadā laika gaitā tika izstrādātas arvien jaunas šī savienojuma sintēzes metodes. Pēdējās desmitgadēs ir pieaudzis literatūras datu skaits par indola atvasinājumu sintēzi, kas pierāda jaunu sintētisko procedūru izstrādes nepieciešamību oriģinālu indola atvasinājumu iegūšanai.[32] Indola gredzens ir fluorescents, tāpēc tam ir potenciāls lietojumam medicīnas ķīmijā, piemēram, pH zondei attēlveidošanā[34] un fluorīda jonu noteikšanā.[35]

Nesen zinātnieki sintezēja purīna-indola konjugātus, lai pārbaudītu to kombinētās īpašības. Viena no šo konjugātu priekšrocībām ir to ierosmes viļņa garums (321 nm), ko var labi atšķirt no parastās DNS absorbcijas (253 nm).[36] Daži purīna-indola konjugāti tiek izmantoti kā fluorescentās zondes procesiem šūnās, piemēram, proteīnu mediētai dupleksa apmaiņai pret G-kvadrupleksu,[37] Hoogstīna (*Hoogsteen*) bāzu pāru izveidei[36] un *Nar*I atpazīšanas sekvences noteikšanai.[38] Tika arī ziņots, ka dažiem no tiem piemīt potenciālas pretvēža[39] īpašības un tie spēj regulēt lipīdu metabolismu.[40]

Šajā promocijas darbā tika iegūti dažādi fluorescenti triazolilpurīna atvasinājumi, pētīts to lietojums kā potenciāliem metāla jonu sensoriem un arī to fotofizikālās īpašības (1. a att.). Tika izstrādāts jauns sintētisks ceļš purīna-indola konjugātu iegūšanai divos soļos no C-C saistītiem triazolilpurīna atvasinājumiem (1. b att.).

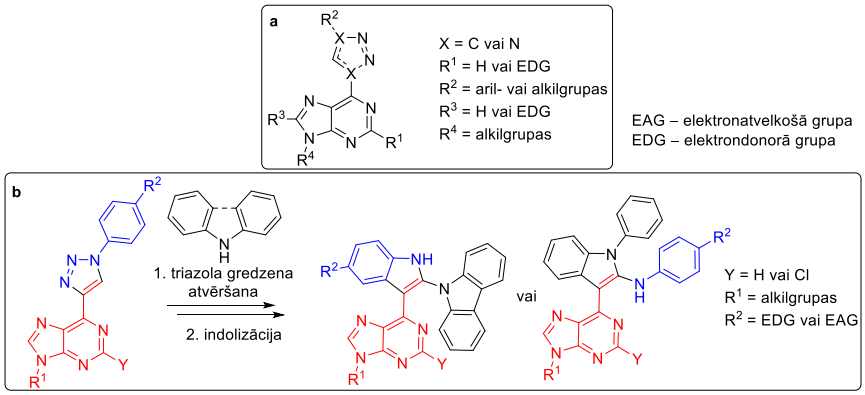

1. att. (a) Vispārīga sintezēto triazolilpurīna atvasinājumu struktūra. (b) Sintētiskais ceļš purīna-indola konjugātu iegūšanai no triazolilpurīniem. EDG (-OMe, -NMe_2); EAG (-CN, -NO_2).

Pētījuma mērķis un uzdevumi

Promocijas darba mērķis ir jaunu funkcionalizētu purīna atvasinājumu sintēze un iegūto fluorescento savienojumu potenciālā lietojuma noteikšana.

Lai sasniegtu mērķi, tika noteikti vairāki uzdevumi.

- Jaunu 2-piperidinil-6-triazolil- un 2,6-bis-triazolilpurīna atvasinājumu ar dažādiem aizvietotājiem triazola gredzenā un purīna *N*9 pozīcijā sintēze, un to fotofizikālo īpašību noteikšana.
- Ūdenī šķīstošo triazolilpurīna atvasinājumu sintēze un to fotofizikālo īpašību noteikšana.
- Triazolilpurīna atvasinājumu kā potenciālo Zn^{2+}, Fe^{2+}, Mn^{2+}, Ca^{2+}, Cu^{2+} un Hg^{2+} metāla jonu sensoru noteikšana, lietojot ^{1}H-KMR titrēšanas eksperimentus.
- Sintētiskā ceļa izstrāde 1,4,7,10-tetraazaciklododecilgrupu saturoša triazolilpurīna atvasinājuma iegūšanai un tā potenciālā lietojuma noteikšana.
- Jauna sintētiskā ceļa izstrāde purīna-indola konjugātu iegūšanai, sākot no triazolilpurīna atvasinājumiem, izstrādātās metodes darbības jomas un ierobežojumu noteikšana.

Zinātniskā novitāte un galvenie rezultāti

Promocijas darba gaitā tika sintezēti jauni 2-piperdinil-6-triazolil- un 2,6-bis-triazolilpurīna atvasinājumi un noteiktas to fotofizikālās īpašības. Tika pārbaudīta izvēlēto 2-piperidinil-6-triazolilpurīna atvasinājumu metālu jonu kompleksu veidošanās organiskajos šķīdinātājos un ūdens šķīdumos. Kompleksveidošanās eksperimentu gaitā bija novērota fluorescences dzēšana, kas liecina, ka šie savienojumi ir piemēroti lietošanai par metāla jonu sensoriem, uzrādot īpaši augstu selektivitāti Hg^{2+} jonu kompleksēšanā. Tika iegūts jauns ūdenī šķīstošs 1,4,7,10-tetraazaciklododecilgrupu saturošs triazolilpurīna atvasinājums ar potenciālu izmantošanai par fotokatalizatoru un pārbaudīta tā kompleksa veidošanās spēja ar Cu^{2+} joniem. Tika izstrādāts jauns divu soļu sintētiskais ceļš purīna-indola konjugātu iegūšanai no triazolilpurīniem, neizmantojot metālu saturošus katalizatorus.

Darba struktūra un apjoms

Promocijas darbs ir sagatavots kā tematiski vienota zinātnisko publikāciju kopa, kas veltīta triazolilpurīnu modificēšanai un sintēzei, izvēlēto atvasinājumu fluorescento īpašību noteikšanai un to lietojumu pētīšanai. Promocijas darbs ietver četras oriģinālpublikācijas *SCI* žurnālos, vienu apskatrakstu, divus patentus un nepublicētus rezultātus.

Darba aprobācija un publikācijas

Promocijas darba rezultāti publicēti četros zinātniskos oriģinālrakstos, vienā apskatrakstā, divos patentos. Galvenie rezultāti tika prezentēti astoņās zinātniskajās konferencēs.

Zinātniskās publikācijas

1) **Burcevs, A.**; Jonusauskas, G.; Turks, M.; Novosjolova, I. Synthesis of purine-1,4,7,10-tetraazacyclododecane conjugate and its complexation modes with copper(II). *Molecules*, **2025**, 30, 1612. https://doi.org/10.3390/molecules30071612.
2) Jovaisaite, J.; Boguševičienė, K.; Jonusauskas, G.; Kreiza, G.; **Burcevs, A.**; Kapilinskis, Z.; Novosjolova, I.; Turks, M.; Hean, L. E.; Chu, H.-W.; Chang, H.-T.; Juršėnas, S. Purine-based chemical probe with HOMO switching for Intracellular Detection of Mercury Ions. Manuskripts iesniegts *Scientific Reports* 11.03.2025.
3) **Burcevs, A.**; Sebris, A.; Novosjolova, I.; Mishnev, A.; Turks, M. Synthesis of Indole Derivatives via Aryl Triazole Ring-Opening and Subsequent Cyclization. *Molecules*, **2025**, 30, 337. https://doi.org/10.3390/molecules30020337.
4) **Burcevs, A.**; Sebris, A.; Traskovskis, K.; Chu, H.; Chang, H.; Jovaišaitė, J.; Juršėnas, S.; Turks, M.; Novosjolova, I. Synthesis of Fluorescent C–C Bonded Triazole-Purine Conjugates. *J. Fluoresc.*, **2024**, 34, 1091–1097. https://doi.org/10.1007/s10895-023-03337-6.
5) **Burcevs, A.**; Turks, M.; Novosjolova, I. Synthesis of Pyridinium Moiety Containing Triazolyl Purines. *Molbank*, **2024**, 2024, M1855. https://doi.org/10.3390/M1855.
6) **Burcevs, A.**; Novosjolova, I. Recent Progress in the Synthesis of *N*7(*N*9)-alkyl(aryl)purines (microreview). *Chem. Heterocycl. Compd.*, **2022**, 58, 400–402. https://doi.org/10.1007/s10593-022-03105-7.

Iesniegtie patenti

1) Novosjolova, I.; **Burcevs, A.**; Tulaite, K.; Kapilinskis, Z.; Jovasaite, J.; Jursenas, S.; Turks, M. 2-Amino-6-triazolilpurīna atvasinājumu izmantošanas paņēmiens par metālu jonu sensoriem. LVP2024000072, 29.11.2024.
2) Kapilinskis, Z.; **Burcevs, A.**; Novosjolova, I.; Turks, M. Ūdenī šķīstoši 2-amino-6-triazolilpurīni un to sintēzes paņēmiens. LV15925A, 20.03.2025.

Zinātniskās konferences, kurās prezentēti promocijas darba rezultāti

1) **Burcevs, A.**; Novosjolova, I. Synthesis of 1*H*-Indole Derivatives through Aryl Triazole Ring Opening and Subsequent Cyclization. No: *Balticum Organicum Syntheticum 2024: Abstract Book*, Rīga, Latvija, 2024. gada 7.–10. jūlijs, 40. lpp.

2) Novosjolova, I.; **Burcevs, A.**; Jonusauskas, G.; Tulaitė, K.; Jovasaite, J.; Juršėnas, S.; Turks, M. Study of Triazolyl Purine Derivatives as Sensors for Metal Ions. No: Balticum Organicum Syntheticum 2024: Abstract Book, Rīga, Latvija, 2024. gada 7.–10. jūlijs, 111. lpp.
3) **Burcevs, A.**; Novosjolova, I. Synthesis of a Cyclen Containing Purine Derivative as a Potential Photo-Catalyst. No: 13th Paul Walden Symposium on Organic Chemistry: Program and Abstract Book, Rīga, Latvija, 2023. gada 14.–15. septembris, 40. lpp.
4) **Burcevs, A.**; Jonusauskas, G.; Tulaitė, K.; Jovasaite, J.; Juršėnas, S.; Novosjolova, I.; Turks, M. Synthetic Pathways Toward Designed Purine Derivative for the Photo-Catalysis. No: International Symposium on Synthesis and Catalysis 2023: Abstract Book, Evora, Portugāle, 2023. gada 5.–9. septembris, 210. lpp.
5) **Burcevs, A.**; Novosjolova, I. Synthetic Pathways towards Purine Derivative as a Potential Molecular System for the Photo-Catalysis. No: 81st International Scientific Conference of the University of Latvia 2023. Chemistry Section and Section of Institute of Chemical Physics: Book of Abstracts, Rīga, Latvija, 2023. gada 17. marts, 47. lpp.
6) **Burcevs, A.**; Sebris, A.; Novosjolova, I.; Turks, M. Synthetic Approaches toward C-C Bonded Triazolylpurines for Use in Materials Science. No: Balticum Organicum Syntheticum 2022: Program and Abstract Book, Viļņa, Lietuva, 2022. gada 3.–6. jūlijs, 58. lpp.
7) **Burcevs, A.**; Sebris, A. Synthesis and Photophysical Properties of C-C Bonded Triazole-Purine Conjugates. No: 12th Paul Walden Symposium on Organic Chemistry: Program and Abstract Book, Latvija, Rīga, 28.–29. oktobris, 2021. Rīga: 2021, 27. lpp.
8) **Burcevs, A.**; Sebris, A.; Novosjolova, I. Synthesis of C-C linked Triazolylpurines. No: *Riga Technical University 62nd International Scientific Conference "*Materials Science and Applied Chemistry 2021": Program and Abstracts, Rīga, Latvija, 2021. gada 22. oktobris, 16. lpp.

PROMOCIJAS DARBA GALVENIE REZULTĀTI

Purīns ir viens no dabā izplatītākajiem slāpekli saturošajiem heterocikliem, kas plaši sastopams dažādos dabas produktos un ārstnieciskajos savienojumos.[3] Medicīnas ķīmijā no dabas produktiem izdalītās vielas bieži vien ir jaunu farmakoloģiski aktīvu savienojumu pamats, un tāpēc ir nerimstoša interese par jaunu purīna atvasinājumu sintēzi un esošo savienojumu modificēšanu. Ir zināmas divas sintētiskas stratēģijas jaunu purīna atvasinājumu iegūšanai – vai nu izmantojot un modificējot purīna gredzena reaģētspējīgās grupas, vai ciklizējot funkcionalizētus pirimidīna vai imidazola prekursorus.[41]

Promocijas darbā aprakstīta jaunu purīna atvasinājumu sintēze, kā arī to fotofizikālās īpašības un metālu jonu kompleksēšanas spējas. Ir aprakstīta arī jauna sintētiskā pieeja purīna-indola konjugātu sintēzei no triazolilpurīniem divos soļos.

1. Purīna gredzena modificēšana

Tā kā tiek sintezēti dažādi purīna atvasinājumi, jo pieaug interese par to iespējamo izmantošanu medicīnas ķīmijā, intensīvi tiek pētīta dažādu purīna gredzena pozīciju reaģētspēja. Komerciāli pieejamākās izejvielas šim nolūkam ir 2,6-dihlorpurīns[42] un 2,6,8-trihlorpurīns,[43] ko parasti iegūst vienā solī attiecīgi no urīnskābes vai ksantīna. Visbiežāk izmantotās pārvērtības halogēnus saturošo purīnu funkcionalizēšanai *C*2, *C*6 un *C*8 pozīcijās ir šķērssametināšanas un S_NAr reakcijas.

Šķērssametināšanas reakcijas ar 2,6- un 6,8-dihalopurīniem ir gan ķīmiskas, gan reģioselektīvas.[16] Ja abi halogēni purīna *C*2 un *C*6 vai *C*6 un *C*8 pozīcijās ir hlora atomi, reakcija ar vienu ekvivalentu metālorganiskā reaģenta notiek selektīvi purīna *C*6 pozīcijā (1. shēma, a–b).[44] Tādos savienojumos joda ievadīšana mazāk reaģētspējīgākajās *C*2 un *C*8 pozīcijās izraisa reakcijas norisi tieši tajā pozīcijā, neskarot *C*6 pozīciju – reakcija notiek ķīmiski selektīvi (1. shēma, c–d).

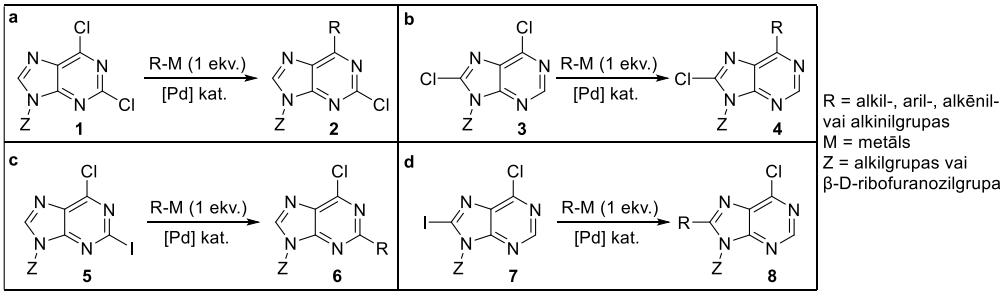

1. shēma. 2,6- un 6,8-dihalopurīnu vispārējā reģioselektivitāte.

Vispārējā reģioselektivitāte, kas redzama 1. shēmā, strādā Stilles (*Stille*),[20, 22] Negiši (*Negishi*)[20–22] un Suzuki-Mijauras (*Suzuki-Miyaura*)[23–25] reakciju apstākļos. Diaizvietotu produktu veidošanās galvenokārt tiek novērota Stilles reakcijā.[20] Iespējamais skaidrojums varētu būt tāds, ka Stilles reakcijā nepieciešama augstāka temperatūra nekā citās pārvērtībās, tādējādi padarot

reakciju neselektīvu. Aril-, alkil- un alkēnilaizvietotājus var ievadīt halopurīna molekulā, izmantojot Negiši vai Stilles reakcijas, savukārt Suzuki-Mijauras šķērssametināšanu pārsvarā lieto arilaizvietotāju ievadīšanai.

2,6,8-Trihlorpurīna gadījumā šķērssametināšanas reakcijas vairumā gadījumu notiek secīgi, reaģētspējas secība samazinās *C*6 > *C*8 > *C*2 pozīcijās.[45] Literatūrā ir ziņots par izņēmumiem, kad atsevišķiem 2,6,8-trihlorpurīna atvasinājumiem nenovēro šo reaģētspējas modeli, jo aizvietošana vispirms notiek *C*8 pozīcijā, kam seko parasti reaģētspējīgākā *C*6 pozīcija.[46] Kā piemērs minēts purīna atvasinājums, kas *N*9 pozīcijā satur glikozīdu, kas, visticamāk, virza aizvietošanās reakcijas norisi uz *C*8 pozīciju.

Halogēna atomus purīna gredzenā var izmantot arī kā aizejošas grupas S_NAr reakcijās, lai ievadītu *N*-,[17] *O*-,[47] *S*-,[18] *P*-,[48] un *Se*-nukleofīlus.[49] S_NAr reakcijās, kamēr purīna gredzena reaģētspēja paliek nemainīga, halogēnu reaģētspēja ir apgriezta, salīdzinot ar šķērssametināšanas reakcijām, un fluora atoms ir visaktīvākais halogēns (F > Cl > Br > I).[50] Lai gan ir zināms, ka purīna *C*6 pozīcija ir visreaģētspējīgākā, ir veikti plaši pētījumi par aizejošo grupu reaģētspēju S_NAr reakcijās tieši šajā pozīcijā (1. tab.).[51]

1. tabula

Aizejošo grupu reaģētspējas secība 6-aizvietotos purīna atvasinājumos

Nr.	Nukleofīls	Piedeva	Reaģētspējas secība
1.	$BuNH_2$	–	F > RSO_2 > Br > Cl > I
2.	MeOH	DBU	RSO_2 > F > Br = Cl > I
3.	*i*-PentilSH	DBU	RSO_2 > F > Br = I > CI
4.	$PhNH_2$	TFA	F > RSO_2 > I > Br > Cl
5.	$PhNH_2$	–	I > Br > RSO_2 > Cl > F

Purīna *C*6 pozīcijas reaģētspēja ir atkarīga no aizejošās grupas, nukleofīla dabas un piedevas. Starp visiem halogēniem fluors ir labākā izvēle S_NAr reakcijām ar butilamīnu un anilīnu skābes katalizatora klātbūtnē, kā arī ar *O*- un *S*-nukleofīliem (1. tab., 1.–4. rinda). Tikai anilīna gadījumā, nelietojot piedevas, 6-fluorpurīna reakcijai nepieciešams ilgāks laiks – sešas stundas, savukārt 6-jodpurīna atvasinājuma reakcija notiek 50 minūšu laikā (1. tab., 5. rinda). Reakcijās ar *O*- un *S*-nukleofīliem 6-alkilsulfonilaizvietotie purīni pārspēj fluoru kā aizejošo grupu, bet to precīzs reakcijas ātrums netika noteikts (1. tab., 2.–3. rinda). Lai gan S_NAr reakcijās visbiežāk izmanto halogēnus, ir zināmi arī piemēri, kad izmanto azīdus, sulfonilgrupas un 1,2,3-triazolus kā aizejošās grupas.[18, 48, 52, 53]

Citas pozīcijas, kuras var modificēt purīna atvasinājumos, ir *N*7 vai *N*9 atomi. Ja vairumā gadījumu *N*9 pozīcija ir reaģētspējīgāka, dažos gadījumos tiek novērota arī *N*7 produktu veidošanās purīna gredzena *N*7/*N*9 pozīciju tautomērijas dēļ. Visizplatītākās pieejas *N*9 pozīcijas funkcionalizēšanai ir alkilēšana ar alkilhalogenīdiem un Micunobu reakcija, taču šajās pārvērtībās joprojām veidojas neliels daudzums nevēlamā *N*7 alkilēšanas produkta.[19] Plaši pētīta tēma ir purīna

*N*9 pozīcijas selektīva glikozilēšana, kur svarīgi iepriekš purīna *C*6 pozīcijā ievest elektronu nabadzīgu virzošo grupu, piemēram, imidazolu,[54] tetrametilsukcīnimīdu[55] vai *O*-difenilkarbamoilgrupas.[56] $SnCl_4$ kā katalizatora izmantošana nodrošina *N*9 glikozilētus purīnus kā produktus, neizmantojot nekādas virzošas grupas purīna *C*6 pozīcijā.[57]

Pēdējos gados ir ziņots par daudzām jaunām sintētiskām pieejām *N*9 pozīcijas selektīvai alkilēšanai. Adenīna vai 6-hlorpurīnu reakcijā ar pirmējiem spirtiem, izmantojot reaģentu P_2O_5 un KI maisījumu trietilamīna un K_2CO_3 klātbūtnē, ar iznākumiem līdz 82 % veidojas *N*9 alkilēti produkti.[58] Lai selektīvi funkcionalizētu purīna *N*9 pozīciju, izmanto cikliskos ēterus un metil-*terc*-butilēteri (MTBE) Umemoto (*Umemoto*) reaģenta un UV gaismas klātbūtnē.[59] *N*9 aizvietotus purīnus iegūst, alkilēšanai izmantojot *N*,*N*-dialkilamīdus, KI un *terc*-butilhidroperoksīdu (TBHP).[60] No otras puses, selektīvu *N*7 alkilēšanu ir grūtāk panākt. Šim nolūkam tiek izmantoti specifiski substrāti, piemēram, glikozildonori ar bis(trimetilsilil)acetamīdu alvas vai titāna tetrahlorīdu klātbūtnē[61] vai elektroniem nabadzīgi ciklopropāna atvasinājumi.[62]

Arilaizvietotus *N*9 purīnus parasti iegūst Čana-Lama reakcijās un šķērssametināšanas reakcijās ar arilhalogenīdiem,[63] savukārt *N*7 arilētos purīnus iegūst purīna cikla *de novo* sintēzē, kā izejvielas izmantojot aizvietotus pirimidīnus vai imidazolus.

Jaunākā informācija par selektīvu *N*7/*N*9 purīna alkilēšanu/arilēšanu ir apkopota apskatrakstā, kas pievienots I pielikumā.

1.1. Fluorescentu purīnu īpašības un to spēja veidot metālu kompleksus

Viens no pirmajiem ziņojumiem par purīna atvasinājumu metālu kompleksiem tika publicēts 1959. gadā, un tajā tika apkopota informācija par sešu 6-aizvietotu purīna atvasinājumu kompleksu veidošanās spēju ar Ni^{2+}, Co^{2+}, Cu^{2+}, Pb^{2+} un Zn^{2+} joniem.[64] Pētījums ietvēra purīna šķīduma pH potenciometriskus mērījumus ūdens-dioksāna šķīdumā metāla jonu klātbūtnē vai bez tiem pēc katras NaOH standartšķīduma pievienošanas. Analizējot šķīduma mainīgās pKa vērtības, šķīduma pH paaugstinoties, tika noteiktas disociācijas konstantes, kas liecina par purīna-metāla kompleksu veidošanos. Pētījumā tika noskaidrots, ka purīnam ir atšķirīgas kompleksēšanās spējas ar dažādu metālu joniem atkarībā no aizvietotājiem purīna *C*6 pozīcijā un izmantotā metāla jona dabas. Vēlāk, 1971. gadā, 6-amino-, 6-hlor-, 6-hidroksi- un 6-merkaptopurīnu kompleksēšanas modelis tika pārbaudīts ar Mn^{2+}, Ca^{2+}, Mg^{2+}, Zn^{2+}, Ni^{2+}, Co^{2+} un Cu^{2+} joniem ūdens šķīdumos, un tika mērītas šo kompleksu stabilitātes konstantes.[65] Izveidoto 6-aizvietoto purīna atvasinājumu un metāla jonu kompleksu stabilitātes secība bija $Cu^{2+} > Ni^{2+} > Zn^{2+} > Co^{2+} > Mn^{2+} > Mg^{2+} > Ca^{2+}$. Autori piedāvāja modeli, kurā veidojas 1 : 1 purīna-metāla kompleksi un metāls tiek koordinēts starp aizvietotāju pie purīna *C*6 atoma un slāpekli pie *N*7 atoma (2. att.).

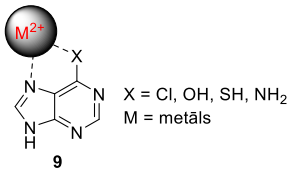

9

2. att. Metālu jonu kompleksēšanas vieta starp aizvietotāju purīna *C*6 pozīcijā un slāpekli *N*7 pozīcijā.

Mūsdienās viens no plaši izmantotajiem pretvēža līdzekļiem ir *cis*-diamīndihlorplatīns(II) vai cisplatīns.[66, 67] Šis komplekss galvenokārt saistās ar guanīna bāzu *N*7 pozīciju atomiem, kas aktivē vairākus signālu transdukcijas ceļus un izraisa apoptozi vai ieprogrammētas šūnu nāves. Lai arī tā ir viena no plaši pieejamajām pretvēža ārstēšanas iespējām, kā trūkumi mināmi toksikoloģiski kaitējumi organismam hepatotoksicitātes (aknas), kardiotoksicitātes (sirds), nefrotoksicitātes (nieres), gastrotoksicitātes (kuņģis) un ototoksicitātes (dzirdes zudums) veidā. [66,67]

Organisko molekulu kompleksēšanas spējas ar metāliem var novērot un detektēt ar ^{1}H-KMR spektroskopijas metodi, kas ir viens no visnoderīgākajiem dinamisko molekulāro procesu pētīšanas paņēmieniem.[68] Izmantojot ^{1}H-KMR titrēšanu, analizējamā savienojuma šķīdumam pakāpeniski tiek pievienots zināmas koncentrācijas metāla jonu kompleksa šķīdums, vienlaikus uzraugot savienojuma protonu ķīmiskās nobīdes izmaiņas spektrā.[69] Nosakot, kuri signāli analizējamā savienojuma spektrā maina ķīmisko nobīdi, ir iespējams noteikt tuvākās kompleksa veidošanās vietas molekulā. Ķīmisko nobīžu analīze vai to izzušanas novērošana sniedz informāciju par kompleksa veidošanās modeli. ^{1}H-KMR titrēšana tiek izmantota, lai noteiktu savienojumu metālu kompleksu saistīšanās konstantes, reakcijas līdzsvara konstantes un pKa vērtības, lai gan ir zināmas grūtības ar rezultātu precizitāti pie zemām (0–2) pH un augstām (12–14) pH vērtībām, jo šajos pH diapazonos aprēķinātās vērtības nedaudz atšķiras no rezultātiem, kas iegūti, izmantojot potenciometriju, un tāpēc to precizitāte ir apšaubāma.[70, 71]

Purīna-metāla kompleksa veidošanās pētījumos tiek izmantoti arī fluorescences mērījumi, ņemot vērā fluorescences intensitātes izmaiņas kompleksa veidošanās laikā. Parasti purīna-metāla kompleksu veidošanās samazina emisijas intensitāti vai pilnībā dzēš fluorescenci. Dabā sastopamajiem purīna nukleozīdiem piemīt vājas fluorescentās īpašības,[72] bet tie ir viena no visizplatītākajām bioloģiski aktīvo savienojumu klasēm, tāpēc ir jāveic papildu modifikācijas purīna struktūrā, lai uzlabotu savienojumu fotofizikālās īpašības. Parasti struktūrā tiek ievadīti akceptori (-CN, -CO_2Me, -CONHR (R = alkil-)) un donori (-NH_2, -NHMe, -NMe_2, -OBn) aizvietotāji, padarot purīnu par "*push-pull*" hromoforu,[73] palielinot tā kvantu iznākumu un ļaujot novērot intracelulāros procesus, izmantojot fluorescences izmaiņās balstītas novērošanas metodes. Ir izstrādāti fluorescenti purīna jonu sensori Hg^{2+} un Pd^{2+} joniem ūdens vidē[29,74] un Cu^{2+} joniem šūnās,[8, 75] to kompleksu fluorescējošās īpašības tika dzēstas pēc kompleksa veidošanās (3. att., **I**–**III**). Tika ziņots arī par pretēju gadījumu, kad uz purīna bāzes veidotam metāla jonu sensoram uzlabojas fluorescence, pievienojot Al^{3+} jonus (3. att., **IV**).[9]

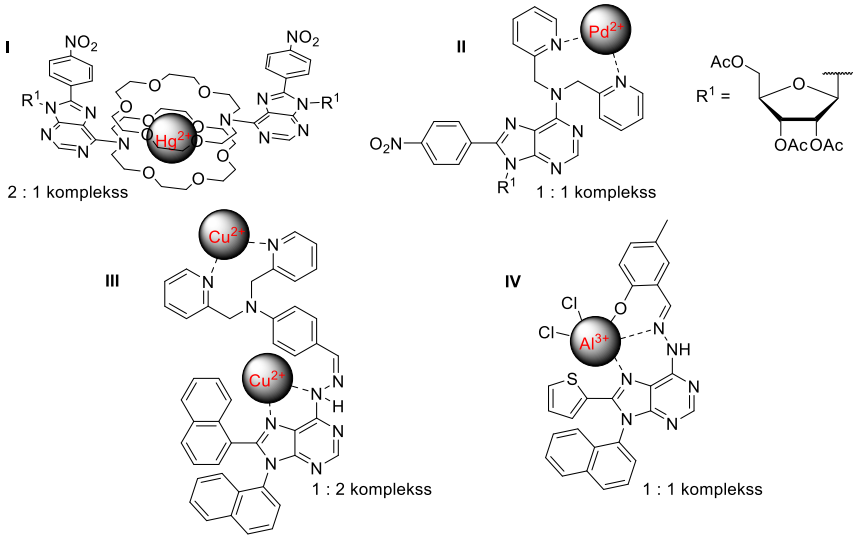

3. att. Uz purīna bāzes veidotu metāla jonu sensoru **I–IV** piemēri.

Minētajos pētījumos fluorescences izmaiņas tika analizētas, izmantojot titrēšanas eksperimentus un UV-Vis spektroskopiju, kas ir metode nepārtrauktai savienojuma absorbcijas vai emisijas intensitātes mērīšanai, mainot metāla jonu koncentrāciju. Izmantojot purīna ciklu, var sintezēt daudz "*push-pull*" hromoforu. Viens no iespējamiem fragmentiem, ko var ievadīt purīna ciklā, ir 1,2,3-triazols, kas darbojas ne tikai kā laba elektronus atvelkoša grupa, bet arī veido stabilu kompleksēšanās vietu metāla joniem (4. att.). Literatūrā ir ziņots, ka 1,2,3-triazoli ir daļa no kompleksēšanās sistēmām ar piridīnu, izohinolīnu un ferocēnu[76, 77] kopā ar citiem *O*-, *S*- un *N*-atomiem molekulā. Šādas sistēmas veido metālu jonu kompleksus ar Pd^{2+}, Cu^{2+}, Ni^{2+}, Ru^{2+}, Au^{+} un Ag^{+} joniem, dažiem no tiem piemīt pretmikrobu, pretvēža un pretsēnīšu aktivitāte.[76–78] Tomēr neviena no minētajām triazola sistēmām neietvēra purīna ciklu. Tā kā promocijas darba autora un kolēģu grupa iepriekš ziņoja par 2,6-bis-triazola-purīna atvasinājumu potenciālu izmantošanu par ratiometriskajiem sensoriem,[28] pētījums rosināja šī promocijas darba izstrādes laikā sintezēt jaunus triazolilpurīna atvasinājumus.

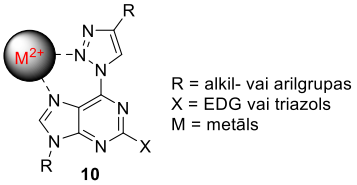

4. att. Metāla jonu kompleksēšanās vieta starp 1,2,3-triazolu un purīna *N*7 pozīciju.

1.2. Triazolilpurīna atvasinājumu sintēze

1,2,3-Triazola fragments ir atrodams atsevišķu medikamentu struktūrā un tiek izmantots kā farmakofors, piemēram, pretvīrusu un pretvēža līdzekļos, tādos kā cefatrizīns, rufinamīds un mubtritinibs.[79–81] 1,2,3-Triazola struktūrai ir tieksme veidot ūdeņraža saites, kā arī veikt π-π un dipola-dipola mijiedarbību, un tai nav noslieces uz degradāciju vielmaiņas rezultātā.[82] 1,2,3-Triazola cikls spēj uzrādīt funkcionālo grupu pazīmes, un to izmanto kā amīda saites, estera saites un karbonskābes bioizostēru grupu.[83]

1,2,3-Triazolus parasti sintezē, izmantojot [3+2] Huisgena (*Huisgen*) vara vai rutēnija katalizētās azīda-alkīna ciklopievienošanās reakcijas.[80, 84] Atkarībā no izejvielu uzbūves ir iespējams iegūt divas savienojumu sērijas, proti, caur C-N un C-C saitēm saistītus triazolilpurīnus **A** un **B** (5. att.).

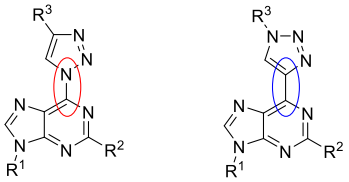

5. att. Caur C-N (**A**) vai C-C (**B**) saitēm saistīto triazola-purīna konjugātu struktūras.

Iepriekš promocijas darba autora un kolēģu grupa pētīja caur C-N saiti saistītos triazolilpurīnus **A**.[28, 85] Ir zināms, ka caur C-N saiti saistītais triazols purīna *C*6 pozīcijā darbojas kā laba aizejošā grupa S_NAr reakcijās ar dažādiem *O*-, *C*-, *P*-, *Se*- un *N*-nukleofīliem.[48, 49, 52, 53] Bet šajā darbā autors izvēlējās sintezēt savienojumus **B**, kuros triazola un purīna cikli ir saistīti ar C-C saiti, tādējādi uzlabojot struktūras stabilitāti potenciālai izmantošanai *OLED* struktūrās.

Ar C-C saiti saistīti triazolilpurīna atvasinājumi tika sintezēti vara katalizētā azīda-alkīna ciklopievienošanās reakcijā (CuAAC), izmantojot attiecīgos alkinilpurīnus un arilazīdus. Pirmkārt, komerciāli pieejamais 2,6-dihlorpurīns (**11**) *N*9 pozīcijā tika funkcionalizēts ar trim dažādām alkilgrupām Micunobu reakcijas apstākļos (2. shēma). Tritilgrupu saturošais fragments (**a**) tika ievests struktūrā, lai piešķirtu savienojumam amorfas īpašības, padarot to piemērotāku fotofizikālo īpašību pētījumiem plānās kārtiņās un potenciālās *OLED* izmantošanas izvērtēšanai.[86] Heptilgrupa (**b**) tika izvēlēta tās inertās uzvedības dēļ, un glicerīnu saturošais fragments (**c**) tika izvēlēts, lai palielinātu galaprodukta šķīdību ūdenī. Pēc tam Sonogaširas (*Sonogashira*) reakcijā molekulā tika ievadītas alkinilgrupas. Tā kā izejvielā ir divi hlora atomi, attiecīgi purīna *C*2 un *C*6 pozīcijās, šajā reakcijā, tikai mainot reakcijas apstākļus, ir iespējams iegūt vai nu 6-alkinilpurīnus **13,** vai arī 2,6-bis-alkinilpurīnus **14**. Tā kā purīna *C*6 pozīcija ir reaģētspējīgāka,[16] vispirms 50 °C temperatūrā izveidojās produkts **13**, un tālākai aizvietošanai purīna *C*2 pozīcijā bija nepieciešama augstākas temperatūras izmantošana, tāpēc temperatūra tika paaugstināta līdz 100 °C, nomainot šķīdinātāju

no tetrahidrofurāna (THF) uz dimetilformamīdu (DMF). Ir vērts atzīmēt, ka 6-alkinilpurīnu **13** sintēzē pat 50 °C temperatūrā, izmantojot tieši vienu ekvivalentu trimetilsilil- (TMS) acetilēna, vienmēr tika novērota 2,6-bis-alkinilpurīnu **14** veidošanās līdz pat 10 % no konversijas.

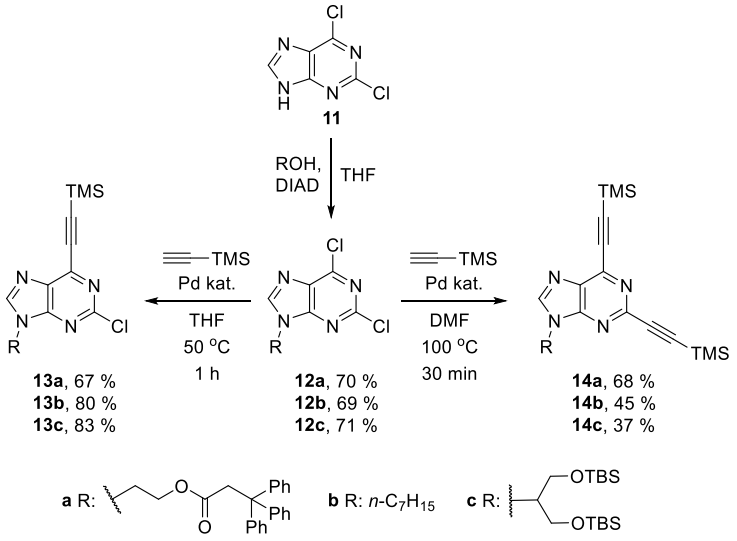

2. shēma. 6-Alkinilpurīnu **13** un 2,6-bis-alkinilpurīnu **14** sintēze.

Tālāk tika veiktas CuAAC reakcijas starp iegūtajiem alkinilpurīniem un aril- (2. tab., 1.–8. rinda) un alkilazīdiem **15** (2. tab., 9.–13. rinda), izmantojot CuI kā katalizatoru. Atbilstošie 2-hlor-6-triazolilpurīni **16a-m** tika iegūti ar 56–91 % iznākumu. 4-Azido-*N*,*N*-dimetilanilīna gadījumā (2. tab., 3. rinda) reakcija tika veikta, izmantojot $CuSO_4 \cdot 5H_2O$/nātrija askorbāta katalītisko sistēmu attiecīgā azīda palielināta elektronu blīvuma dēļ. Vara jodīda klātbūtnē tas reducējās par atbilstošo amīnu ātrāk, nekā reakcija tiek pabeigta. Pēc tam savienojumi **16a-m** tika izmantoti S_NAr reakcijās ar piperidīnu, iegūstot 2-piperidinil-6-triazolilpurīnus **17a-m**. Piperidīns tika izvēlēts kā elektronu donorā daļa, kas veido pilnīgu "*push-pull*" hromoforu pretstatā elektronu deficītajam triazola fragmentam, tādējādi uzlabojot produkta fluorescenci. Savienojuma **16j** gadījumā (2. tab., 10. rinda) tika novērota estera aminolīze, un attiecīgā metilestera vietā tika iegūts piperidilamīds.

2. tabula

Alkinilpurīnu **13** un alkil-/arilazīdu **15** CuAAC reakcija ar sekojošu S_NAr reakciju piperidīna fragmenta ievadīšanai molekulā

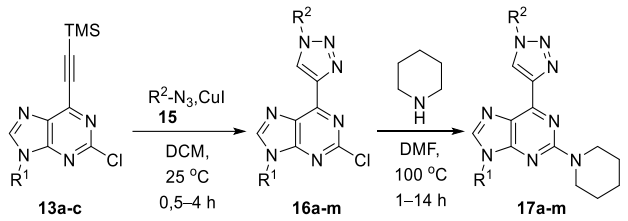

Nr.	R^1	R^2	Reakcijas **13** →**16** iznākums, %	Reakcijas **16** → **17** iznākums, %
1.	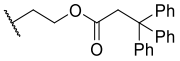	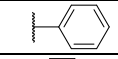	**16a**, 66	**17a**, 67
2.		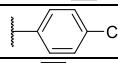	**16b**, 82	**17b**, 76
3.		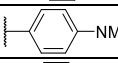	**16c**, 56[a]	**17c**, 41
4.		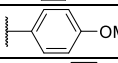	**16d**, 89	**17d**, 67
5.	*n*-C_7H_{15}	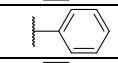	**16e**, 86	**17e**, 77
6.		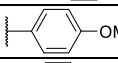	**16f**, 91	**17f**, 81
7.		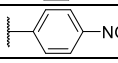	**16g**, 69	**17g**, 71
8.	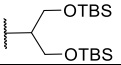	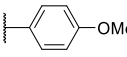	**16h**, 89	**17h**, 75
9.	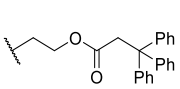	CH_2CN	**16i**, 59	**17i**, 75
10.		CH_2COOMe	**16j**, 74	**17j**, 75[b]
11.		Cy[c]	**16k**, 77	**17k**, 66
12.		*n*-$C_{10}H_{23}$	**16l**, 88	**17l**, 89
13.		Bn	**16m**, 83	**17m**, 83

[a] Reakcijas **13** → **16** apstākļi – $CuSO_4 \cdot 5H_2O$, nātrija askorbāts, AcOH, DMF, 70 °C.

[b] Reakcijā **16** → **17** novērota estera aminolīze, un attiecīgā metilestera vietā tika iegūts piperidilamīds.

[c] Cy – cikloheksilgrupa.

Tika izmantota arī CuAAC reakcija starp 2,6-bis-alkinilpurīniem **14** un atbilstošajiem alkil-/arilazīdiem **15**, lai iegūtu bis-triazolilpurīnus **18a-m** (3. tab.). Ir zināms, ka nitrogrupa, kas ievadīta feniltriazola daļā (2. tab., 7. rinda), pilnībā dzēš fluorescenci, savukārt 4-azido-*N*,*N*-dimetilanilīna gadījumā reakcijas maisījumā nekad netika novērota otrā triazola veidošanās.

3. tabula

2,6-Bis-alkinilpurīnu **14** un azīdu **15** CuAAC reakcija

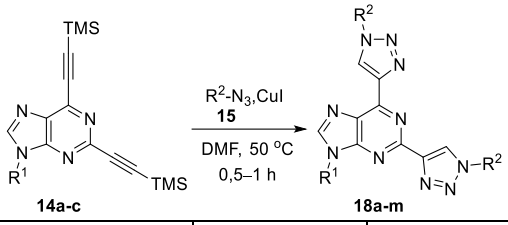

Nr.	R^1	R^2	Reakcijas **14** → **18** iznākums, %
1.	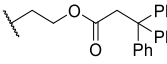	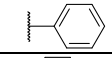	**18a**, 60
2.		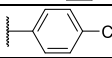	**18b**, 50
3.		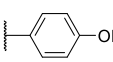	**18c**, 60
4.	*n*-C_7H_{15}		**18d**, 44
5.	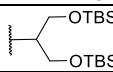		**18e**, 38
6.	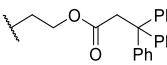	CH_2CN	**18f**, 62
7.		CH_2COOMe	**18g**, 67
8.		Cy[a]	**18h**, 81
9.		*n*-$C_{10}H_{23}$	**18i**, 45
10.		Bn	**18j**, 85

[a]Cy – cikloheksilgrupa.

Pēc plaša caur C-C saiti saistītu mono- un bis-triazolilpurīnu klāsta iegūšanas tika nolemts sintezēt dažus caur C-N saiti saistītos triazolilpurīna analogus, lai savstarpēji salīdzinātu abu produktu sēriju fotofizikālās īpašības. Turklāt, tā kā metālu jonu kompleksu veidošanas eksperimentus ir labāk veikt ūdens vidē, tika nolemts ievadīt glicerīnu saturošu fragmentu izvēlētajos ar C-N saiti saistītajos triazola-purīna analogos. C-N triazolilpurīna produktu sintēzei tika izvēlēta mūsu laboratorijā iepriekš izstrādāta metode.[31, 53, 85, 87] Pirmajā solī S_NAr reakcijā starp iepriekš iegūto purīna atvasinājumu **12c** un NaN_3 tika iegūts 2,6-diazidopurīns **19** (3. shēma). Tālāk CuAAC reakcijā starp diazīdu **19** un 1-etinil-4-metoksibenzolu tika iegūts 2,6-bis-triazolilpurīns **20**. Līdzīgā veidā, izmantojot S_NAr un CuAAC reakciju secību, tika sintezēts caur C-N saiti saistīts 2-piperidinil-6-triazolilpurīns **23**. S_NAr reakcijā starp diazīdu **19** un piperidīnu azīda-tetrazola līdzsvara dēļ izveidojās produkts **22**, kas vēlāk tika izmantots CuAAC reakcijā ar 1-etinil-4-metoksibenzolu. Pēdējā solī savienojumos **20** un **23** tika nošķeltas *terc*-butildimetilsilil- (TBS) aizsarggrupas, izmantojot etiķskābi THF/H_2O maisījumā, iegūstot attiecīgos produktus **21** un **24**. Tie paši apstākļi tika izmantoti arī TBS grupu nošķelšanai caur C-C saiti saistītajiem analogiem **17h** un **18e** (4. tab., 11. un 14. rindas).

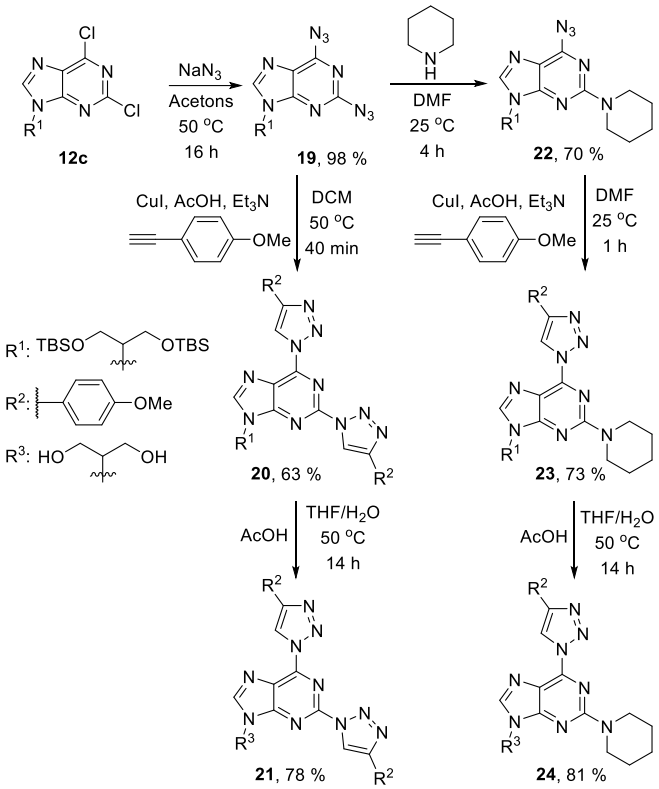

3. shēma. Ar C-N saiti saistītu bis-triazolilpurīna atvasinājumu **21** un mono-triazolilpurīna atvasinājumu **24** sintēze.

Tālāk tika pētītas mērķsavienojumu **17**, **18**, **21** un **24** fotofizikālās īpašības (4. tab.). Amorfo savienojumu **17a**, **17d** un **17m**, kas bija paredzēti potenciālai izmantošanai *OLED* iekārtās, kvantu iznākumu mērījumi tika veikti plānās kārtiņās un sasniedza līdz 35 %. Pētījuma laikā tika atklāts, ka tritilgrupu saturošie purīna atvasinājumi tomēr ir nepiemēroti *OLED* izstrādei, jo šie savienojumi strauji degradējās elektriskās strāvas ietekmē, tāpēc turpmāki eksperimenti un purīna struktūras modifikācijas potenciālai *OLED* izstrādei netika veikti.

4. tabula

Triazolilpurīnu **17**, **18**, **21** un **24** fotofizikālās īpašības

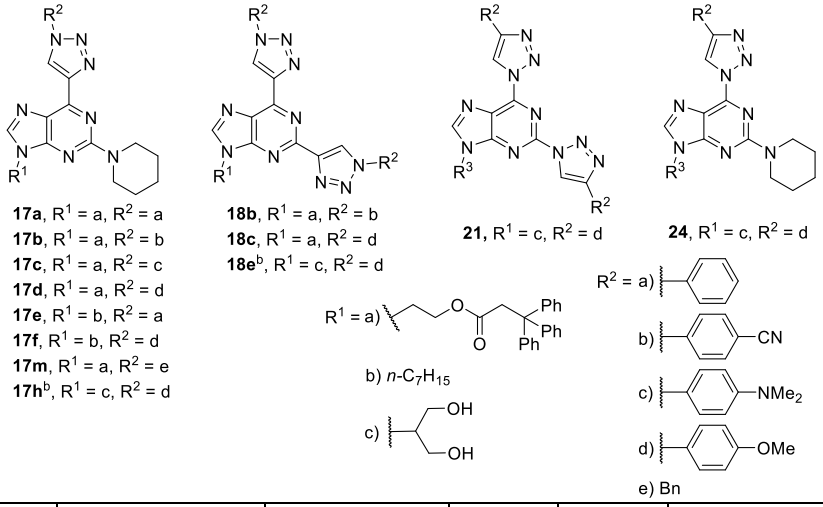

Nr.	Savienojums	Šķīdinātājs[a]	$\lambda_{abs\ max}$, nm	$\lambda_{em\ max}$, nm	Kvantu iznākums, %
1.	**17a**	DCM	365	443	75
2.		plānā kārtiņā	366	447	35
3.	**17b**	DCM	371	452	68
4.	**17c**	DCM	311	437	76
5.	**17d**	DCM	363	439	71
6.		plānā kārtiņā	381	545	12
7.	**17e**	DCM	364	443	81
8.	**17f**	DCM	365	441	74
9.	**17m**	DCM	362	438	75
10.		plānā kārtiņā	361	443	23
11.	**17h**[b]	DMSO	363	450	95
12.	**18b**	DCM	282	---	0
13.	**18c**	DCM	281	394	26
14.	**18e**[b]	DMSO	283	452	49
15.	**21**	DMSO	261	506	24
16.	**24**	DMSO	362	457	98

[a] $C = 10^{-5}$ mol/L.

[b] Pēc TBS grupas nošķelšanas no sākotnējā substrāta.

Glicerīna fragmentu saturošu purīna atvasinājumu **17h**, **18e**, **21** un **24** gadījumā tika novērots, ka tie praktiski nešķīst ūdenī un dihlormetānā (DCM), bet šķīst tikai dimetilsulfoksīdā (DMSO), tāpēc visi fotofizikālie mērījumi tika veikti DMSO šķīdumos. 2,6-Bis-triazolilpurīna atvasinājums **18b** neuzrādīja fluorescenci, savukārt savienojumi **18c**, **18e** un **21** uzrādīja mērenus kvantu

iznākumus diapazonā no 24 % līdz 49 %. Pētīto deviņu 6-triazolil-2-piperidinilpurīna atvasinājumu **17a-h** un **24** gadījumā kvantu iznākumi DCM un DMSO bija robežās no 68 % līdz 98 %.

Oriģinālpublikācija par šajā nodaļā aprakstītajiem pētījumiem ir pievienota II pielikumā.

1.3. Ūdenī šķīstošo triazolilpurīna atvasinājumu sintēze

Tā kā glicerīna fragmentu saturošajam savienojumam **24** bija augsts kvantu iznākums, bet tomēr slikta šķīdība ūdenī, tika nolemts hidroksilgrupas aizvietot ar piridīnija fragmentiem, kas ļautu veidot sāļus ar pretjoniem, tā palielinot savienojuma šķīdību ūdenī.[88, 89] Šim nolūkam no hidroksilgrupām tika izveidoti tozilatvasinājumi **25**, kas pēc tam tika karsēti piridīnā 120 °C temperatūrā, kamēr veidojas atvasinājums **26** (4. shēma).

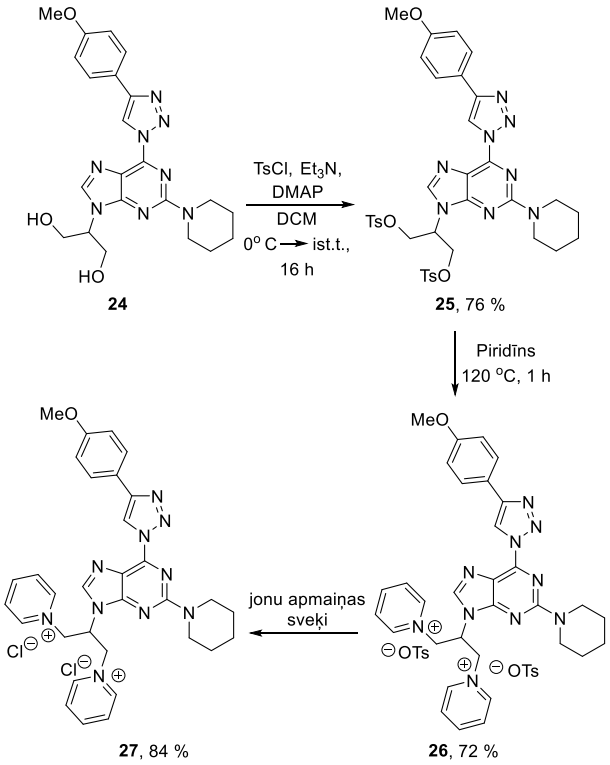

24 **25**, 76 %

27, 84 % **26**, 72 %

4. shēma. Ūdenī šķīstošu caur C-N saiti saistītu mono-triazolilpurīnu **27** sintēze.

Savienojums **26** bija ūdenī šķīstošs, tomēr tas saturēja tozilāta anjonus, kas potenciāli varētu ietekmēt fluorescenci, tāpēc tika nolemts šos jonus apmainīt pret hlorīdjoniem, izmantojot jonu apmaiņas sveķus. Savienojumu **24**–**27** šķīdība ūdenī tika noteikta, izmantojot kvantitatīvo

^{1}H-KMR metodi, iegūstot šādus datus: sav. **24** – 0,21 mg/mL, sav. **25** – 0,19 mg/mL, sav. **26** – 57 mg/mL un sav. **27** – 133 mg/mL.

Fotofizikālās īpašības tika noteiktas savienojumiem **26** un **27** (5. tab.). Absorbcijas un emisijas spektri savienojumam **26** tika reģistrēti H_2O, DMSO un DCM un savienojumam **27** acetonitrilā (MeCN), metanolā (MeOH), H_2O, DMSO un DCM 10^{-4} M koncentrācijā. Abu triazolilpurīna atvasinājumu kvantu iznākums bija zem noteikšanas robežas (< 0,5 %), savukārt izejvielai **24** 10^{-5} M koncentrācijā tas sasniedza 98 % DMSO (4. tab., 16. rinda). Nomainot savienojuma **24** glicerīnu saturošo daļu purīna *N*9 pozīcijā ar piridīnija fragmentiem, vienlaikus ievērojami uzlabojas savienojuma šķīdība ūdenī, bet pilnīgi tika dzēsta fluorescence.

5. tabula

Triazolilpurīnu **26** un **27** fotofizikālās īpašības

	Savienojums **26**			Savienojums **27**		
Šķīdinātājs[a]	$\lambda_{abs\ max}$, nm	$\lambda_{abs\ min}$, nm	Kvantu iznākums, %	$\lambda_{abs\ max}$, nm	$\lambda_{abs\ min}$, nm	Kvantu iznākums, %
MeCN	–	–	–	360	457	< 0,5
MeOH	–	–	–	362	461	< 0,5
H_2O	362	457	< 0,5	363	463	< 0,5
DMSO	361	428	< 0,5	362	454	< 0,5
DCM	359	565	< 0,5	360	452	< 0,5

[a] C = 10^{-4} mol/L.

Oriģinālpublikācija par šajā nodaļā aprakstītajiem pētījumiem ir pievienota III pielikumā.

1.4. Ūdenī šķīstoši purīna atvasinājumi metālu jonu kompleksēšanai

Pamatojoties uz literatūras datiem, tetraetilēnglikola (TEG) grupas ievadīšana purīna atvasinājumos paaugstina savienojumu šķīdību ūdenī.[90, 91] TEG fragmentu saturoši purīna atvasinājumi **31** un **32** tika iegūti vairāku stadiju sintēzē, sākot ar 2,6-dihlorpurīnu (**11**) (5. shēma).

Izmantojot Micunobu reakcijas apstākļus, ar tetrahidropiranil- (THP) grupu aizsargāts TEG fragments tika ievadīts 2,6-dihlorpurīna (**11**) *N*9 pozīcijā. Pēc tam 6-alkinilpurīna atvasinājums **29** tika iegūts Sonogaširas reakcijā un tālāk tika izmantots CuAAC reakcijā ar 1-azido-4-metoksibenzolu, kam sekoja S_NAr reakcija ar piperidīnu, kas ļāva iegūt triazolilpurīna atvasinājumu **30**. THP aizsarggrupa tika noņemta ar trifluoretiķskābi (TFA) metanolā, rezultātā tika iegūts savienojums **31**. Pēc tam savienojuma **31** reakcijā ar *terc*-butil-2-bromacetātu ar sekojošu aizsarggrupas noņemšanu, tika iegūts produkts **32**. Savienojumu **31** un **32** šķīdība ūdenī tika noteikta, mērot piesātināto šķīdumu UV absorbciju un salīdzinot to ar atbilstošajām kalibrēšanas līknēm. Noteiktā savienojumu **31** un **32** šķīdība ūdenī bija attiecīgi 0,24 mg/mL un 110 mg/mL.

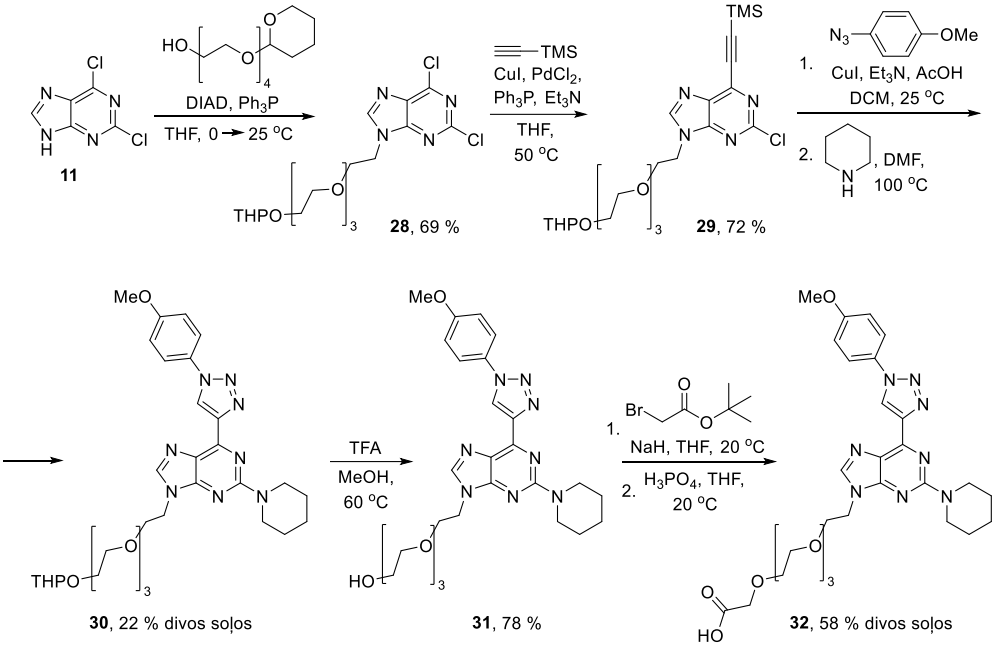

5. shēma. TEG fragmentu saturoša purīna atvasinājuma **32** iegūšana.

Tālāk tika pētītas savienojumu **17f**, **31** un **32** fotofizikālās īpašības (6. tab.). Tā kā savienojums **17f** nešķīst ūdenī, mērījumi tika veikti dažādas polaritātes aprotonos šķīdinātājos – cikloheksānā (CyHex), dietilēterī (DEE), etilacetātā (EA), dimetoksietānā (DME), MeCN un DMSO. TEG grupu saturošo triazolilpurīnu **31** un **32** fotofizikālās īpašības tika pārbaudītas ūdenī. Savienojuma **17f** kvantu iznākums dažādos šķīdinātājos bija robežās no 48 % līdz 72 %, tā fluorescences dzīves laiks bija no 9 ns līdz 15,7 ns. Starojuma pārejas varbūtības laiks (τ_{rad}) apzīmē ātrumu, ar kādu molekula izstaro fluorescenci, savukārt bezizstarojuma pārejas varbūtības laiks (τ_{nonrad}) ir fluorescences dzēšanas ātrums.[92] Šie ir konkurējošie procesi, un augstam kvantu iznākumam atbilst maksimālais τ_{rad} un minimālais τ_{nonrad}. Augstākais sasniegtais kvantu iznākums savienojumam **17f** bija 72 % DMSO, kas izskaidrojams ar to, ka viskozākos šķīdinātājos molekulu kustības ir lēnākās, tādējādi samazinot fluorescences dzēšanu. Zemākais kvantu iznākums 17 % tika novērots savienojumiem **31** un **32** ūdenī. Izteikta fluorescences dzēšana ūdenī bija sagaidāma hidroksilgrupu augstas vibrāciju enerģijas dēļ.[93] Novērotais kvantu iznākums joprojām tika uzskatīts par pietiekamu turpmākiem metālu jonu noteikšanas eksperimentiem ūdens vidē.

6. tabula

Triazolilpurīnu **17f**, **31** un **32** fotofizikālās īpašības

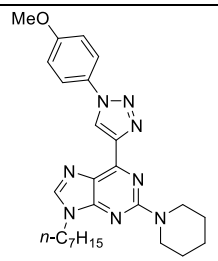

17f

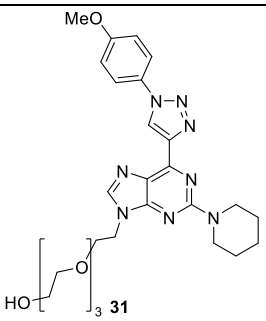

31

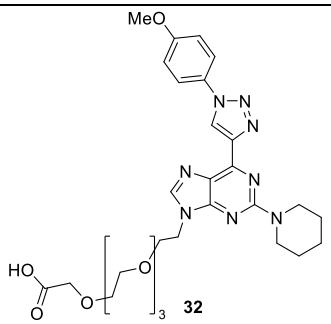

32

Nr.	Savienojums	Šķīdinātājs	λ_{abs}, nm	λ_{em}, nm	Kvantu iznākums, %	τ,[a] ns	τ_{rad},[b] ns	τ_{nonrad},[c] ns
1	**17f**	CyHex	365	415 395	61	9	14,8	23,1
2		DEE	360	425	52	9,4	18,1	19,6
3		EA	360	425	48	9,3	19,4	17,9
4		DME	360	425	50	9,7	19,4	19,4
5		MeCN	360	435	49	12,4	25,3	24,3
6		DMSO	360	445	72	15,7	21,8	56,1
7	**31**	H_2O	363	462	17	7,1	41,5	8,5
8	**32**		363	462	17	7,1	41,8	8,6

[a] Fluorescences dzīves laiks.

[b] Starojuma pārejas varbūtības laiks, $\tau_{\mathrm{rad}} = \frac{\tau}{QY}$.

[c] Bezizstarojuma pārejas varbūtības laiks, $\tau_{\mathrm{nonrad}} = \frac{\tau}{1 - QY}$.f

Tika pārbaudītas savienojumu **31**, **32** un iepriekš iegūtā purīna atvasinājuma **17f** metālu jonu kompleksēšanas īpašības. Eksperimentiem tika izvēlēti dzīvsudraba(II) joni. Dzīvsudrabs ir bioloģiski nedegradējams smagais metāls, kam ir augsta toksicitāte attiecībā uz dzīvajiem organismiem. Dzīvsudraba savienojumi, izšķīdinot saldūdenī vai jūras ūdenī, veido metildzīvsudrabu, kas uzkrājas jūras produktos un tādējādi nonāk cilvēku uzturā.[94] Dzīvsudraba uzkrāšanās cilvēku organismā palielina sirds saslimšanu risku, izraisa Minamatas (*Minamata*) slimību, kā arī bojā DNS un hromosomas.[95] Minēto problēmu dēļ ir nepieciešams detektēt Hg^{2+} jonus ūdenī un šūnās. Ir zināmi savienojumi, kas spēj kompleksēt Hg^{2+} jonus, balstoties dažādos darbības mehānismos, tai skaitā kompleksēšanai izmantojot *S*-atomus un *N*-atomus, kā arī tioacetālu aizsarggrupu noņemšanu kompleksa veidošanās rezultātā.[96] Promocijas darba izstrādes gaitā triazolilpurīni tika pētīti, jo Hg^{2+} joniem ir tendence koordinēties ar slāpekļa atomiem, bet triazolilpurīnu struktūrā ir pietiekams daudzums slāpekļa atomu.

Izmantojot ^{1}H-KMR titrēšanas metodi, triazolilpurīna atvasinājums **17f** tika titrēts MeCN-d_3 šķīdumā, izmantojot $Hg(ClO_4)_2 \cdot 3H_2O$ kā Hg^{2+} avotu un benzolu kā iekšējo standartu. Analizējamā

parauga ^{1}H-KMR spektrs tika reģistrēts pēc katras 0,1 ekvivalenta Hg^{2+} jonu pievienošanas reizes (6. att.).

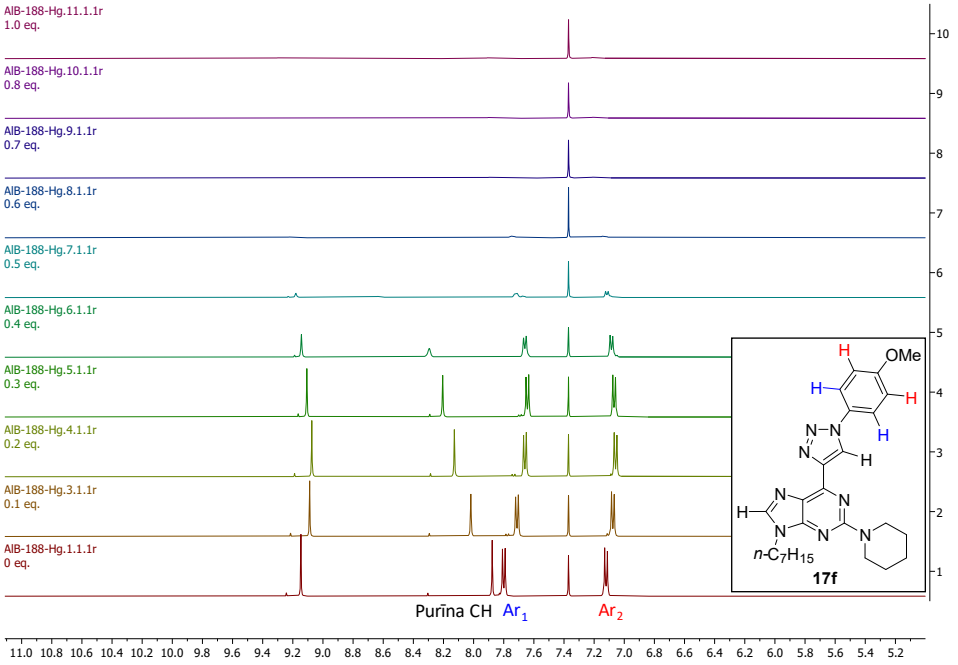

6. att. Savienojuma **17f** ^{1}H-KMR titrēšanas ar Hg^{2+} joniem eksperiments MeCN-d_3 šķīdumā, spektrā attēlots tikai aromātiskais reģions.

Pēc katras Hg^{2+} jonu porcijas pievienošanas aromātisko protonu signāliem tika novērotas nobīdes, visstraujāko nobīdi novēroja purīna *C*8-H signāla gadījumā, kam sekoja triazola CH un Ar_1 CH signālu nobīdes. Jau pēc pirmās Hg^{2+} jonu porcijas pievienošanas lēnām sāka veidoties nogulsnes, pie 0,5 ekvivalentiem Hg^{2+} jonu tika novērots tikai neliels daudzums savienojuma **17f**, kas pilnībā izzuda, pievienojot nākamos 0,1 ekvivalentus Hg^{2+} jonu šķīduma. Visticamāk, izveidojušās nogulsnes bija purīna **17f** un Hg^{2+} jonu komplekss ar koordinācijas modeli 2 : 1, kur Hg^{2+} koordinējās starp purīna *N*7 un triazola *N*3 atomiem (7. att.).

Savienojumu **31** un **32** kompleksu veidošanās ar Hg^{2+} joniem tika pārbaudīta ūdenī, kompleksi veidojas attiecībā 1 : 1, jo ūdenī samazinās saistīšanas konstante. Kā bija sagaidāms, visiem pārbaudītajiem substrātiem Hg^{2+} jonu pievienošana dzēsa fluorescenci, pierādot šo savienojumu potenciālu izmantošanai par Hg^{2+} jonu sensoriem. Citu metālu jonu, tādu kā Na^+, K^+, Mg^{2+}, Ca^{2+}, Fe^{2+}, Cu^{2+}, Zn^{2+}, Hg^{2+} un Pb^{2+}, kompleksēšanās ar savienojumiem **17f**, **31** un **32** arī tika pārbaudīta attiecīgi acetonitrilā vai ūdenī (8. att.).

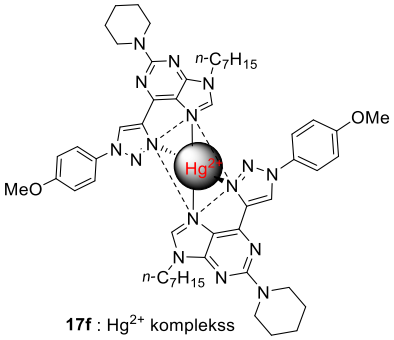

17f : Hg^{2+} komplekss

7. att. Iespējamais **17f** : Hg^{2+} komplekss, pamatojoties uz titrēšanas eksperimentu novērojumiem.

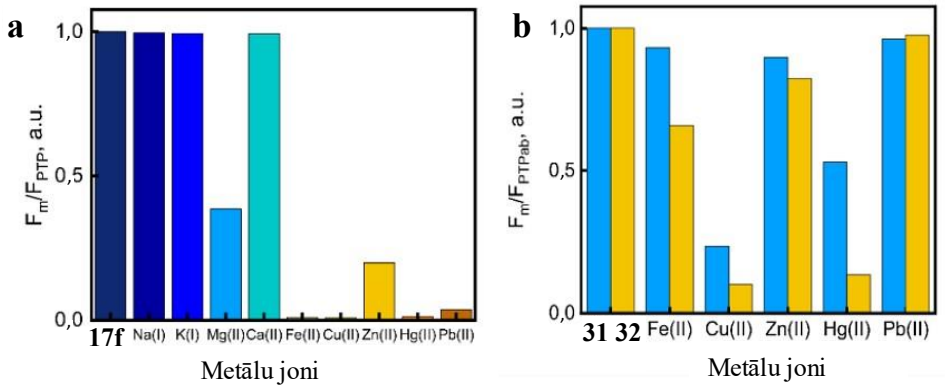

8. att. a) Fluorescences intensitāte pēc metāla jonu pievienošanas savienojumam **17f** acetonitrilā. b) Fluorescences intensitāte pēc metāla jonu pievienošanas savienojumam **31** (zila josla) un **32** (dzeltena josla) ūdenī.

Triazolilpurīna atvasinājums **17f**, neskaitot Hg^{2+} jonus, veido kompleksus ar Fe^{2+}, Cu^{2+}, Pb^{2+}, Mg^{2+} un Zn^{2+} joniem. Savukārt ūdens vidē TEG saturošie triazolilpurīna atvasinājumi **31** un **32** stipri koordinējas ar Hg^{2+} un Cu^{2+} joniem (8. b att.), kas izskaidrojams ar vara jonu azafīlo dabu, kas pat ūdens vidē dod priekšroku koordinācijai pie slāpekļa atomiem.[97] Savukārt citi metālu joni, piemēram, Fe^{2+} un Pb^{2+}, dod priekšroku koordinācijai pie skābekļa atoma un tā vietā veido kompleksus ar ūdeni. Visiem pārbaudītajiem savienojumiem bija lieliska kompleksēšanās spēja ar Hg^{2+} joniem šķīdumos. Sadarbībā ar kolēģiem no Taivānas tālākie eksperimenti ar savienojumiem **31** un **32** tika veikti šūnās. Savienojums **32**, kas saturēja COOH grupu, bija pārāk reaģētspējīgs un pielipa pie šūnu plates, tāpēc eksperimenti tika turpināti tikai ar savienojumu **31**. MDA-MB-231 šūnas tika apstrādātas ar $HgCl_2$, kam sekojoši tika pievienots savienojums **31**. Lai novērotu izmaiņas šūnās, tika izmantota gaišā lauka un fluorescences spektroskopija (9. att.).

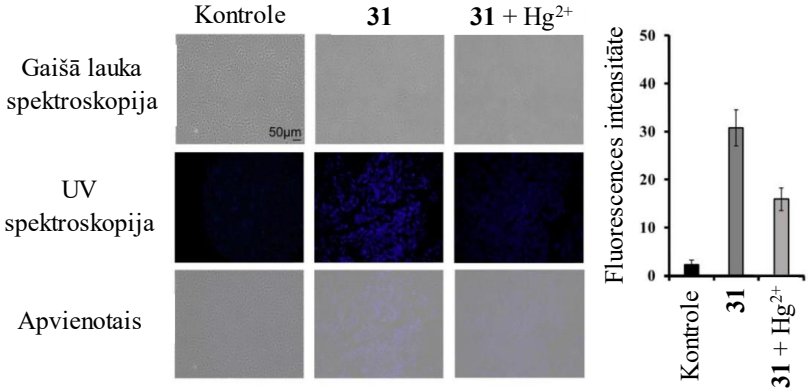

9. att. Fluorescences un gaišā lauka spektroskopijas attēli MDA-MB-231 šūnām marķētām ar savienojumu **31** ar vai bez Hg^{2+} joniem.

Šūnas veiksmīgi iekļāva savienojumu **31**, un fluorescence tika dzēsta pēc apstrādes ar dzīvsudrabu. Šis eksperiments apstiprināja savienojuma **31** iespējamo izmantošanu par dzīvsudraba jonu detektoru bioloģiskajās sistēmās.

Oriģinālpublikācijas manuskripts par šajā nodaļā aprakstītajiem pētījumiem ir pievienots IV pielikumā.

Savienojumi **17f**, **31** un **32** ir aprakstīti arī LVP2024000059 un LVP2024000072 patentu pieteikumos, kas iesniegti Latvijas Republikas Patentu valdē un ir pievienoti V un VI pielikumos.

1.5. Ūdenī šķīstoši purīna atvasinājumi kā potenciālie fotokatalizatori

Sadarbībā ar kolēģiem no Viļņas Universitātes (VU) un Akvitānijas viļņu un materiālu laboratorijas Bordo Universitātē, kuriem ir pieredze fotokatalītisko sistēmu pētījumos,[98, 99] tika dizainēts jauns potenciāls purīna ciklu un ciklēna (1,4,7,10-tetraazaciklododekāna) fragmentu saturošs fotokatalizators, kuru izdevās iegūt deviņu soļu sintēzē (10. att.).

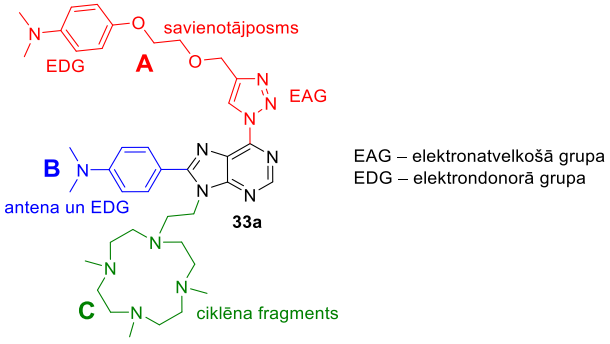

10. att. Piedāvātā mērķsavienojuma **33a** struktūra.

Fragments **A** sastāv no trīs daļām – 1,2,3-triazola, savienotājposma un *N*,*N*-dimetilanilīna. Triazols strādā kā elektronatvelkošā grupā šīs "*push-pull*" sistēmas molekulā, savukārt *N*,*N*-dimetilanilīns pēc ierosināšanas ir stiprs lādiņa donors, kas nav savienots ar citām aromātiskām sistēmām. Fragments **B** ir *N*,*N*-dimetilanilīns, kas ir savienots tieši ar purīna ciklu, strādā kā stipra elektrondonorā grupa "*push-pull*" sistēmā un kā antena elektronu pārnesei. Fragments **B** arī pagarina triazolilpurīna π-konjugēto elektronu sistēmu, pazeminot tā absorbcijas maksimuma viļņa garumu un pārvēršot to par fragmentu ar izteiktām lādiņa pārneses īpašībām. Ciklēna daļu saturošais fragments **C** tika izvēlēts, jo tam piemīt lieliskās spējas kompleksēt metāla jonus, tādus kā Cu^{2+}, Ni^{2+} un Zn^{2+}.[100,101] Šajā molekulā esošais **C** fragments ir paredzēts Cu^{2+} jonu koordinācijai ar visiem četriem ciklā esošajiem slāpekļa atomiem, pateicoties labajai koordinācijas tieksmei pret tiem, termodinamiskajai stabilitātei un kinētiskajam inertumam skābā vidē.[102] Vispārējs piedāvātais šī fotokatalizatora darbības mehānisms ir šāds: 1) pēc fotoierosināšanas tiek ierosināts elektrons antenā un tas nonāk zemākajā neaizņemtajā molekulārajā orbitālē (LUMO), kam ātri seko elektrona pārvietošana no donora grupas uz brīvu vietu antenas augstākajā aizņemtajā molekulārajā orbitālē (HOMO); 2) notiek elektronu pārnese no antenas LUMO uz metālu ciklēnā, reducējot metāla jonus no Cu^{2+} līdz Cu^{+} (11. att.).

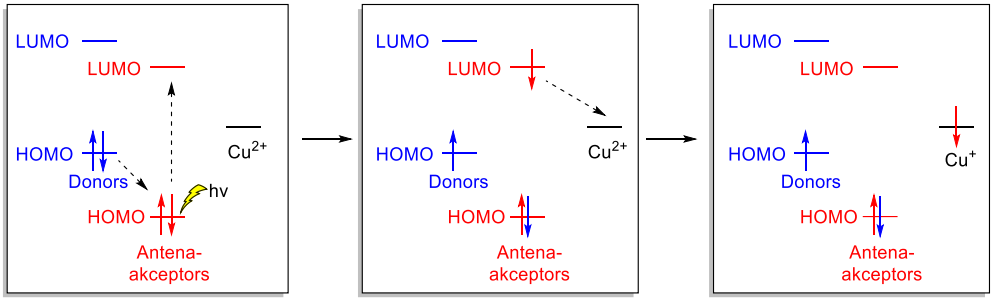

11. att. Piedāvātais fotokatalizatora **33a** darbības mehānisms.

Lai iegūtu vēlamo savienojumu, purīna ciklu nepieciešams modificēt ar **A**, **B** un **C** fragmentiem *C*6, *C*8 un *N*9 pozīcijās. Tika izstrādāti seši iespējamie sintēzes ceļi mērķprodukta **33a** iegūšanai atkarībā no izvēlēto fragmentu ievadīšanas secības purīna gredzenā. Vispārējās stratēģijas mērķsavienojuma sintēzei redzamas 6. shēmā. **A** fragmentu var ievadīt, izmantojot CuAAC reakciju (6. a shēma). Būvbloka **36** sintēze tika veikta četros soļos, sākot no 1-brom-4-nitrobenzola (VII pielikums). Purīna *C*8 pozīcijas arilēšanu var veikt, izmantojot pallādija katalizētu šķērssametināšanas reakciju, šim nolūkam tika izvēlēta Stilles reakcija (6. b shēma); būvbloks **39** viegli tika iegūts vienā solī.[103] Būvbloku **C** var ievadīt purīna *N*9 pozīcijā S_N2 reakcijā, izmantojot ciklēna atvasinājumu **42**, kas iegūts pēc literatūrā zināmas metodes (6. c shēma).[104]

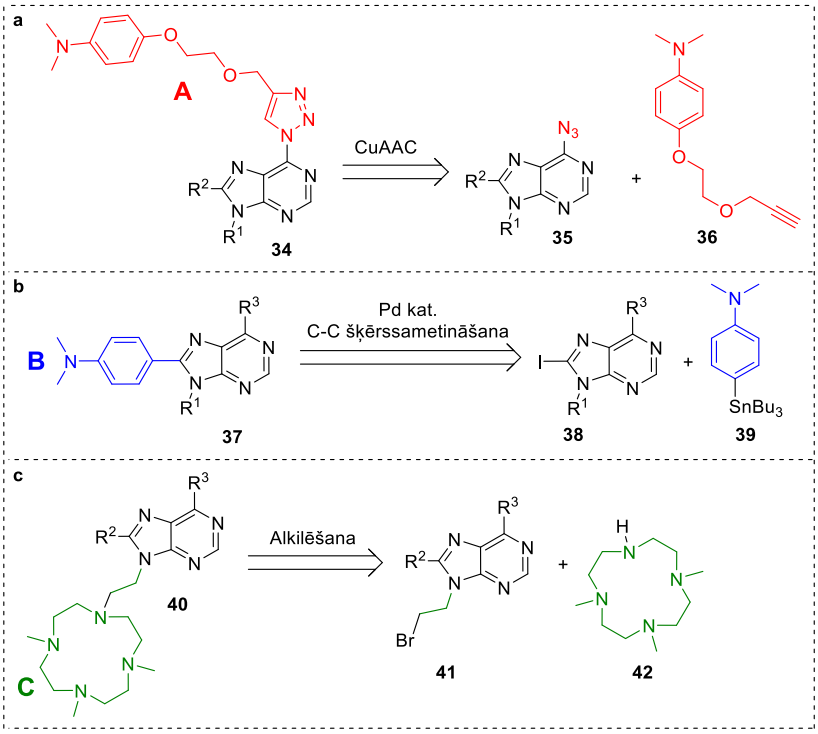

6. shēma. Retrosintētiskā pieeja **A**, **B** un **C** fragmentu ievadīšanai purīnu ciklā.

Vispirms ciklēnu saturošā produkta **33a** iegūšanai tika izmantots savienojums **43**, kura S_NAr reakcijā ar nātrija azīdu tika iegūts 6-azidopurīna atvasinājums **44** (7. shēma). Sekojošā CuAAC reakcijā ar 2-(prop-2-īn-1-iloksi)etan-1-olu tika iegūts triazolilpurīns **45**. Savienojuma **45** tālāka modificēšana ar 4-brom-*N*,*N*-dimetilanilīnu, izmantojot vara katalizētas Ulmaņa (*Ulmann*) tipa reakcijas ar dažādām bāzēm (Cs_2CO_3, K_2CO_3) un ligandiem (3,4,7,8-tetrametil-1,10-fenantrolīns, 8-hidroksihinolīns), bija neveiksmīgas. Tā vietā tika izmantots būvbloks **36**, un CuAAC reakcijā tika iegūts produkts **46**, kura THP aizsarggrupa tika viegli noņemta AcOH/H_2O/THF maisījumā 50 °C temperatūrā 16 h. Turpmākie šī savienojuma funkcionalizēšanas mēģinājumi, izmantojot Micunobu reakciju vai *N*9 pozīcijas alkilēšanu, bija neveiksmīgi.

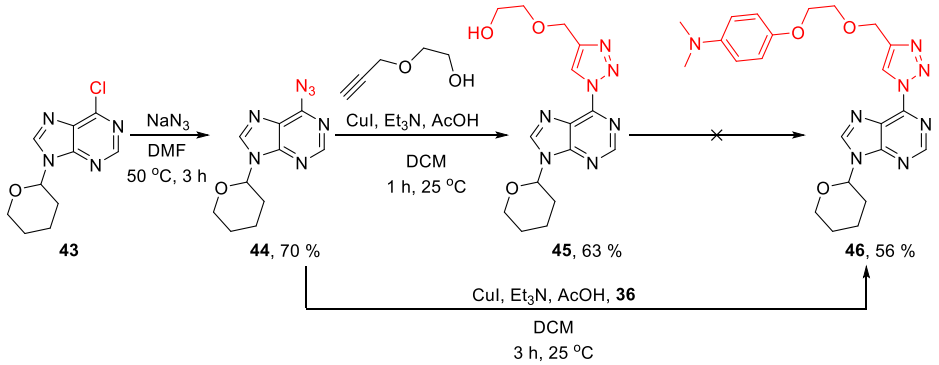

7. shēma. Pirmais savienojuma **33a** sintēzes ceļš, sākot ar purīna *C*6 pozīcijas modificēšanu.

Pēc tam tika nolemts mainīt modificēšanas secību un sākt ar purīna *N*9 pozīcijas funkcionalizēšanu. Vispirms Micunobu reakcijā starp 6-hlorpurīnu (**47**) un THP aizsargātu etilēnglikolu tika iegūts produkts **48**, kas tika izmantots azidēšanas un CuAAC reakcijās, rezultātā triazolilpurīns **50** tika iegūts ar 46 % iznākumu (8. shēma). Tālāk tika mēģināts ievadīt halogēna atomu purīna *C*8 pozīcijā, lai to varētu izmantot C-C šķērssametināšanas reakcijā. Reakcijā ar NBS sagaidāmās purīna bromēšanas vietā notika elektrofīla aizvietošānās fenilgredzenā, un tika iegūts savienojums **51**, savukārt litija diizopropilamīda (LDA) vai citu bāzu izmantošanas rezultātā tika novērota triazola deprotonēšana. Tika secināts, ka *C*8 pozīcijas funkcionizēšana jāveic agrākās stadijās.

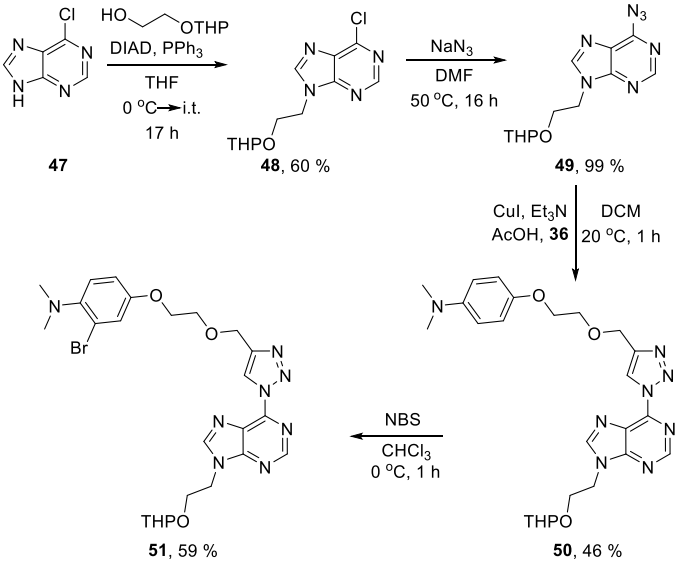

8. shēma. Otrais sintēzes ceļš, mēģinājumi secīgi modificēt purīna *C*6 un *C*8 pozīcijas.

Trešo sintēzes ceļš tika sākts ar iepriekš iegūtā savienojuma **48** jodēšanas reakciju, kam sekoja Stilles šķērssametināšanas reakcija ar *N*,*N*-dimetil-4-(tributilstannil)anilīnu (**39**), lai ievadītu nepieciešamo fragmentu purīna *C*8 pozīcijā, iegūstot savienojumu **53** (9. shēma). Šajā posmā tika nolemts, ka analogi mērķsavienojumam **33a** jāiegūst arī savienojums **33b**, kas pie triazola gredzena satur *n*-pentilgrupu, lai varētu pierādīt spēcīgas donoras grupas nozīmi aizvietotājā purīna *C*6 pozīcijā. Lai iegūtu savienojumus **33**, tika veikta savienojuma **52** azidēšana un secīga CuAAC reakcija ar dažādiem alkīniem. Pēc tam THP grupas nošķelšana ar tai sekojošu mezilēšanu tika realizēta ar augstu iznākumu. Iegūtie mezilāti **57a-b** bija inerti S_N2 reakcijā ar ciklēna atvasinājumu **42**, un tika nolemts aizvietot mezilāta grupu ar bromu un iegūto savienojumu izmantot alkilēšanas reakcijā ar būvbloku **42**. Reakcija noritēja pēc E2 mehānisma, un eliminēšanas produkti **58a-b** veidojās kā galvenie produkti. Pēc reakcijas apstākļu optimizēšanas tika noteikts, ka vislabākā konversija vēlamajiem produktiem **33a-b** tiek sasniegta tikai 20 % (**33a**) un 30 % (**33b**) līmenī, attiecīgi ar 6 % un 23 % iznākumiem izolētajiem produktiem.

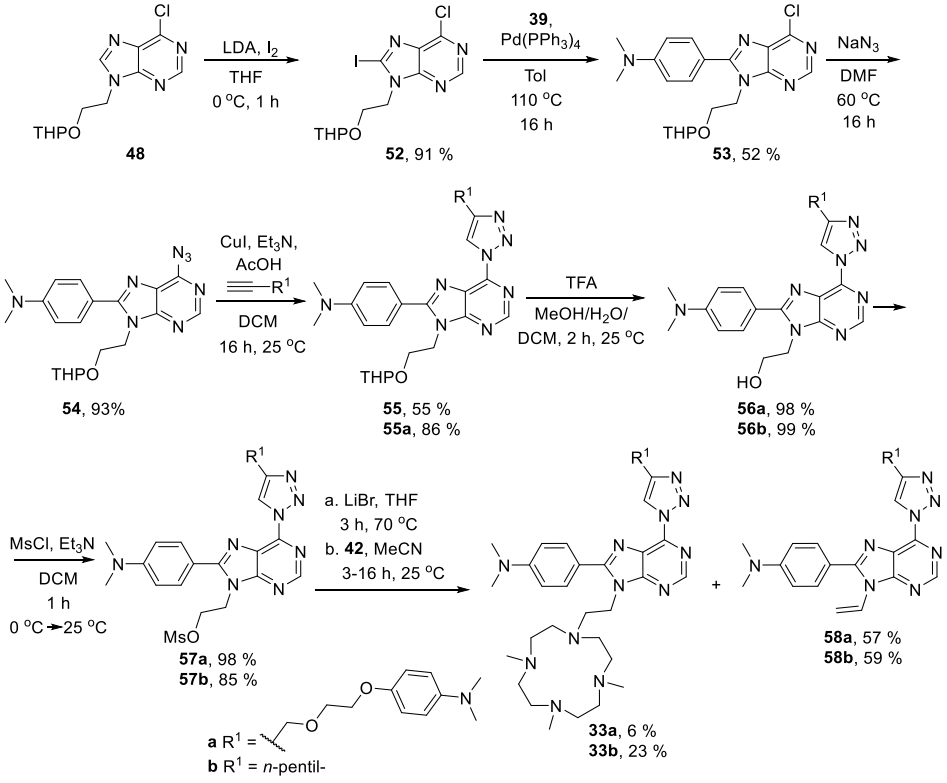

9. shēma. Trešais sintēzes ceļš ar purīna gredzena modificēšanas secību *C*8 → *C*6 → *N*9 pozīcijās.

Izmantojot ^{1}H-KMR titrēšanas metodi, produkts **33a** tika titrēts MeCN-d_3 šķīdumā, izmantojot $Cu(ClO_4)_2 \cdot 6H_2O$ kā Cu^{2+} avotu un benzolu kā iekšējo standartu. Analizējamā parauga ^{1}H-KMR spektrs tika reģistrēts pēc katras 0,1 ekvivalenta Cu^{2+} jonu pievienošanas reizes (12. att.).

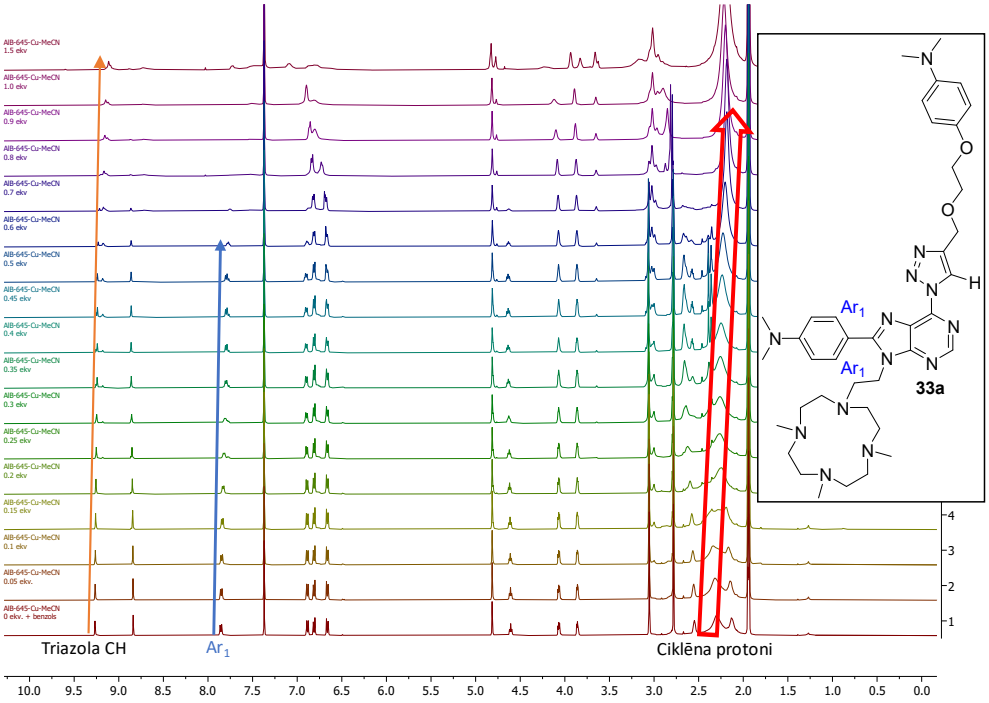

12. att. Spektru dati savienojuma **33a** ^{1}H-KMR titrēšanai ar Cu^{2+} joniem MeCN-d_3 šķīdumā.

Reģistrētie ^{1}H-KMR spektri parāda sarežģītu savienojuma **33a** kompleksēšanos ar Cu^{2+} joniem. Vissvarīgākā pazīme, kas atspoguļo Cu^{2+} saistīšanos ciklēnā, ir attēlota spektrā ar biezu bultiņu pie 2,0–2,5 ppm. Sākot no 0,7 ekvivalentiem metāla jonu, visi ciklēna ^{1}H-KMR signāli saplūst vienā signālā pie apmēram 2,2 ppm, kas nepārvietojas pie augstākām Cu^{2+} koncentrācijām. Šis fakts liecina, ka metāla jons tiek koordinēts ciklēna gredzena iekšpusē un visi četri cikla slāpekļa atomi ir koordinēti ar Cu^{2+} joniem. Vislielākās izmaiņas, izņemot ciklēna daļu, tika novērotas triazola protona un fenilgredzena aromātisko protonu *C*8 pozīcijā nobīdē. Pastāv liela iespēja, ka molekulai ir divas konkurējošas kompleksēšanas vietas – ciklēna fragmentā un starp triazolu un purīnu.

Oriģinālpublikācija par šajā nodaļā aprakstītajiem pētījumiem ir pievienota VII pielikumā.

2. Triazola gredzena atvēršana un enamīnu ciklizācija par indoliem

Iepriekš literatūrā tika aprakstītas triazola gredzena atvēršanas reakcijas ar sekojošu slāpekļa izdalīšanos. Ļoti augstā temperatūrā (400–800 °C) (10. a shēma) vakuumā pirolīzes apstākļos triazola gredzens atveras, veidojot karbēnu saturošu fragmentu **58**, kas tālāk pārgrupējas dažādos indola **59** vai hinolona **62** atvasinājumos.[105–107] Citos pētījumos ir aprakstīta rodija vai niķeļa katalizatoru izmantošana *N*-toziltriazola atvasinājumu cikla atvēršanai daudz maigākos apstākļos (70–140 °C), iegūstot metālkarbēnu **64**, kas tālāk reaģē ar alkīniem vai nitriliem, veidojot imidazola vai pirola atvasinājumus **65** (10. b shēma).[108, 109] Izmantojot *H*-fosfīna oksīdus niķeļa katalizatora klātbūtnē, *N*-toziltriazola cikls atveras, rezultātā rodas α-aminovinilfosforilatvasinājumi **66** (10. c shēma).[110] Ja viens no aizvietotājiem pie triazola C atomiem ir aminogrupa, ir iespējama Dimrota (*Dimroth*) pārgrupēšanās (10. d shēma). Šī termiskā gredzena transformācijas reakcija sākas tad, kad triazols **67** veido līdzsvaru ar savu vaļējo formu **68** un notiek dubultsaites nobīde starp diviem slāpekļa atomiem, kam seko gredzena saslēgšanās, veidojot triazolu **70**.[111]

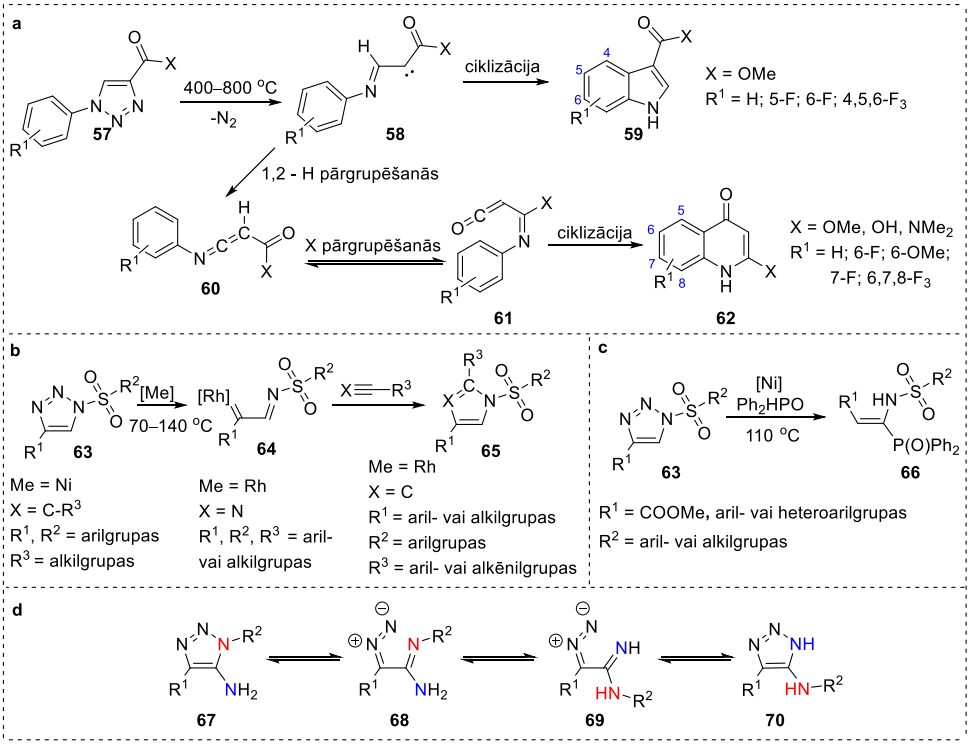

10. shēma. Literatūrā zināmās triazola gredzena atvēršanas reakcijas.[105–111]

Indols ir viens no nozīmīgākajiem un izplatītākajiem heterocikliem dabā. Tas bieži atrodams bioloģiski nozīmīgu dabasvielu sastāvā, piemēram, serotonīnā un vinblastīnā.[32] Pēdējā gadsimtā ir bijusi interese par dažādu indola atvasinājumu sintēzi,[112, 113] un joprojām ir nepieciešamība izstrādāt jaunas sintēzes metodes un ceļus, lai iegūtu vēlamos indola atvasinājumus, ko varētu izmantot kā farmaceitiskus līdzekļus.[33, 114]

1*H*-indolu sintēze no aromātiskajiem enamīniem ir plaši pētīta. Viens no pirmajiem pētījumiem par šo reakciju bija pallādija katalizēta intramolekulāra oksidatīvā šķērssametināšana, ko izstrādājusi Gloriusa (*Glorius*) grupa (11. a shēma).[115] Reakcijas norisei bija nepieciešams katalītisks daudzums pallādija un stehiometrisks vara acetāta daudzums, kas tika izmantots kā oksidētājs kopā ar K_2CO_3 DMF 80–140 °C temperatūrā. Vēlāk vairākas grupas ziņoja par reakcijas apstākļiem bez pallādija klātbūtnes. Lianga (*Liang*) grupa publicēja pētījumu, kurā šai ciklizācijas reakcijai joprojām bija nepieciešams stehiometrisks vara daudzums, bet pallādija katalizators tika aizstāts ar Fe(III) (11. b shēma).[116] Šī metode (11. a–b shēma) tika izmantota sintēzēm, ja indola *C*2 pozīcijā ir metilaizvietotājs, tāpēc vēlāk tika atrastas jaunas katalītiskas sistēmas *C*2 arilaizvietotu indolu sintēzei (11. c–d shēma).[117, 118] Šīm reakcijām bija nepieciešams vai nu stehiometrisks vara daudzums (11. d shēma)[118] un mezitilēns kā šķīdinātājs 170 °C temperatūrā, vai arī CuI un 1,10-fenantrolīna ligands kopā ar litija karbonātu pārākumā (11. c shēma).[117] Ju (*Yu*) grupa 2014. gadā ziņoja par jauniem reakcijas apstākļiem (DMF/DMSO 7 : 1 maisījums; 120 °C; 3 ekv. $CuCl_2$ un 3 ekv. K_3PO_4), kuru rezultātā veidojās indola atvasinājumi ar alkiltioaizvietotājiem *C*2 pozīcijā (11. e shēma).[119]

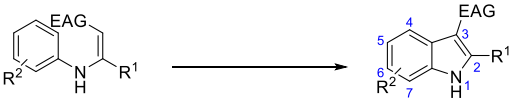

71 **72**

a) kat. Pd, ekv. Cu, bāze (Glorius, 2008)
R^1 = Me; R^2 = H, Me, Cl, F, CN, OMe, COMe, CO_2Et, $CONEt_2$; EAG = CO_2Me

b) kat. Fe(III), ekv. Cu(II), bāze (Liang, 2010)
R^1 = Me; R^2 = H, Me, Cl, Br, I, OMe, COMe; EAG = CO_2Me, CO_2Et

c) kat. Cu(I), ligands, bāze (Cacchi, 2009)
R^1 = arilgrupa; R^2 = H, Me, F, Cl, Br, I, OMe, COMe, CO_2Et; EAG = COAr

d) ekv. Cu(I) (Taylor, 2015)
R^1 = arilgrupa; R^2 = H, OMe; EAG = CO_2Et

e) ekv. Cu(II), bāze (Yu, 2014)
R^1 = SMe, SEt; R^2 = H, Me, Cl, F, OMe, OEt; EAG = COMe, COAr

f) ekv. I(III) (Zhao, 2009)
R^1 = alkil- vai arilgrupas, CO_2Et; R^2 = H, Me, OMe, Br, F; EAG = CN, NO_2, CO_2Me, COPh

g) kat. I_2, oksidētājs (Li, 2011)
R^1 = alkil- vai arilgrupas; R^2 = H, Me, OMe, Br, I, CF_3; EAG = CO_2Me, CO_2Et, CO_2Ph, CONHPh

h) kat. *n*-Bu_4NI, oksidētājs (Chan, 2013)
R^1 = arilgrupa; R^2 = H, Me, OMe, Br, Cl, I, NO_2, CF_3; EAG = COPh, CO_2Et, CONHPh

i) ekv. CBr_4, bāze (Li, 2021)
R^1 = alkil- vai arilgrupas; R^2 = H, OMe, F, Cl, alkilgrupa, Br, Ph; EAG = COMe, CO_2Et, COPh

11. shēma. Literatūrā publicētie pētījumi par 2,3-aizvietotu 1*H*-indolu sintēzēm no enamīniem.[115–122]

Žao (*Zhao*) grupa izstrādāja reakcijas apstākļus indola atvasinājumu sintēzei no enamīna bez metāla klātbūtnes, izmantojot ekvimolāru daudzumu hipervalenta joda reaģenta (11. f shēma).[120]

Reakciju rezultātā tika iegūti produkti ar 33–91 % iznākumu, reakcijas notika arī tad, ja savienojumi saturēja tādas EAG grupas kā -CN un -NO_2. Li (*Li*) grupa publicēja pētījumu, kurā indola sintēzei tika izmantoti elementārais jods kā katalizators un NBS kā oksidētājs. Ir pierādīts, ka šī reaģentu sistēma darbojas labāk, ja enamīnā kā aizvietotājs ir arilgrupa, nevis alkilgrupa (11. g shēma). Katalītisks *n*-tetrabutilamonija bromīda un stehiometrisks *terc*-butilhidroperoksīda daudzumi arī veicināja šādu indola ciklizāciju, taču tam bija nepieciešams daudz ilgāks reakcijas laiks – 24 stundas (11. h shēma).[121] Jaunākos pētījumus par šo tēmu ir publicējusi Li grupa, kam izdevās veikt indola ciklizāciju CBr_4 un bāzes klātbūtnē (11. i shēma), taču šajos apstākļos kā blakusreakcija iespējama aromātiskā gredzena bromēšana.[122]

Lai gan pētījumu apjoms par reakcijām, kurās izmanto aromātiskos enamīnus, lai iegūtu indolus, ir iespaidīgs, aizvietotāju daudzveidība indola *C*2 un *C*3 pozīcijās ir ierobežota, jo nav zināmi aizvietotāji, kas indola *C*2 pozīcijā savienoti caur C-N saiti. Heteroarilstruktūras, kas satur indola daļas, ir plaši sastopamas bioloģiski aktīvās molekulās un farmaceitiskajos līdzekļos, piemēram, *Eudistomin U, Topsentin* un *Wakayin*.[123, 124] Ierastā indolu heteroarilēšanas reakcija notiek caur C-H saites aktivāciju, un indola struktūrā ir brīvas sešas C-H pozīcijas.[124, 125] Indola *C*3 un *C*2 pozīcijas ir visreaģētspējīgākās, un, mainot reakcijas norises temperatūru un reaģentus, var kontrolēt C-H aktivācijas reģioselektivitāti. Lai funkcionalizētu indola cikla citas pozīcijas, izmantojot C-H aktivāciju, indola ciklā ir jāievada virzošās grupas. Iepriekšminētais motivēja izstrādāt jaunu sintētisku ceļu 1*H*-indolu, kas saturētu estera un heterocikliskus aizvietotājus *C*2 un *C*3 pozīcijās, sintēzei, kas ir aprakstīts šajā promocijas darbā.

Savienojums **73** ar divām elektronus atvelkošām grupām pie triazola cikla tika iegūts, izmantojot triazola cikla atvēršanas reakciju. Kā nukleofīls tika izvēlēts karbazols, jo tas tiek plaši izmantots fluorescentajos materiālos[126] un ir atrodams aktīvos dabas alkaloīdos.[127] Sajaucot triazolu **73**, *t*-BuOK un karbazolu DMF 100 °C temperatūrā (12. shēma), tika iegūts etēn-1,1-diamīna atvasinājums **74** ar 64 % iznākumu. Pēc tam tika meklēti reakcijas apstākļi iegūtā savienojuma **74** ciklizācijai, lai izveidotos indols. Izpētot literatūrā aprakstītās metodes (11. shēma), tika nolemts izmantot Pd un Cu metālu katalizētas reakcijas, tika izmēģināti apstākļi bez metāla klātbūtnes un noskaidrots, ka I_2/K_2CO_3 kombinācija nodrošina mērķa indola **75** veidošanos. Izmantojot secīgo pieeju produktu **73** → **74** → **75** pārvērtībām, produkts **75** tika iegūts ar kopējo iznākumu 26 %, savukārt viena reaktora sintēze deva savienojumu **75** ar nedaudz mazāku (19 %) iznākumu.

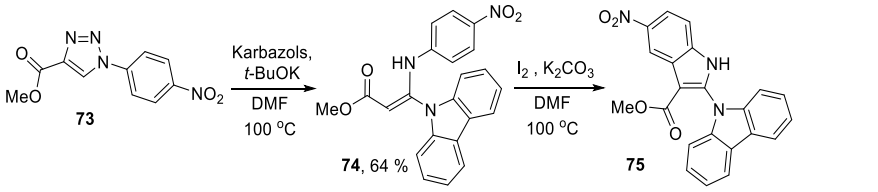

12. shēma. Triazola **73** cikla atvēršanas reakcija un ciklizācija par indolu.

Pēc tam tika mēģināts paplašināt aizvietotāju klāstu, lai noteiktu šīs sintēzes metodes darbības jomu un ierobežojumus, un tika sintezēti triazola atvasinājumi **76a-g**, kuriem tika pētītas cikla atvēršanas reakcijas (13. shēma). Savienojumu **76a-c** gadījumā tika noskaidrots, ka triazola gredzena atvēršanas produkti **77a-c** veidojās, taču tos neizdevās veiksmīgi izdalīt, jo tie ātri degradējās izdalīšanas un attīrīšanas gaitā. Lai šo problēmu novērstu, reakcijas maisījumam uzreiz pēc triazola gredzena atvēršanas produkta rašanās apstiprināšanas tika pievienots I_2 un K_2CO_3, bet tika novērota tikai produktu **78a-c** veidošanās.

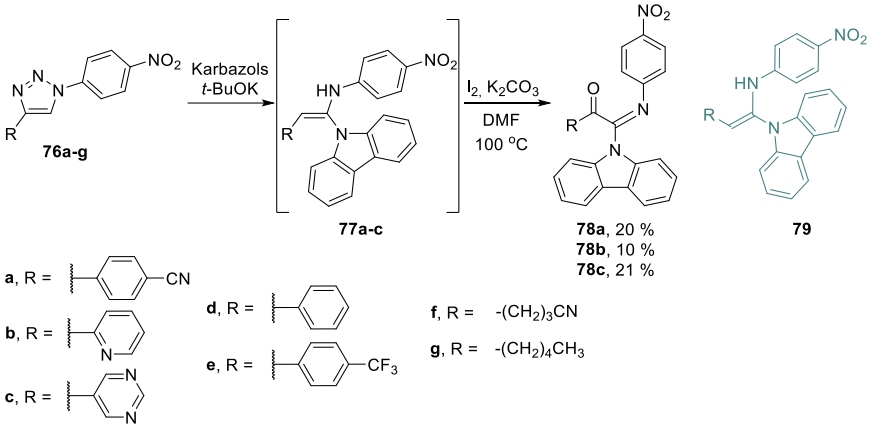

13. shēma. Triazola atvasinājumu **76** cikla atvēršanas reakcijas shēma.

Triazola atvasinājumu **76d**–**g** gadījumā reakcijas laikā ātri radās dažādu neidentificējamu produktu maisījums. Savienojuma **78b** struktūra tika pierādīta ar kristālu rentgenstruktūranalīzi (13. att.). Tika secināts, ka triazola cikla atvēršanas reakcija ar sekojošu ciklizāciju par indolu darbojas tikai ar izejvielām, kas satur spēcīgus elektronus atvelkošus aizvietotājus triazola gredzenā.

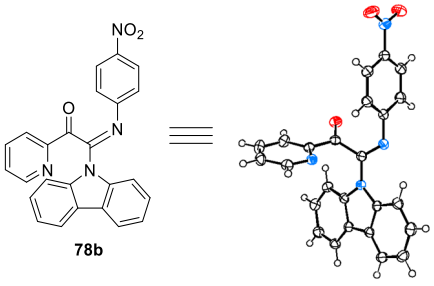

13. att. Savienojuma **78b** kristāla rentgenstruktūranalīze.

Tālāk tika izmantota uz triazolilpurīna atvasinājumiem **80** izstrādātā sintēzes sekvence, veidojot aromātiskos enamīnus **81**, kas pēc tam tika ciklizēti par 1*H*-indola atvasinājumiem **82** (7. tab.). Sintēzēm tika izmantota gan pakāpeniska, gan viena reaktora pieeja.

7. tabula

Triazola atvasinājumu **80** cikla atvēršanas reakcijas ar sekojošo ciklizāciju par indola atvasinājumiem

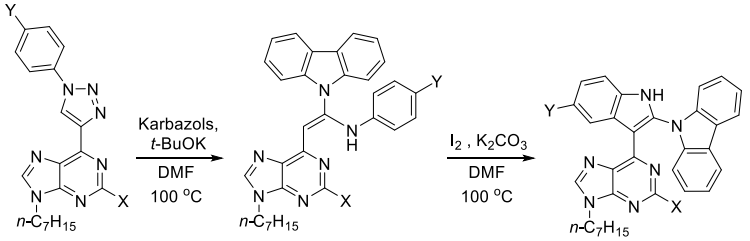

80 **81** **82**

Nr.	Izejviela	Aizvietotāji		Iznākums **81**, % **80→81**	Iznākums **82**, % **81→82**	Iznākums **82**, % **80→[81]→82**
		X	Y			
1.	**80a**	Cl	H	**81a**, 63	**82a**, 84	**82a**, 63
2.	**80b**	Cl	NO_2	**81b**, 84	**82b**, 60	**82b**, 48
3.	**80c**	Cl	OMe	**81c**, 69	**82c**, 75	**82c**, 48
4.	**80d**	Cl	CN	**81d**, 88	**82d**, 57	**82d**, 70
5.	**80e**	Cl	NMe_2	**81e**, 68[a]	–	–
6.	**80f**	H	H	–	–	**82f**, 35
7.	**80g**	H	NO_2	–	–	**82g**, 55
8.	**80h**		H	**81h**, 33	–	–

[a] Reakcija notika 25 °C.

Pētītajās reakcijās tika izmantoti triazolilpurīna atvasinājumi **80**, kas purīna *C*2 pozīcijā saturēja dažādus aizvietotājus. *N*,*N*-Dimetilaminogrupu saturošā atvasinājuma **80e** gadījumā triazola ciklu atvēršanās reakcija notika, tikai pazeminot temperatūru, bet ciklizācijas produkts nākamajā solī netika iegūts, iespējams, *N*,*N*-dimetilaminogrupas spēcīgā donorā efekta dēļ.

Visos triazola cikla atvēršanas reakcijas gadījumos savienojums **81** radās kā vienīgais produkts. Viena reaktora sintēzes gadījumā galaproduktu **82** iznākums bija vai nu ievērojami lielāks, vai tikai nedaudz zemāks, salīdzinot ar kopējo iznākumu pakāpeniskā pieejā, tāpēc savienojumus **80f-g** tika nolemts sintezēt, izmantojot viena reaktora sintēzes pieeju. Ja izmanto purīna atvasinājumu **80h** ar diviem triazola gredzeniem purīna *C*2 un *C*6 pozīcijās, šādos reakcijas apstākļos tiek atvērts tikai cikls *C*6 pozīcijā (7. tab., 8. rinda).

Lai pierādītu produkta **81** dubultsaites konfigurāciju, kā arī pārbaudītu purīna-indola konjugāta **82** struktūru un noskaidrotu, kurš triazola cikls atveras savienojuma **81h** gadījumā, savienojumiem **81b**, **81h** un **82b** tika veiktas kristālu rentgenstruktūranalīzes (14. att.).

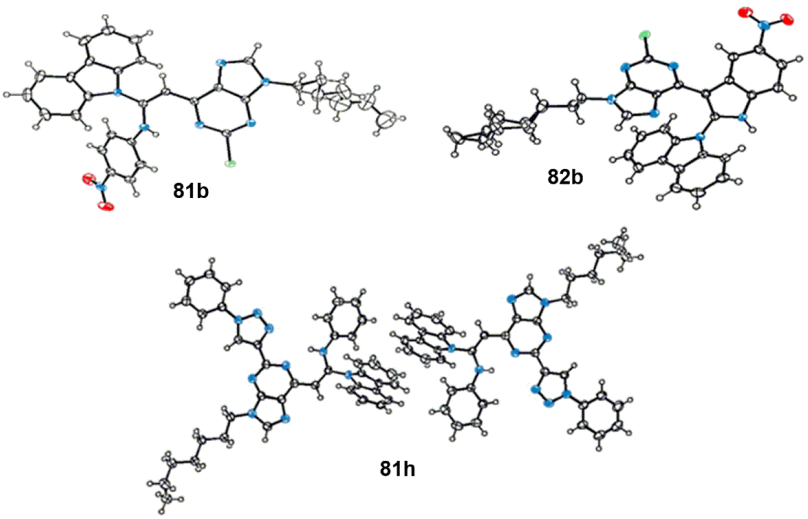

14. att. Savienojumu **81b**, **81h** un **82b** kristālu rentgenstruktūranalīzes attēli.

Tālāk tika izpētīts citu *N*-nukleofīlu lietojums izstrādātajā reakciju sekvencē. Triazolilpurīni **80a** un **80b** tika izmantoti reakcijā ar difenilamīnu kā nukleofīlu, kā produktus sagaidot etēn-1,1-diamīnus **83a-b** (14. shēma). Savukārt ciklizācijas reakcijās tika novērota *N*-fenilaizvietotu indolu **84** veidošanās – ciklizācija notika pie nukleofīla fenilgredzena, nevis ar anilīna fragmentu. Viena reaktora sintēzēs iznākums bija lielāks nekā kopējais iznākums, izmantojot pakāpenisko sintēzes pieeju.

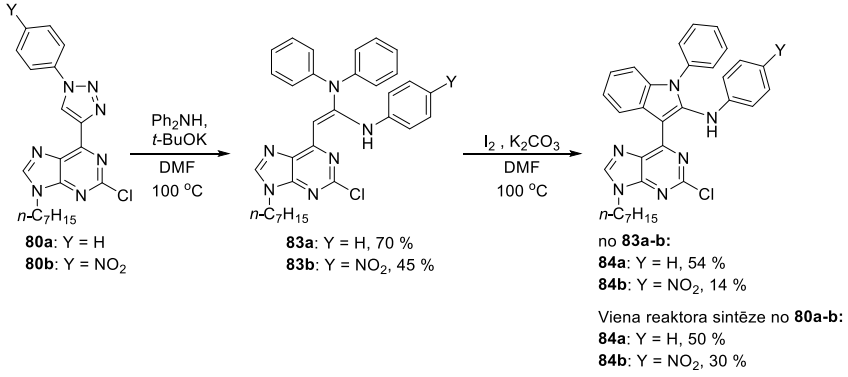

14. shēma. *N*-Fenilsaturošu indola atvasinājumu **84** sintēze no triazolilpurīna atvasinājumiem **80a-b**.

Produktu **84a-b** struktūra tika pierādīta ar savienojuma **84b** kristāla rentgenstruktūranalīzi (15. att.).

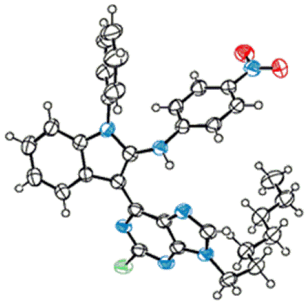

15. att. Savienojuma **84b** kristāla rentgenstruktūranalīzes attēls.

Triazola cikla atvēršanas laikā ir iespējama starpprodukta **A** veidošanās (10. a shēma), kam uzbrūk nukleofīls, veidojot produktus **B** (15. shēma). Ciklizācijas reakcijās ar karbazolu etēn-1,1-diamīna **C** dubultsaite ciklizējas ar arilgrupu pat tad, ja pie cikla ir ar elektroniem nabadzīgi aizvietotāji, piemēram, ciano- un nitrogrupas. Tas liecina, ka *N*-savienotājposma elastīgais raksturs šai reakcijai ir svarīgāks nekā elektroniskie efekti. Difenilamīnu saturošu savienojumu **D** gadījumā ciklizācija indolos **84** notiek selektīvi, pat ar savienojumu **84a**, kas satur trīs fenilgredzenus bez aizvietotājiem, kas liek domāt, ka ciklizācijā liela nozīme ir gan elektroniskajiem efektiem, gan fenilgredzena pieejamībai.

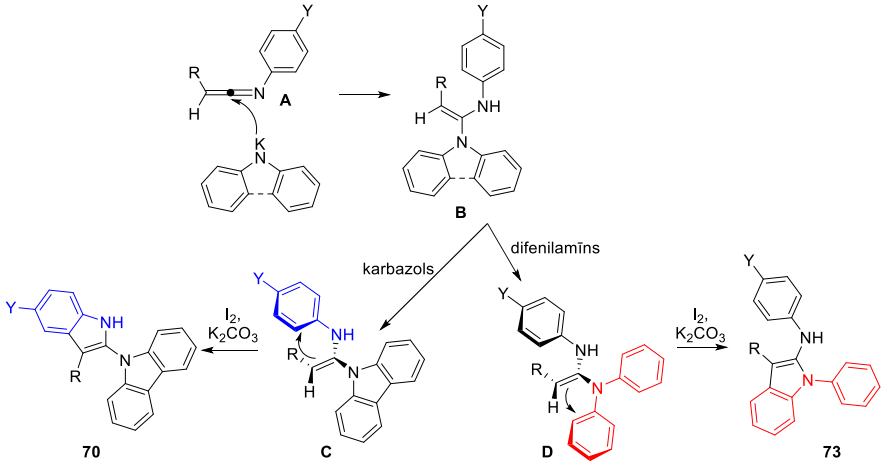

15. shēma. Triazola cikla atvēršana un ciklizācijas reakcijas reģioselektivitāte.

Oriģinālpublikācija par šajā nodaļā aprakstītajiem pētījumiem ir pievienota VIII pielikumā.

SECINĀJUMI

1. Jaunie 2-piperidinil-6-(1*H*-1,2,3-triazol-4-il)-9*H*-purīna atvasinājumi sasniedz kvantu iznākumus līdz 81 % DCM, 95 % DMSO un 35 % plānajās kārtiņās. Kvantu iznākumi C-C un C-N saistītiem triazolilpurīnu analogiem, kas satur 4-metoksifenilgrupu triazola fragmentā, ir attiecīgi 95 % un 98 %. 2,6-Bis-(1*H*-1,2,3-triazol-4-il)-9*H*-purīna atvasinājumi sasniedz kvantu iznākumus līdz 49 % DMSO, savukārt C-N saiti saturošā 2,6-bis-(1*H*-1,2,3-triazol-1-il)-9*H*-purīna atvasinājuma kvantu iznākums DMSO ir tikai 24 %, kas ir divreiz mazāks nekā tā C-C analogam.

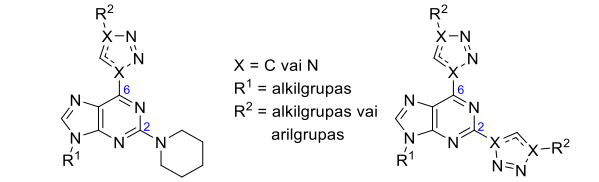

Φ līdz 81 % DCM un 98 % DMSO
Φ līdz 35 % plānajās kārtiņās

Φ līdz 26 % DCM un 49 % DMSO

2. Piridīnija fragmentu ievadīšana 2-amino-6-triazolilpurīna atvasinājuma *N*9 pozīcijā, salīdzinot ar 1,3-propāndiola grupas ievadīšanu, palielina savienojumu šķīdību ūdenī no 0,21 mg/mL līdz 133 mg/mL, bet pilnīgi dzēš tā fluorescenci.

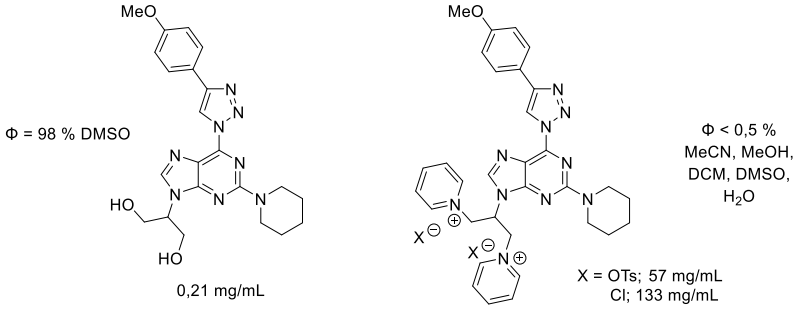

3. 6-Metoksifeniltriazolil-2-piperidinilpurīna atvasinājumi ar *n*-heptilgrupām vai TEG grupām purīna *N*9 pozīcijā koordinē Hg^{2+} jonus starp purīna *N*7 un triazola *N*3 atomiem, un kompleksēšanas rezultātā tiek dzēsta savienojuma fluorescence, tādējādi minētos savienojumus var potenciāli lietot kā Hg^{2+} metāla jonu sensorus šķīdumos vai šūnās.

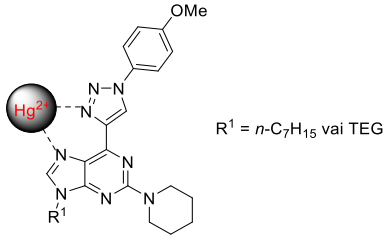

4. 6-Triazolil-8-arilpurīna atvasinājumu, kas satur 1,4,7,10-tetraazaciklododekāna (ciklēna) fragmentu purīna *N*9 pozīcijā, var iegūt deviņos soļos, izmantojot Micunobu, jodēšanas, Stilles, S_NAr, CuAAC un alkilēšanas reakcijas kā galvenās pārvērtības, secīgi modificējot *N*9→*C*8→*C*6→*N*9 pozīcijas purīna molekulā. Balstoties KMR titrēšanas rezultātos, tika noteikts, ka purīna-ciklēna konjugāts veido kompleksus ar Cu^{2+} metāla joniem ar iespējamajām kompleksēšanas vietām ciklēnā un starp triazola *N*2 un purīna *N*7 slāpekļa atomiem, dzēšot fluorescenci.

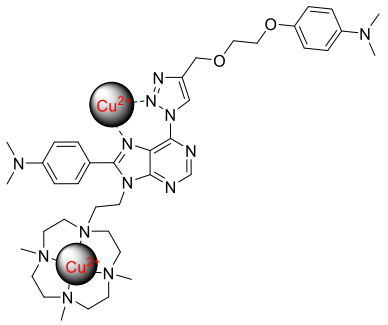

5. Triazola cikla atvēršanas reakcijās ar karbazola un difenilamīna nukleofīliem veidojas etēn-1,1-diamīni, kas atkarībā no aizvietotāja dabas pie etēna dubultsaites var tikt tālāk ciklizēti par 1*H*-brīviem vai 1-fenilaizvietotiem indola atvasinājumiem. Lai šī pārvērtība notiktu, pie triazola gredzena ir nepieciešamas spēcīgas elektronus atvelkošas grupas. Viena no šādām EAG grupām ir purīns, kas veicina purīna-indola konjugātu veidošanos.

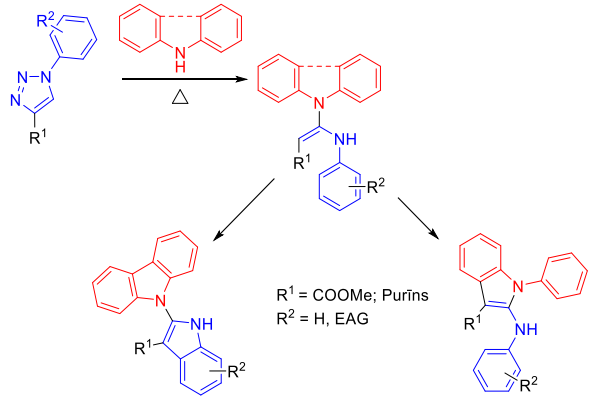

DOCTORAL THESIS PROPOSED TO RIGA TECHNICAL UNIVERSITY FOR PROMOTION TO THE SCIENTIFIC DEGREE OF DOCTOR OF SCIENCE

To be granted the scientific degree of Doctor of Science (Ph. D.), the present Doctoral Thesis has been submitted for defense at at the open meeting of RTU Promotion Council on June 17, 2025, at the Faculty of Natural Sciences and Technology of Riga Technical University, 3 Paula Valdena Street, Room 272.

OFFICIAL REVIEWERS

Senior Researcher Dr. Chem. Aiva Plotniece,
Latvian Institute of Organic Synthesis, Latvia

Dr. Chem. Māra Jure,
Corresponding Member of the Latvian Academy of Sciences

Docent Dr. Chem. Jeļena Kirilova,
Daugavpils University, Latvia

DECLARATION OF ACADEMIC INTEGRITY

I declare that the Doctoral Thesis submitted for review to Riga Technical University for promotion to the scientific degree of Doctor of Science (Ph. D.) is my own. I confirm that this Doctoral Thesis has not been submitted to any other university for promotion to a scientific degree.

Aleksejs Burcevs ……..….
(*signature*)

Date …...……...….

The Doctoral Thesis has been prepared as a collection of thematically related scientific publications complemented by summaries in both Latvian and English. The Thesis unites four publications in SCI journals, one review, two patents and unpublished results. The scientific publications have been written in English, with a total volume of 60 pages, not including supplementary data. The manuscript for publication has been written in English, with a total volume of 29 pages, not including supplementary data.

CONTENTS

Appendix I: Burcevs, A.; Novosjolova, I. Recent Progress in the Synthesis of *N*7(*N*9)-alkyl(aryl)purines (microreview). *Chem. Heterocycl. Compd*., **2022**, 58, 400–402.

Appendix II: Burcevs, A.; Sebris, A.; Traskovskis, K.; Chu, H.; Chang, H.; Jovaišaitė, J.; Juršėnas, S.; Turks, M.; Novosjolova, I. Synthesis of Fluorescent C–C Bonded Triazole-Purine Conjugates. *J. Fluoresc*., **2024**, 34, 1091–1097.

Appendix III: Burcevs, A.; Turks, M.; Novosjolova, I. Synthesis of Pyridinium Moiety Containing Triazolyl Purines. *Molbank*, **2024**, 2024, M1855.

Appendix IV: Jovaisaite, J.; Boguševičienė, K.; Jonusauskas, G.; Kreiza, G.; Burcevs, A.; Kapilinskis, Z.; Novosjolova, I.; Turks, M.; Hean, L. E.; Chu, H.-W.; Chang, H.-T.; Juršėnas, S. Purine-based chemical probe with HOMO

switching for Intracellular Detection of Mercury Ions. Manuscript submitted to *Scientific Reports* on 11.03.2025.

Appendix V: Novosjolova, I.; Burcevs, A.; Tulaite, K.; Kapilinskis, Z.; Jovasaite, J.; Jursenas, S.; Turks, M. A method of application of 2-amino-6-triazolyl purine derivatives as metal ion sensors. LVP2024000072, 29.11.2024.

Appendix VI: Kapilinskis, Z.; Burcevs, A.; Novosjolova, I.; Turks, M. Water soluble 2-amino-6-triazolyl purines and their synthesis approach. LV15925A, 20.03.2025.

Appendix VII: Burcevs, A.; Jonusauskas, G.; Turks, M.; Novosjolova, I. Synthesis of purine-1,4,7,10-tetraazacyclododecane conjugate and its complexation modes with copper(II). *Molecules*, **2025**, 30, 1612.

Appendix VIII: Burcevs, A.; Sebris, A.; Novosjolova, I.; Mishnev, A.; Turks, M. Synthesis of Indole Derivatives via Aryl Triazole Ring-Opening and Subsequent Cyclization. *Molecules*, **2025**, 30, 337.

ABBREVIATIONS

AcOH	acetic acid
Ar	aryl
Bn	benzyl
Bu	butyl
cat.	catalyst
CuAAC	copper-catalyzed azide-alkyne cycloaddition
Cy	cyclohexyl
CyHex	cyclohexane
DBU	diazabicycloundecene
DCM	dichloromethane
DEE	diethyl ether
DIAD	diisopropyl azodicarboxylate
DMAP	4-dimethylaminopyridine
DME	dimethoxyethane
DMF	*N*,*N*-dimethylformamide
DMSO	dimethyl sulfoxide
DNA	deoxyribonucleic acid
E2	bimolecular elimination reaction
EA	ethyl acetate
EDG	electron-donating group
eq.	equivalents
Et	ethyl
EWG	electron-withdrawing group
h	hour
HIV	human immunodeficiency virus
HOMO	highest occupied molecular orbital
LDA	lithium diisopropylamide
LUMO	lowest unoccupied molecular orbital
Me	methyl
MeCN	acetonitrile
MeCN-d_3	trideuteroacetonitrile
MeOH	methanol
Ms	mesyl-
MTBE	methyl-*tert*-butylether
NBS	*N*-bromosuccinimide
NMR	nuclear magnetic resonance spectroscopy
OLED	organic light-emitting diode
Ph	phenyl
ppm	parts per million
RNA	ribonucleic acid
S_N2	nucleophilic substitution reaction
S_NAr	nucleophilic aromatic substitution reaction
t-Bu	*tert*-butyl
TADF	thermally activated delayed fluorescence
TBHP	*tert*-butyl hydroperoxide
TBS	*tert*-butyldimethylsilyl
TEG	tetraethylene glycol
TFA	trifluoroacetic acid
THF	tetrahydrofuran
THP	tetrahydropiranyl
TMS	trimethylsilyl
Tol	toluene
Ts	tosyl
UV	ultraviolet radiation
UV-Vis	ultraviolet-visible spectroscopy
$\lambda_{abs\ max}$	absorption maxima wavelength
$\lambda_{em\ max}$	emission maxima wavelength
τ_{rad}	radiative fluorescence decay
τ_{nonrad}	non-radiative fluorescence decay

GENERAL OVERVIEW OF THE THESIS

Introduction

Purines, being one of the building blocks of DNA and RNA, are one of the most occurring heterocycles in nature, playing an important role in the transfer of genetic information.[1] Purine structures are also present in various metabolic processes, such as energy transfer and intracellular signaling, and thus, they are of great interest to biochemists.[2] Some classes of purine derivatives, for example, cytokinines and sinefungins, have been found and isolated from bacteria and proven to have growth-stimulating activity or antiviral and anticancer properties.[3] Overall, the purine ring provides a great molecular core for the synthesis of new compounds that possess biological activity and have potential use in pharmaceuticals. Most purine derivatives also possess luminescent properties, which can be used for cell imaging and studies of biological processes.

Many literature reports describe the use of fluorescent purine derivatives. They are used as organic light-emitting diodes (OLED),[4, 5] as thermally activated delayed fluorescence (TADF) emitters,[6] as pH sensors,[7] as metal ion detectors, and for cell imaging.[8–12] In recent years, more and more fluorescent purine derivatives have been synthesized, having new structural patterns that influence their photophysical properties. Nevertheless, there is still a necessity for synthesizing new compounds due to several limitations of existing structures – such as insufficient solubility in aqueous media, and low receptor selectivity or reactivity. Many simple purine derivatives, such as 6-methylpurine, 6-aminopurine, and 6-mercaptopurine, exhibit phosphorescence.[13–15] Purines can be derivatized at carbon and nitrogen atoms − *C*2, *C*6, *C*8, and *N*7, *N*9 positions, respectively.[16] There are many methods described in the literature with high selectivity for derivatization at selected positions, but usually, the most used reactions for functionalizing purine *C*2, *C*6, and *C*8 positions are nucleophilic aromatic substitution reactions (S_NAr)[17–19] and cross-coupling reactions.[20–25] For the *N*9 position, either direct alkylation, Mitsunobu, or Chan-Lam reactions are used.[19, 26] But it is challenging to achieve selective derivatization of the purine *N*7 position, often requiring construction of the purine ring via *de novo* synthesis[27] from corresponding imidazole or pyrimidine derivative.

Purine derivatives form metal complexes with certain metal ions (for example, Ca^{2+}, Fe^{2+}, Cu^{2+}, Pd^{2+}, and Zn^{2+}), and their photophysical properties change with the formation of those complexes.[28, 29] This usually results in the emission wavelength shift and quenching of the fluorescence, although the situation when the compound increases its fluorescent properties upon complexation is also present.[9] Dissolution of such compounds and observation of the fluorescence change are the principles behind metal ion analysis in solutions by ultraviolet-visible (UV-Vis) spectroscopy. Formation of the compound-metal complexes can also be observed by using the ^{1}H-NMR titration approach.

Triazolyl purines are notable structures of fluorescent purine derivatives that belong to the push-pull chromophore category.[17] Such compounds possess good photophysical properties, reaching quantum yields up to 91 %,[30, 31] and potentially can have various applications in cell imaging, optoelectronics, or as sensors.

Another heterocycle, alongside purine, that is also abundant in nature and has a wide array of biological activities is indole. Indole derivatives, for example, serotonin, play an important role in human biology, acting as a neurotransmitter, while mitomycin C is known for its anticancer properties.[32] Report on indole derivatives being a new promising antiviral medicine was made against such viruses as Hepatitis C, HIV and influenza.[33] Since the first report of indole synthesis in 1883 by Fischer, new synthetic procedures have been developed over the years. In recent decades, the number of literature references on the synthesis of indoles has increased, which proves the importance of the development of novel synthetic procedures towards a wide range of new indole derivatives.[32] Indole ring is also fluorescent and has potential applications in medicinal chemistry as a probe for pH imaging[34] and the detection of fluoride ions[35] in cells.

Recently, chemists synthesized purine-indole conjugates to test their combined properties. One of the advantages of these purine-indole conjugates is their excitation wavelength (321 nm), which is well separated from the usual absorption of DNA (253 nm).[36] Some purine-indole conjugates are used as fluorescent probes for such processes in cells as a protein-mediated duplex to G-quadruplex exchange,[37] Hoogsteen base pairing,[36] and *Nar*I recognition sequence.[38] It was also reported that some of them potentially have antitumor[39] properties and are able to regulate lipid metabolism.[40]

In this Doctoral Thesis, various fluorescent triazolyl purine derivatives were obtained, and their use as potential metal ion sensors was studied alongside their photophysical properties (Fig. 1 a). The new synthetic pathway towards purine-indole conjugates was developed in two steps from C-C bonded triazole purine derivatives (Fig. 1 b).

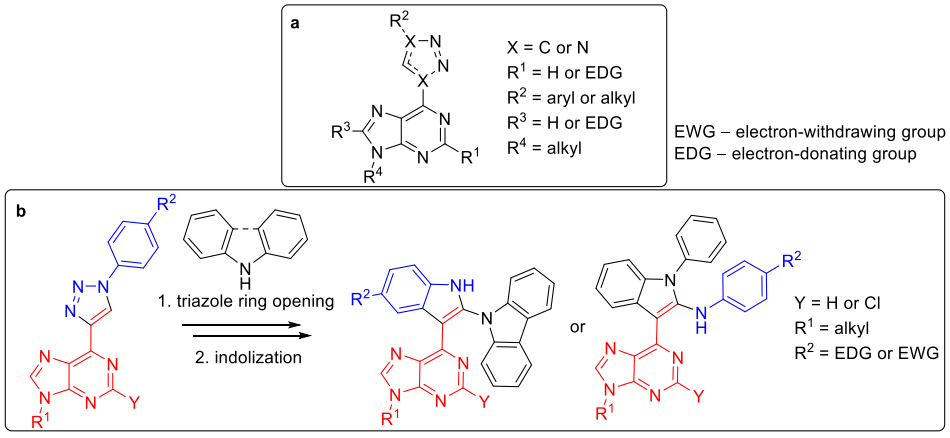

Fig. 1. a – Overall structure of synthesized triazolyl purine derivatives; b – the synthetic route towards purine-indole conjugates from triazolyl purines. EDG (-OMe, -NMe_2); EWG (-CN, -NO_2).

Aims and objectives

The aim of the Thesis is the synthesis of new functionalized purine derivatives and the determination of the potential uses for the obtained fluorescent compounds.

To achieve the goal, the following tasks were set:

- Synthesis of novel 2-piperidinyl-6-triazolyl and 2,6-bis-triazolyl purine derivatives with various substituents at triazole ring and purine *N*9 position, and the examination of their photophysical properties.
- Synthesis of water-soluble triazolyl purine derivatives and the examination of their photophysical properties.
- Evaluation of triazolyl purine derivatives as potential metal ion sensors using ^{1}H-NMR titration experiments with Zn^{2+}, Fe^{2+}, Mn^{2+}, Ca^{2+}, Cu^{2+}, and Hg^{2+} metal ions.
- Development of a synthetic pathway towards 1,4,7,10-tetraazacyclododecane moiety containing triazolyl purine derivative and determination of its potential use.
- Development of a new synthetic pathway towards purine-indole conjugates starting from triazolyl purines and determination of the scope and limitations of the developed method.

Scientific novelty and main results

During the course of the Doctoral Thesis, new 2-piperidinyl-6-triazolyl and 2,6-bis-triazolyl purine derivatives were synthesized, and their photophysical properties were measured. Selected 2-piperidinyl-6-triazolylpurine derivatives were tested for metal ion complexation in organic solvents and water solutions. Quenching of the fluorescence was observed during complexation experiments, indicating that these compounds are suitable for use as metal ion sensors, especially demonstrating a great selectivity towards the complexation of Hg^{2+} ions. Novel water-soluble 1,4,7,10-tetraazacyclododecane containing triazolyl purine derivative, with the potential to be used as a photo-catalyst, was obtained and tested for complexation ability with Cu^{2+} ions. A new metal-free two-step synthetic pathway towards purine-indole conjugates from triazolyl purines was developed.

Structure and volume of the Thesis

The Doctoral Thesis has been prepared as a collection of thematically related scientific publications dedicated to the synthesis and derivatization of triazolyl purines, measuring the fluorescence properties of selected compounds, and studying their applications. The Thesis consists of four publications in SCI journals, one review, two patents and unpublished results.

Publications and approbation of the Thesis

Results of the Thesis have been reported in four scientific publications. One review has been published. Two patents have been submitted. The main results have been presented at eight conferences.

Scientific publications

1. **Burcevs, A.**; Jonusauskas, G.; Turks, M.; Novosjolova, I. Synthesis of purine-1,4,7,10-tetraazacyclododecane conjugate and its complexation modes with copper(II). *Molecules*, **2025**, 30, 1612. https://doi.org/10.3390/molecules30071612
2. Jovaisaite, J.; Boguševičienė, K.; Jonusauskas, G.; Kreiza, G.; **Burcevs, A.**; Kapilinskis, Z.; Novosjolova, I.; Turks, M.; Hean, L. E.; Chu, H.-W.; Chang, H.-T.; Juršėnas, S. Purine-based chemical probe with HOMO switching for Intracellular Detection of Mercury Ions. Manuscript submitted to *Scientific Reports* on 11.03.2025.
3. **Burcevs, A.**; Sebris, A.; Novosjolova, I.; Mishnev, A.; Turks, M. Synthesis of Indole Derivatives via Aryl Triazole Ring-Opening and Subsequent Cyclization. *Molecules*, **2025**, *30*, 337. https://doi.org/10.3390/molecules30020337
4. **Burcevs, A.**; Sebris, A.; Traskovskis, K.; Chu, H.; Chang, H.; Jovaišaitė, J.; Juršėnas, S.; Turks, M.; Novosjolova, I. Synthesis of Fluorescent C–C Bonded Triazole-Purine Conjugates. *J. Fluoresc.*, **2024**, 34, 1091–1097. https://doi.org/10.1007/s10895-023-03337-6
5. **Burcevs, A.**; Turks, M.; Novosjolova, I. Synthesis of Pyridinium Moiety Containing Triazolyl Purines. *Molbank*, **2024**, *2024*, M1855. https://doi.org/10.3390/M1855
6. **Burcevs, A.**; Novosjolova, I. Recent Progress in the Synthesis of *N*7(*N*9)-alkyl(aryl)purines (microreview). *Chem. Heterocycl. Compd*., **2022**, 58, 400–402. https://doi.org/10.1007/s10593-022-03105-7

Submitted patents

1. Novosjolova, I.; **Burcevs, A.**; Tulaite, K.; Kapilinskis, Z.; Jovasaite, J.; Jursenas, S.; Turks, M. A method of application of 2-amino-6-triazolyl purine derivatives as metal ion sensors. LVP2024000072, 29.11.2024.
2. Kapilinskis, Z.; **Burcevs, A.**; Novosjolova, I.; Turks, M. Water soluble 2-amino-6-triazolyl purines and their synthesis approach. LV15925A, 20.03.2025.

Results have been presented at the following conferences

1. **Burcevs, A.**; Novosjolova, I. Synthesis of 1*H*-Indole Derivatives through Aryl Triazole Ring Opening and Subsequent Cyclization. In: *Balticum Organicum Syntheticum 2024: Abstract Book*, Latvia, Riga, 7–10 July 2024. Riga: 2024, p. 40.

2. Novosjolova, I.; **Burcevs, A.**; Jonusauskas, G.; Tulaitė, K.; Jovasaite, J.; Juršėnas, S.; Turks, M. Study of Triazolyl Purine Derivatives as Sensors for Metal Ions. In: *Balticum Organicum Syntheticum 2024: Abstract Book*, Latvia, Riga, 7–10 July 2024. Riga: 2024, p. 111.
3. **Burcevs, A.**; Novosjolova, I. Synthesis of a Cyclen Containing Purine Derivative as a Potential Photo-Catalyst. In: *13th Paul Walden Symposium on Organic Chemistry: Program and Abstract Book*, Latvia, Riga, 14–15 September 2023. Riga: 2023, p. 40.
4. **Burcevs, A.**; Jonusauskas, G.; Tulaitė, K.; Jovasaite, J.; Juršėnas, S.; Novosjolova, I.; Turks, M. Synthetic Pathways Toward Designed Purine Derivative for the Photo-Catalysis. In: *International Symposium on Synthesis and Catalysis 2023: Abstract Book*, Portugal, Evora, 5–9 September 2023. Evora: 2023, p. 210.
5. **Burcevs, A.**; Novosjolova, I. Synthetic Pathways towards Purine Derivative as a Potential Molecular System for the Photo-Catalysis. In: *81st International Scientific Conference of the University of Latvia 2023. Chemistry Section and Section of Institute of Chemical Physics: Book of Abstracts.*, Latvia, Riga, March 17, 2023. Riga: University of Latvia Press, 2023, p. 47.
6. **Burcevs, A.**; Sebris, A.; Novosjolova, I.; Turks, M. Synthetic Approaches toward C-C Bonded Triazolylpurines for Use in Materials Science. In: *Balticum Organicum Syntheticum 2022: Program and Abstract Book*, Lithuania, Vilnius, 3–6 July 2022. Online: 2022, p. 58.
7. **Burcevs, A.**; Sebris, A. Synthesis and Photophysical Properties of C-C Bonded Triazole-Purine Conjugates. In: *12th Paul Walden Symposium on Organic Chemistry: Program and Abstract Book*, Latvia, Riga, 28–29 October 2021. Riga: RTU Press, 2021, p. 27.
8. **Burcevs, A.**; Sebris, A.; Novosjolova, I. Synthesis of C-C linked Triazolylpurines. In: *Riga Technical University 62nd International Scientific Conference "Materials Science and Applied Chemistry 2021": Program and Abstracts*, Latvia, Riga, October 22, 2021. Riga: Riga Technical University, 2021, p. 16.

MAIN RESULTS OF THE THESIS

Purine is one of the most occurring nitrogen-containing heterocycles in nature, widely found in various natural products and medicinal compounds.[3] In medicinal chemistry, substances isolated from natural products often act as a framework for new pharmacologically active compounds, and because of that, there is a constant interest in the synthesis and derivatization of purine-based derivatives. Overall, there are two synthetic strategies for the synthesis of new purine derivatives – either by replacing previous reactive functionalities on a purine ring or by cyclization of a functionalized pyrimidine or imidazole precursors.[41]

In the Thesis, the synthesis of novel purine derivatives is described alongside their photophysical properties and their metal ion complexation abilities. A new synthetic approach for the synthesis of purine-indole conjugates in two steps from triazolyl purines is described.

1. Derivatization of the purine ring

Since a variety of purine derivatives is being synthesized due to the increased interest in their potential use in medicinal chemistry, the reactivity of different positions at the purine ring has been intensively studied. The most readily and commercially available starting materials for this purpose are 2,6-dichloropurine[42] and 2,6,8-trichloropurine,[43] which are usually obtained in one step from uric acid and xanthine, respectively. For halopurines, the most commonly used reactions for their derivatization at *C*2, *C*6, and *C*8 positions are cross-coupling and S_NAr reactions.

Cross-coupling reactions at 2,6- and 6,8-dihalopurine derivatives are both chemo- and regioselective.[16] If both halogens at purine *C*2 and *C*6 or *C*6 and *C*8 positions are chlorines, a reaction with one equivalent of organometallic reagent occurs regioselectively at purine *C*6 position (Scheme 1 a–b).[44] Introduction of iodine at less reactive *C*2 and *C*8 positions in such compounds leads to the reaction occurring at that position, leaving the *C*6 position untouched – respectively, the reaction is happening chemoselectively (Scheme 1 c–d).

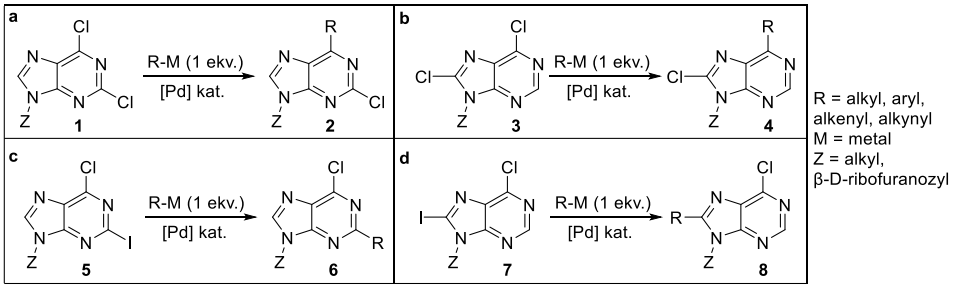

Scheme 1. General regioselectivity of 2,6- and 6,8-dihalopurines.

General regioselectivity depicted in Scheme 1 works well with Stille,[20, 22] Negishi[20–22] and Suzuki-Miyaura[23–25] reaction conditions. The formation of disubstituted products is mostly

observed in Stille reactions.[20] A possible explanation could be that the Stille reaction, in general, requires higher temperatures than others, thus making the reaction non-selective. By using Negishi and Stille reactions, aryl, alkyl, and alkenyl substituents could be introduced to the halogenated purine, while Suzuki-Miyaura cross-coupling is mostly used for the introduction of aryl substituents.

In the case of 2,6,8-trichloropurine derivatives, cross-coupling reactions in most cases occur sequentially, the order of reactivity being *C*6 > *C*8 > *C*2 positions.[45] There is a report in the literature on exceptions not following this reactivity pattern in selected 2,6,8-trichloropurine derivatives, where substitution occurs at the *C*8 position first, followed by the usually more reactive *C*6 position.[46] The example includes glycoside at the purine *N*9 position, which probably directs the reaction to happen at the *C*8 position.

Halogen atoms on the purine ring can also be used as leaving groups in S_NAr reactions to introduce various nucleophiles, such as *N*-,[17] *O*-,[47] *S*-,[18] *P*-,[48] and *Se*-nucleophiles.[49] For S_NAr reactions, while the order of reactivity on the purine ring remains the same, the reactivity of halogens is reversed in comparison to cross-coupling reactions, and fluorine being the most reactive halogen (F > Cl > Br > I).[50] Although it is known that the *C*6 position is more reactive, there have been extensive studies on leaving groups reactivities in S_NAr reactions for that position (Table 1).[51]

Table 1

Orders of leaving groups reactivities in 6-substituted purine derivatives

Entry	Nucleophile	Additive	Reactivity
1	$BuNH_2$	---	F > RSO_2 > Br > Cl > I
2	MeOH	DBU	RSO_2 > F > Br = Cl > I
3	*i*-PentylSH	DBU	RSO_2 > F > Br = I > CI
4	$PhNH_2$	TFA	F > RSO_2 > I > Br > Cl
5	$PhNH_2$	---	I > Br > RSO_2 > Cl > F

The reactivity of the purine *C*6 position depends on the leaving group, nucleophile, and the additive. Among all halogens, fluorine is the best choice for S_NAr reactions with butylamine and aniline in the presence of an acid catalyst, as well as with *O*- and *S*-nucleophiles (Table 1, entries 1–4). Only in the case of aniline without any additive, 6-fluoropurine takes the most time to react – 6 hours, as opposed to the 50-minute reaction time of 6-iodopurine derivative (Table 1, entry 5). 6-Alkylsulfonyl substituted purines surpass fluorine as a leaving group in reactions with *O*- and *S* nucleophiles, but the exact speed of the reaction was not determined (Table 1, entries 2–3). While halogens are the most commonly used for the S_NAr reactions, there are known examples of azides, sulfonyl groups, and 1,2,3-triazoles being used as leaving groups.[18, 48, 52, 53]

Other positions that can be derivatized in purines are either the *N*7 or *N*9 atoms. While in most cases, the *N*9 position is more reactive, in some cases, the formation of *N*7 products is also observed due to the purine ring *N*7/*N*9 position tautomerism. The most common procedures for the

functionalization of the *N*9 position are alkylation with alkyl halides and Mitsunobu reaction, but in these transformations, a small amount of undesired *N*7 alkylation product is still forming.[19] Selective glycosylation of purine *N*9 position is a well-studied topic that requires the previous introduction of an electron-poor directing group at *C*6 position, such as imidazole,[54] tetramethylsuccinimide,[55] or *O*-diphenylcarbamoyl groups.[56] The use of $SnCl_4$ as a catalyst also provides *N*9 glycosylated purines without any directing groups at the purine *C*6 position.[57]

In recent years, many novel synthetic procedures have been reported for the selective alkylation of the *N*9 position. In the reaction between adenine or 6-chloropurine with primary alcohols, using a mixture of P_2O_5, KI in the presence of Et_3N and K_2CO_3, *N*9 alkylated products are formed with yields up to 82 %.[58] In the presence of Umemoto's reagent and UV light, cyclic ethers and methyl-*tert*-butylether (MTBE) are used to selectively derivatize purine at the *N*9 position.[59] *N*9-substituted purines are obtained by using *N*,*N*-dialkyl amides, KI, and *tert*-butylhydroperoxide (TBHP) for the alkylation.[60] On the other hand, selective *N*7 alkylation is more challenging to achieve. For this purpose, specific substrates like glycosyl donors in the presence of bis(trimethylsilyl)acetamide with tin or titanium tetrachlorides[61] or very electron-poor cyclopropanes are exploited.[62]

Aryl-substituted *N*9 purines are usually obtained in Chan-Lam reactions[26] and in cross-couplings with aryl halides,[63] while *N*7-arylated purines are achieved in *de novo* synthesis of purine ring using substituted pyrimidines or imidazoles as starting materials.

The most recent information on selective *N*7/*N*9 purine alkylation/arylation is summarized in the review found in Appendix I.

1.1. Fluorescent properties of purines and their ability to form metal complexes

One of the first reports on purine derivative metal complexes was published in 1959, where six 6-substituted purine derivatives were tested for their complexation ability with Ni^{2+}, Co^{2+}, Cu^{2+}, Pb^{2+}, and Zn^{2+} ions.[64] It involved potentiometric measurements of pH values of water-dioxane solution of purine in or without the presence of metal ions after each addition of standard NaOH solution. By monitoring the changing pKa values of the solution, as the solution pH went higher, dissociation constants were determined, indicating the formation of purine-metal complexes. The study elucidated that purine has different complexation abilities with metal ions, depending on the substituents at the purine *C*6 position and the nature of the used metal ions. Later, in 1971, complexation patterns of 6-amino-, 6-chloro-, 6-hydroxy- and 6-mercaptopurines were tested with Mn^{2+}, Ca^{2+}, Mg^{2+}, Zn^{2+}, Ni^{2+}, Co^{2+}, and Cu^{2+} ions in water, and their stability constants were measured.[65] Stability of formed metal complexes with 6-substituted purine derivatives followed the order of $Cu^{2+} > Ni^{2+} > Zn^{2+} > Co^{2+} > Mn^{2+} > Mg^{2+} > Ca^{2+}$. The authors proposed that 1:1 purine-metal complexes were formed and the metal was coordinated between the substituent at purine *C*6 and nitrogen at *N*7 (Fig. 2).

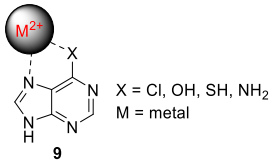

Fig. 2. Metal ion complexation site between the substituent at *C*6 position and the purine *N*7 position.

Nowadays, one of the widely used anti-cancer drugs is *cis*-diamminedichloroplatinum(II) or cisplatin.[66, 67] This metal complex primarily binds with the *N*7 positions of guanine bases, which activates several signal transduction pathways and leads to apoptosis or programmed cell death. While it is one of the widely available anti-cancer treatment options, its drawbacks include toxicological damage to the organism in the form of hepatotoxicity (liver), cardiotoxicity (heart), nephrotoxicity (kidney), gastrotoxicity (stomach) and ototoxicity (hearing loss).[66, 67]

The complexation ability of organic molecules with metals can be observed and determined with ^{1}H-NMR spectroscopy, one of the most useful techniques for the observation of dynamic molecular processes.[68] By using a methodology called ^{1}H-NMR titration, a metal ion complex solution with known concentration is gradually added to the solution of the analyzed compound while monitoring the change of the compound's chemical shifts.[69] By defining which signals in the analyzed compound shifted, it is possible to pinpoint the closest complexation sites in the molecule. Analysis of chemical shifts or observation of their disappearance gives information on the complexation pattern. ^{1}H-NMR titration is used to determine metal complex binding constants, reaction equilibrium constants, and pK_a values of compounds, although some difficulties with the precision of the results at low (0–2) and high (12–14) pH values are present – in these pH ranges calculated values slightly differ from the results gained using potentiometry and thereof their precision is doubtful.[70, 71]

Measurements of fluorescence are also used in the studies of purine-metal complex formation due to the change in the fluorescence intensities when the complexation occurs. Usually, the formation of purine-metal complexes lowers the emission intensities or completely quenches the fluorescence. Since naturally occurring purine nucleosides possess weak fluorescent properties,[72] while being one of the most widespread biologically active compounds, it is required to make extra modifications in the molecular structure of purine to enhance their photophysical properties. Usually, acceptor (-CN, -CO_2Me, -CONHR (R = alkyl)) and donor (-NH_2, -NHMe, -NMe_2, -OBn) substituents are introduced in the structure, making purine a push-pull chromophore,[73] increasing its quantum yield and enabling monitoring of the intracellular processes by using fluorescence-based observation methods. Fluorescent purine-based ion sensors for Hg^{2+} and Pd^{2+} in aqueous media[29, 74] and for Cu^{2+} in cells,[8, 75] were developed, with their fluorescent properties quenched upon complexation (Fig. 3 **I**–**III**). A case of a purine-based metal ion sensor, which increases its fluorescence upon the addition of Al^{3+} ions, was also reported (Fig. 3 **IV**).[9]

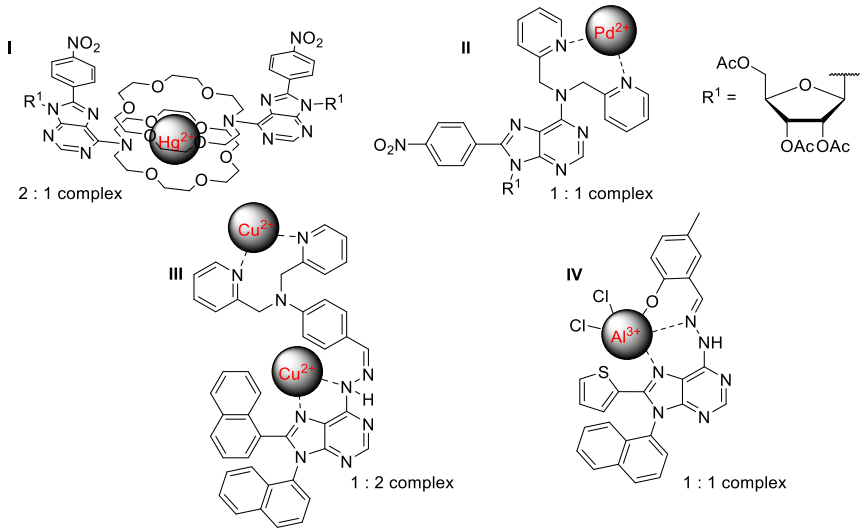

Fig 3. Examples of purine-based metal ion sensors **I**–**IV**.

In the mentioned studies, fluorescence change was analyzed using titration experiments by UV-Vis spectroscopy, a method of continuously measuring the absorption or emission intensities of a compound upon the addition of metal ions. The countless number of push-pull chromophores can be synthesized using a purine base. One of the possible moieties that can be introduced to the purine is 1,2,3-triazole, which functions not only as a good electron-withdrawing group but also adds a stable complexation site (Fig. 4) for the metal ion. 1,2,3-Triazoles have been reported to be parts of the complexation systems with pyridine, isoquinoline, and ferrocene[76, 77] alongside other *O*-, *S*-, and *N*-atoms in the molecule. Such systems make metal ion complexes with Pd^{2+}, Cu^{2+}, Ni^{2+}, Ru^{2+}, Au^{+}, and Ag^{+}, with some of them possessing antimicrobial, anticancer, and antifungal properties.[76–78] None of those systems with triazoles included purine in it, and since our group previously reported the use of 2,6-bis-triazole purine derivatives as potential ratiometric sensors,[28] this encouraged us to synthesize novel triazolyl purine derivatives during the development of this Doctoral Thesis.

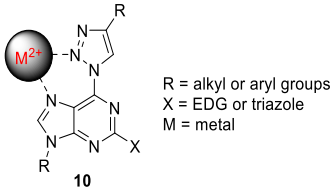

Fig. 4. Metal ion complexation site between 1,2,3-triazole and the purine *N*7 position.

1.2. Synthesis of triazolyl purine derivatives

1,2,3-Triazole moiety is found in some medicines and used as a pharmacophore, for example, in antiviral and anticancer drugs, such as cefatrizine, rufinamide, and mubtritinib.[79–81] The structure of 1,2,3-triazole has a tendency to form hydrogen bonds, as well as to provide π-π stacking and dipole-dipole interactions, and is not prone to metabolic degradation.[82] It is able to mimic the features of other different functional groups, and it is used as an amide bond, ester bond, and carboxylic acid bioisoster.[83]

1,2,3-Triazoles are usually synthesized through [3+2] Huisgen, copper-catalyzed, or ruthenium-catalyzed azide-alkyne cycloadditions.[80, 84] Depending on the starting materials, two sets of compounds were obtained, C-N and C-C bonded triazolyl-purine conjugates **A** and **B** (Fig. 5).

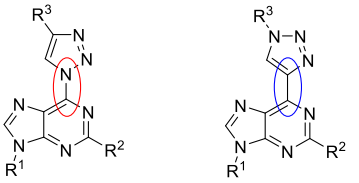

Fig. 5. General structures of C-N (**A**) or C-C (**B**) bonded triazole-purine conjugates.

Previously, our group studied C-N bonded triazolyl purines **A**.[28, 85] It is known that C-N bonded triazole at the *C*6 position of purine acts as a leaving group in S_NAr reactions with different *O*-, *C*-, *P*-, *Se*- and *N*-nucleophiles.[48, 49, 52, 53] So, we opted to synthesize compounds **B**, where triazole and purine were connected via the C-C bond, improving structure stability for potential use in OLEDs.

C-C bonded triazolyl purines were synthesized in copper-catalyzed azide-alkyne cycloaddition (CuAAC) using corresponding alkynyl purines and aryl azides. Firstly, commercially available 2,6-dichloropurine (**11**) was derivatized at the *N*9 position in the Mitsunobu reaction with three different alkyl groups (Scheme 2). Trityl group containing moiety (**a**) was introduced into the structure to make it more amorphous and suitable for the studies of photophysical properties in films and the discovery of potential use for OLEDs.[86] Heptyl group (**b**) was chosen for its inert behavior, and glycerol-containing moiety (**c**) was selected to increase the end-product solubility in aqueous solutions. Next, in the Sonogashira reaction, alkynyl groups were introduced into the molecule. Since the starting material has two chlorine atoms at purine *C*2 and *C*6 positions, it is possible to obtain either 6-alkynyl purines **13** or 2,6-bis-alkynyl purines **14**, solely changing the reaction conditions. Since the purine *C*6 position is more reactive,[16] product **13** formed first at 50 °C temperature, and the further substitution at the purine *C*2 position required a higher temperature, thus resulting in an increase in temperature to 100 °C and the change of solvent from

tetrahydrofuran (THF) to dimethylformamide (DMF). It is worth noticing that in the synthesis of 6-alkynyl purines **13**, even by lowering the temperature and using exactly one equivalent of TMS acetylene, the formation of 2,6-bis-alkynyl purines **14** always was observed up to 10 % of conversion.

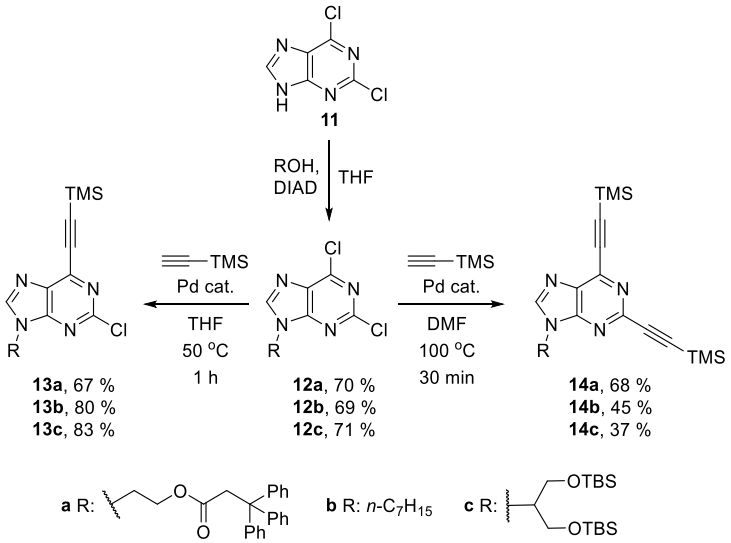

Scheme 2. Synthesis of 6-alkynyl purines **13** and 2,6-bis-alkynyl purines **14**.

With alkynyl purines in hand, CuAAC reactions were carried out with aryl (Table 2, entries 1–8) and alkyl (Table 2, entries 9–13) azides **15** using CuI as a catalyst. Corresponding 2-chloro-6-triazolylpurines **16a-m** were obtained in 56–91 % yields. In the case of 4-azido-*N*,*N*-dimethylaniline (Table 2, entry 3), the CuAAC reaction was performed using $CuSO_4 \cdot 5H_2O$/sodium ascorbate catalytic system due to the electron-rich nature of the corresponding azide. In the presence of the copper iodide, it was reducing itself to the corresponding amine way faster than the reaction was complete. Next, compounds **16a-m** were used in S_NAr reactions with piperidine, yielding 2-piperidinyl-6-triazolylpurines **17a-m**. Piperidine was introduced to the structure as an electron-donating moiety, forming the complete push-pull chromophore in opposition to electron-deficient triazole, thus enhancing product fluorescence. In the case of compound **16j** (Table 2, entry 10), aminolysis of the ester was observed, and piperidylamide was obtained instead of the corresponding methyl ester.

Table 2

CuAAC between alkynyl purines **13** and alkyl/aryl azides **15**, followed by an S_NAr reaction with piperidine

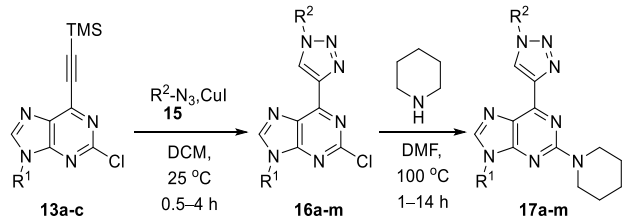

Entry	R^1	R^2	Reaction **13** → **16**, yield, %	Reaction **16** → **17**, yield, %
1	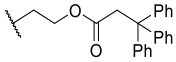	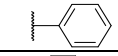	**16a**, 66	**17a**, 67
2		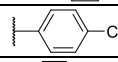	**16b**, 82	**17b**, 76
3[a]		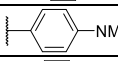	**16c**, 56	**17c**, 41
4		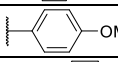	**16d**, 89	**17d**, 67
5	*n*-C_7H_{15}	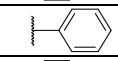	**16e**, 86	**17e**, 77
6		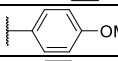	**16**, 91	**17f**, 81
7		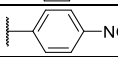	**16g**, 69	**17g**, 71
8	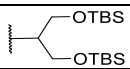	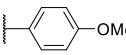	**16h**, 89	**17h**, 75
9	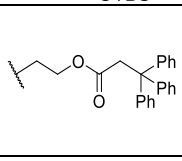	CH_2CN	**16i**, 59	**17i**, 75
10[b]		CH_2COOMe	**16j**, 74	**17j**, 75
11		Cy	**16k**, 77	**17k**, 66
12		*n*-$C_{10}H_{23}$	**16l**, 88	**17l**, 89
13		Bn	**16m**, 83	**17m**, 83

[a] For the reaction **13** → **16**, reaction conditions were $CuSO_4{\cdot}5H_2O$, sodium ascorbate, AcOH, DMF, 70 °C.
[b] For the reaction **16** → **17**, aminolysis of the ester was observed, and piperidylamide was obtained instead of the corresponding methyl ester.
[c] Cy – cyclohexyl group.

We also used CuAAC reaction between 2,6-bis-alkynyl purines **14** and corresponding alkyl/aryl azides **15** to result in bis-triazolyl purines **18a-m** (Table 3). The nitro group that was introduced to the phenyl triazole moiety (Table 3, entry 7) fully quenched the fluorescence, and in the case of 4-azido-*N*,*N*-dimethylaniline, formation of the second triazole was never observed in the reaction mixture.

Table 3

CuAAC between 2,6-bis-alkynyl purines **14** and azides **15**

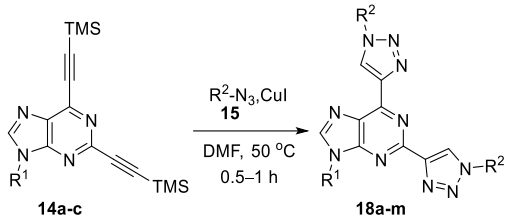

Entry	R^1	R^2	Reaction **14** → **18**, yield, %
1	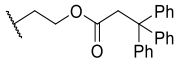		**18a**, 60
2		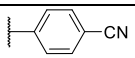	**18b**, 50
3		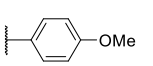	**18c**, 60
4	*n*-C_7H_{15}		**18d**, 44
5	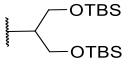		**18e**, 38
6	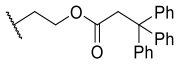	CH_2CN	**18f**, 62
7		CH_2COOMe	**18g**, 67
8		Cy[a]	**18h**, 81
9		*n*-$C_{10}H_{23}$	**18i**, 45
10		Bn	**18j**, 85

[a] Cy – cyclohexyl group.

After acquiring a wide range of C-C bonded mono- and bis-triazolyl purines, we decided to synthesize some C-N bonded triazolyl purine analogs for comparison of their photophysical properties among themselves. Since ion complexing tests are better achieved in aqueous media, we chose to introduce a glycerol-containing moiety into selected C-N bonded analogs. For the synthesis of C-N triazolyl purine products, we used an approach developed in our laboratory before.[31, 53, 85, 87] In the first step, we used previously obtained purine derivative **12c** in S_NAr reaction with NaN_3, acquiring 2,6-diazidopurine **19** (Scheme 3). Next, in the CuAAC reaction between diazide **19** and 1-ethynyl-4-methoxybenzene, we obtained 2,6-bis-triazolylpurine **20**. C-N bonded 2-piperidinyl-6-triazolylpurine **23** was synthesized in a similar manner using the sequence of S_NAr and CuAAC reactions. In the S_NAr reaction, diazide **19** reacted with piperidine, and due to azide-tetrazole equilibrium, product **22** formed and was later used in the CuAAC with 1-ethynyl-4-methoxybenzene. The last step was the cleavage of the *tert*-butyldimethylsilyl (TBS) protecting groups in compounds **20** and **23**, using acetic acid in THF/H_2O, yielding products **21**

and **24**, respectively. The same TBS deprotection protocol was used for their C-C bonded analogs **17h** and **18e** (Table 4, entries 11 and 14).

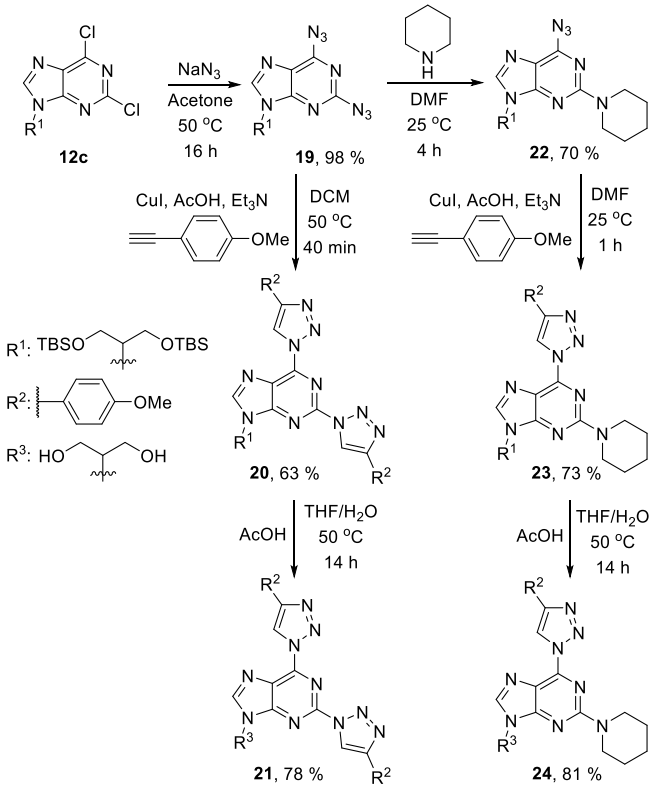

Scheme 3. Synthesis of C-N bonded bis-triazolyl purine **21** and mono-triazolyl purine **24**.

Next, the photophysical properties of target compounds **17**, **18**, **21**, and **24** were studied (Table 4). Quantum yield measurements of amorphous compounds **17a**, **17d**, and **17m**, which were designed for potential use in OLEDs, were taken in the thin films and reached up to 35 %. During the research, the trityl group containing purine derivatives proved to be unsuitable for the development of OLED devices due to the rapid degradation under the influence of electrical current, so we did not perform any experiments or further purine structure modifications for the potential OLED development.

Table 4

Photophysical properties of triazolyl purines **17**, **18**, **21** and **24**

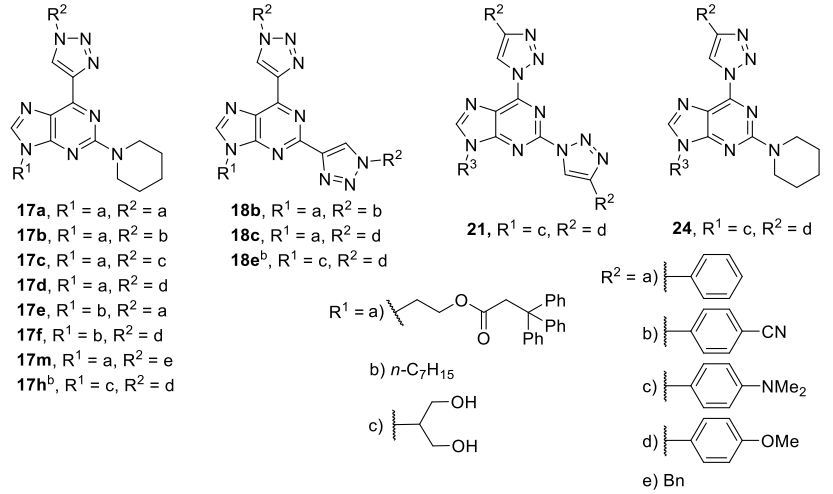

Entry	Compound	Solvent[a]	$\lambda_{abs\ max}$, nm	$\lambda_{em\ max}$, nm	Quantum yield, %
1	**17a**	DCM	365	443	75
2		in the film	366	447	35
3	**17b**	DCM	371	452	68
4	**17c**	DCM	311	437	76
5	**17d**	DCM	363	439	71
6		in the film	381	545	12
7	**17e**	DCM	364	443	81
8	**17f**	DCM	365	441	74
9	**17m**	DCM	362	438	75
10		in the film	361	443	23
11	**17h**[b]	DMSO	363	450	95
12	**18b**	DCM	282	---	0
13	**18c**	DCM	281	394	26
14	**18e**[b]	DMSO	283	452	49
15	**21**	DMSO	261	506	24
16	**24**	DMSO	362	457	98

[a] C = 10^{-5} mol/L.

[b] TBS group being cleaved from the initial substrate.

In the case of glycerol containing purine derivatives **17h**, **18e**, **21**, and **24**, we observed that they were practically insoluble in water and dichloromethane (DCM), but soluble in dimethylsulfoxide (DMSO), so all measurements were taken in DMSO. 2,6-Bis-triazolyl purine derivative **18b** did not exhibit fluorescence, while compounds **18c**, **18e**, and **21** showed moderate quantum yields in the range of 24–49 %. In the case of the nine studied 6-triazolyl-2-piperidinyl purines **17a-h** and **24,** quantum yields in DCM and DMSO were in the range of 68–98 %.

The original publication of the research described in this chapter can be found in Appendix II.

1.3. Synthesis of water-soluble triazolyl purines

Since glycerol moiety containing compound **24** possessed an excellent quantum yield but had poor solubility in water, we decided to transform hydroxyl groups into pyridinium moieties, which form the salts with counter ions, increasing compound solubility in water.[88, 89] For this purpose, we exchanged hydroxyl groups for tosylates and then heated tosylate derivative **25** in pyridine at 120 °C temperature until pyridinium tosylate salt **26** was formed (Scheme 4).

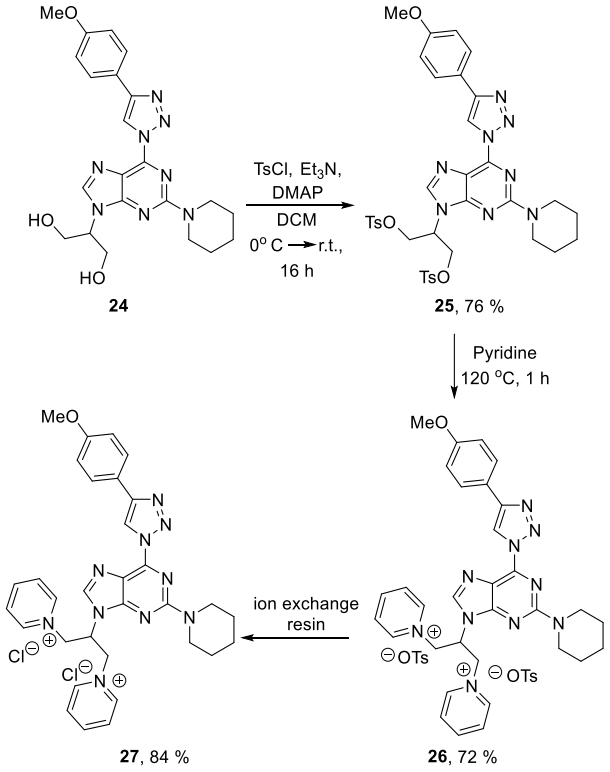

Scheme 4. Synthesis of water-soluble C-N bonded mono-triazolyl purine **27**.

Although compound **26** was already soluble in water, it still possessed two aromatic tosylate anions that potentially could impact fluorescence, so we decided to exchange these ions for chlorides using ion exchange resin. The solubility of compounds **24**–**27** in water was determined by using quantitative ^{1}H-NMR (**24** – 0.21 mg/mL, **25** – 0.19 mg/mL, **26 –** 57 mg/mL, **27** – 133 mg/mL).

Photophysical properties were measured for compounds **26** and **27** (Table 5). Absorption and emission spectra were measured for compound **26** in H_2O, DMSO, and DCM and for compound **27** in acetonitrile (MeCN), methanol (MeOH), H_2O, DMSO, and DCM at 10^{-4} M concentration. The quantum yields for both triazolyl purine derivatives were below the detection range (< 0.5 %) while starting material **24** had a 98 % QY in DMSO solution at 10^{-5} M concentration (Table 4, entry 16). Upon derivatization of glycerol containing moiety of compound **24** at the purine *N*9 position with pyridinium salts, while the solubility of compounds in water was greatly enhanced, the fluorescence was quenched.

Table 5

Photophysical properties of triazolyl purines **26** and **27**

	Compound **26**			Compound **27**		
Solvent[a]	$\lambda_{abs\ max}$, nm	$\lambda_{em\ max}$, nm	Quantum yield, %	$\lambda_{abs\ max}$, nm	$\lambda_{em\ max}$, nm	Quantum yield, %
MeCN	–	–	–	360	457	< 0.5
MeOH	–	–	–	362	461	< 0.5
H_2O	362	457	< 0. 5	363	463	< 0.5
DMSO	361	428	< 0.5	362	454	< 0.5
DCM	359	565	< 0.5	360	452	< 0.5

[a] C = 10^{-4} mol/L.

The original publication of the research described in this chapter can be found in Appendix III.

1.4. Water-soluble purine derivatives for metal ion complexation

According to the example in the literature, the introduction of the tetraethylene glycol (TEG) moiety into the purine derivative should increase compound solubility in water.[90, 91] TEG moiety containing purine derivatives **31** and **32** were synthesized in multiple steps from 2,6-dichloropurine (**11**) (Scheme 5).

TEG moiety protected with the tetrahydropiranil (THP) group was introduced into 2,6-dichloropurine (**11**) *N*9 position using the Mitsunobu reaction conditions. Next, 6-alkynyl purine derivative **29** was synthesized in the Sonogashira reaction and later was used in the subsequent CuAAC reaction with 1-azido-4-methoxybenzene, followed by S_NAr reaction with piperidine, yielding triazolyl purine derivative **30**. The THP group was deprotected with trifluoroacetic acid

(TFA) in MeOH, resulting in compound **31**. Next, in the reaction between compound **31** and *tert*-butyl-2-bromoacetate, followed by the removal of the protecting group, product **32** was obtained. Solubilities in water of compounds **31** and **32** were determined by measuring and comparing the UV absorptions of their saturated solutions with corresponding calibration curves. The resulting solubility in water was 0.24 mg/mL for compound **31** and 110 mg/mL for compound **32**.

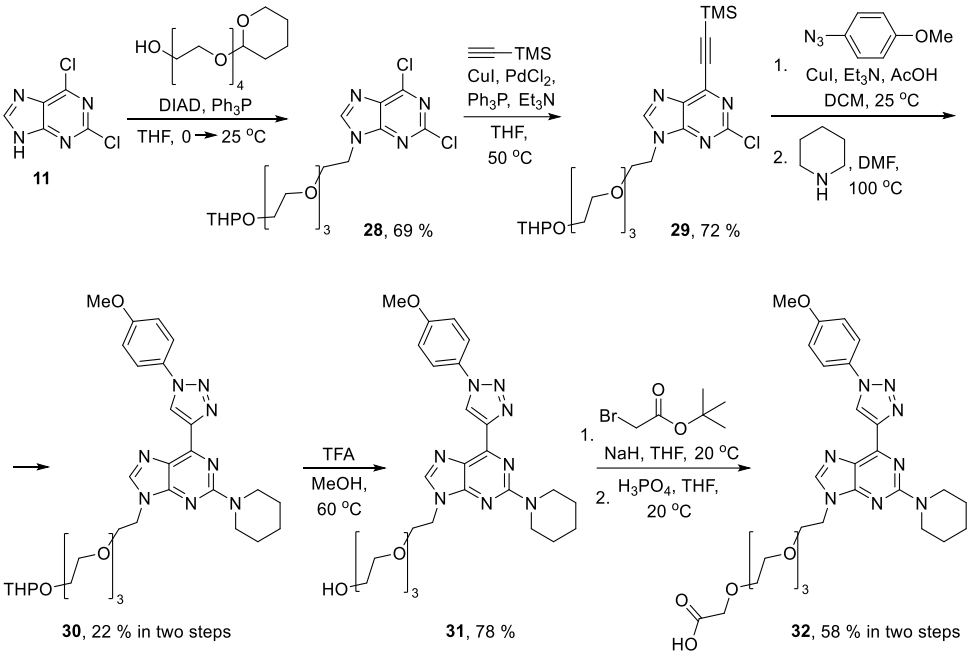

Scheme 5. Synthesis of purine derivative **32** with the TEG moiety.

The photophysical properties of compounds **17f**, **31**, and **32** were studied (Table 6). Since compound **17f** was insoluble in water, measurements were made in aprotic solvents of different polarities – in cyclohexane (CyHex), diethyl ether (DEE), ethyl acetate (EA), dimethoxy ethane (DME), MeCN and DMSO. The TEG group containing triazolyl purines **31** and **32** were tested in water. Quantum yields of compound **17f** in different solvents were in the range of 48−72 %, its fluorescence lifetime being from 9 ns to 15.7 ns. Radiative fluorescence decay (τ_{rad}) represents the speed by which a molecule emits fluorescence, while non-radiative fluorescence decay (τ_{nonrad}) is the speed of fluorescence quenching.[92] Both processes are competing, and for high quantum yield, τ_{rad} should be faster than τ_{nonrad} and vice versa. The highest quantum yield achieved was 72 % for compound **17f** in DMSO, which is explained by the fact that in more viscous solvents, molecular motions are slower, thus lowering fluorescence quenching. The lowest quantum yield was 17 % in water for compounds **31** and **32**. This rapid quenching of fluorescence was expected due to the

high-energy vibrations of hydroxyl groups.[93] But the observed quantum yield was still considered sufficient for further metal ion sensing experiments in water.

Table 6

Photophysical properties of triazolyl purines **17f**, **31** and **32**

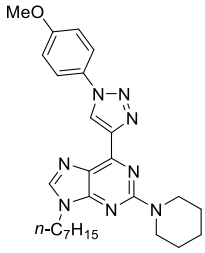

17f

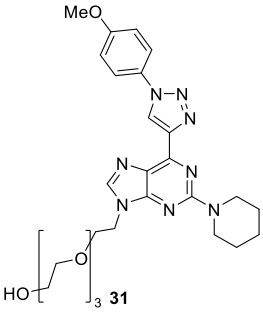

31

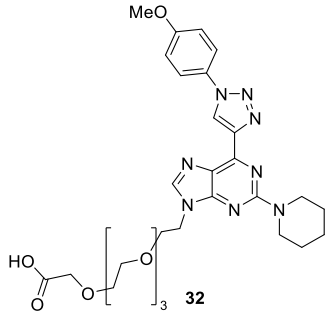

32

Entry	Compound	Solvent	λ_{abs}, nm	λ_{em}, nm	Quantum yield, %	τ,[a] ns	τ_{rad},[b] ns	τ_{nonrad},[c] ns
1	**17f**	CyHex	365	415 395	61	9.0	14.8	23.1
2		DEE	360	425	52	9.4	18.1	19.6
3		EA	360	425	48	9.3	19.4	17.9
4		DME	360	425	50	9.7	19.4	19.4
5		MeCN	360	435	49	12.4	25.3	24.3
6		DMSO	360	445	72	15.7	21.8	56.1
7	**31**	H_2O	363	462	17	7.1	41.5	8.5
8	**32**		363	462	17	7.1	41.8	8.6

[a] Fluorescence lifetimes.

[b] Radiative fluorescence decay lifetimes, $\tau_{rad} = \frac{\tau}{QY}$.

[c] Non-radiative fluorescence decay lifetimes, $\tau_{nonrad} = \frac{\tau}{1 - QY}$.

Compounds **31** and **32**, alongside previously synthesized **17f**, were tested for their ability to complex metal ions. For the experiments, mercury(II) ions were chosen. Mercury is a non-biodegradable heavy metal that possesses high toxicity for living organisms. Mercury compounds, upon dissolution in freshwater or seawater, create methylmercury, which accumulates in marine products and is easily ingested by humans.[94] Accumulation of mercury into humans increases the risk of heart complications, causes Minamata disease, and damages the DNA and chromosomes.[95] Due to the mentioned issues, there is a necessity for the detection of Hg^{2+} ions in water and living cells. There are known compounds capable of complexing the Hg^{2+} ions with different complexation mechanisms, including *S*-atom complexation, deprotection of thioacetals, and *N*-

atom complexation.[96] Since Hg^{2+} ions have a tendency towards coordination of nitrogen atoms, and triazolyl purines structure possesses a sufficient amount of nitrogen atoms, our triazolyl-purine conjugates were examined.

By using the ^{1}H-NMR titration technique, triazolyl purine **17f** was titrated in MeCN-d_3 using $Hg(ClO_4)_2 \cdot 3H_2O$ as an Hg^{2+} source and benzene as an internal standard. ^{1}H-NMR spectra of the analyzed sample were taken after each addition of 0.1 eq. of Hg^{2+} ions (Fig. 6).

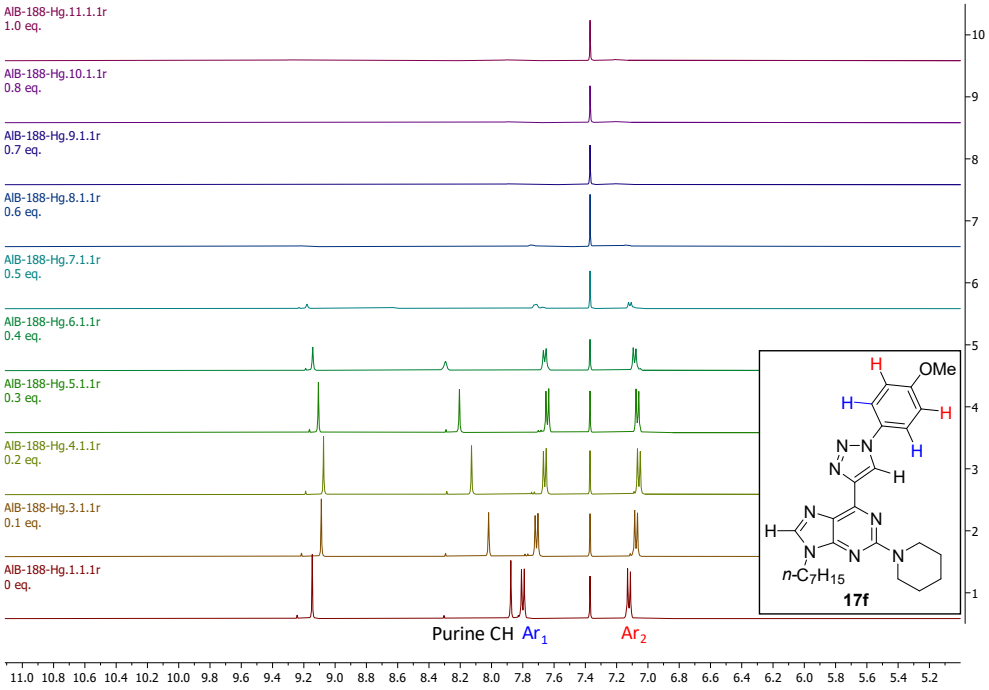

Fig. 6. ^{1}H-NMR titration of compound **17f** with Hg^{2+} ions in MeCN-d_3, aromatic region is shown.

After each addition of Hg^{2+} ions, aromatic proton signals shifted, and the most rapid shift was observed by the purine *C*8-H signal, followed by the triazole and Ar_1 signals. Upon the first addition of ions, precipitate started forming slowly, and at 0.5 eq. of Hg^{2+} ions, only traces of **17f** were found, completely disappearing at 0.6 eq. The most likely formed precipitate is compound **17f** and Hg^{2+} ion complex with a coordination pattern 2 : 1, with the Hg^{2+} coordination site being between purine *N*7 and triazole *N*3 atoms (Fig. 7).

Compounds **31** and **32** were also tested for the complexation pattern to the Hg^{2+} ions, but the formed complexes in water were with a 1 : 1 ratio, as a result of reducing binding constant in water. As expected, for all tested substrates, every addition of Hg^{2+} ions quenched the fluorescence,

making them potential metal ion sensors. Other metal ions such as Na^+, K^+, Mg^{2+}, Ca^{2+}, Fe^{2+}, Cu^{2+}, Zn^{2+}, Hg^{2+}, and Pb^{2+} were tested for their complexation potential with compounds **17f**, **31** and **32** in water or acetonitrile (Fig. 8).

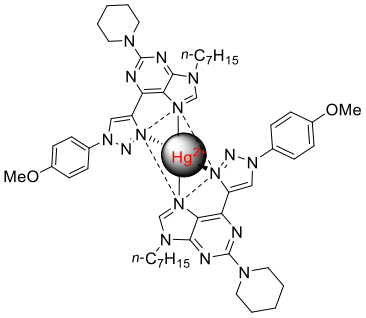

Fig. 7. Possible **17f** : Hg^{2+} complex based on the observations in the titration experiments.

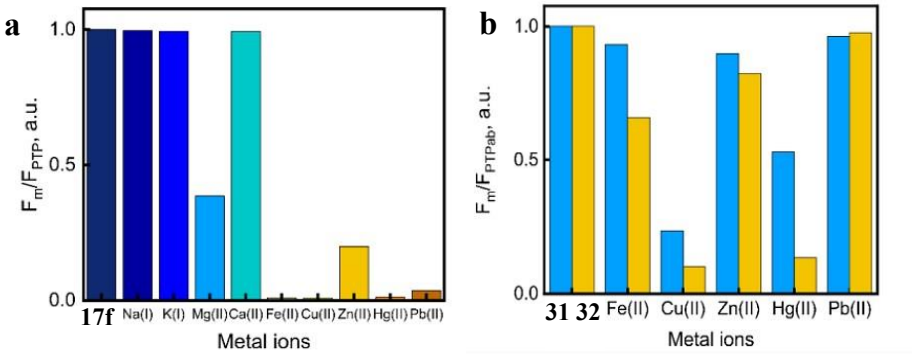

Fig. 8. a – Fluorescence intensity upon addition of metal ions to the compound **17f** in acetonitrile; b – fluorescence intensity upon addition of metal ions to the compounds **31** (blue bar) and **32** (yellow bar) in H_2O.

Triazolyl purine derivative **17f** has shown a complexation pattern towards Fe^{2+}, Cu^{2+}, Pb^{2+}, Mg^{2+}, and Zn^{2+} ions, similar to that observed with Hg^{2+} ions. In aqueous media TEG containing triazolyl purine derivatives **31** and **32**, besides Hg^{2+}, strongly coordinated only with Cu^{2+} ions (Fig. 8 b), which is explained with azafilic nature of copper, that even in aqueous media prefers to coordinate with nitrogen,[97] while metal ions such as Fe^{2+}, Pb^{2+}, and Zn^{2+} prefer to coordinate with oxygen and are making complexes with water instead. All tested compounds displayed excellent complexation ability towards Hg^{2+} ions in solutions. Next, the experiments with compounds **31** and **32** were performed on the living cells in collaboration with Taiwan colleagues. However, compound **32**, which contained -COOH moiety, was too reactive and adhered to the cultural plate, and experiments were continued only with compound **31**. MDA-MB-231 cells were treated with

$HgCl_2$, followed by compound **31**. Bright-field and fluorescence spectroscopy were used to observe changes in the cells (Fig. 9).

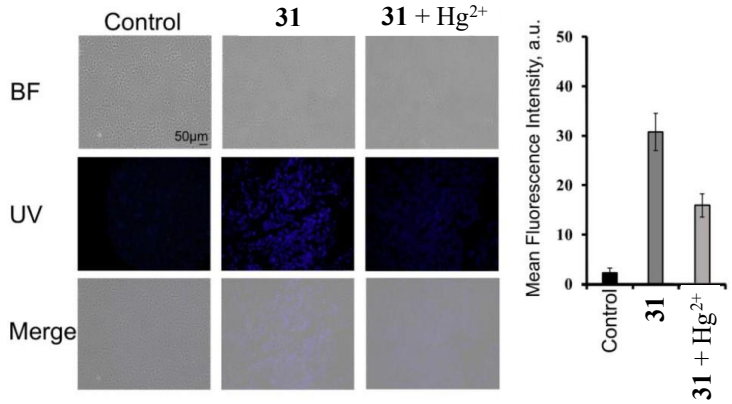

Fig. 9. Bright-field and fluorescence spectroscopy of MDA-MB-231 cells stained with compound **31** with or without Hg^{2+} ions.

Cells successfully internalized compound **31,** and the fluorescence was quenched after treating them with mercury. This experiment confirmed the potential use of derivative **31** as a mercury ion detector in biological systems.

The manuscript of the research described in this chapter can be found in Appendix IV.

Compounds **17f**, **31**, and **32** are part of the LVP2024000059 and LVP2024000072 patent applications submitted to the Patent Office of the Republic of Latvia and can be found in Appendices V and VI.

1.5. Water-soluble purines as potential photocatalysts

In collaboration with colleagues from Vilnius University (VU) and Laboratoire Ondes et Matière d'Aquitaine in Bordeaux University, who have experience in the studies of photocatalytic systems,[98, 99] a new potential photocatalyst based on purine containing cyclen (1,4,7,10-tetraazacyclododecane) moiety was designed and synthesized in 9 steps (Fig. 10).

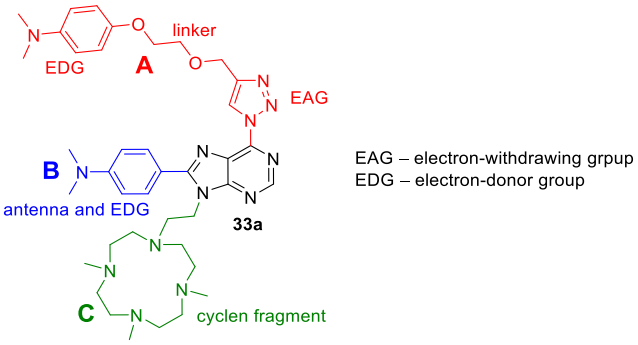

Fig. 10. Structure of the designed target compound **33a**.

Moiety **A** consists of several parts – triazole, alkyl linker, and *N*,*N*-dimethylaniline. Triazole acts as an electron-withdrawing group in the push-pull system in this molecule, while *N*,*N*-dimethylaniline moiety is a strong charge donor, not connected to any other aromatic system. Moiety **B** consists solely of *N*,*N*-dimethylaniline, which is connected to the purine ring directly, acting as a strong electron donor group for the push-pull system and as an antenna for the electron transfer. Moiety **B** also extends the π-conjugated electron system of triazolyl purine, lowering its absorption wavelength and transforming it into a fragment with well-expressed charge transfer properties. The cyclen part of the moiety **C** was chosen due to its excellent ability to complex metal ions such as Cu^{2+}, Ni^{2+}, and Zn^{2+}.[100, 101] In this molecule, moiety **C** is meant for the coordination of Cu^{2+} ions to all four nitrogens in cyclen due to good coordination strength towards them, thermodynamical stability, and kinetic inertness in acidic media.[102] General mechanism of the envisioned operation scheme of this photocatalyst is: 1) upon photoexcitation, an electron from the antenna is excited and goes to its lowest unoccupied molecular orbital (LUMO), quickly followed by an electron from the donor group occupying a free spot in the antenna's highest occupied molecular orbital (HOMO); 2) electron transfer from LUMO happens from the antenna to the metal in cyclen position, reducing it from Cu^{2+} to Cu^{+} (Fig. 11).

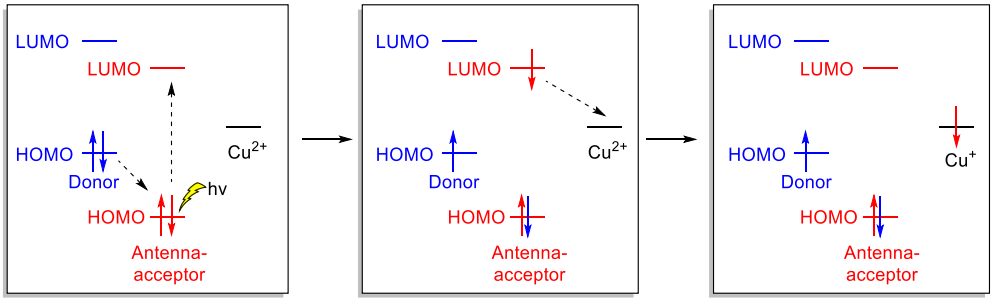

Fig. 11. Proposed mechanism of action for the photocatalyst **33a**.

To synthesize the desired compound, the purine core requires derivatization at the *C*6, *C*8, and *N*9 positions with **A**, **B**, and **C** moieties. We designed six possible synthetic routes towards the target product, depending on the introduction order of the chosen moieties into the purine ring. The general synthetic strategies for the synthesis of the goal product are presented in Scheme 6. Moiety **A** was planned to be constructed via CuAAC reaction (Scheme 6 a). The synthesis of building block **36** was done in 4 steps starting from 1-bromo-4-nitrobenzene (see Appendix VII). Arylation of the purine *C*8 position was planned to be achieved via a palladium-catalyzed cross-coupling reaction, and we chose the Stille reaction (Scheme 6 b); building block **39** was easily obtained in one step.[103] Building block **C** could be introduced to the purine *N*9 position via S_N2 reaction using cyclen derivative **42**, which was obtained by using known literature methods (Scheme 6 c).[104]

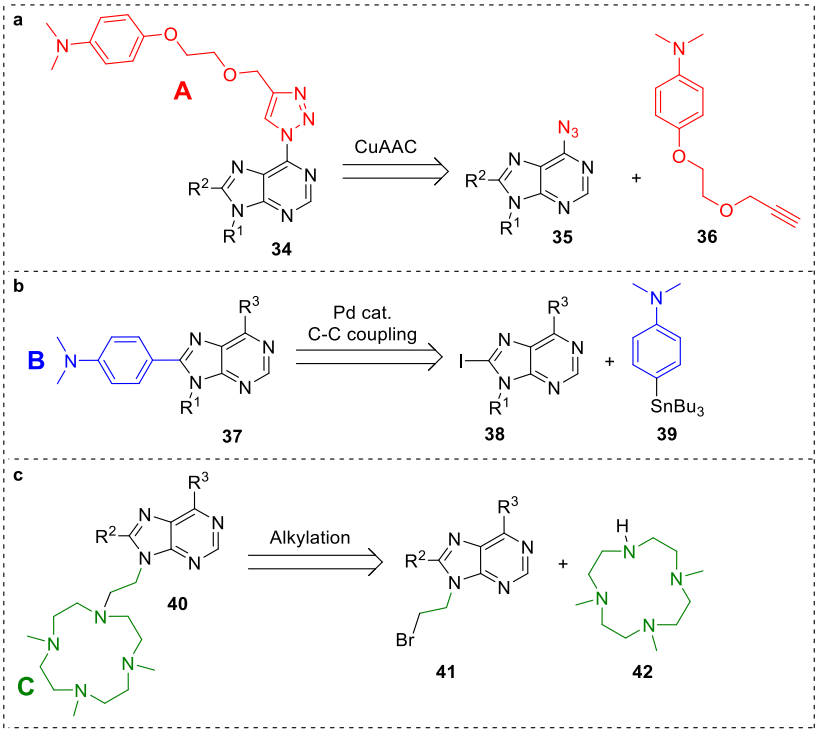

Scheme 6. Retrosynthetic approach for the introduction of **A**, **B**, and **C** moieties into the purine core.

In our initial synthetic route towards cyclen moiety-containing product **33a**, we used compound **43** in the S_NAr reaction with sodium azide and obtained 6-azidopurine derivative **44** (Scheme 7). Subsequent CuAAC reaction with 2-(prop-2-yn-1-yloxy)ethan-1-ol resulted in triazolyl purine **45**. Further derivatization of compound **45** with 4-bromo-*N*,*N*-dimethylaniline by using copper-catalyzed Ullmann-type reactions with different bases (Cs_2CO_3, K_3PO_4, K_2CO_3) and ligands

(3,4,7,8-tetramethyl-1,10-phenanthroline, 8-hydroxyquinoline) was unsuccessful. Instead, building block **36** was used, and in the CuAAC reaction, product **46** was obtained, in which the THP-protecting group was easily cleaved in AcOH/H_2O/THF mixture at 50 °C temperature in 16 h. Further derivatization attempts of this compound using the Mitsunobu reaction or alkylation of the *N*9 position were unsuccessful.

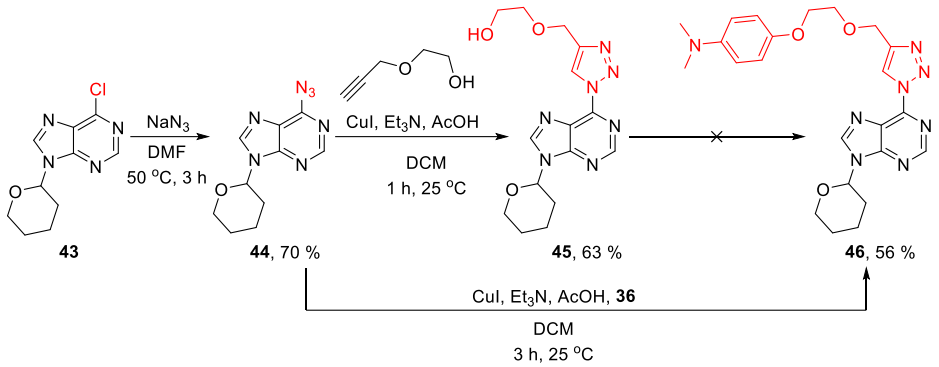

Scheme 7. The first synthetic route, starting with the derivatization of the purine *C*6 position.

Then, we decided to change the derivatization sequence and start the modification at the purine *N*9 position. First, the Mitsunobu reaction between 6-chloropurine (**47**) and THP-protected ethylene glycol yielded product **48**, which underwent azidation and CuAAC reactions, and triazolylpurine **50** was obtained in 46 % yield (Scheme 8). Next, we tried to introduce a halogen atom to the purine *C*8 position for further C-C cross-coupling reaction. In the reaction with NBS, the phenyl ring was brominated instead of purine, leading to the formation of compound **51**, while the use of lithium diisopropilamide (LDA) and other deprotonation reagents resulted in the deprotonation of triazole. We concluded that the derivatization of the *C*8 position should be done earlier.

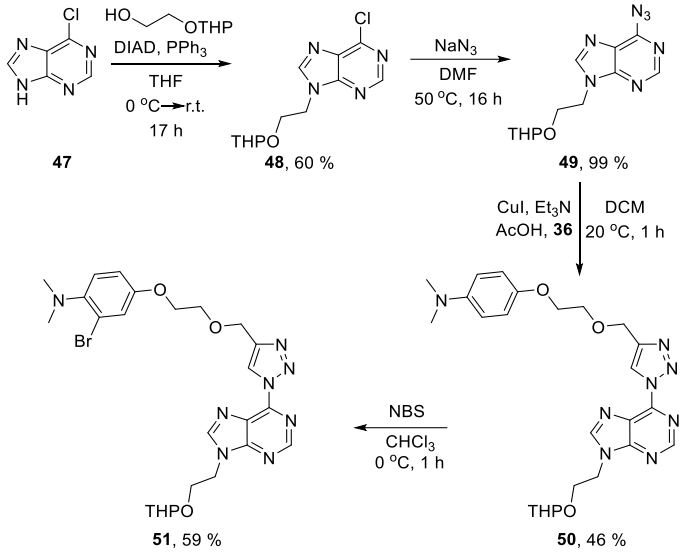

Scheme 8. The second synthetic route, attempts to modify subsequently purine *C*6 and *C*8 positions.

We started the third synthetic route with the iodination of previously obtained compound **48**, followed by a Stille cross-coupling reaction with *N*,*N*-dimethyl-4-(tributylstannyl)aniline (**39**) to introduce the necessary moiety into the purine *C*8 position, obtaining compound **53** (Scheme 9). In this stage, we decided that alongside target compound **33a**, we would also synthesize compound **33b**, which contained the *n*-pentyl group in the triazole ring, so we could prove the importance of the strong donor group in the substituent at the purine *C*6 position. To acquire desired products **33**, the sequence of azidation and CuAAC reactions with different alkynes was performed with compound **52**. Further, THP group cleavage with the following mesylation resulted in high yields. Acquired mesylates **57a-b** were inert in the S_N2 reaction with cyclen derivative **42**, and we decided to substitute the mesylate group with bromine and then use it in the alkylation reaction with building block **42**. The reaction proceeded via the preferred E2 mechanism, forming the elimination products **58a-b** as the main products. After screening the reaction conditions, we noticed that the best conversion to desired products is achieved only in 20 % (for **33a**) and 30 % (for **33b**), with 6 % and 23 % isolated yields, respectively.

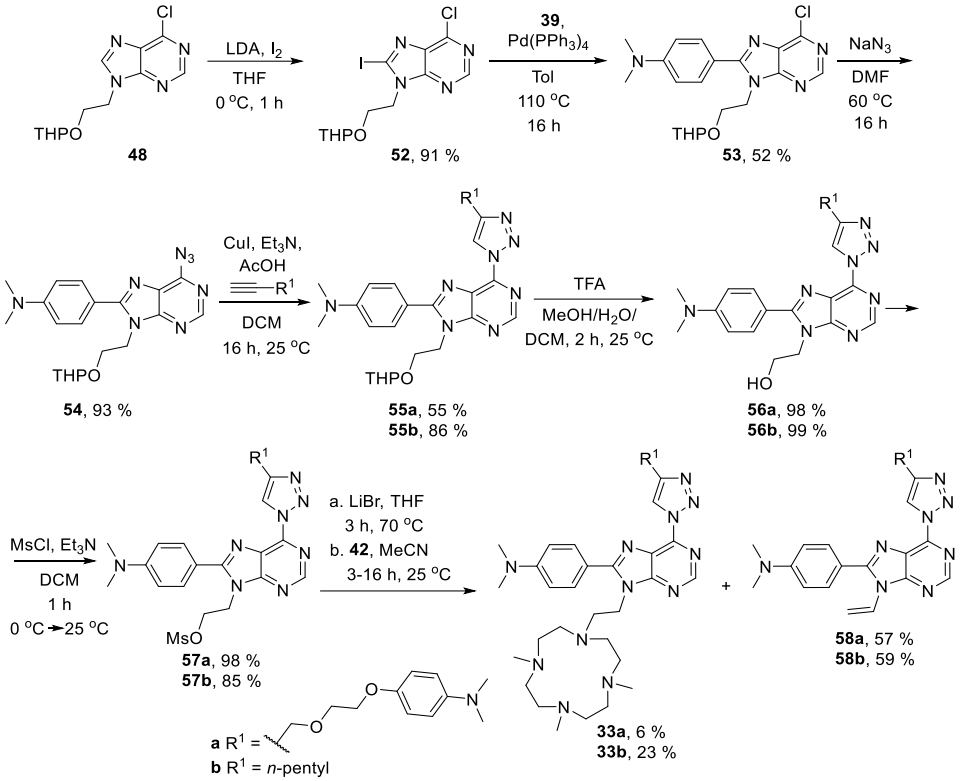

Scheme 9. The third synthetic route, order of purine ring derivatization being *C*8 → *C*6 → *N*9 positions.

By using the ^{1}H-NMR titration technique, product **33a** was titrated in MeCN-d_3 using $Cu(ClO_4)_2 \cdot 6H_2O$ as a Cu^{2+} source and benzene as an internal standard. ^{1}H-NMR spectra of the analyzed sample were taken after each addition of 0.1 eq. of Cu^{2+} ions (Fig. 12).

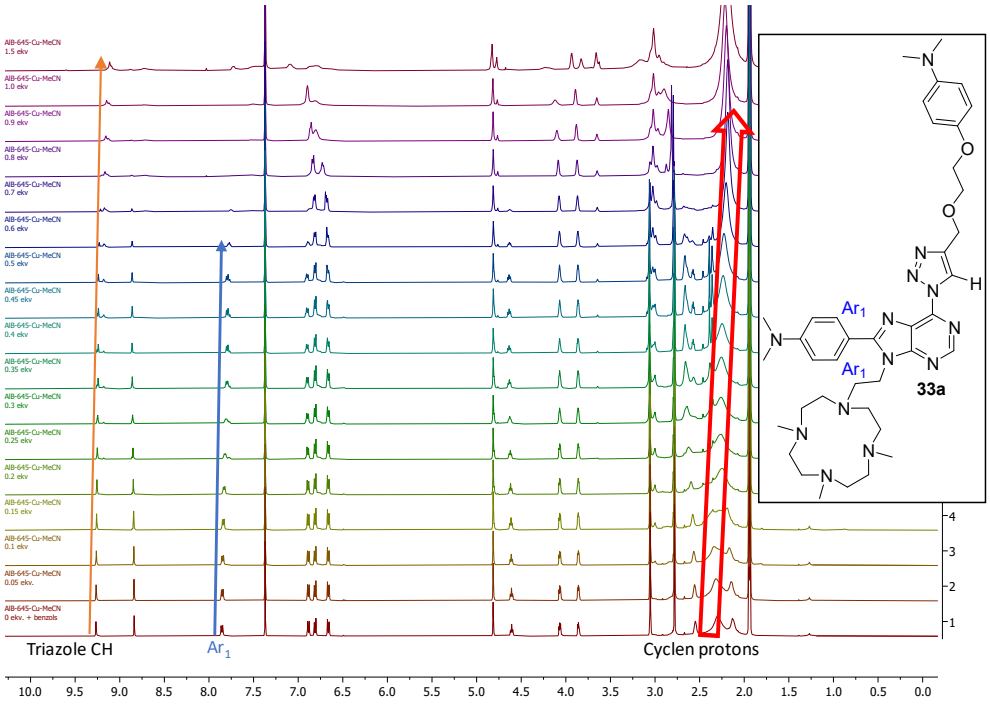

Fig. 12. ^{1}H-NMR titration of compound **33a** with Cu^{2+} ions in MeCN-d_3.

^{1}H-NMR spectra show compound **33a** complicated complexation pattern with Cu^{2+} ions. The most important sign that reflects the binding of Cu^{2+} to the cyclen is depicted in the spectrum by a thick arrow at 2.0–2.5 ppm. Starting from 0.7 equivalents of metal ions, all ^{1}H-NMR signals of cyclen merge into a single signal at about 2.2 ppm, which does not shift at higher Cu^{2+} concentrations. This fact indicates that the metal ion is coordinated inside the cyclen ring and all 4 nitrogens of the cycle are coordinated to Cu^{2+} ions. The largest changes, except for the cyclen fragment, were observed in the shift of the triazole proton and the aromatic protons at *C*8 of the phenyl ring. There is a strong possibility that the molecule has two competing complexation sites – in the cyclen fragment and between the triazole and the purine.

The unpublished results of the research described in this chapter can be found in Appendix VII.

2. Triazole ring opening and cyclization of the enamines into indoles

Triazole ring opening reactions with the release of nitrogen gas were reported before. At very high temperatures (400−800 °C) (Scheme 10 a) under flash vacuum pyrolysis conditions, the triazole ring opens with the formation of carbene species **58** that further rearrange into various indoles **59** or quinolones **62**.[105–107] Other studies report the use of rhodium or nickel catalysts for the opening of *N*-tosyl type triazole derivatives at much milder conditions (70−140 °C) that results in metallocarbene **64**, which reacts further with alkynes or nitriles with the formation of imidazole or pyrrole **65** (Scheme 10 b).[108, 109] *N*-Tosyl type triazoles in the presence of nickel catalyst open using *H*-phospine oxides resulting in the formation of α-aminovinylphosphoryl derivatives **66** (Scheme 10 c).[110] If one of the substituents at the triazole *C* atoms is an amino group, then the Dimroth rearrangement is possible (Scheme 10 d). This thermal ring-transformation reaction starts when triazole **67** forms an equilibrium with its open form **68**, where a double bond shift happens between two nitrogen atoms, followed by a ring closure with the formation of triazole **70**.[111]

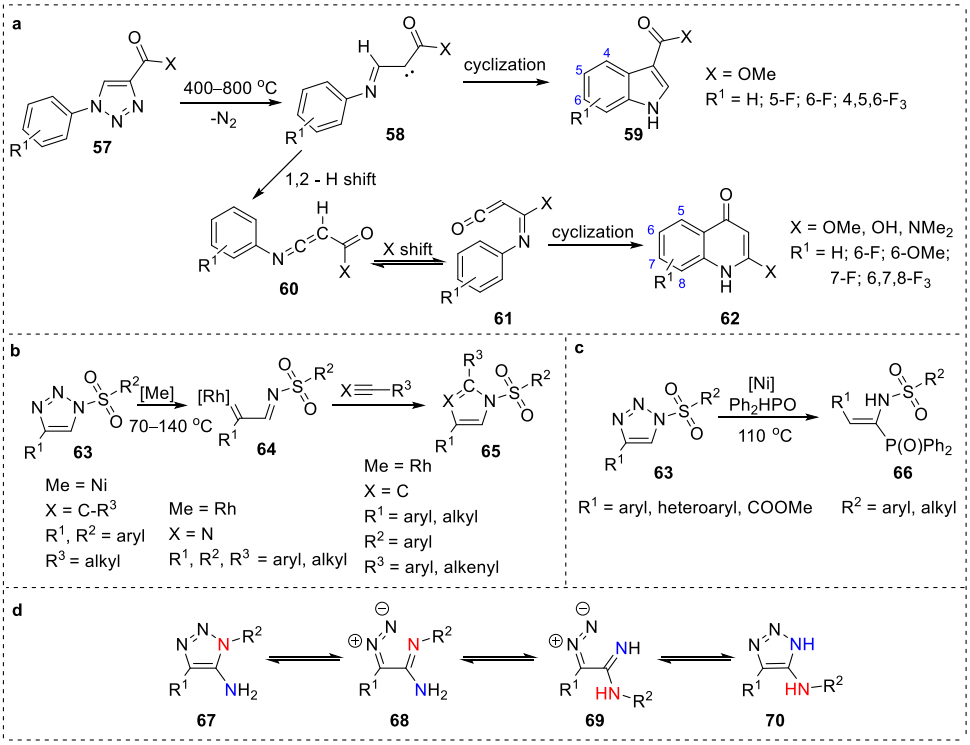

Scheme 10. Triazole ring opening reactions known in the literature.[105–111]

Indole is one of the most significant and prevalent heterocycles in nature, being present in a wide array of biologically significant natural compounds, such as serotonin and vinblastine.[32] The synthesis of various indole derivatives has always been a topic of interest in the last century,[112, 113] and there is still a necessity for the development of new synthetic methods and pathways towards desired indole derivatives with potential use as pharmaceuticals.[33, 114]

The synthesis of 1*H* indoles from aromatic enamines has been extensively studied. One of the first reported examples of this transformation was palladium-catalyzed intramolecular oxidative coupling developed by the Glorius group (Scheme 11 a).[115] The course of the reaction required a catalytic amount of palladium and a stoichiometric amount of copper acetate that was used as an oxidant alongside the excess of K_2CO_3 in DMF at 80–140 °C. Later, palladium-free reaction conditions were reported by multiple groups. Liang's group published the research where this cyclization reaction still required a stoichiometric amount of copper, but the palladium catalyst was substituted by Fe(III) species (Scheme 11 b).[116] These methods (Scheme 11 a–b) included methyl substituent at the indole *C*2 position, so later new catalytic systems were developed for the synthesis of *C*2 aryl-substituted indoles (Scheme 11 c–d).[117, 118] Transformations required either a stoichiometric amount of copper (Scheme 11 d)[118] in mesitylene as a solvent at 170 °C or they were catalyzed by CuI and required the presence of 1,10-phenanthroline ligand alongside an excess amount of lithium carbonate (Scheme 11 c).[117] Yu group in 2014 developed reaction conditions (DMF/DMSO 7 : 1 mixture; 120 °C; 3 eq. of $CuCl_2$ and 3 eq. of K_3PO_4) that resulted in the formation of indoles with alkylthio substituents at the indole *C*2 position (Scheme 11 e).[119]

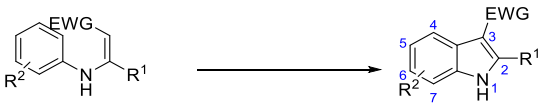

a) cat. Pd, eq. Cu, base (Glorius, 2008)
R^1 = Me; R^2 = H, Me, Cl, F, CN, OMe, COMe, CO_2Et, $CONEt_2$; EWG = CO_2Me

b) cat. Fe(III), eq. Cu(II), base (Liang, 2010)
R^1 = Me; R^2 = H, Me, Cl, Br, I, OMe, COMe; EWG = CO_2Me, CO_2Et

c) cat. Cu(I), ligand, base (Cacchi, 2009)
R^1 = aryl; R^2 = H, Me, F, Cl, Br, I, OMe, COMe, CO_2Et; EWG = COAr

d) eq. Cu(I) (Taylor, 2015)
R^1 = aryl; R^2 = H, OMe; EWG = CO_2Et

e) eq. Cu(II), base (Yu, 2014)
R^1 = SMe, SEt; R^2 = H, Me, Cl, F, OMe, OEt; EWG = COMe, COAr

f) eq. I(III) (Zhao, 2009)
R^1 = alkyl, aryl, CO_2Et; R^2 = H, Me, OMe, Br, F; EWG = CN, NO_2, CO_2Me, COPh

g) cat. I_2, oxidant (Li, 2011)
R^1 = alkyl, aryl; R^2 = H, Me, OMe, Br, I, CF_3; EWG = CO_2Me, CO_2Et, CO_2Ph, CONHPh

h) cat. *n*-Bu_4NI, oxidant (Chan, 2013)
R^1 = aryl; R^2 = H, Me, OMe, Br, Cl, I, NO_2, CF_3; EWG = COPh, CO_2Et, CONHPh

i) eq. CBr_4, base (Li, 2021)
R^1 = alkyl, aryl; R^2 = H, alkyl, OMe, F, Cl, Br, Ph; EWG = COMe, CO_2Et, COPh

Scheme 11. Reported studies on the synthesis of 2,3-substituted 1*H*-indoles starting from enamines.[115–122]

The Zhao group developed metal-free conditions for enamine conversion to indoles using an equimolar amount of hypervalent iodine reagent (Scheme 11 f).[120] Reactions yielded products in 33–91 % yields and also worked with such EWG as -CN and -NO_2 groups. The Li group published work where elemental iodine was used as a catalyst and NBS as an oxidant for indole synthesis. This system of reagents is proven to work better for aryl than alkyl substituents in enamine (Scheme 11 g). A catalytic amount of *n*-butylammonium bromide and a stoichiometric amount of *tert*-butyl hydroperoxide also promoted this indole cyclization but required a much longer reaction time – 24 h (Scheme 11 h).[121] The most recent studies on the topic are from the Li group that succeeded in the indole cyclization in the presence of CBr_4 and a base (Scheme 11 i), but under those conditions, bromination of the aromatic ring was possible as a side reaction.[122]

Although the amount of research on aromatic enamine transformations into indoles is impressive, the diversity of substituents at indole *C*2 and *C*3 positions is limited, lacking in substituents connected via the C-N bond to the indole *C*2 position. Heteroaryl structures that contain indole moieties are found extensively in bioactive molecules and pharmaceuticals, for example, Eudistomin U, Topsentin, and Wakayin.[123, 124] The usual way of heteroarylation of indoles includes C-H activation, and the indole core possesses six free C-H bonds.[124, 125] Indole *C*3 and *C*2 positions are the most reactive, and by changing reaction temperature and substrate, the regioselectivity of C-H activations could be controlled. To derivatize other positions through C-H activation, the introduction of the directing groups into the indole core is required. This all prompted the development of a new synthetic pathway for the synthesis of 1*H*-indoles, which contain ester and heterocyclic substituents at *C*2 and *C*3 positions, reported in this Doctoral Thesis.

Compound **73**, which possessed two electron-withdrawing moieties connected to triazole, was synthesized using a triazole ring-opening reaction. For this transformation, we chose carbazole as a nucleophile due to its extensive use in fluorescent materials[126] and its presence in active natural alkaloids.[127] By mixing triazole **73**, *t*-BuOK, and carbazole in DMF at 100 °C (Scheme 12), we obtained ethene-1,1-diamine derivative **74** in 64 % yield. Afterwards, we sought reaction conditions for the indole cyclization from the obtained compound **74**. After examination of the reported methods in the literature (Scheme 11), we applied some of the Pd and Cu metal-catalyzed reaction conditions alongside metal-free approaches and found out that the I_2/K_2CO_3 combination led to the formation of target indole **75**. Using a stepwise approach for the reaction sequence **73** → **74** → **75**, product **75** was obtained in a 26 % total yield, but the one-pot approach gave compound **75** in a bit lower 19 % yield.

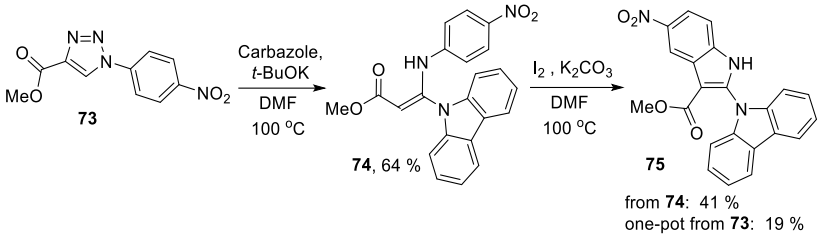

Scheme 12. Triazole **62** ring-opening reaction with carbazole and cyclization into indole.

After that, we tried to expand the scope of the substituents and synthesized triazoles **76a-g** for the ring-opening reactions (Scheme 13). In the case of compounds **76a-c**, we have found out that while triazole ring-opening products **77a-c** were forming, they were never successfully isolated, rapidly degrading during isolation and purification processes. So, we started adding I_2 and K_2CO_3 to the reaction mixture after confirming the triazole ring opening and observed only the formation of products **78a-c**.

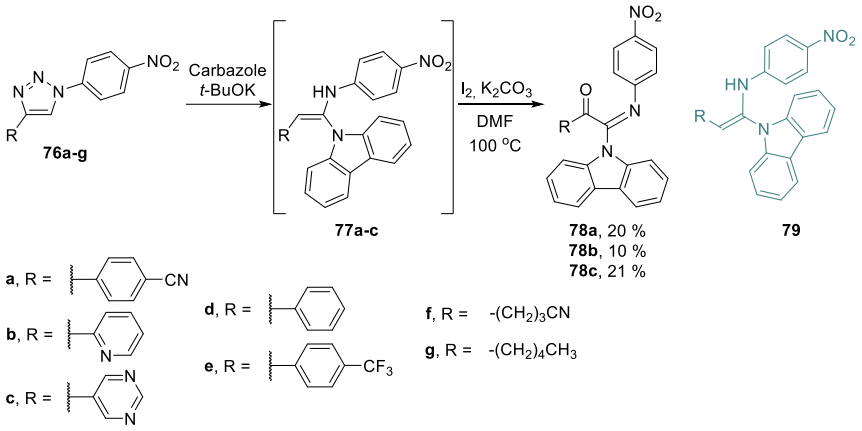

Scheme 13. Ring-opening reactions of triazoles **76** with carbazole.

In the case of triazole derivatives **76d-g**, they rapidly degraded during the reactions into various unidentifiable mixtures of products. The structure of compound **78b** was proven by a single-crystal X-ray analysis (Fig. 13). We concluded that the triazole ring-opening reaction, followed by a cyclization reaction into indole, works only with starting materials that possess strong electron-withdrawing substituents at the triazole ring.

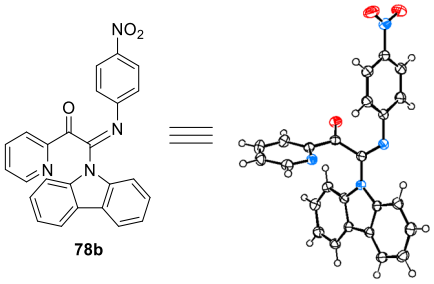

Fig. 13. X-ray crystallographic analysis of compound **78b**.

Next, we applied the developed synthetic sequence to triazolyl purines **80**, creating aromatic enamines **81** that we subsequently cyclized into 1*H*-indole derivatives **82** (Table 7). Both stepwise and one-pot approaches were used.

Table 7

Ring-opening reactions of triazoles **80** with subsequent ring cyclization into indoles

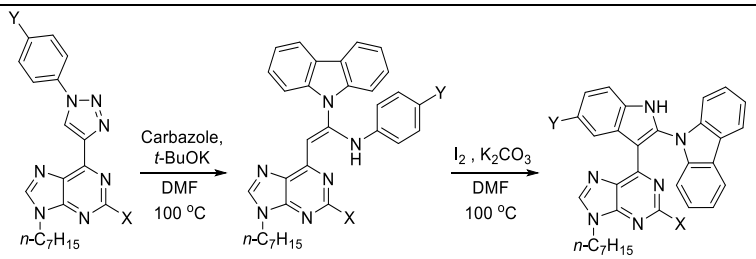

Entry	Starting Material	Substituents		Yield of **81**, %	Yield of **82**, %	Yield of **82**, %
		X	Y	**80→81**	**81→82**	**80→[81]→82**
1	**80a**	Cl	H	**81a**, 63	**82a**, 84	**82a**, 63
2	**80b**	Cl	NO_2	**81b**, 84	**82b**, 60	**82b**, 48
3	**80c**	Cl	OMe	**81c**, 69	**82c**, 75	**82c**, 48
4	**80d**	Cl	CN	**81d**, 88	**82d**, 57	**82d**, 70
5	**80e**	Cl	NMe_2	**81e**, 68[a]	–	–
6	**80f**	H	H	–	–	**82f**, 35
7	**80g**	H	NO_2	–	–	**82g**, 55
8	**80h**		H	**81h**, 33	–	–

[a] The reaction performed at 25 °C.

In the reaction, we used triazolyl purines **80**, with different substituents at the purine *C*2 position. In the case of the *N*,*N*-dimethylamino group containing derivative **80e**, the triazole ring-

opening reaction occurred only by lowering the temperature, while the cyclization product in the next step was not obtained, probably due to the strong donor effect of *N*,*N*-dimethylamino group.

In all cases, the triazole ring-opening reactions produced compounds **81** as the only products. The yields of the final products **82** were either significantly higher or just slightly lower in the case of one-pot reactions when compared to the stepwise approach, so for starting materials **80f-g,** we decided to use only the one-pot approach. If purine derivative **80h** with two triazole rings at *C*2 and *C*6 positions is used, then, under our reaction conditions, only one triazole at *C*6 position is opened (Table 7, entry 8).

In order to prove the double bond configuration of the formed products **81**, to verify the structure of the target purine–indole conjugates **82**, and elucidate which triazole ring opened in the case of compound **81h**, single crystal X-ray crystallographic analyses were performed for compounds **81b**, **81h** and **82b** (Fig. 14).

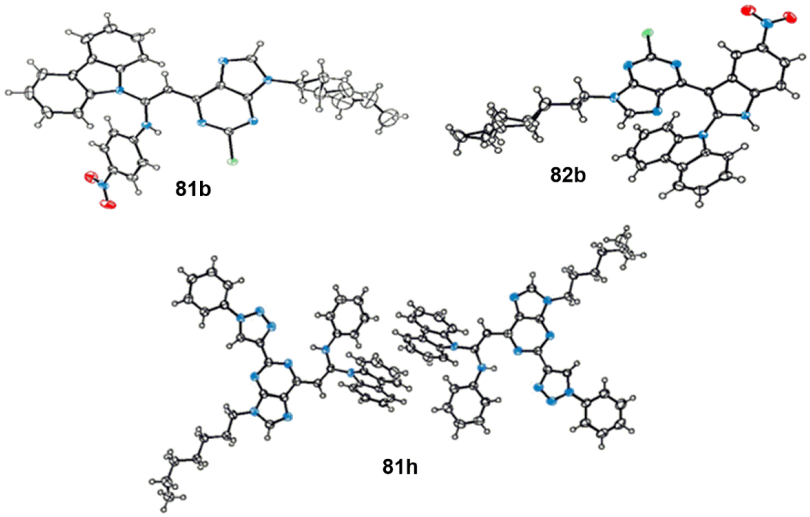

Fig. 14. X-ray crystallographic analyses of compounds **81b**, **81h**, and **82b**.

Next, we explored the application of other *N*-nucleophiles in our developed reaction sequence. Triazolyl purines **80a** and **80b** underwent reactions with diphenylamine as a nucleophile, yielding expected ethene-1,1-diamines **83a-b** (Scheme 14). In the cyclization reactions, however, the formation of *N*-phenyl substituted indoles **84** was observed – cyclization occurred at the phenyl ring of the nucleophile instead of the aniline moiety. The total yield of the one-pot approach was higher than that of using the same reactions in a stepwise approach.

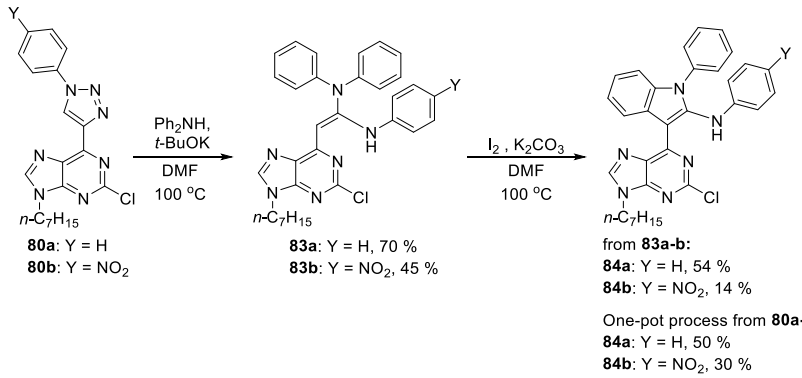

80a: Y = H
80b: Y = NO_2

83a: Y = H, 70 %
83b: Y = NO_2, 45 %

from **83a-b:**
84a: Y = H, 54 %
84b: Y = NO_2, 14 %

One-pot process from **80a-b:**
84a: Y = H, 50 %
84b: Y = NO_2, 30 %

Scheme 14. Synthesis of *N*-phenyl-containing indole derivatives **84** from triazolyl purines **80a-b**.

The chemical structure of products **84a-b** was proven by crystallographic analysis of compound **84b** (Fig. 15).

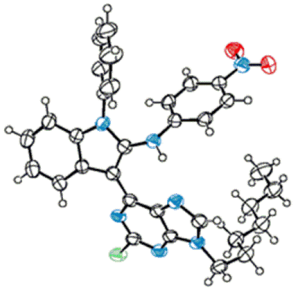

Fig. 15. X-ray crystallographic analysis of compound **84b**.

During triazole ring opening, the formation of intermediate **A** is possible (Scheme 10 a), which is attacked by a nucleophile, forming products **B** (Scheme 15). In cyclization reactions with carbazole, a double bond of ethene-1,1-diamine **C** cyclizes with the aryl moiety, even with electron-deficient substituents like CN and NO_2 groups on it. This indicates that the flexible nature of the *N*-linker is more important for this transformation than electronic effects. In the case of diphenylamine-containing compounds **D**, cyclization into indoles **84** occurs selectively, even with compound **84a**, which contained three phenyl rings without any substituents, making us suggest that both electronic effects and accessibility to the phenyl ring play an important role in it.

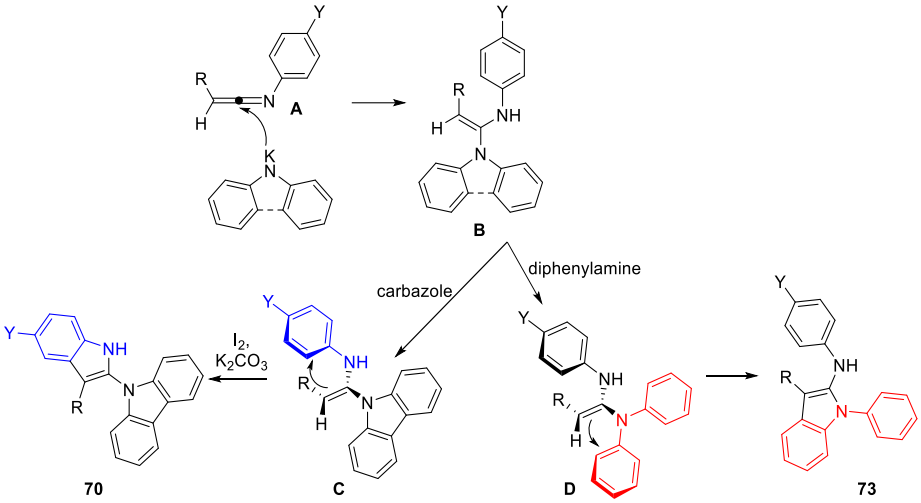

Scheme 15. Triazole ring opening and regioselectivity of cyclization reactions.

The original publication of the research described in this chapter can be found in Appendix VIII.

CONCLUSIONS

1. Quantum yields of novel 2-piperidinyl-6-(1*H*-1,2,3-triazol-4-yl)-9*H*-purine derivatives reach up to 81 % in DCM, 95 % in DMSO and 35 % in thin layer films. Quantum yields for C-C and C-N bonded triazolylpurine analogs that contain 4-methoxyphenyl group at the triazole are 95 % and 98 %, respectively. Quantum yields of 2,6-bis-(1*H*-1,2,3-triazol-4-yl)-9*H*-purine derivatives reach up to 49 % in DMSO, whereas the quantum yield of C-N bonded 2,6-bis-(1*H*-1,2,3-triazol-1-yl)-9*H*-purine derivative is only 24 % in DMSO, which is twice lower than for its C-C analog.

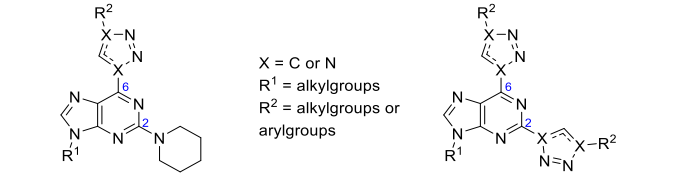

QY up to 81 % in DCM or 98 % in DMSO
QY up to 35 % in thin layer films

QY up to 26 % in DCM or 49 % in DMSO

2. The introduction of pyridinium moieties to the *N*9 position of 2-amino-6-triazolyl purine derivatives, when compared to the introduction of 1,3-propandiol group, increases the compound's solubility in water from 0.21 mg/mL to 133 mg/mL but completely quenches the fluorescence.

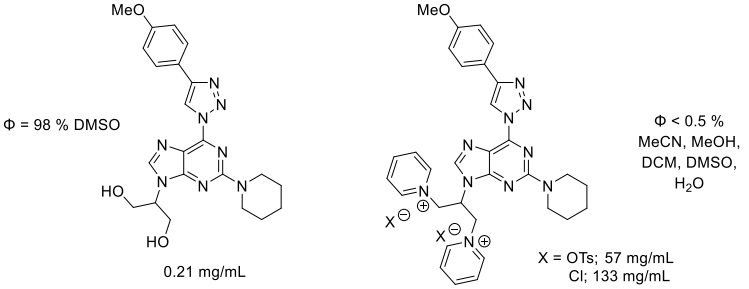

3. 6-Methoxyphenyltriazolyl-2-piperidinyl purine derivatives with *n*-heptyl or TEG moieties at the purine *N*9 position coordinate Hg^{2+} ions between the purine *N*7 and triazole *N*3 atoms. As a result of complexation, the fluorescence of the compound is quenched; thus, these compounds can potentially be used as Hg^{2+} metal ion sensors in solutions or living cells.

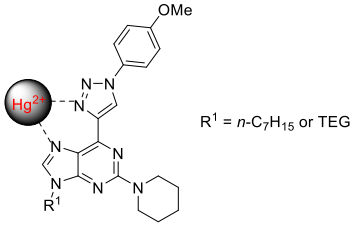

4. 6-Triazolyl-8-aryl purine derivative that contains 1,4,7,10-tetraazacyclododecane (cyclen) moiety at the purine *N*9 position can be synthesized in 9 steps using Mitsunobu, iodination, Stille, S_NAr, CuAAC, and alkylation reactions as main transformations, sequentially modifying the *N*9→*C*8→*C*6→*N*9 positions of the purine core. NMR titration studies indicate that the purine-cyclen conjugate forms complexes with Cu^{2+} metal ions with possible complexation sites in the cyclen moiety and between the triazole *N*2 and purine *N*7 nitrogen atoms, quenching fluorescence.

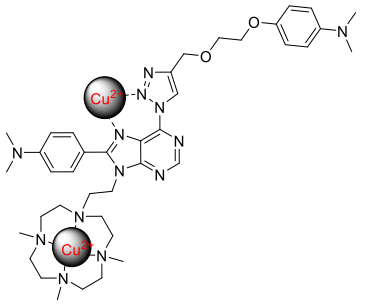

5. Triazole ring-opening reactions using carbazole and diphenylamine nucleophiles result in the formation of ethene-1,1-diamines, which can be cyclized into 1*H*-free or 1-phenyl substituted indoles, depending on the nature of the substituents at the ethene double bond. For this transformation to happen, a strong EWG is required at the triazole ring. One such EWG is purine, which promotes the formation of purine-indole conjugates.

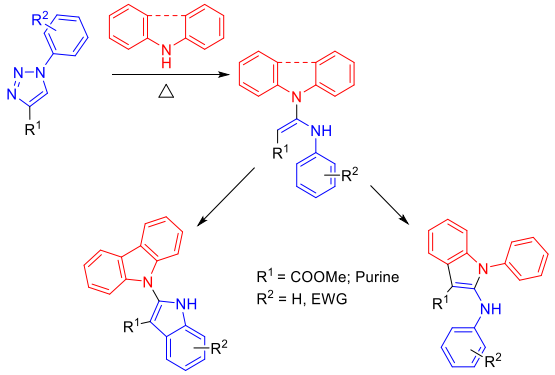

LITERATŪRAS SARAKSTS / REFERENCES

(1) Shaw, G. 4.09-Purines. In Comprehensive Heterocyclic Chemistry; Katritzky, A.R., Rees, C.W., Eds.; Elsevier: Pergamon, Turkey, 1984; Volume 5, pp. 499–605.

(2) Schmidt, A. P.; Lara, D. R.; Souza, D. O. *Pharmacol. Ther.* **2007**, *116* (3), 401–416.

(3) Rosemeyer, H. The Chemodiversity of Purine as a Constituent of Natural Products. *Chem. Biodivers.* **2004**, *1* (3), 361–401.

(4) Yang, Y.; Cohn, P.; Dyer, A. L.; Eom, S.-H.; Reynolds, J. R.; Castellano, R. K.; Xue, J. *Chem. Mater.* **2010**, *22* (12), 3580–3582.

(5) Yang, Y.; Cohn, P.; Eom, S. H.; Abboud, K. A.; Castellano, R. K.; Xue, J. *J. Mater. Chem. C.* **2013**, *1* (16), 2867–2874.

(6) Wang, Z.; Yao, J.; Zhan, L.; Gong, S.; Ma, D.; Yang, C. *Dye. Pigment.* **2020**, *180*, 108437.

(7) Wang, H.; Zhang, J.; Shi, R.; Yang, J.; Song, W.; Bai, Q.; Shen, Y. *Opt. Mater.* **2023**, *138*, 113708.

(8) Chen, X.; Mao, Y.; Wang, A.; Lu, L.; Shao, Q.; Jiang, C.; Lu, H. *Spectrochim. Acta – Part A Mol. Biomol. Spectrosc.* **2024**, *304*, 123291.

(9) Xu, H.; Chen, W.; Ju, L.; Lu, H. *Spectrochim. Acta – Part A Mol. Biomol. Spectrosc.* **2021**, *247*, 119074.

(10) Shao, Q.; Jiang, C.; Chen, X.; Wang, A.; Lu, L.; Chen, L.; Lu, H. *Spectrochim. Acta – Part A Mol. Biomol. Spectrosc.* **2023**, *296*, 122676.

(11) Wang, A.; Mao, Y.; Chen, X.; Lu, L.; Jiang, C.; Lu, H. *Spectrochim. Acta – Part A Mol. Biomol. Spectrosc.* **2024**, *308*, 123674.

(12) Dong, Y.; Yang, Y.; Tao, Y.; Fang, M.; Li, C.; Zhu, W. *J. Fluoresc.* **2024**. https://doi.org/10.1007/s10895-024-03961-w.

(13) Jin, W. J.; Zhu, R. H.; Shang, X. H.; Dong, C.; Zhang, W. Y.; Liu, C. S. *Spectrochim. Acta – Part A Mol. Biomol. Spectrosc.* **1997**, *53* (11), 1735–1742.

(14) Aaron, J. J.; Winefordner, J. D. *Anal. Chem.* **1972**, *44* (13), 2127–2131.

(15) Wei, Y.; Ding, L.; Li, J.; Wei, Y.; Dong, C. *Anal. Lett.* **2004**, *37* (3), 435–448.

(16) Hocek, M.; Pohl, R. *Synthesis.* **2004**, *17*, 2869–2876.

(17) Novosjolova, I.; Bizdena, E.; Turks, M. *European J. Org. Chem.* **2015**, *2015* (17), 3629–3649.

(18) Zaķis, J. M.; Ozols, K.; Novosjolova, I.; Vilšķērsts, R.; Mishnev, A.; Turks, M. *J. Org. Chem.* **2020**, *85* (7), 4753–4771.

(19) Mahajan, T. R.; Ytre-Arne, M. E.; Strøm-Andersen, P.; Dalhus, B.; Gundersen, L. L. *Molecules* **2015**, *20* (9), 15944–15965.

(20) Nolsøe, J. M. J.; Gundersen, L. L.; Rise, F. *Acta Chem. Scand.* **1999**, *53*, 366–372.

(21) Wang, D. C.; Niu, H. Y.; Qu, G. R.; Liang, L.; Wei, X. J.; Zhang, Y.; Guo, H. M. *Org. Biomol. Chem.* **2011**, *9* (22), 7663–7666.

(22) Gundersen, L. L.; Langli, G.; Rise, F. *Tetrahedron Lett.* **1995**, *36* (11), 1945–1948.

(23) Strouse, J. J.; Ješelnik, M.; Arterburn, J. B. *Acta Chim. Slov.* **2005**, *52* (3), 187–199.
(24) Havelková, M.; Dvořák, D.; Hocek, M. *Synthesis* **2001**, *11*, 1704–1710.
(25) Čerňa, I.; Pohl, R.; Klepetářová, B.; Hocek, M. *J. Org. Chem.* **2008**, *73* (22), 9048–9054.
(26) Abdoli, M.; Mirjafary, Z.; Saeidian, H.; Kakanejadifard, A. *RSC Adv.* **2015**, *5* (55), 44371–44389.
(27) Sebris, A.; Novosjolova, I.; Turks, M. *Synthesis* **2022**, *54* (24), 5529–5539.
(28) Jovaisaite, J.; Cīrule, D.; Jeminejs, A.; Novosjolova, I.; Turks, M.; Baronas, P.; Komskis, R.; Tumkevicius, S.; Jonusauskas, G.; Jursenas, S. *Phys. Chem. Chem. Phys.* **2020**, *22* (45), 26502–26508.
(29) Li, J. P.; Wang, H. X.; Wang, H. X.; Xie, M. S.; Qu, G. R.; Niu, H. Y.; Guo, H. M. *European J. Org. Chem.* **2014**, *2014* (11), 2225–2230.
(30) Sebris, A.; Novosjolova, I.; Traskovskis, K.; Kokars, V.; Tetervenoka, N.; Vembris, A.; Turks, M. *ACS Omega* **2022**, *7* (6), 5242–5253.
(31) Sebris, A.; Traskovskis, K.; Novosjolova, I.; Turks, M. *Chem. Heterocycl. Compd.* **2021**, *57* (5), 560–567.
(32) Inman, M.; Moody, C. J. *Chem. Sci.* **2013**, *4* (1), 29–41.
(33) Dorababu, A. *RSC Med. Chem.* **2020**, *11* (12), 1335–1353.
(34) Nan, M.; Niu, W.; Fan, L.; Lu, W.; Shuang, S.; Li, C.; Dong, C. *RSC Adv.* **2015**, *5* (121), 99739–99744.
(35) Wang, Q.; Li, D.; Rao, N.; Zhang, Y.; Le, Y.; Liu, L.; Huang, L.; Yan, L. *Dye. Pigment.* **2021**, *188*, 109166.
(36) Schlitt, K. M.; Millen, A. L.; Wetmore, S. D.; Manderville, R. A. *Biomol. Chem.* **2011**, *9* (5), 1565–1571.
(37) Fadock, K. L.; Manderville, R. A.; Sharma, P.; Wetmore, S. D. *Org. Biomol. Chem.* **2016**, *14* (19), 4409–4419.
(38) Rankin, K. M.; Sproviero, M.; Rankin, K.; Sharma, P.; Wetmore, S. D.; Manderville, R. A. *J. Org. Chem.* **2012**, *77* (23), 10498–10508.
(39) Ye, F.; Chen, L.; Hu, L.; Xiao, T.; Yu, S.; Chen, D.; Wang, Y.; Liang, G.; Liu, Z.; Wang, S. *Bioorganic Med. Chem. Lett.* **2015**, *25* (7), 1556–1560.
(40) Guo, S. Y.; Wei, L. Y.; Song, B. B.; Hu, Y. T.; Jiang, Z.; Zhao, D. D.; Xu, Y. H.; Lin, Y. W.; Xu, S. M.; Chen, S. Bin; Huang, Z. S. *Eur. J. Med. Chem.* **2023**, *260*, 115729.
(41) Debnath, P. *ChemistrySelect* **2023**, *8* (26). https://doi.org/10.1002/slct.202300998.
(42) Zeng, Q.; Huang, B.; Danielsen, K.; Shukla, R.; Nagy, T. *Org. Process Res. Dev.* **2004**, *8* (6), 962–963.
(43) Davoll, J.; Lowy, B. A. *J. Am. Chem. Soc.* **1951**, *73* (6), 2936.
(44) Hocek, M. *European J. Org. Chem.* **2003**, 245–254.
(45) Seela, F.; Ramzaeva, N.; Rosemeyer, H. Product Class 17: Purines. In *Science of Synthesis, 16: Category 2, Hetarenes and Related Ring Systems*. Yamamoto, Y.; Shinkai, I., Eds.; Georg Thieme Verlag, Germany; Volume 16, pp. 945–1108.

(46) Seela, F. *Nucleosides and Nucleotides* **1995**, *14* (6), 1403–1414.
(47) Kania, J.; Gundersen, L. L. *European J. Org. Chem.* **2013**, *10*, 2008–2019.
(48) Kriķis, K. Ē.; Novosjolova, I.; Mishnev, A.; Turks, M. *Beilstein J. Org. Chem.* **2021**, *17*, 193–202.
(49) Duarte, L. F. B.; Oliveira, R. L.; Rodrigues, K. C.; Voss, G. T.; Godoi, B.; Schumacher, R. F.; Perin, G.; Wilhelm, E. A.; Luchese, C.; Alves, D. *Bioorganic Med. Chem.* **2017**, *25* (24), 6718–6723.
(50) Legraverend, M. *Tetrahedron* **2008**, *64* (37), 8585–8603.
(51) Liu, J.; Robins, M. J. *J. Am. Chem. Soc.* **2007**, *129* (18), 5962–5968.
(52) Cīrule, D.; Novosjolova, I.; Bizdēna, Ē.; Turks, M. *Beilstein J. Org. Chem.* **2021**, *17*, 410–419.
(53) Kovaļovs, A.; Novosjolova, I.; Bizdēna, E.; Bižane, I.; Skardziute, L.; Kazlauskas, K.; Jursenas, S.; Turks, M. *Tetrahedron Lett.* **2013**, *54* (8), 850–853.
(54) Zhong, M.; Nowak, I.; Robins, M. J. *Org. Lett.* **2005**, *7* (21), 4601–4603.
(55) Arico, J. W.; Calhoun, A. K.; Salandria, K. J.; McLaughlin, L. W. *Org. Lett.* **2010**, *12* (1), 120–122.
(56) Robins, M. J.; Zou, R.; Guo, Z.; Wnuk, S. F. *J. Org. Chem.* **1996**, *61* (26), 9207–9212.
(57) Saneyoshi, M.; Satoh, E. *Chem. Pharm. Bull.* **1979**, *27* (10), 2518–2521.
(58) Behrouz, S.; Soltani Rad, M. N.; Ahmadi, S. *Tetrahedron* **2019**, *75* (36), 130499.
(59) Mao, R.; Sun, L.; Wang, Y. S.; Zhou, M. M.; Xiong, D. C.; Li, Q.; Ye, X. S. *Chinese Chem. Lett.* **2018**, *29* (1), 61–64.
(60) Xu, S.; Luo, Z.; Jiang, Z.; Lin, D. *Synlett* **2017**, *28* (7), 868–872.
(61) Tranová, L.; Stýskala, J. *J. Org. Chem.* **2021**, *86* (19), 13265–13275.
(62) Niu, H. Y.; Su, L. Y.; Bai, S. X.; Li, J. P.; Feng, X. L.; Guo, H. M. *Chinese Chem. Lett.* **2017**, *28* (1), 105–108.
(63) Larsen, A. F.; Ulven, T. *Chem. Commun.* **2014**, *50* (39), 4997–4999.
(64) Cheney, G. E.; Freiser, H.; Fernando, Q.; Freiser, H. *J. Am. Chem. Soc.* **1959**, *81* (11), 2611–2615.
(65) Taqui Khan, M. M.; Krishnamoorthy, C. R. *J. Inorg. Nucl. Chem.* **1971**, *33*, 1417–1425.
(66) Ghosh, S. *Bioorg. Chem.* **2019**, *88*, 102925.
(67) Dasari, S.; Bernard Tchounwou, P. *Eur. J. Pharmacol.* **2014**, *740*, 364–378.
(68) Macomber, R. S. *J. Chem. Educ.* **1992**, *69* (5), 375–378.
(69) Jopa, S.; Wójcik, J.; Ejchart, A.; Nowakowski, M. *J. Incl. Phenom. Macrocycl. Chem.* **2024**, *104* (11), 547–568.
(70) Popov, K.; Rönkkömäki, H.; Lajunen, L. H. J. *Pure Appl. Chem.* **2006**, *78* (3), 663–675.
(71) Szakács, Z.; Hägele, G. *Talanta* **2004**, *62* (4), 819–825.
(72) Matsika, S. *J. Phys. Chem. A* **2004**, *108* (37), 7584–7590.
(73) Butler, R. S.; Cohn, P.; Tenzel, P.; Abboud, K. A.; Castellano, R. K. *J. Am. Chem. Soc.* **2009**, *131* (2), 623–633.

(74) Gao, S. H.; Xie, M. S.; Wang, H. X.; Niu, H. Y.; Qu, G. R.; Guo, H. M. *Tetrahedron* **2014**, *70* (33), 4929–4933.
(75) Tao, X.; Mao, Y.; Alam, S.; Wang, A.; Qi, X.; Zheng, S.; Jiang, C.; Chen, S. Y.; Lu, H. *Spectrochim. Acta – Part A Mol. Biomol. Spectrosc.* **2024**, *314*, 124226.
(76) Joseph, M. C.; Swarts, A. J.; Mapolie, S. F. *Coord. Chem. Rev.* **2023**, *493*, 215317.
(77) Todorov, L.; Kostova, I. *Front. Chem.* **2023**, *11*, 1–9.
(78) Sumrra, S. H.; Habiba, U.; Zafar, W.; Imran, M.; Chohan, Z. H. *J. Coord. Chem.* **2020**, *73*, 2838–2877.
(79) Raman, A. P. S.; Aslam, M.; Awasthi, A.; Ansari, A.; Jain, P.; Lal, K.; Bahadur, I.; Singh, P.; Kumari, K. *Mol. Divers.* **2024**, *29*, 899–964.
(80) Dai, J.; Tian, S.; Yang, X.; Liu, Z. *Front. Chem.* **2022**, *10*, 1–24.
(81) Matin, M. M.; Matin, P.; Rahman, M. R.; Ben Hadda, T.; Almalki, F. A.; Mahmud, S.; Ghoneim, M. M.; Alruwaily, M.; Alshehri, S. *Front. Mol. Biosci.* **2022**, *9*, 1–8.
(82) Rahman, M. T.; Decker, A. M.; Laudermilk, L.; Maitra, R.; Ma, W.; Ben Hamida, S.; Darcq, E.; Kieffer, B. L.; Jin, C. *J. Med. Chem.* **2021**, *64* (16), 12397–12413.
(83) Bonandi, E.; Christodoulou, M. S.; Fumagalli, G.; Perdicchia, D.; Rastelli, G.; Passarella, D. *Drug Discov. Today* **2017**, *22* (10), 1572–1581.
(84) Johansson, J. R.; Beke-Somfai, T.; Said Stålsmeden, A.; Kann, N. *Chem. Rev.* **2016**, *116* (23), 14726–14768.
(85) Šišuļins, A.; Bucevičius, J.; Tseng, Y. T.; Novosjolova, I.; Traskovskis, K.; Bizdēna, Ē.; Chang, H. T.; Tumkevičius, S.; Turks, M. *Beilstein J. Org. Chem.* **2019**, *15* (9), 474–489.
(86) Traskovskis, K.; Rudušs, A.; Kokars, V.; Mihailovs, I.; Lesina, N.; Vembris, A. *New J. Chem.* **2019**, *43* (1), 37–47.
(87) Novosjolova, I.; Bizdēna, E.; Turks, M. *Tetrahedron Lett.* **2013**, *54* (48), 6557–6561.
(88) Islam, M. B.; Islam, M. I.; Nath, N.; Emran, T. Bin; Rahman, M. R.; Sharma, R.; Matin, M. M. *Biomed Res. Int.* **2023**, *2023*, 9967591.
(89) Sajomsang, W.; Gonil, P.; Ruktanonchai, U. R.; Petchsangsai, M.; Opanasopit, P.; Puttipipatkhachorn, S. *Carbohydr. Polym.* **2013**, *91* (2), 508–517.
(90) Janssen, P. G. A.; Ruiz-Carretero, A.; González-Rodriguez, D.; Meijer, E. W.; Schenning, H. J. *Angew. Chemie - Int. Ed.* **2009**, *48* (43), 8103–8106.
(91) Stevens, A. L.; Janssen, P. G. A.; Ruiz-Carretero, A.; Surin, M.; Schenning, H. J.; Herz, L. M. *J. Phys. Chem. C* **2011**, *115* (21), 10550–10560.
(92) Kumar, V.; Schlücker, S.; Hasselbrink, E. Chapter 16 - Ultrafast Time-Resolved Molecular Spectroscopy In Molecular and Laser Spectroscopy; Gupta, V. P., Ozaki, Y.. Eds.; Elsevier, 2020; Volume 2, pp. 563–594.
(93) Maillard, J.; Klehs, K.; Rumble, C.; Vauthey, E.; Heilemann, M.; Fürstenberg, A. *Chem. Sci.* **2021**, *12* (4), 1352–1362.
(94) Hong, Y. S.; Kim, Y. M.; Lee, K. E. *J. Prev. Med. Public Heal.* **2012**, *45* (6), 353–363.
(95) Briffa, J.; Sinagra, E.; Blundell, R. *Heliyon* **2020**, *6* (9), e04691.

(96) Wang, Y.; Zhang, L.; Han, X.; Zhang, L.; Wang, X.; Chen, L. *Chem. Eng. J.* **2021**, *406*, 127166.
(97) Kobayashi, S.; Busujima, T.; Nagayama, S. *Chem. – A Eur. J.* **2000**, *6* (19), 3491–3494.
(98) Harmand, L.; Cadet, S.; Kauffmann, B.; Scarpantonio, L.; Batat, P.; Jonusauskas, G.; McClenaghan, N. D.; Lastécouères, D.; Vincent, J. M. *Angew. Chemie – Int. Ed.* **2012**, *51* (29), 7137–7141.
(99) Mongin, C.; Pianet, I.; Jonusauskas, G.; Bassani, D. M.; Mongin, C.; Pianet, I.; Jonusauskas, G.; Bassani, D. M.; Bibal, B. *ACS Catal.* **2015**, *5* (1), 380–387.
(100) Tosato, M.; Asti, M.; Dalla Tiezza, M.; Orian, L.; Häussinger, D.; Vogel, R.; Köster, U.; Jensen, M.; Andrighetto, A.; Pastore, P.; Marco, V. Di. *Inorg. Chem.* **2020**, *59* (15), 10907–10919.
(101) Delgado, R.; Félix, V.; Lima, L. M. P.; Price, D. W. *Dalt. Trans.* **2007**, *26*, 2734–2745.
(102) Lima, L. M. P.; Esteban-Gómez, D.; Delgado, R.; Platas-Iglesias, C.; Tripier, R. *Inorg. Chem.* **2012**, *51* (12), 6916–6927.
(103) Sessler, J. L.; Sathiosatham, M.; Doerr, K.; Lynch, V.; Abboud, K. A. *Angew. Chem. Int. Ed. Engl.* **2000**, *39* (7), 1300–1303.
(104) Ohashi, M.; Konkol, M.; Del Rosal, I.; Poteau, R.; Maron, L.; Okuda, J. *J. Am. Chem. Soc.* **2008**, *130* (22), 6920–6921.
(105) Fulloon, B. E.; Wentrup, C. *Org. Chem.* **1996**, *61* (4), 1363–1367.
(106) Rao, V. V. R.; Wentrup, C. *J. Chem. Soc. Perkin Trans. 1* **1998**, *16*, 2583–2586.
(107) Fulloon, B. E.; Wentrup, C. *Aust. J. Chem.* **2009**, *62* (2), 115–120.
(108) Davies, H. M. L.; Alford, J. S. *Chem. Soc. Rev.* **2014**, *43* (15), 5151–5162.
(109) Horneff, T.; Chuprakov, S.; Chernyak, N.; Gevorgyan, V.; Fokin, V. V. *J. Am. Chem. Soc.* **2008**, *130* (45), 14972–14974.
(110) Liu, Y.; Xie, P.; Li, J.; Bai, W. J.; Jiang, J. *Org. Lett.* **2019**, *21* (13), 4944–4949.
(111) Fan, W.; Katritzky, A. R. 5.01 - 1,2,3-Triazoles. In Comprehensive Heterocyclic Chemistry; Katritzky, A.R., Rachwal, S. Eds.: Elsevier, 2008; Volume 5, pp. 1–158.
(112) Gribble, G. W. *J. Chem. Soc. Perkin Trans. 1* **2000**, *7*, 1045–1075.
(113) Humphrey, G. R.; Kuethe, J. T. *Chem. Rev.* **2006**, *106* (7), 2875–2911.
(114) Kochanowska-Karamyan, A. J.; Hamann, M. T. *Chem. Rev.* **2010**, *110* (8), 4489–4497.
(115) Würtz, S.; Rakshit, S.; Neumann, J. J.; Dröge, T.; Glorius, F. *Angew. Chemie – Int. Ed.* **2008**, *47* (38), 7230–7233.
(116) Guan, Z. H.; Yan, Z. Y.; Ren, Z. H.; Liu, X. Y.; Liang, Y. M. *Chem. Commun.* **2010**, *46* (16), 2823–2825.
(117) Bernini, R.; Fabrizi, G.; Sferrazza, A.; Cacchi, S. *Angew. Chemie - Int. Ed.* **2009**, *48* (43), 8078–8081.
(118) Drouhin, P.; Taylor, R. J. K. *European J. Org. Chem.* **2015**, *2015* (11), 2333–2336.
(119) Huang, F.; Wu, P.; Wang, L.; Chen, J.; Sun, C.; Yu, Z. *J. Org. Chem.* **2014**, *79* (21), 10553–10560.

(120) Yu, W.; Du, Y.; Zhao, K. *Org. Lett.* **2009**, *11* (11), 2417–2420.
(121) Jia, Z.; Nagano, T.; Li, X.; Chan, A. S. C. *European J. Org. Chem.* **2013**, *5*, 858–861.
(122) Zhao, L.; Qiu, C.; Zhao, L.; Yin, G.; Li, F.; Wang, C.; Li, Z. *Org. Biomol. Chem.* **2021**, *19* (24), 5377–5382.
(123) Wang, Z.; Li, K.; Zhao, D.; Lan, J.; You, J. *Angew. Chemie - Int. Ed.* **2011**, *50* (23), 5365–5369.
(124) Chen, S.; Zhang, M.; Su, R.; Chen, X.; Feng, B.; Yang, Y.; You, J. *ACS Catal.* **2019**, *9* (7), 6372–6379.
(125) Yang, Y.; Shi, Z. *Chem. Commun.* **2018**, *54* (14), 1676–1685.
(126) Wex, B.; Kaafarani, B. R. *J. Mater. Chem. C* **2017**, *5* (34), 8622–8653.
(127) Greger, H. *Phytochem. Rev.* **2017**, *16* (6), 1095–1153.

Pielikumi / Appendices

Pielikums I
Appendix I

Burcevs, A.; Novosjolova, I.

Recent Progress in the Synthesis of *N*7(*N*9)-alkyl(aryl)purines (microreview)

Chem. Heterocycl. Compd., **2022**, 58, 400–402.

doi:10.1007/s10593-022-03105-7

Chemistry of Heterocyclic Compounds **2022**, *58*(8/9), 400–402

HETERO CYCLES IN FOCUS

Recent progress in the synthesis of N^7(N^9)-alkyl(aryl)purines (microreview)

Aleksejs Burcevs[1], **Irina Novosjolova**[1]*

[1] *Institute of Technology of Organic Chemistry, Faculty of Materials Science and Applied Chemistry, Riga Technical University, 3 P. Valdena St., Riga LV-1048, Latvia; e-mail: irina.novosjolova@rtu.lv*

Published in Khimiya Geterotsiklicheskikh Soedinenii, 2022, *58*(8/9), 400–402

Submitted July 19, 2022
Accepted July 29, 2022

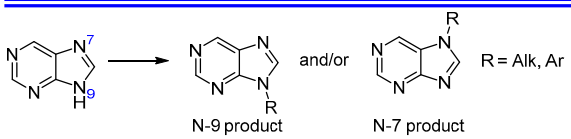

Recent progress from 2015 to 2022 in alkylation and arylation reactions of purine N-7 and N-9 positions is shown.

Introduction

Purine derivatives play important role in the field of medicinal, chemical, and biological research,[1] but one of the major problems in the synthesis of such compounds is the selectivity of alkylation/arylation reactions. Sometimes the mixture of N-9- and N-7-derived products is obtained. Usual methods of purine alkylation include the use of carbon electrophiles, such as alkyl halides, epoxides, ethers,[2] and Mitsunobu and aza-Michael reactions.[3] While arylation of purines is selective and occurs at N-9 position, few new methods have been developed over these years. Approaches toward purine derivatization at N-7 and N-9 positions from 2015 to 2022 are summarized in this review.

N-7 Alkylation

Stýskala group[4] has developed a method for the synthesis of N-7-alkylated purine glycosides **2**, starting with an introduction of a TMS group in 6-chloropurine or 2,6-dichloropurine **1** using *N*,*O*-bis(trimethylsilyl)acetamide (BSA) as a silylating reagent. The following glycosylation step of purine compounds with appropriately protected monosaccharides catalyzed by $SnCl_4$ or $TiCl_4$ in 1,2-dichloroethane provided N-7-alkylated products as the prevailing regioisomers. Formation of N-7 products was favored by kinetically controlled conditions, performing the glycosylation reaction at low or room temperature for shorter time.

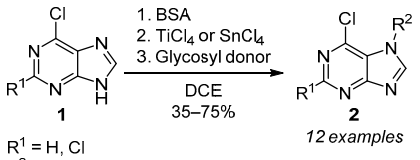

R^1 = H, Cl
R^2 = Glc-Ac, Gal-Ac, Man-Ac, Xyl-Ac, Rib-Ac, Glc-Tfc, Gal-Bz

In 2015, ring opening reaction of vinyl cyclopropane **4** with purine **3** has been reported for the construction of acyclic nucleosides.[3] In the presence of a catalytic amount of MgI_2 regioselectivity of reactions was achieved, and N-7-alkylated derivatives **5** formed as main products. Further, double bond of products **5** can be easily reduced.

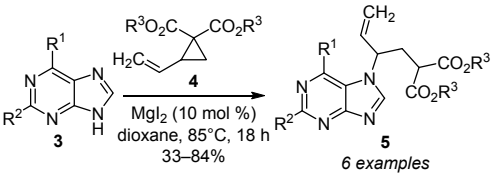

R^1 = Cl, I; R^2 = H, Cl; R^3 = Me, Et, *i*-Pr, *t*-Bu

Aleksejs Burcevs obtained his MSc in chemical engineering in 2021 from the Riga Technical University (RTU). Currently he is working toward PhD thesis under supervision of Associate Professor Irina Novosjolova at RTU. His research focuses on design and synthesis of novel purine derivatives and their application studies as TADF materials.

Irina Novosjolova obtained her doctoral degree in organic chemistry from RTU under the supervision of Professors Māris Turks and Ērika Bizdēna. Dr. Novosjolova spent two years as Postdoctoral Research Associate at the Binghamton University under the supervision of Professor Ēriks Rozners. Currently she is Associate Professor at RTU Faculty of Materials Science and Applied Chemistry and her research interests deal with chemistry and materials science of fused pyrimidines.

N-9 Alkylation

On the other hand, in the presence of an equimolar amount of $AlCl_3$, N-9-alkylated products **6** were selectively formed in the reaction between purines **3** and cyclopropanes **4**.[3] When other Lewis acids like $Sc(OTf)_3$, $In(OTf)_3$, $Cu(OTf)_2$, or $Mg(OTf)_2$ were used as catalysts, the reaction did not occur at all.

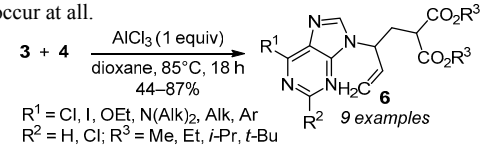

Selective synthetic approach for one-pot N-9 alkylation of purines **7** using alcohols and a mixture of P_2O_5 and KI in the presence of Et_3N and K_2CO_3, was described by Ahmadi group.[2] The main advantage of this approach was formation of water-soluble byproducts which were easily separated from products **8** by water extraction.

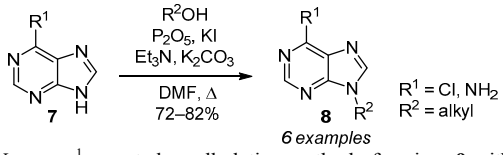

Ye group[1] reported an alkylation method of purines **9** with ethers **10** in the presence of Umemoto's reagent (**11**). C-radical of ether **10** generated in this transformation is transformed into oxocarbenium ion by an excess of Umemoto's reagent (**11**) which reacts with purine. Similarly, N-9 alkylation of purine with thioethers in the presence of phenyliodoacetate for the synthesis of compounds **12** was reported by Li group.[5]

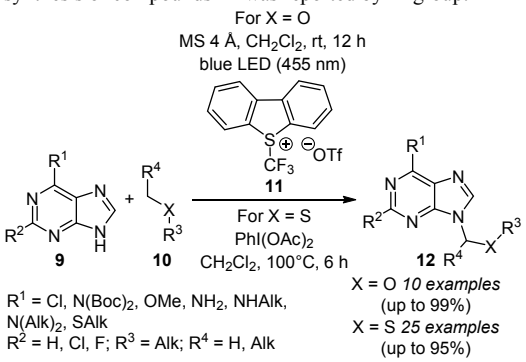

Taylor group[6] described a regioselective method of opening of epoxy alcohols **14** in the presence of diarylboronic acid catalyst **15**. Although epoxide ring was opened with purine (**13**) at compound's **14** C-3 position with good regioselectivity, the alkylation itself was less selective, yielding a 2:1 mixture of N-9 (shown on the scheme) and N-7 products **16**.

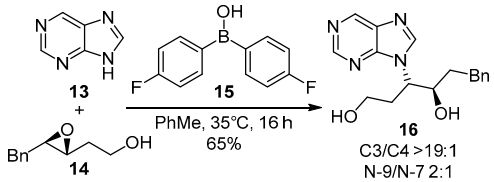

Selective N-9 amidoalkylation of purines **17** is possible using *N*,*N*-dialkylamides **18** in the presence of KI and *tert*-butyl hydroperoxide (TBHP).[7] Alkylation for the formation of products **19** occurs *via* activation of C(sp^3)–H bond adjacent to an amide nitrogen atom.

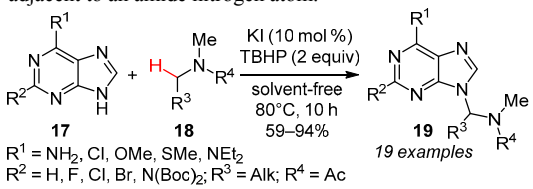

Purine **22** was synthesized *via* selective copper-catalyzed cross coupling between dichloropurine **20** and benzylic C–H-containing substrate **21** in the presence of *N*-fluorobenzenesulfonimide (NFSI), $BF_3{\cdot}Et_2O$, and diisopropylphosphite.[8]

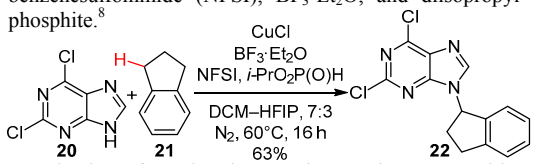

Introduction of *tert*-butyl group into purine N-9 position can be achieved in an organophotoredox-catalyzed decarboxylative cross coupling between 6-chloropurine (**23**) and compound **24** under mild and transition-metal-free conditions in the presence of pyridinium additive **26** and catalyst **25**.[9] Catalyst **25** initiates single electron transfer (SET) to ester **24**, starting the reaction, while pyridinium additive **26** inhibits the formation of elimination byproducts from the carbocation intermediate. Compound **27** was obtained in 55% yield.

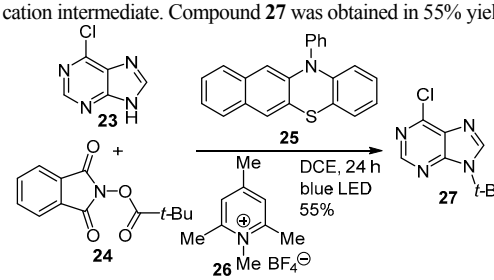

6-Chloropurine (**23**) was used in decarboxylative C–N coupling with compound **28** *via* visible light and transition-metal-mediated photoredox catalysis using iodine(III) reagent **29** for the synthesis of compound **30**.[10] In comparison, the same transformation with 2,6-dichloropurine gave mixture of N-9/N-7-alkylated products with regioselectivity 3:2.

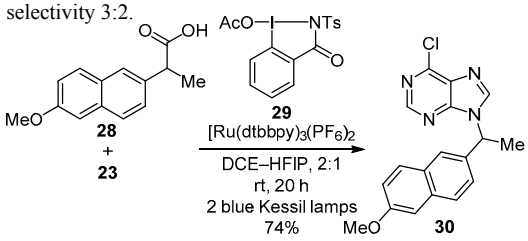

N-9 Alkylation (continued)

The use of microwave irradiation significantly reduces the standard reaction time of purine **31** alkylation with alkyl halides, and also increases reaction regioselectivity toward N-9 product **32** without any traces of other regioisomer.[11]

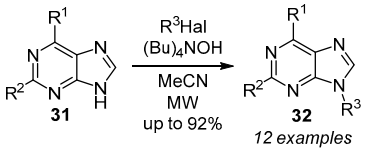

R^1 = Cl, SMe; R^2 = H, Cl, NH_2; R^3 = Me, Bn, cyclopentyl

N-9 Arylation and alkenylation

An effective and green method of N-9 arylation was described by Esmaeilpour group.[12] It included the use of nickel(0) nanoparticles on EDTA-modified Fe_3O_4@SiO_2 nanospheres as a reusable catalyst. This method avoids the usual disadvantages of nickel catalysts such as air sensitivity, use of complex phosphine ligands, and high catalyst loading.

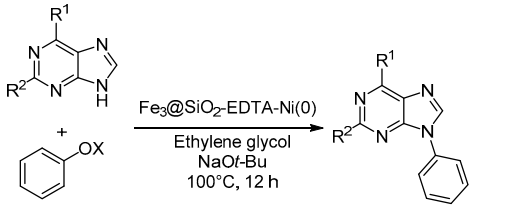

R^1, R^2 = H, NH_2
X = C(O)N(Alk)$_2$, SO_2N(Alk)$_2$

Diaryliodonium salts were widely used for *N*-arylation of amines in the past decades. Recently, a novel solvent-free method of such *N*-arylation was described, where iodonium salt, CuI, Na_2CO_3, and silica gel were milled with stainless steel balls and gave the product in 51% yield.[13]

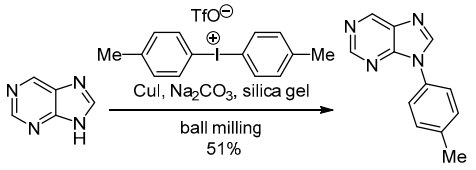

In 2021, Novák group[14] reported the use of iodonium salt **33** for stereoselective synthesis of alkenylpurines **34** in mild conditions. Previous methods for the synthesis of fluorinated enamines included the use of copper- or palladium-catalyzed trifluoromethylation of vinyl derivatives or the use of 3,3,3-trifluoropropene gas.

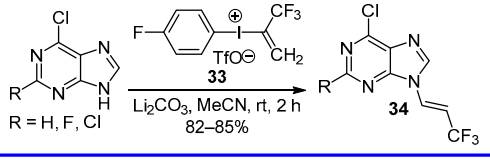

Synthesis of N-7-arylated purines

There are few methods for N-7 arylation of purines, and the ones that exist, have limitations in functional group scope at other positions of purine. Recently, a synthetic pathway toward N^7-arylpurines **36** *via* a *de novo* synthesis starting from substituted pyrimidines **35** was reported.[15] The products can be further functionalized at C-2, C-6, and C-8 positions.

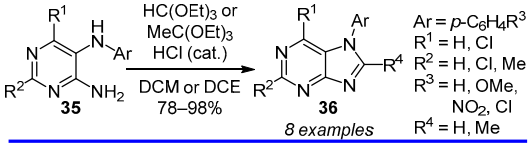

Conclusion

From 2015 to 2022, a selective purine alkylation was achieved using modification of known methods to favor either N-7- or N-9-substituted product or by developing new synthetic methodologies. In this review, the described methods of selective N-7 alkylation are very specific and limited in terms of alkyl substrate, it being either a monosaccharide or vinyl cyclopropane. In the case of N-9 alkylation, the substrate scope is more extensive and allows the introduction of various moieties in purine core. Better results, in general, are obtained in reactions where purine ring possesses electron-donating group while alkyl substrate has short sp^3 carbon chain or cycle with possible aromatic system attached. Two new methods of purine N-9 arylation have been reported. The use of iodonium salts is still a good way to attach sp^2 carbon to the purine cycle, introducing aryl or alkenyl groups. The only way to obtain N^7-arylpurines is through imidazole ring closure using substituted pyrimidines as starting materials.

Financial support by the Latvian Council of Science grant No. LZP-2020/1-0348 is gratefully acknowledged.

References

1. Mao, R.; Sun, L.; Wang, Y.-S.; Zhou, M.-M.; Xiong, D.-C.; Li, Q.; Ye, X.-S. *Chin. Chem. Lett.* **2018**, *29*, 61.
2. Behrouz, S.; Soltani Rad, M. N.; Ahmadi, S. *Tetrahedron* **2019**, *75*, 130499.
3. Niu, H.-Y.; Du, C.; Xie, M.-S.; Wang, Y.; Zhang, Q.; Qu, G.-R.; Guo, H.-M. *Chem. Commun.* **2015**, *51*, 3328.
4. Tranová, L.; Stýskala, J. *J. Org. Chem.* **2021**, *86*, 13265.
5. Li, X.; Qi, P.; Du, H. *Org. Biomol. Chem.* **2022**, *20*, 1058.
6. Desai, S. P.; Taylor, M. S. *Org. Lett.* **2021**, *23*, 7049.
7. Xu, S.; Luo, Z.; Jiang, Z.; Lin, D. *Synlett* **2017**, 868.
8. Chen, S.-J.; Golden, D. L.; Krska, S. W.; Stahl, S. S. *J. Am. Chem. Soc.* **2021**, *143*, 14438.
9. Kobayashi, R.; Shibutani, S.; Nagao, K.; Ikeda, Z.; Wang, J.; Ibáñez, I.; Reynolds, M.; Sasaki, Y.; Ohmiya, H. *Org. Lett.* **2021**, *23*, 5415.
10. Li, P.; Zbieg, J. R.; Terrett, J. A. *Org. Lett.* **2021**, *23*, 9563.
11. Vinuesa, A.; Viñas, M.; Jahani, D.; Ginard, J.; Mur, N.; Pujol, M. D. *J. Heterocycl. Chem.* **2022**, *59*, 597.
12. Dindarloo Inaloo, I.; Majnooni, S.; Eslahi, H.; Esmaeilpour, M. *New J. Chem.* **2020**, *44*, 13266.
13. Jiang, J.; Li, J. *ChemistrySelect* **2020**, *5*, 542.
14. Csenki, J. T.; Mészáros, Á.; Gonda, Z.; Novák, Z. *Chem.–Eur. J.* **2021**, *27*, 15638.
15. Sebris, A.; Novosjolova, I.; Turks, M. *Synthesis* **2022**. DOI: 10.1055/a-1898-9675.

Pielikums II
Appendix II

Burcevs, A.; Sebris, A.; Traskovskis, K.; Chu, H.; Chang, H.; Jovaišaitė, J.; Juršėnas, S.; Turks, M.; Novosjolova, I.

Synthesis of Fluorescent C–C Bonded Triazole-Purine Conjugates

J. Fluoresc., **2024**, 34, 1091–1097.

doi:10.1007/s10895-023-03337-6

Journal of Fluorescence (2024) 34:1091–1097
https://doi.org/10.1007/s10895-023-03337-6

RESEARCH

Synthesis of Fluorescent C–C Bonded Triazole-Purine Conjugates

Aleksejs Burcevs[1] · Armands Sebris[1] · Kaspars Traskovskis[2] · Han-Wei Chu[3] · Huan-Tsung Chang[3,4,5,6] · Justina Jovaišaitė[7] · Saulius Juršėnas[7] · Māris Turks[1] · Irina Novosjolova[1]

Received: 16 June 2023 / Accepted: 3 July 2023 / Published online: 18 July 2023

Abstract
A design toward C–C bonded 2,6-bis(1*H*-1,2,3-triazol-4-yl)-9*H*-purine and 2-piperidinyl-6-(1*H*-1,2,3-triazol-4-yl)-9*H*-purine derivatives was established using the combination of Mitsunobu, Sonogashira, copper (I) catalyzed azide-alkyne cycloaddition, and S_NAr reactions. 11 examples of 2,6-bistriazolylpurine and 14 examples of 2-piperidinyl-6-triazolylpurine intermediates were obtained, in 38–86% and 41–89% yields, respectively. Obtained triazole-purine conjugates expressed good fluorescent properties which were studied in the solution and in the thin layer film for the first time. Quantum yields reached up to 49% in DMSO for bistriazolylpurines and up to 81% in DCM and up to 95% in DMSO for monotriazolylpurines. Performed biological studies in mouse embryo fibroblast, human keratinocyte, and transgenic adenocarcinoma of the mouse prostate cell lines showed that most of obtained triazole-purine conjugates are not cytotoxic. The 50% cytotoxic concentration of the tested derivatives was in the range from 59.6 to 1528.7 μM.

Keywords Fluorescent purines · Sonogashira reaction · CuAAC · Fluorescence

The Sonogashira reaction is a facile way of introducing alkynyl substituents onto purine C2, C6, and C8 positions by exchanging triflates or halogens [1–13]. Further alkynyl groups have the potential to be modified via C–C coupling with alkyl halides in the presence of a Pd/Cu catalyst and a base [14]. They can also undergo modification through cyclization reactions with alkyl/aryl azides, cyclopentadiene, diazomethane, and isonitrile [15, 16]. Obtained cycloadducts are widely studied as agonists or antagonists of A_1 or A_3 adenosine receptors [17–20] or used for cytostatic activity studies [15]. On the other hand, alkynylpurine nucleosides have potential as A_1 and A_2 adenosine receptor agonists, as antihypertensive [21] and antiviral [22] agents and they also possess photophysical properties [23]. Alkynylated purine-pyridazine base pairs are studied for their pairing stability and selectivity and have proven to form thermally stable and sequence-specific DNA duplexes [24]. 8-Ethynyl-2'-deoxyguanosine analogs are important in the study of G quadruplex formation and in the development of their fluorescent analogs in copper (I) catalyzed azide-alkyne cycloaddition (CuAAC) reaction with phenyl azide [25]. Furthermore, fluorescent or reporter markers are incorporated into purine derivatives using CuAAC between alkynylpurines as starting materials and appropriate azides [26, 27]. A wide range of C8 triazolyl purine analogs exhibits fluorescent characteristics [28]. Quantum yields for nucleosides reach up to 64% [29] and for their modified DNA up to 20% [30]. Click reaction between alkynyl group at the C8 position of purine and azido group at the sugar 2' position leads to fluorescent adenosine-based fluorosides developed by M. Grøtli [31]. In addition, 2,6,9-substituted 8-triazolylpurines are used as

✉ Irina Novosjolova
irina.novosjolova@rtu.lv

1 Institute of Technology of Organic Chemistry, Faculty of Materials Science and Applied Chemistry, Riga Technical University, P. Valdena Str. 3, Riga LV-1048, Latvia

2 Institute of Applied Chemistry, Faculty of Materials Science and Applied Chemistry, Riga Technical University, P. Valdena Str. 3, Riga LV-1048, Latvia

3 Department of Biomedical Sciences, Chang Gung University, Taoyuan 33302, Taiwan

4 Graduate Institute of Biomedical Sciences, Chang Gung University, Taoyuan 33302, Taiwan

5 Center for Advanced Biomaterials and Technology Innovation, Chang Gung University, Taoyuan 33302, Taiwan

6 Division of Breast Surgery, Department of General Surgery, Chang-Gung Memorial Hospital, Linkou, Taoyuan 33305, Taiwan

7 Institute of Photonics and Nanotechnology, Faculty of Physics, Vilnius University, Saulėtekis av. 3, Vilnius LT-10257, Lithuania

mimics of α-helices and have shown an inhibitory activity in protein–protein interaction studies [32]. Therefore, the Sonogashira reaction and the utilization of the resulting products have proven to be a powerful tool for the construction of diverse purine derivatives with unique properties and enhanced biological activities.

Despite extensive research on present alkynylpurine derivatives, there is still potential for designing novel structures and exploring their potential applications. One particularly challenging area is the development of new photophysical structures for use in materials science and biological systems. With this in mind, a library of new-type purine-triazole conjugates was designed, employing Mitsunobu, Sonogashira, CuAAC, and S_NAr reactions. During the research, monotriazolyl- and bistriazolylpurine derivatives were obtained. Although alkynyl group introduction in purines is already known, our developed structural pattern is new, especially for 2,6-bistriazolylpurine intermediates. And fluorescence studies of 2-(1,2,3-triazol-4-yl)purine and 6-(1,2,3-triazol-4-yl)purine derivatives have been conducted for the first time. Cytotoxicity studies of obtained products were established to discover suitability of developed structures for biological/environmental applications.

Our previous studies demonstrated that 2/6-amino-6/2-(1,2,3-triazol-1-yl)-purine and 2,6-bis(1,2,3-triazol-1-yl) purine derivatives possess photophysical properties [33–37]. In this study, we developed a method for synthesizing their analogs connecting the triazolyl ring to the purine core via C–C bond. For the synthesis of target compounds Mitsunobu, Sonogashira, CuAAC, and S_NAr reactions were used. The C–C bond is more stable and prevents triazole from acting as a leaving group at C6 position of purine. Our previous studies proved that 1,2,3-triazol-1-yl moiety is a good leaving group in nucleophilic reactions with *N*-, *S*-, *O*-, *C*-, and *P*-nucleophiles [33, 38–40].

Firstly, purine derivatives **2** were obtained via Mitsunobu reaction conditions between 2,6-dichloropurine (**1**) and appropriate alcohols, giving products **2** in yields up to 71% (Scheme 1) [34, 41, 42]. *n*-Heptanol was commercially available, but 2-hydroxyethyl 3,3,3-triphenylpropanoate and 1,3-di-*tert*-butyldimethylsilyl glycerol were synthesized based on the literature procedures [43, 44].

Trityl moiety containing alkyl group was chosen to improve amorphous characteristics of target compounds to study their photophysical properties in films [45, 46]. Heptyl group was used due to its inert behavior. And glycerol-containing moiety was selected to increase the solubility of triazolylpurine derivatives in aqueous solutions. With starting materials **2** in hand, the Sonogashira reaction was carried out using TMS acetylene and $PdCl_2$ as a catalyst. To compare, in the presence of $Pd(OAc)_2$ the conversion to the product was slower. Optimization of reaction conditions was done on the synthesis of derivatives **3a** and **4a** (Scheme 1, Table 1). Optimal temperature for the synthesis of monoalkynylproducts was 50 °C, in room temperature conversion took 18 h, and for bisalkynylproducts – 100 °C. Depending on temperature and equivalents of TMS acetylene monoalkynyl purines **3** and bisalkynyl purines **4** were selectively obtained (Scheme 1, Table 2). For the synthesis of product **3**, reactions were performed in the presence of 4 equivalents of TMS acetylene in THF at 50 °C for 30 min. During the synthesis disubstituted products **4** as byproducts were also observed, reaching up to 11% by HPLC (in synthesis of **3c**), but were easily separated by column chromatography. On the other hand, for the synthesis of product **4**, using 10 equivalents of TMS acetylene was necessary, stirring the reaction mixture in DMF at 100 °C for 30 min (Table 1). The moderate yields of the disubstituted products **4** were due to the possible formation of Glaser-type coupling products [47–49] connecting two purine moieties via dialkynyl bond which were not isolated.

In CuAAC reaction between 6-alkynylpurines **3** and azides 6-triazolylpurine derivatives **5** were obtained in yields up to 91% (Scheme 2, Table 3). Azides were synthesized from the relevant amines or bromides and stored as solids or in DCM solution (C = 0.15–0.74 M) prior to use [50–57]. CuAAC reaction occurred at room temperature in the presence of CuI and Et_3N in DCM or DMF as a solvent. Product **5c** was synthesized using $CuSO_4 \cdot 5H_2O$/sodium ascorbate system in DMF at 70 °C because the formation of the

Table 1 Optimization of reaction conditions for the synthesis of **3a** and **4a**

Entry	Solvent	Equiv. of cat	Equiv. of TMS acetylene	T, °C	Time, h	3a, %[a]	4a, %[a]	Yield, %
1	DMF	0.1	6	60	1	69	9	50
2	THF	0.1	4	50	0.5	77	5	66
3			1	50	0.5	77	8	64
4			1	25	18	83	7	56
5	DMF	0.1	10	100	1	-	64	43
6		0.2			0.5	-	79	68

[a]Ratio obtained from HPLC; integration was done for all the signals in the chromatogram

Scheme 1 Synthesis of alkynyl purine derivatives **3** and **4**

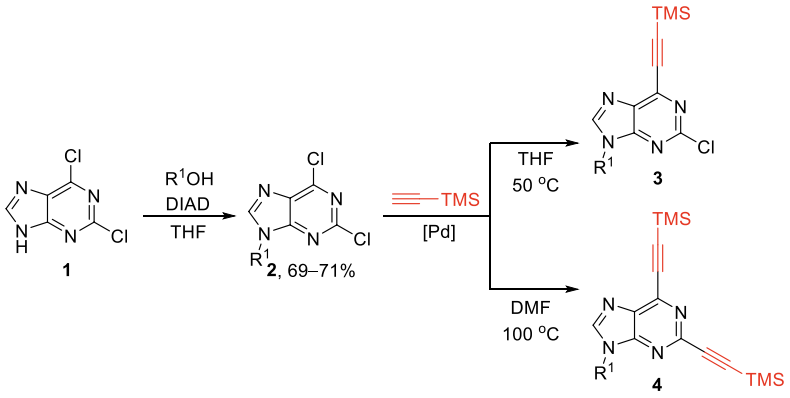

product was not observed using CuI/Et_3N/AcOH catalytic system even after 24h of stirring. Target compounds **7** were synthesized in S_NAr reaction between intermediate **5** and piperidine in DMF at 100 °C (Scheme 2, Table 3).

CuAAC reaction between 2,6-bisalkynylpurines **4** and azides took place in DMF at 50 °C for 30 min and 2,6-bis-triazolylpurines **6** were obtained in yields up to 85% (Scheme 3, Table 4). For products **7h** and **6e** TBS groups were cleaved using AcOH in THF/H_2O and products **8a** and **8b** were obtained in 57 and 86% yields, respectively (see SI, pp. S75–S77).

For the comparison of photophysical properties, C-N analogs of purine-triazole conjugates were synthesized. For their design known approach was used [33, 34, 37], and products were obtained in good yields (see SI, p. S68).

Table 2 Variety and yields of alkynyl purine derivatives **3** and **4** (Scheme 1)

Entry	R^1	Time, min	Yield of 3 and 4, %
1	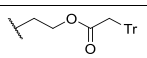	30	**3a**, 67
2			**4a**, 68
3	*n*-C_7H_{15}	60	**3b**, 80
4		30	**4b**, 45
5	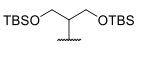	60	**3c**, 83
6		40	**4c**, 37

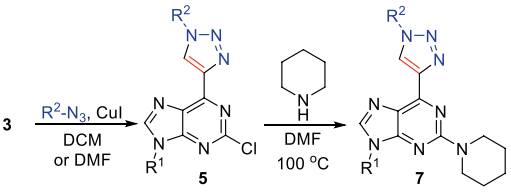

Scheme 2 Synthesis of monotriazolylpurine derivatives **5** and **7**

From previous observations, bistriazolylpurines with 4-metoxyphenyl moiety on the triazole ring possessed photophysical properties [35]. Bistriazolylpurine derivative **6b** did not show fluorescence, but compound **6c** reached 26%

Table 3 Variety and yields of monotriazolylpurine derivatives **5** and **7**

Entry	Starting material	R^2	Yield of 5, %	Yield of 7, %
1	**3a**		**5a**, 66	**7a**, 67
2			**5b**, 82	**7b**, 76
3			**5c**, 56	**7c**, 41
4			**5d**, 89	**7d**, 67
5	**3b**		**5e**, 86	**7e**, 77
6			**5f**, 91	**7f**, 81
7			**5g**, 69	**7g**, 71
8	**3c**		**5h**, 89	**7h**, 75
9	**3a**	-CH_2CN	**5i**, 59	**7i**, 75
10[a]		-CH_2COOMe	**5j**, 74	**7j**, 75
11		-Cy	**5k**, 77	**7k**, 66
12		-decyl	**5l**, 88	**7l**, 89
13		-Bn	**5m**, 83	**7m**, 83

[a]For the product **7j** substitution of -OMe was observed and the final product contained 

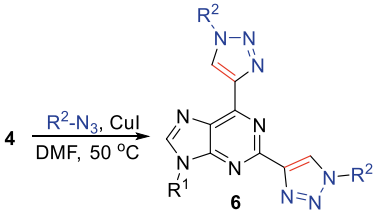

Scheme 3 Synthesis of 2,6-bistriazolylpurine derivatives **6**

Table 4 Variety and yields of 2,6-bistriazolylpurine derivatives **6**

Entry	Starting material[a]	R^2	Yield, %
1	4a		**6a**, 60
2		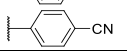	**6b**, 50
3	**4a**		**6c**, 60
4	**4b**	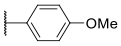	**6d**, 44
5	**4c**		**6e**, 38
6		$-CH_2CN$	**6f**, 62
7		$-CH_2COOMe$	**6g**, 67
8	**4a**	-Cy	**6h**, 81
9		-decyl	**6i**, 45
10		-Bn	**6j**, 85

[a]Aryl azides were used as solutions in DCM

Table 5 Photophysical properties of target purine-triazole conjugates

Entry	Compound	Solvent[a]	$\lambda_{abs\ max}$, nm	$\lambda_{em\ max}$, nm	Quantum yield, %
1	**6b**	DCM	282	---	0
2	**6c**	DCM	281	394	26
3	**8b**	DMSO	283	452	49
4	**7a**	DCM	365	443	75
5		in the film	366	447	35
6	**7b**	DCM	371	452	68
7	**7c**	DCM	311	437	76
8	**7d**	DCM	363	439	71
9		in the film	381	545	12
10	**7e**	DCM	364	443	81
11	**7f**	DCM	365	441	74
12	**7m**	DCM	362	438	75
13		in the film	361	443	23
14	**8a**	DMSO	363	450	95
15	**13**	DMSO	261	506	24
16	**15**	DMSO	362	457	98

[a]C = 10^{-5} mol/l

quantum yield (QY) in DCM solution with emission maxima of 394 nm (Table 5, Fig. 1).

In the end derivatives with glycerol moiety at the N9 position were not soluble in water and DMSO was used instead. QY for compound **8b** reached 49% in DMSO solution, but for analog **13** with C-N bond connected triazolyl ring QY reached only 24% in DMSO. Between compounds **8b** and **13** a bathochromic shift of emission maxima was observed, 452 nm for **8b** and 506 nm for **13** (Fig. 1). Photophysical properties of derivatives **7a**, **7d** and **7m** were studied both in DCM solution and in the film. The emission maxima in the thin film were slightly elevated, especially for the compound **7d** (Table 5). Quantum yields of 2-piperidinyl-6-triazolylpurines **7a-f** and **7m** were in range from 68 to 81% in DCM, but for compounds **8a** and **15** in DMSO QY reached 95 and 98%, respectively (Table 5). Their emission maxima were in range from 437 to 457 nm (Fig. 2).

During the research, was found that trityl group containing purine derivatives were unsuitable for OLED development due to rapid degradation under the influence of electrical current, so we did not perform any experiments for OLED development.

To ensure that the synthesized purine derivatives can be employed in biological systems in future, MTT (3-(4,5-dimethylthiazol-2-yl)-2,5-diphenyltetrazolium bromide) test was used to ascertain their cytotoxicity (Table 6). NIH-3T3 (mouse embryo fibroblast), HaCaT (human keratinocytes) and TrampC1 (transgenic adenocarcinoma of the mouse prostate) were chosen for this evaluation. The 50% cytotoxic concentration (CC_{50}) of the tested samples ranged from 59.6 to 1528.7 μM. Out of 9 tested materials, 7 compounds exhibit slightly lower CC_{50} towards HaCaT compared to the other two cell lines. Compound **15**, in particularly, has lower CC_{50} and is shown to be more toxic towards both HaCaT and NIH-3T3 (normal cell line) with a CC_{50} of 73.0 and 172.3 μM respectively. Whereas, compounds **5g**

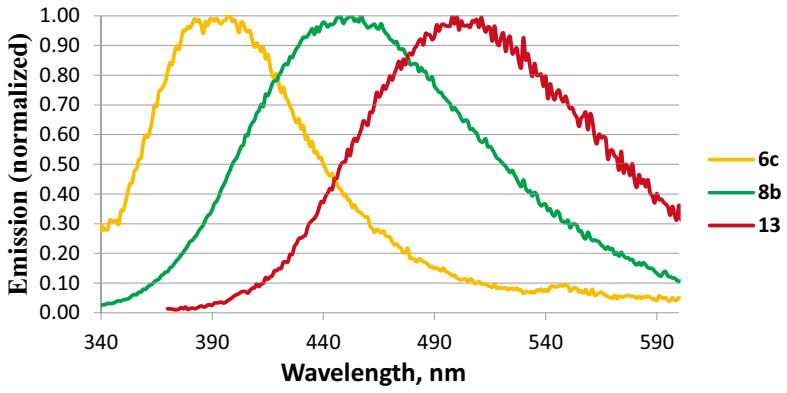

Fig. 1 Emission spectra of bistriazolylpurine derivatives

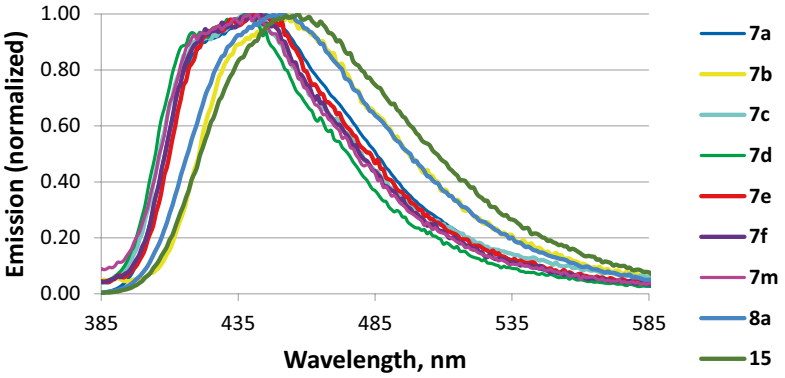

Fig. 2 Emission spectra of target compounds **7**, **8** and **15**

and **7e** demonstrated significantly lower CC_{50} in TrampC1 cancer cell line compared to NIH-3T3 and HaCaT with a CC_{50} of 206.2 and 59.6 µM respectively.

To conclude, 2,6-bis(1*H*-1,2,3-triazol-4-yl)-9*H*-purine and 2-piperidinyl-6-(1*H*-1,2,3-triazol-4-yl)-9*H*-purine derivatives were obtained in this study and their photophysical properties were studied and compared to their C-N bonded triazolyl analogs. Quantum yields for bistriazolylpurine derivatives reached up to 49% in DMSO solution and for C–C bonded monotriazolylpurines up to 81% in DCM and up to 95% in DMSO. The introduction of glycerol group at purine *N*(9) position did not enhance product solubility in H_2O. Acquired triazolylpurine derivatives were soluble only in such polar solvents as DMSO and DMF. In addition,

Table 6 Cytotoxicity evaluation of the 9 synthesized purine derivatives and their CC_{50} (µM) in 3 different cell lines

	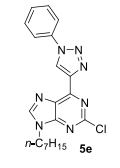 5e	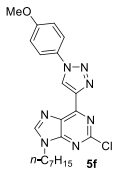 5f	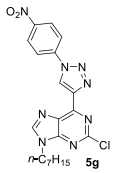 5g
NIH3T3	885.8	1427.5	719.2
HaCaT	598.1	703.4	736.2
TrampC1	919.7	1092.0	206.2
	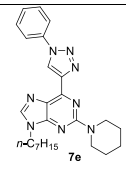 7e	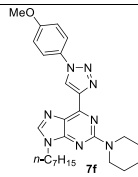 7f	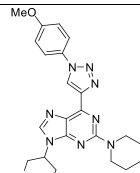 8a
NIH3T3	875.4	1212.8	1528.7
HaCaT	438.6	603.6	827.7
TrampC1	59.6	1124.5	1533.0
	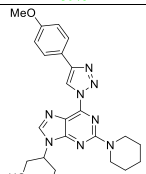 15	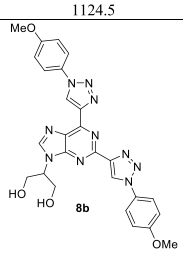 8b	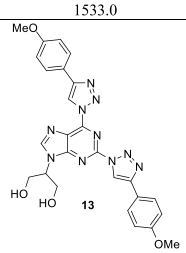 13
NIH3T3	172.3	1104.6	1012.1
HaCaT	73.0	558.9	552.4
TrampC1	784.9	1179.4	650.6

cytotoxicity studies demonstrated that most part of compounds are not cytotoxic and are applicable for the studies in biological systems which will be discussed in other publications.

Supplementary Information The online version contains supplementary material available at https://doi.org/10.1007/s10895-023-03337-6.

Acknowledgements The authors thank the Latvia-Lithuania-Taiwan joint grant "Molecular Electronics in functionalized Purines: fundamental Study and applications (MEPS)" for financial support and *Dr. chem*. Kristine Lazdoviča for IR analysis. A.B. thanks the European Social Fund within Project No. 8.2.2.0/20/I/008 "Strengthening of PhD students and academic personnel of Riga Technical University and BA School of Business and Finance in the strategic fields of specialization".

Authors' Contributions M.T. and I.N. contributed to the study conception and design, and supervision. A.B. and A.S. performed the synthesis and analysis of purine derivatives, and wrote the experimental part. K.T., J.J. and S.J. performed the photophysical studies and analysis of data. H.W.C. and H.T.C. performed cytotoxicity experiments and analysis. The first draft of the manuscript was written by I.N. and all authors commented on previous versions of the manuscript. All authors read and approved the final manuscript.

Funding The Latvia-Lithuania-Taiwan joint grant "Molecular Electronics in functionalized Purines: fundamental Study and applications (MEPS)". The European Social Fund within Project No. 8.2.2.0/20/I/008.

Availability of Data and Materials Below is the link to the electronic supporting information.

Declarations

Ethical Approval Not applicable.

Competing Interests The authors declare no competing financial or personal interest.

References

1. Sonogashira K, Tohda Y, Hagihara N (1975) A convenient synthesis of acetylenes: catalytic substitutions of acetylenic hydrogen with bromoalkenes, iodoarenes and bromopyridines. Tetrahedron Lett 16:4467–4470. https://doi.org/10.1016/S0040-4039(00)91094-3
2. Chinchilla R, Nájera C (2007) The Sonogashira reaction: A booming methodology in synthetic organic chemistry. Chem Rev 107:874–922. https://doi.org/10.1021/cr050992x
3. Biffis A, Centomo P, Del Zotto A, Zecca M (2018) Pd Metal catalysts for cross-couplings and related reactions in the 21st century: A critical review. Chem Rev 118:2249–2295. https://doi.org/10.1021/acs.chemrev.7b00443
4. Johansson Seechurn CCC, Kitching MO, Colacot TJ, Snieckus V (2012) Palladium-catalyzed cross-coupling: A historical contextual perspective to the 2010 nobel prize. Angew Chemie - Int Ed 51:5062–5085. https://doi.org/10.1002/anie.201107017
5. Bag SS, Jana S, Kasula M (2018) Sonogashira cross-coupling: Alkyne-modified nucleosides and their applications. Elsevier Inc
6. Hocek M (2003) Syntheses of purines bearing carbon substituents in positions 2, 6 or 8 by metal- or organometal-mediated C–C bond-forming reactions. Eur J Org Chem 2003:245–254. https://doi.org/10.1002/ejoc.200390025
7. Agrofoglio LA, Gillaizeau I, Saito Y (2003) Palladium-assisted routes to nucleosides. Chem Rev 103:1875–1916. https://doi.org/10.1021/cr010374q
8. Manvar A, Shah A (2013) Microwave-assisted chemistry of purines and xanthines. An overview Dedicated to the late Professor V.M. Thakor on his 94th birthday. Tetrahedron 69:8105–8127. https://doi.org/10.1016/j.tet.2013.06.034
9. Fang X, Gao Q, Zhang W et al (2020) Multisensing emissive 8-phenylethynylated 2′-deoxyadenosines and 2′-deoxyisoguanosines. Tetrahedron 76:8–16. https://doi.org/10.1016/j.tet.2019.130795
10. Ibrahim N, Chevot F, Legraverend M (2011) Regioselective Sonogashira cross-coupling reactions of 6-chloro-2,8-diiodo-9-THP-9H-purine with alkyne derivatives. Tetrahedron Lett 52:305–307. https://doi.org/10.1016/j.tetlet.2010.11.033
11. Malthum S, Polkam N, Allaka TR et al (2017) Synthesis, characterization and biological evaluation of purine nucleoside analogues. Tetrahedron Lett 58:4166–4168. https://doi.org/10.1016/j.tetlet.2017.09.041
12. Bilbao N, Vázquez-González V, Aranda MT, González-Rodríguez D (2015) Synthesis of 5-/8-halogenated or ethynylated lipophilic nucleobases as potential synthetic intermediates for supramolecular chemistry. Eur J Org Chem 2015:7160–7175. https://doi.org/10.1002/ejoc.201501026
13. Sedláček O, Břehová P, Pohl R et al (2011) The synthesis of the 8-C-substituted 2,6-diamino-9-[2-(phosphonomethoxy)ethyl] purine (PMEDAP) derivatives by diverse cross-coupling reactions. Can J Chem 89:488–498. https://doi.org/10.1139/V11-001
14. Nagy A, Kotschy A (2008) Synthesis of 6-ethynylpurine derivatives. Tetrahedron Lett 49:3782–3784. https://doi.org/10.1016/j.tetlet.2008.04.011
15. Křováček M, Dvořáková H, Votruba I et al (2011) 6-Alkynylpurines bearing electronacceptor substituents: Preparation, reactivity in cycloaddition reactions and cytostatic activity. Collect Czechoslov Chem Commun 76:1487–1527. https://doi.org/10.1135/cccc2011176
16. Buchanan HS, Pauff SM, Kosmidis TD et al (2017) Modular, step-efficient palladium-catalyzed cross-coupling strategy to access C6-heteroaryl 2-aminopurine ribonucleosides. Org Lett 19:3759–3762. https://doi.org/10.1021/acs.orglett.7b01602
17. Mathew SC, By Y, Berthault A et al (2010) Expeditious synthesis and biological evaluation of new C-6 1,2,3-triazole adenosine derivatives A1 receptor antagonists or agonists. Org Biomol Chem 8:3874–3881. https://doi.org/10.1039/c0ob00017e
18. Cosyn L, Palaniappan KK, Kim S-K et al (2006) 2-triazole-substituted adenosines: a new class of selective A_3 adenosine receptor agonists, partial agonists, and antagonists. J Med Chem 49:7373–7383. https://doi.org/10.1021/jm0608208
19. Tosh DK, Chinn M, Yoo LS et al (2010) 2-Dialkynyl derivatives of (N)-methanocarba nucleosides: "Clickable" A_3 adenosine receptor-selective agonists. Bioorganic Med Chem 18:508–517. https://doi.org/10.1016/j.bmc.2009.12.018
20. Luan F, Melo A, Borges F, Cordeiro MNDS (2011) Affinity prediction on A_3 adenosine receptor antagonists: The chemometric approach. Bioorganic Med Chem 19:6853–6859. https://doi.org/10.1016/j.bmc.2011.09.032
21. Matsuda a, Shinozaki M, Yamaguchi T, et al (1992) Nucleosides and nucleotides. 103. 2-Alkynyladenosines: a novel class of selective adenosine A_2 receptor agonists with potent antihypertensive effects. J Med Chem 35:241–252
22. Sági G, Ötvös L, Ikeda S et al (1994) Synthesis and antiviral activities of 8-alkynyl-, 8-alkenyl-, and 8-alkyl-2′-deoxyadenosine analogs. J Med Chem 37:1307–1311. https://doi.org/10.1021/jm00035a010
23. He X, Kuang S, Gao Q et al (2022) Bright fluorescent purine analogues as promising probes. Nucleosides Nucleotides Nucleic Acids 41:45–60. https://doi.org/10.1080/15257770.2021.2004418

24. Okamura H, Trinh GH, Dong Z et al (2022) Selective and stable base pairing by alkynylated nucleosides featuring a spatially-separated recognition interface. Nucleic Acids Res 50:3042–3055. https://doi.org/10.1093/nar/gkac140
25. Da XC, He ZY, Guo CX et al (2020) Conformation of G-quadruplex controlled by click reaction. Molecules 25:1–8. https://doi.org/10.3390/molecules25184339
26. Creech C, Kanaujia M, Causey CP (2015) Synthesis and evaluation of 2-ethynyl-adenosine-5′-triphosphate as a chemical reporter for protein AMPylation. Org Biomol Chem 13:8550–8555. https://doi.org/10.1039/c5ob01081k
27. Kele P, Li X, Link M et al (2009) Clickable fluorophores for biological labeling - with or without copper. Org Biomol Chem 7:3486–3490. https://doi.org/10.1039/b907741c
28. Redwan IN, Bliman D, Tokugawa M et al (2013) Synthesis and photophysical characterization of 1- and 4-(purinyl)triazoles. Tetrahedron 69:8857–8864. https://doi.org/10.1016/j.tet.2013.08.023
29. Dyrager C, Börjesson K, Dinér P et al (2009) Synthesis and photophysical characterisation of fluorescent 8-(1 *H*-1,2,3-triazol-4-yl) adenosine derivatives. Eur J Org Chem 1515–1521. https://doi.org/10.1002/ejoc.200900018
30. Dierckx A, Dinér P, El-Sagheer AH et al (2011) Characterization of photophysical and base-mimicking properties of a novel fluorescent adenine analogue in DNA. Nucleic Acids Res 39:4513–4524. https://doi.org/10.1093/nar/gkr010
31. O'Mahony G, Ehrman E, Grøtli M (2005) Synthesis of adenosine-based fluorosides containing a novel heterocyclic ring system. Tetrahedron Lett 46:6745–6748. https://doi.org/10.1016/j.tetlet.2005.07.115
32. Pettersson M, Bliman D, Jacobsson J et al (2015) 8-Triazolylpurines: Towards fluorescent inhibitors of the MDM2/p53 interaction. PLoS ONE 10:1–17. https://doi.org/10.1371/journal.pone.0124423
33. Kovaļovs A, Novosjolova I, Bizdēna Ē et al (2013) 1,2,3-Triazoles as leaving groups in purine chemistry: a three-step synthesis of N6-substituted-2-triazolyl-adenine nucleosides and photophysical properties thereof. Tetrahedron Lett 54:850–853. https://doi.org/10.1016/j.tetlet.2012.11.095
34. Šišuļins A, Bucevičius J, Tseng Y-T et al (2019) Synthesis and fluorescent properties of N(9)-alkylated 2-amino-6-triazolylpurines and 7-deazapurines. Beilstein J Org Chem 15:474–489. https://doi.org/10.3762/bjoc.15.41
35. Jovaisaite J, Cīrule D, Jeminejs A et al (2020) Proof of principle of a purine D-A-D′ ligand based ratiometric chemical sensor harnessing complexation induced intermolecular PET. Phys Chem Chem Phys 22:26502–26508. https://doi.org/10.1039/d0cp04091f
36. Sebris A, Traskovskis K, Novosjolova I, Turks M (2021) Synthesis and photophysical properties of 2-azolyl-6-piperidinylpurines. Chem Heterocycl Compd 57:560–567. https://doi.org/10.1007/s10593-021-02943-1
37. Sebris A, Novosjolova I, Traskovskis K et al (2022) Photophysical and electrical properties of highly luminescent 2/6-triazolyl-substituted push-pull purines. ACS Omega 7:5242–5253. https://doi.org/10.1021/acsomega.1c06359
38. Novosjolova I, Bizdēna Ē, Turks M (2013) Application of 2,6-diazidopurine derivatives in the synthesis of thiopurine nucleosides. Tetrahedron Lett 54:6557–6561. https://doi.org/10.1016/j.tetlet.2013.09.095
39. Cīrule D, Novosjolova I, Bizdēna Ē, Turks M (2021) 1,2,3-Triazoles as leaving groups: S_NAr reactions of 2,6-bistriazolylpurines with O- and C-nucleophiles. Beilstein J Org Chem 17:410–419. https://doi.org/10.3762/bjoc.17.37
40. Kriķis KE, Novosjolova I, Mishnev A, Turks M (2021) 1,2,3-Triazoles as leaving groups in S_NAr-Arbuzov reactions: Synthesis of C6-phosphonated purine derivatives. Beilstein J Org Chem 17:193–202. https://doi.org/10.3762/BJOC.17.19
41. Kapilinskis Z, Novosjolova I, Turks M (2018) Purine-furan and purine-thiophene conjugates. Molbank. https://doi.org/10.3390/M1024
42. Kim HS, Barak D, Harden TK et al (2001) Acyclic and cyclopropyl analogues of adenosine bisphosphate antagonists of the P2Y1 receptor: Structure-activity relationships and receptor docking. J Med Chem 44:3092–3108. https://doi.org/10.1021/jm010082h
43. Lv J, Luo T, Zou D, Dong H (2019) Using DMF as both a catalyst and cosolvent for the regioselective silylation of polyols and diols. Eur J Org Chem 2019:6383–6395. https://doi.org/10.1002/ejoc.201901195
44. Hellerman L (1927) The preparation of β-triphenylethylamine. Rearrangement of β-triphenylpropionhydroxamic acid. J Am Chem Soc 49:1735–1742. https://doi.org/10.1021/ja01406a013
45. Traskovskis K, Mihailovs I, Tokmakovs A et al (2012) Triphenyl moieties as building blocks for obtaining molecular glasses with nonlinear optical activity. J Mater Chem 22:11268–11276. https://doi.org/10.1039/c2jm30861d
46. Traskovskis K, Ruduss A, Kokars V et al (2019) Thiphenylmethane based structural fragments as building blocks towards solution-processable heteroleptic iridium(III) complexes for OLED use. New J Chem 43:37–47. https://doi.org/10.1039/c8nj04484h
47. Glaser C (1869) Beitrage zur Kenntnifs des Acetenylbenzols. Ber Dtsch Chem Ges 2:422–424
48. Glaser C (1870) Untersuchungen über einige Derivate der Zimmtsäure. Justus Liebigs Ann Chem 154:137–171. https://doi.org/10.1002/jlac.18701540202
49. Sindhu KS, Anilkumar G (2014) Recent advances and applications of Glaser coupling employing greener protocols. RSC Adv 4:27867–27887. https://doi.org/10.1039/c4ra02416h
50. Alvarez SG, Alvarez MT (1997) A Practical procedure for the synthesis of alkyl azides at ambient temperature in dimethyl sulfoxide in high purity and yield. Synthesis (Stuttg) 1997:413–414. https://doi.org/10.1055/s-1997-1206
51. Barral K, Moorhouse AD, Moses JE (2007) Efficient conversion of aromatic amines into azides: A one-pot synthesis of triazole linkages. Org Lett 9:1809–1811. https://doi.org/10.1021/ol070527h
52. Zhang D, Fan Y, Yan Z et al (2019) Reactions of α-haloacroleins with azides: Highly regioselective synthesis of formyl triazoles. Green Chem 21:4211–4216. https://doi.org/10.1039/c9gc01129c
53. Vereshchagin LI, Kizhnyaev VN, Verkhozina ON et al (2004) Synthesis of polycyclic functionally-substituted triazole- and tetrazole-containing systems. Russ J Org Chem 40:1156–1161. https://doi.org/10.1023/B:RUJO.0000045898.10072.7f
54. Schmitz J, Li T, Bartz U, Gütschow M (2016) Cathepsin B inhibitors: combining dipeptide nitriles with an occluding loop recognition element by click chemistry. ACS Med Chem Lett 7:211–216. https://doi.org/10.1021/acsmedchemlett.5b00474
55. Schulz A, Thomas M, Villinger A (2019) Tetrazastannoles versus distannadiazanes-a question of the tin(ii) source. Dalt Trans 48:125–132. https://doi.org/10.1039/C8DT04295K
56. Gribanov PS, Topchiy MA, Golenko YD et al (2016) An unprecedentedly simple method of synthesis of aryl azides and 3-hydroxytriazenes. Green Chem 18:5984–5988. https://doi.org/10.1039/c6gc02379g
57. Verkhozina ON, Kizhnyaev VN, Vereshchagin LI et al (2003) Synthesis of polynuclear nonfused azoles. Russ J Org Chem 39:1792–1796. https://doi.org/10.1023/B:RUJO.0000019746.10504.f3

Pielikums III
Appendix III

Burcevs, A.; Turks, M.; Novosjolova, I.

Synthesis of Pyridinium Moiety Containing Triazolyl Purines

Molbank, **2024**, 2024, M1855.

doi.org/10.3390/M1855

molbank

MDPI

Communication

Synthesis of Pyridinium Moiety Containing Triazolyl Purines

Aleksejs Burcevs, Māris Turks * and Irina Novosjolova *

Institute of Chemistry and Chemical Technology, Faculty of Natural Sciences and Technology, Riga Technical University, P. Valdena Str. 3, LV-1048 Riga, Latvia; aleksejs.burcevs@rtu.lv
* Correspondence: maris.turks@rtu.lv (M.T.); irina.novosjolova@rtu.lv (I.N.)

Abstract: Pyridinium salts of 2-piperidinyl-6-triazolylpurine derivatives were obtained by the introduction of pyridinium moieties into the propane-1,3-diol fragment at the *N*(9) position of purine to enhance the solubility of 2-amino-6-triazolylpurine derivatives in water. Target structures were obtained using the tosylation of hydroxyl groups of 2-(6-(4-(4-methoxyphenyl)-1*H*-1,2,3-triazol-1-yl)-2-(piperidin-1-yl)-9*H*-purin-9-yl)propane-1,3-diol, the subsequent introduction of pyridine, and ion exchange. The compounds were characterized using ^{1}H- and ^{13}C-NMR spectra, FTIR, UV–Vis, and HRMS data.

Keywords: purines; triazolyl purines; pyridinium salts

Citation: Burcevs, A.; Turks, M.; Novosjolova, I. Synthesis of Pyridinium Moiety Containing Triazolyl Purines. *Molbank* **2024**, *2024*, M1855. https://doi.org/10.3390/M1855

Academic Editor: Nicholas Leadbeater

Received: 4 July 2024
Revised: 22 July 2024
Accepted: 23 July 2024
Published: 24 July 2024

1. Introduction

Purine derivatives are extensively studied due to their biological activity [1]. Purines are one of the most common naturally occurring heterocycles and can easily undergo modifications at *C*2, *C*6, *C*8, *N*9, and *N*7 positions [2–9], leading to countless new compounds with new reactivities and possible applications in biochemistry. They can be used as adenosine receptor agonists and antagonists, inhibitors of phosphodiesterases, sulfotransferases, and Src tyrosine and P38α MAP kinase inhibitors [10,11].

Many purine derivatives also possess fluorescent properties and are widely used in studies of biological and biochemical processes in cells and nucleic acids [12–14] due to the fact that a purine moiety works as a building block in DNA and RNA syntheses. Such compounds should usually have low cytotoxicity and are soluble in water. Many derivatization approaches are used to increase the solubility of purine derivatives in aqueous media, for example, introducing an amine-containing moiety to the purine *N*9 position [15], making purine derivatives co-crystals with benzenetricarboxylic acids [16] or obtaining purine-based ionic liquids [17].

In addition, a variety of reported novel fluorescent purine derivatives are also exploited as pH sensors [18], photocatalysts [19] and metal ion sensors [20].

2-Piperidinyl-6-triazolylpurine derivatives are known as push–pull chromophores that possess photophysical properties [21–23]. In our study, we decided to enhance their solubility, especially in water, and synthesize pyridinium salts of 2-piperidinyl-6-triazolylpurine derivatives, and then examine how much the fluorescence is quenched upon introduction of pyridine moieties in the structure. There are a few examples in the literature that report that the introduction of pyridinium moieties in organic structures can increase the solubility [24,25] and also quench the fluorescence [26,27].

2. Results and Discussion

Starting material **1** was prepared according to the literature [21]. Then, two hydroxyl groups of propane-1,3-diol at the *N*9 position of purine derivative **1** were tosylated using TsCl, DMAP, and Et_3N in DCM, resulting in product **2** with a 76% yield (Scheme 1).

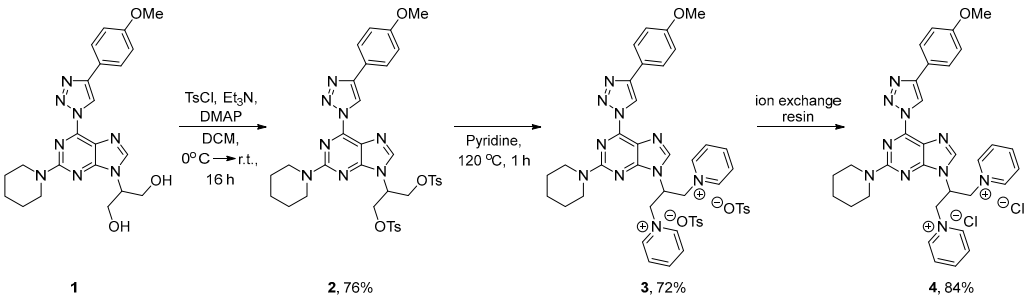

Scheme 1. Synthesis of pyridinium moiety containing triazolyl purine derivatives **3** and **4**.

To make the triazolyl purine derivative's pyridinium tosylate salt **3**, the solution of compound **2** in pyridine was heated in the pressure vial at 120 °C for 1 h. After workup, compound **3** was acquired with a 72% yield with no need for further purification. Although pyridinium salt **3** was soluble in water, it still possessed bulky and aromatic tosylate anions that potentially could limit the solubility and impact fluorescence. Therefore, the tosylate anions were exchanged to chlorides using ion exchange resin, and product **4** was obtained in an 84% yield. Next, the solubility of compounds **1**–**4** in water was determined by using qNMR (**1**—0.21 mg/mL, **2**—0.19 mg/mL, **3**—57 mg/mL, **4**—133 mg/mL).

Absorption and emission spectra were measured for compound **3** in H_2O, DMSO, and DCM (Figure 1) and for compound **4** in MeCN, MeOH, H_2O, DMSO, and DCM (Figure 2). Compound **3** exhibited absorption maxima at 359–362 nm and emission maxima at 428–565 nm (Table 1). Compound **4** exhibited absorption maxima at 360–363 nm and emission maxima at 452–463 nm (Table 1). Purine derivative **3** showed a blue shift in DCM and red shift in DMSO for emission spectra compared to derivative **4**, probably due to the presence of tosylate ions (Figures 1 and 2). The quantum yields for 10^{-4} M solutions of both compounds were below the detection range (<0.5%). In contrast, starting material **1** was reported to have a 98% QY in DMSO solution at 10^{-5} M concentration [21]. Thus, upon derivatization of propane-1,3-diol fragments at the purine *N*(9) position with pyridinium moieties, the solubility of compounds in water was greatly enhanced, but the fluorescence was practically quenched.

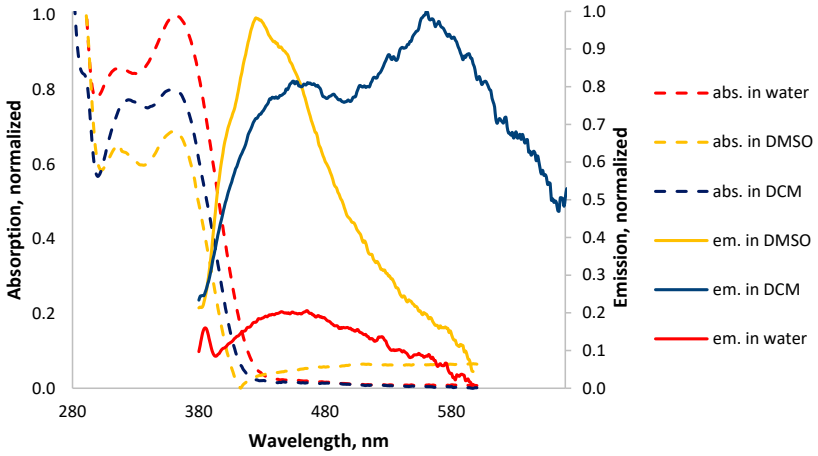

Figure 1. Absorption (dashed lines) and emission (solid lines) spectra for compound **3** at 10^{-4} M concentration in various solvents.

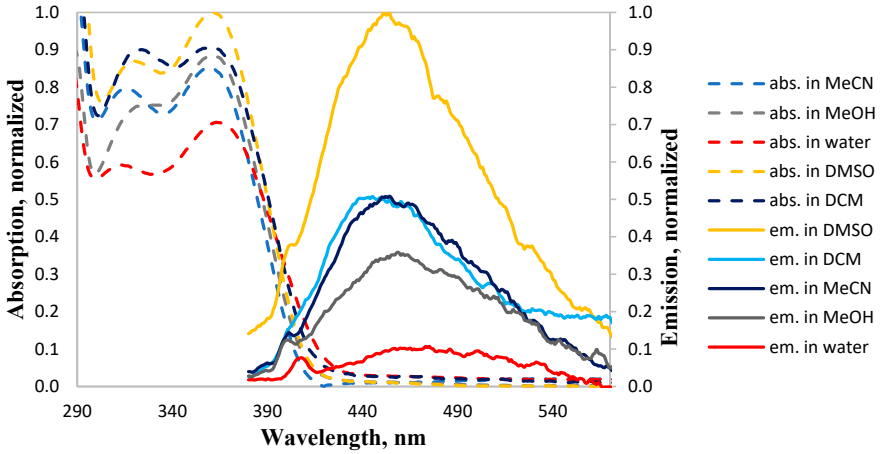

Figure 2. Absorption (dashed lines) and emission (solid lines) spectra for compound **4** at 10^{-5} M concentration in various solvents.

Table 1. Photophysical properties of compounds **3** and **4** in various solvents.

Solvent	Compound 3			Compound 4		
	$\lambda_{abs\ max}$, nm	$\lambda_{em\ max}$, nm	QY, %	$\lambda_{abs\ max}$, nm	$\lambda_{em\ max}$, nm	QY, %
MeCN	-	-	-	360	457	<0.5
MeOH	-	-	-	362	461	<0.5
H_2O	362	457	<0.5	363	463	<0.5
DMSO	361	428	<0.5	362	454	<0.5
DCM	359	565	<0.5	360	452	<0.5

3. Materials and Method

NMR spectra were recorded on Bruker Avance 300 and Bruker Avance 500 spectrometers. ^{1}H-NMR spectra were recorded at 300 or 500 MHz with internal references from nondeuterated solvents (δ = 7.26 for $CDCl_3$, δ = 2.50 for DMSO-d_6) at 20° or 80 °C. ^{13}C-NMR spectra were recorded at 75.5 or 125.7 MHz with internal references from nondeuterated solvents (δ = 77.16 for $CDCl_3$, δ = 39.52 for DMSO-d_6) at 20° or 80 °C. Coupling constants are reported in Hz, chemical shifts of signals are given in ppm, and standard abbreviations are used for multiplicity assignments. Fourier transform infrared (FTIR) spectra were recorded using a Thermo Scientific Nicolet™ iSTM50 (Thermo Fisher, Waltham, MA, USA) spectrometer in the Attenuated Total Reflectance (ATR) mode. Spectra were obtained over a range of wavenumbers from 400 to 4000 cm^{-1}, co-adding 64 scans at 4 cm^{-1} resolution. Before every measurement, a background spectrum was taken and deducted from the sample spectrum. An Orbitrap Exploris 120 (Thermo Scientific, Waltham, MA, USA) mass spectrometer was used for high-resolution mass spectra (ESI). UV–Vis absorption spectra were recorded with a PerkinElmer Lambda 35 spectrometer. Emission spectra and quantum yields for solutions were recorded using a QuantaMaster 40 steady-state spectrofluorometer (Photon Technology International, Inc., Birmingham, NJ, USA) equipped with a 6-inch integrating sphere by LabSphere (North Sutton, NH, USA), using the software package provided by the manufacturer.

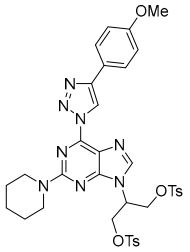

2-{6-[4-(4-Methoxyphenyl)-1H-1,2,3-triazol-1-yl]-2-[piperidin-1-yl]-9H-purin-9-yl}propane-1,3-diyl bis(4-methylbenzenesulfonate) **2**. To a suspension of compound **1** (250 mg, 0.56 mmol, 1.0 eq.) and 4-dimethylaminopyridine (7 mg, 0.056 mmol, 0.1 eq.) in dry DCM (30 mL), Et_3N (0.19 mL, ρ = 0.73 g/cm^3, 1.34 mmol, 2.4 eq.) was added, and the reaction mixture was cooled to 0 °C temperature. Tosyl chloride (253 mg, 1.34 mmol, 2.4 eq.) was added in small portions to the reaction mixture at 0 °C temperature, and the reaction was left stirring for 2 h and then overnight at room temperature. DCM was washed with water (2 × 30 mL) and brine (30 mL), dried over anhydrous Na_2SO_4, filtered and evaporated. Recrystallization from hot ethanol (15 mL) provided product **2** (322 mg, 76%) as a beige amorphous solid. ^{1}H-NMR (500 MHz, $CDCl_3$) δ (ppm): 9.01 (s, 1H, H-C(triazole)), 7.80 (d, 2H, ^3J = 9.0 Hz, 2×H-C(Ar)), 7.53 (s, 1H, H-C(purine)), 7.45 (d, 4H, ^3J = 8.2 Hz, 4×H-C(Ts)), 7.07 (d, 2H, ^3J = 9.0 Hz, 2×H-C(Ar)), 7.03 (d, 4H, ^3J = 8.2 Hz, 4×H-C(Ts)), 4.75 (tt, 1H, ^3J = 8.0, 4.6 Hz, (-CH-)), 4.59 (dd, 2H, ^2J = 10.7 Hz, ^3J = 8.0 Hz, (-CH_2-)), 4.42 (dd, 2H, ^2J = 10.7 Hz, ^3J = 4.6 Hz, (-CH_2-)), 3.90 (s, 3H, (-CH_3)), 3.83–3.70 (m, 4H, 2×(-CH_2-)), 2.27 (s, 6H, 2×(-CH_3)), 1.74–1.68 (m, 2H, (-CH_2-)), 1.68–1.62 (m, 4H, 2×(-CH_2-)). ^{13}C-NMR (125.7 MHz, $CDCl_3$) δ (ppm): 160.2, 158.3, 152.8, 147.6, 145.7, 144.5, 140.7, 131.4, 130.4, 129.9, 127.6, 124.7, 123.0, 122.5, 115.0, 65.2, 55.8, 54.5, 45.4, 26.0, 25.0, 21.8. IR (neat) ν (cm^{-1}): 2934, 2853, 1628, 1564, 1445, 1362, 1250, 1175, 1095, 1017, 977, 808, 785, 640, 554. HRMS (ESI): m/z calculated for $[C_{36}H_{38}N_8O_7S_2 + H]^+$ 759.2378, found 759.2349.

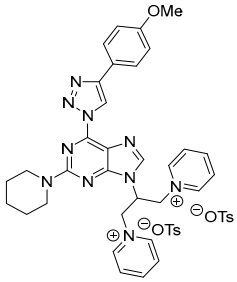

1,1′-(2-{6-[4-(4-Methoxyphenyl)-1H-1,2,3-triazol-1-yl]-2-[piperidin-1-yl]-9H-purin-9-yl}propane-1,3-diyl)bis(pyridin-1-ium) di-4-methylbenzenesulfonate **3**. In the pressure vial, compound **2** (120 mg, 0.158 mmol) in pyridine (7 mL) was heated at 120 °C temperature for 1 h. The reaction mixture was evaporated, then dissolved in DCM (20 mL) and washed with cold water (2 × 30 mL) and cold brine (30 mL). The organic phase was concentrated in a vacuum, giving product **3** (104 mg, 72%) as a yellow oil. ^{1}H-NMR (300 MHz, DMSO-d_6, 80 °C) δ (ppm): 9.22 (s, 1H, H-C(triazole)), 9.02 (d, 4H, ^3J = 6.0 Hz, 4×H-C(Pyridine)), 8.58 (t, 2H, ^3J = 7.7 Hz, 2×H-C(Pyridine)), 8.34 (s, 1H, H-C(purine)), 8.06 (d, 4H, ^3J = 7.0 Hz, 4×H-C(Pyridine)), 7.92 (d, 2H, ^3J = 8.7 Hz, 2×H-C(Ar)), 7.58 (d, 4H, ^3J = 8.1 Hz, 4×H-C(Ts)), 7.12 (d, 4H, ^3J = 8.1 Hz, 4×H-C(Ts)), 7.06 (d, 2H, ^3J = 8.7 Hz, 2×H-C(Ar)), 6.05–5.90 (m, 1H, (-CH-)), 5.72–5.52 (m, 4H, 2×(-CH_2-)), 3.83 (s, 3H, (-CH_3)), 3.83–3.75 (m, 4H, 2×(-CH_2-)), 2.30 (s, 6H, 2×(-CH_3)), 1.74–1.53 (m, 6H, 3×(-CH_2-)). ^{13}C-NMR (75.5 MHz, DMSO-d_6, 80 °C) δ (ppm): 159.4, 157.2, 155.8, 146.4, 146.3, 145.5, 144.9, 144.6, 141.5, 137.3, 128.0, 127.6, 126.9, 125.2, 121.9, 118.7, 114.5, 114.2, 59.4, 56.2, 55.0, 44.7, 24.9, 23.7, 20.3. IR (neat) ν (cm^{-1}): 3058, 2936, 1627, 1560, 1490, 1444,

1176, 1120, 1009, 910, 782, 680, 564. HRMS (ESI): m/z calculated for $[C_{32}H_{34}N_{10}O]^{2+}$ 287.1453, found 287.1449.

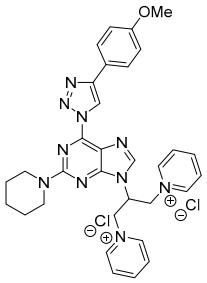

1,1′-(2-{6-[4-(4-Methoxyphenyl)-1H-1,2,3-triazol-1-yl]-2-[piperidin-1-yl]-9H-purin-9-yl}propane-1,3-diyl)bis(pyridin-1-ium) dichloride **4**. Compound **3** (52 mg, 0.057 mmol) was dissolved in water (0.3 mL) and flashed through wet Bio-Rex® 9 ion exchange resin (2 mL), using water (5 mL) as an eluent. Water was evaporated, giving product **4** (31 mg, 84%) as a yellow oil. ^{1}H-NMR (500 MHz, DMSO-d_6, 80 °C) δ (ppm): 9.43 (d, 4H, ^3J = 6.0 Hz, 4×H-C(Pyridine)), 9.22 (s, 1H, H-C(triazole)), 8.78 (s, 1H, H-C(purine)), 8.57 (t, 2H, ^3J = 7.7 Hz, 2×H-C(Pyridine)), 8.08 (t, 4H, ^3J = 7.0 Hz, 4×H-C(Pyridine)), 7.92 (d, 2H, ^3J = 8.7 Hz, 2×H-C(Ar)), 7.06 (d, 2H, ^3J = 8.7 Hz, 2×H-C(Ar)), 6.27 (tt, 1H, ^3J = 10.4, 3.5 Hz, (-CH-)), 5.92 (dd, 2H, ^2J = 13.7 Hz, ^3J = 3.5 Hz, (-CH_2-)), 5.74 (dd, 2H, ^2J = 13.7 Hz, ^3J = 10.4 Hz, (-CH_2-)), 3.83 (s, 3H, (-CH_3)), 3.75 (t, 4H, ^3J = 5.3 Hz, 2×(-CH_2-)), 1.71–1.64 (m, 2H, (-CH_2-)), 1.64–1.54 (m, 4H, 2×(-CH_2-)). ^{13}C-NMR (125.7 MHz, DMSO-d_6, 80 °C) δ (ppm): 159.4, 157.1, 155.9, 146.29, 146.27, 145.0, 144.4, 142.0, 127.8, 126.8, 121.9, 118.7, 114.3, 114.2, 59.1, 56.8, 55.0, 44.6, 24.9, 23.7. IR (neat) ν (cm^{-1}): 3046, 2935, 2853, 1626, 1560, 1489, 1442, 1249, 1177, 1017, 910, 838, 782, 684. HRMS (ESI): m/z calculated for $[C_{32}H_{34}N_{10}O]^{2+}$ 287.1453, found 287.1446.

4. Conclusions

1,1′-(2-{6-[4-(4-Methoxyphenyl)-1*H*-1,2,3-triazol-1-yl]-2-[piperidin-1-yl]-9*H*-purin-9-yl} propane-1,3-diyl)bis(pyridin-1-ium) di-4-methylbenzenesulfonate and 1,1′-(2-{6-[4-(4-methoxy phenyl)-1*H*-1,2,3-triazol-1-yl]-2-[piperidin-1-yl]-9*H*-purin-9-yl}propane-1,3-diyl)bis(pyridin-1-ium) dichloride salts were obtained in 72 and 84% yields by substitution of tosylates of propane-1,3-diol fragments at the *N9* position of purine with pyridinium moieties. 2-Amino-6-triazolyl purine pyridinium conjugates were easily soluble in water, and this opens the possibility of using them in biological studies in the future. 1,1′-(2-{6-[4-(4-Methoxyphenyl)-1*H*-1,2,3-triazol-1-yl]-2-[piperidin-1-yl]-9*H*-purin-9-yl}propane-1,3-diyl)bis(pyridin-1-ium) dichloride salt showed decreased fluorescence intensity in MeCN, MeOH, H_2O, DMSO, and DCM and had a QY below 0.5% in comparison to its highly fluorescent analog 2-(6-(4-(4-methoxyphenyl)-1*H*-1,2,3-triazol-1-yl)-2-(piperidin-1-yl)-9*H*-purin-9-yl)propane-1,3-diol.

Supplementary Materials: The following supporting information can be downloaded: the procedure for the determination of the solubility of compounds **1**–**4** in water by qNMR, ^{1}H- and ^{13}C-NMR spectra of 2-{6-[4-(4-methoxyphenyl)-1*H*-1,2,3-triazol-1-yl]-2-[piperidin-1-yl]-9*H*-purin-9-yl}propane-1,3-diyl bis(4-methylbenzenesulfonate) (**2**), 1,1′-(2-{6-[4-(4-methoxyphenyl)-1*H*-1,2,3-triazol-1-yl]-2-[piperidin-1-yl]-9*H*-purin-9-yl}propane-1,3-diyl)bis(pyridin-1-ium) di-4-methylbenzenesulfonate (**3**), 1,1′-(2-{6-[4-(4-methoxyphenyl)-1*H*-1,2,3-triazol-1-yl]-2-[piperidin-1-yl]-9*H*-purin-9-yl}propane-1,3-diyl)bis(pyridin-1-ium) dichloride (**4**); FTIR spectra and HRMS results of compounds **2**, **3**, and **4**.

Author Contributions: A.B. performed the synthetic experiments and prepared the manuscript draft; I.N. and M.T. designed the experiments, managed the research and reviewed the manuscript. All authors have read and agreed to the published version of the manuscript.

Funding: This research was funded by the Latvian Council of Science Latvia-Lithuania-Taiwan co-project MEPS LV-LT-TW/2024/5.

Data Availability Statement: The original contributions presented in the study are included in the article/Supplementary Material; further inquiries can be directed to the corresponding authors.

Acknowledgments: The authors thank Emanuels Šūpulnieks for their assistance with the FTIR analysis and Kaspars Traskovskis and Armands Rudušs for the absorption and emission spectra measurements.

Conflicts of Interest: The authors declare no conflicts of interest.

References

1. Seley-Radtke, K.L.; Yates, M.K. The evolution of nucleoside analogue antivirals: A review for chemists and non-chemists. Part 1: Early structural modifications to the nucleoside scaffold. *Antivir. Res.* **2018**, *154*, 66–86. [CrossRef] [PubMed]
2. Legraverend, M. Recent advances in the synthesis of purine derivatives and their precursors. *Tetrahedron* **2008**, *64*, 8585–8603. [CrossRef]
3. Shaw, G. 4.09-Purines. In *Comprehensive Heterocyclic Chemistry*; Katritzky, A.R., Rees, C.W., Eds.; Elsevier: Pergamon, Turkey, 1984; Volume 5, pp. 499–605.
4. Joule, J.A.; Mills, K. Purines. In *Heterocyclic Chemistry at a Glance*; John Wiley & Sons, Ltd.: Chichester, UK, 2012; pp. 122–131.
5. Hocek, M. Syntheses of purines bearing carbon substituents in positions 2, 6 or 8 by metal- or organometal-mediated C-C bond-forming reactions. *Eur. J. Org. Chem.* **2003**, *2003*, 245–254. [CrossRef]
6. Manvar, A.; Shah, A. Microwave-assisted chemistry of purines and xanthines. An overview Dedicated to the late Professor V.M. Thakor on his 94th birthday. *Tetrahedron* **2013**, *69*, 8105–8127. [CrossRef]
7. Novosjolova, I.; Bizdēna, Ē.; Turks, M. Synthesis and applications of azolylpurine and azolylpurine nucleoside derivatives. *Eur. J. Org. Chem.* **2015**, *2015*, 3629–3649. [CrossRef]
8. Kovaļovs, A.; Novosjolova, I.; Bizdēna, Ē.; Bižane, I.; Skardziute, L.; Kazlauskas, K.; Jursenas, S.; Turks, M. 1,2,3-Triazoles as leaving groups in purine chemistry: A three-step synthesis of *N6*-substituted-2-triazolyl-adenine nucleosides and photophysical properties thereof. *Tetrahedron Lett.* **2013**, *54*, 850–853. [CrossRef]
9. Zaķis, J.M.; Ozols, K.; Novosjolova, I.; Vilšķērsts, R.; Mishnev, A.; Turks, M. Sulfonyl group dance: A tool for the synthesis of 6-azido-2-sulfonylpurine derivatives. *J. Org. Chem.* **2020**, *85*, 4753–4771. [CrossRef] [PubMed]
10. Legraverend, M.; Grierson, D.S. The purines: Potent and versatile small molecule inhibitors and modulators of key biological targets. *Bioorg. Med. Chem.* **2006**, *14*, 3987–4006. [CrossRef] [PubMed]
11. Sharma, S.; Singh, J.; Ojha, R.; Singh, H.; Kaur, M.; Bedi, P.M.S.; Nepali, K. Design strategies, structure-activity relationship and mechanistic insights for purines as kinase inhibitors. *Eur. J. Med. Chem.* **2016**, *112*, 298–346. [CrossRef]
12. Matarazzo, A.; Brow, J.; Hudson, R.H.E. Synthesis and photophysical evaluation of new fluorescent 7-arylethynyl-7-deazaadenosine analogs. *Can. J. Chem.* **2018**, *96*, 1093–1100. [CrossRef]
13. Saito, Y.; Hudson, R.H.E. Base-modified fluorescent purine nucleosides and nucleotides for use in oligonucleotide probes. *J. Photochem. Photobiol. C Photochem. Rev.* **2018**, *36*, 48–73. [CrossRef]
14. Venkatesham, A.; Pillalamarri, S.R.; Wit, F.; Lescrinier, E.; Debyser, Z.; Aerschot, A. Propargylated purine deoxynucleosides: New tools for fluorescence imaging strategies. *Molecules* **2019**, *24*, 1–16. [CrossRef] [PubMed]
15. He, H.; Zatorska, D.; Kim, J.; Aguirre, J.; Llauger, L.; She, Y.; Wu, N.; Immormino, R.M.; Gewirth, D.T.; Chiosis, G. Identification of potent water-soluble purine-scaffold inhibitors of the heat shock protein 90. *J. Med. Chem.* **2006**, *49*, 381–390. [CrossRef] [PubMed]
16. Gołdyn, M.R.; Larowska, D.; Bartoszak-Adamska, E. Novel Purine Alkaloid Cocrystals with Trimesic and Hemimellitic Acids as Coformers: Synthetic Approach and Supramolecular Analysis. *Cryst. Growth Des.* **2021**, *21*, 396–413. [CrossRef] [PubMed]
17. Carreira, A.R.F.; Veloso, T.; Schaeffer, N.; Pereira, J.L.; Ventura, S.P.M.; Rizzi, C.; Plénet, J.S.; Passos, H.; Coutinho, J.A.P. Synthesis of purine-based ionic liquids and their applications. *Molecules* **2021**, *26*, 6958. [CrossRef] [PubMed]
18. Sun, K.M.; McLaughlin, C.K.; Lantero, D.R.; Manderville, R.A. Biomarkers for phenol carcinogen exposure act as pH-sensing fluorescent probes. *J. Am. Chem. Soc.* **2007**, *129*, 1894–1895. [CrossRef] [PubMed]
19. Kumar, A.; Mital, S. Electronic and photocatalytic properties of purine(s)-capped CdS nanoparticles in the presence of tryptophol. *J. Mol. Catal. A Chem.* **2004**, *219*, 65–71. [CrossRef]
20. Jovaisaite, J.; Cīrule, D.; Jeminejs, A.; Novosjolova, I.; Turks, M.; Baronas, P.; Komskis, R.; Tumkevicius, S.; Jonusauskas, G.; Jursenas, S. Proof of principle of a purine D-A-D′ ligand based ratiometric chemical sensor harnessing complexation induced intermolecular PET. *Phys. Chem. Chem. Phys.* **2020**, *22*, 26502–26508. [CrossRef]
21. Burcevs, A.; Sebris, A.; Traskovskis, K.; Chu, H.W.; Chang, H.T.; Jovaišaitė, J.; Juršėnas, S.; Turks, M.; Novosjolova, I. Synthesis of Fluorescent C–C Bonded Triazole-Purine Conjugates. *J. Fluoresc.* **2024**, *34*, 1091–1097. [CrossRef]
22. Sebris, A.; Novosjolova, I.; Traskovskis, K.; Kokars, V.; Tetervenoka, N.; Vembris, A.; Turks, M. Photophysical and Electrical Properties of Highly Luminescent 2/6-Triazolyl-Substituted Push-Pull Purines. *ACS Omega* **2022**, *7*, 5242–5253. [CrossRef]
23. Šišuļins, A.; Bucevičius, J.; Tseng, Y.T.; Novosjolova, I.; Traskovskis, K.; Bizdēna, Ē.; Chang, H.T.; Tumkevičius, S.; Turks, M. Synthesis and fluorescent properties of N(9)-alkylated 2-amino-6-triazolylpurines and 7-deazapurines. *Beilstein J. Org. Chem.* **2019**, *15*, 474–489. [CrossRef] [PubMed]

24. Sajomsang, W.; Gonil, P.; Ruktanonchai, U.R.; Petchsangsai, M.; Opanasopit, P.; Puttipipatkhachorn, S. Effects of molecular weight and pyridinium moiety on water-soluble chitosan derivatives for mediated gene delivery. *Carbohydr. Polym.* **2013**, *91*, 508–517. [CrossRef] [PubMed]
25. Islam, M.B.; Islam, M.I.; Nath, N.; Emran, T.B.; Rahman, M.R.; Sharma, R.; Matin, M.M. Recent Advances in Pyridine Scaffold: Focus on Chemistry, Synthesis, and Antibacterial Activities. *BioMed Res. Int.* **2023**, *2023*, 9967591. [CrossRef] [PubMed]
26. Wade, D.A.; Tucker, S.A. Spectrochemical evaluation of pyridinium chloride as a possible selective fluorescence quenching agent of polycyclic aromatic hydrocarbons in water and neat acetonitrile. *Talanta* **2000**, *53*, 571–578. [CrossRef]
27. Hann, R.A.; Rosseinsky, D.R.; White, T.P. Inter- and intra-molecular quenching of anthracene fluorescence by pyridinium ion in solution. *J. Chem. Soc. Faraday Trans. 2* **1974**, *70*, 1522–1525. [CrossRef]

Pielikums IV
Appendix IV

Jovaisaite, J.; Boguševičienė, K.; Jonusauskas, G.; Kreiza, G.; Burcevs, A.; Kapilinskis, Z.; Novosjolova, I.; Turks, M.; Hean, L. E.; Chu, H.-W.; Chang, H.-T.; Juršėnas, S.

Purine-based chemical probe with HOMO switching for Intracellular Detection of Mercury Ions

Manuskripts iesniegts Scientific Reports 11.03.2025. /

Manuscript submitted to Scientific Reports on 11.03.2025.

Purine-based chemical probe with HOMO switching for Intracellular Detection of Mercury Ions

Kamilė Boguševičienė[1†], Justina Jovaišaitė[1†*], Gediminas Jonusauskas[1,2*], Gediminas Kreiza[1], Aleksejs Burcevs[3], Zigfrīds Kapilinskis[3], Irina Novosjolova[3], Maris Turks[3], Li Er Hean[4], Han-Wei Chu[4], Huang-Tsung Chang[4,5] and Saulius Juršėnas[1]

[1] Institute of Photonics and Nanotechnology, Faculty of Physics, Vilnius University, Saulėtekis Av. 3, Vilnius, LT-10222 Lithuania

[2] Laboratoire Ondes et Matière d'Aquitaine, Bordeaux University, UMR CNRS 5798, 351 Cours de la Libération, Talence, 33405, France

[3] Institute of Chemistry and Chemical Technology, Faculty of Natural Sciences and Technology, Riga Technical University, P. Valdena Str. 3, Riga, LV-1048, Latvia

[4] Department of Biomedical Sciences, College of Medicine, Chang Gung University, Taoyuan, 33302, Taiwan

[5] College of Pharmacy, Kaohsiung Medical University, Kaohsiung 80708, Taiwan

† These authors contributed equally to this work

* Corresponding authors: Justina Jovaišaitė (justina.jovaisaite@ff.vu.lt) and Gediminas Jonusauskas (gediminas.jonusauskas@u-bordeaux.fr)

Abstract

The detailed photophysical characterization of 2-piperidinyl-6-triazolylpurine derivatives and their complexes with metal ions is presented. The studied compounds bear two electron donating units – piperidine and methoxyphenyl, while triazolyl-purine acts as electron acceptor. The present derivatives possess good fluorescence quantum yields in both aprotic and aqueous environments. All piperidine-triazole-purine compounds revealed a fluorescence "turn-off" sensing behavior to different metal ions, including Hg^{2+}. We are discussing the changes in photophysical properties occurring under complexation including switching between highest occupied molecular orbitals (HOMOs) of different electron donating units and the entire electron charge shift possibility in the complex with mercury ion. The sensing concept was further applied for newly synthesized water-soluble compounds, that demonstrated better selectivity towards Hg^{2+} in aqueous media. Further, the selected 2-piperidinyl-6-triazolylpurine water-soluble derivative was employed as "turn-off" chemical probe for mercury ion detection in living cells.

Keywords

Purine, chemical probe, mercury ion sensing, "turn-off" fluorescence, HOMO switching, mercury ion imaging

Introduction

Purine is the most widely distributed nitrogen heterocycle in nature and can be regarded as a unique heterocyclic base with respect to diverse possibilities of its chemical modifications[1]. The exceptional biological activity of purine-based derivatives, including antitumor[2], antiviral[3,4] antibacterial[5] and antioxidant properties[6], encouraged it's development towards medical applications[7,8]. Furthermore, the additional characteristics, such as good biocompatibility, large π-conjugated plane and multiple readily available modification sites have raised a scientific interest to develop multifunctional purine-based fluorescent materials[9–13]. Recently, there has been an increasing number of publications presenting the potential applications of these derivatives, including organic light emitting diodes (OLEDs)[14–17], information encryption and anti-counterfeiting[18], bioimaging[19,20], also, optical probes for metal ion sensing[21,22], including heavy metals, such as cadmium (II)[23] or palladium (II)[24].

Mercury is one of the heavy metals continuously raising concern due to its non-biodegradable nature, high toxicity and harmful effects on living organisms. Inorganic Hg^{2+} can transform into methylmercury, which readily bioaccumulates in animals and plants[25]. This bioaccumulation can ultimately lead to methylmercury's entry into the human body, most commonly through the consumption of contaminated fish and seafood[26]. It has been noticed that small amounts of methylmercury can be traced almost in all humans, indicating its widespread occurrence in the environment[27,28], including crops or terrestrial ecosystems[29]. The exposure to high levels of methylmercury may cause serious health problems, such as damage and disorder of nervous, digestive and immune systems[27,30,31]. As a result, ongoing efforts are focused on developing real-time detection and monitoring techniques for mercury in food, environment and biological samples, including Hg^{2+} imaging in living cells[29,32].

Chemical metal ion detection via colorimetry or fluorimetry is a promising tool due to its simplicity, non-sophisticated equipment, quick, sensitive and selective detection and no need of specific sample pre-treatment[33,34]. The fast-evolving field of molecular sensor chemistry is closely connected to versatile of organic compounds and possibility to govern photophysical properties upon chemosensor-analyte complexation[35]. On the other hand, it still remains a challenging task to create water-soluble, biocompatible, non-toxic and well coordinating organic molecular sensors that could additionally penetrate cell membrane and expand the range of applications in biological systems[36,37]. The promising candidates for mercury ion detection are nitrogen heterocycles. The widely demonstrated Hg^{2+} chemosensors

based on pyrrole, imidazole, pyrazole, pyridine or porphyrin derivatives have proven the possibility to form stable complexes with Hg^{2+} via coordination with N atoms. Purine heterocyclic skeleton is characterized by an electron delocalization and there are four nitrogen atoms in the ring providing potential coordination sites for metal ions[21]. Regarding this and above-mentioned reasons, especially biocompatibility and possible cell membrane permittivity, we believe that purine-based compounds could be a prominent material in terms of optical mercury ion probe development.

In this study, we present a detailed photophysical characterization of 2-piperidinyl-6-triazolylpurine (**PTP**) and its newly synthesized water-soluble derivatives (**PTPa** and **PTPb**). The introduction of electron rich piperidine unit at C2 position of purine core enabled to create a desirable push-pull system while maintaining high fluorescence quantum yields[38,39]. The triazolyl ring was connected to purine core at C6 position via stable C-C bond[40]. This prevented the triazole from acting as a leaving group[41–44] and introduced a metal ion complexing site between nitrogen atoms of the triazole N3 and the purine N7[40,45]. The molecular structure was further extended by electron donating 4-methoxyphenyl at C4 position of triazolyl ring, that allowed to create a donor-acceptor-donor' (D-A-D') type material. **PTP** and its water-soluble derivatives were able to form complexes with several different metal ions. Consequently, the photophysical response and the sensing mechanism were further studied in the presence of metal ions with special attention to Hg^{2+} in aprotic solvents, aqueous medium and living cells. To the best of our knowledge, there are only limited examples in the literature of purine-based fluorescent dyes demonstrated as Hg^{2+} chemical probes[46]. Moreover, this is the first time water-soluble purine-based compounds were developed for mercury ion detection and were further applied for intracellular Hg^{2+} imaging.

Results and Discussion

Synthesis of PTP and its water-soluble derivatives PTPa and PTPb

The design and synthesis concept of 2-piperidinyl-6-triazolylpurine (**PTP**) was already reported by us recently (Fig. 1a)[40]. Now we have developed an approach for the synthesis of modified purine-based chemical sensors **PTPa** and **PTPb** with groups at the N9 position of purine which increase the product solubility in water (Fig. 1b). Firstly, we introduced tetraethylene glycol moiety protected with the THP[47] group at the N9 position via the

Mitsunobu reaction. Next, in the Sonogashira reaction, we obtained purine derivative **5**, which was subsequently used in CuAAC with 1-azido-4-methoxybenzene and S_NAr with piperidine, yielding the derivative **6**. The deprotection of the THP group with TFA in methanol (MeOH) gave the first target product, **PTPa**, which was used in photophysical studies and titration experiments and for further modifications. The second target product - a derivative of 3,6,9,12-tetraoxatetradecanoic acid **PTPb** was obtained by alkylation of tetraethylene glycol with *tert*-butyl 2-bromoacetate and further removal of *tert*-butyl protecting group. More details on synthesis procedures are given in section **Methods** and Electronic Supplementary Information (ESI), Fig. S1 – S14.

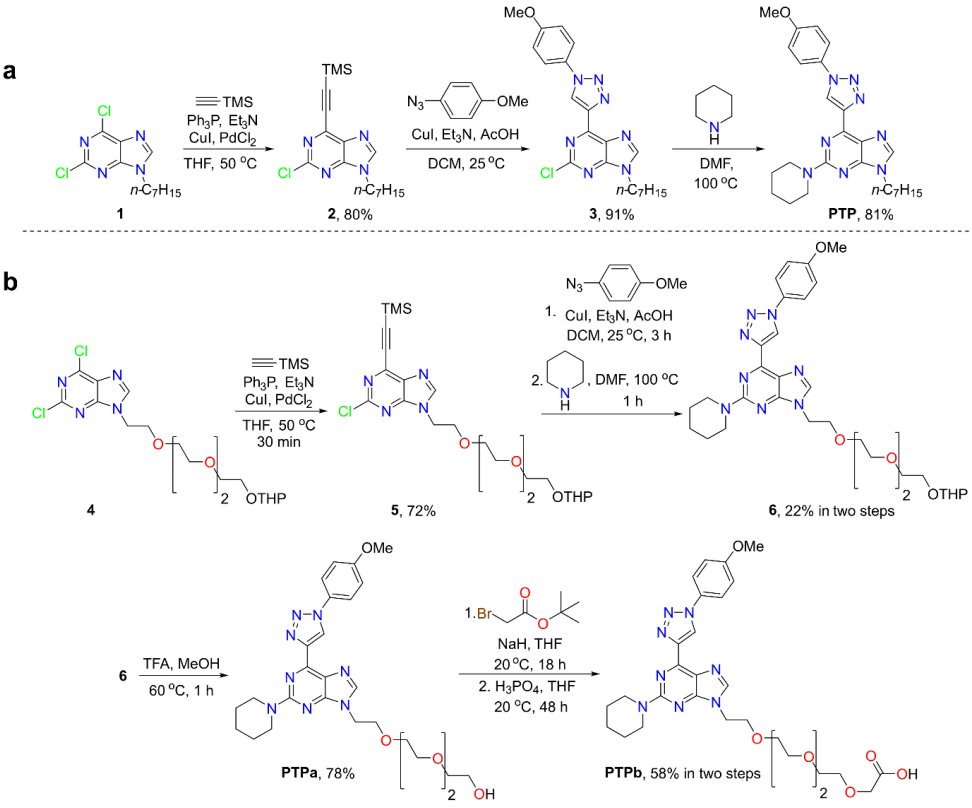

Figure 1. Synthesis of **PTP** (a) and its water-soluble derivatives **PTPa** and **PTPb** (b).

Photophysical characterisation of PTP compounds

The photophysical characterization of **PTP** compound was performed in aprotic solvents of different polarities (cyclohexane (CyHex), diethyl ether (Et_2O), ethyl acetate (EtOAc), dimethoxyethane (DME), acetonitrile (MeCN) and dimethyl sulfoxide (DMSO)), while materials **PTPa** and **PTPb** were tested in water (see summarized results in Fig. 2 and Table 1).

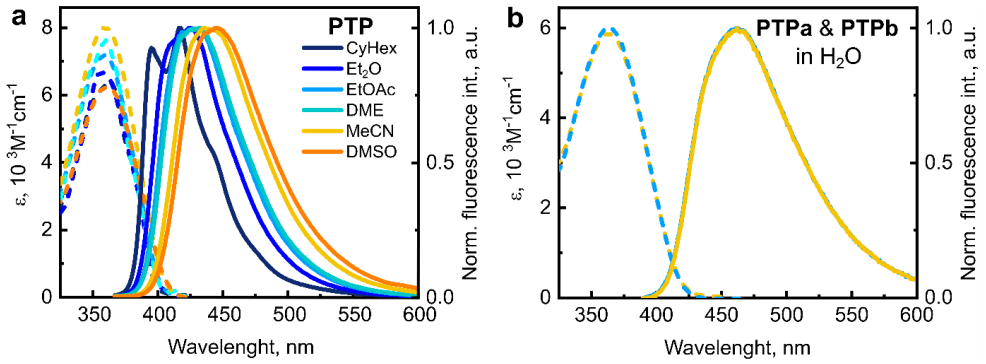

Figure 2. The absorption (dotted lines) and fluorescence (solid lines) spectra of **PTP** in different solvents, indicated in the legend (a) and **PTPa** (blue lines) and **PTPb** (yellow lines) in water (b).

Table 1. Steady-state absorption, fluorescence and time-resolved fluorescence spectroscopic data of compound **PTP** in different solvents and compounds **PTPa** and **PTPb** in water.

Compound	Solvent	ε[1], l/(mol*cm)	λ_{ab}[2], nm	λ_{fl}[3], nm	QY[4], %	τ[5], ns	τ_{rad}[6], ns	τ_{nonrad}[7], ns
PTP	CyHex	6447	365	415 395	61	9	14.8	23.1
	Et_2O	6715	360	425	52	9.4	18.1	19.6
	EtOAc	7162	360	425	48	9.3	19.4	17.9
	DME	7639	360	425	50	9.7	19.4	19.4
	MeCN	8026	360	435	49	12.4	25.3	24.3
	DMSO	6268	360	445	72	15.7	21.8	56.1
PTPa	H_2O	6005	363	462	17	7.1	41.5	8.5
PTPb		5273	363	462	17	7.1	41.8	8.6

[1] Molar extinction coefficients at wavelengths of absorption maxima. [2] Wavelengths of absorption spectra maxima. [3] Wavelengths of fluorescence spectra maxima, obtained by excitation at absorption maxima.

[4] Fluorescence quantum yields, determined by the comparative method using quinine sulfate as an etalon. [5] Fluorescence lifetimes. [6] Radiative fluorescence decay lifetimes, $\tau_{rad} = \frac{\tau}{QY}$. [7] Non-radiative fluorescence decay lifetimes, $\tau_{nonrad} = \frac{\tau}{1-QY}$.

The absorption band for **PTP** is positioned at ca. 360 nm and remains stable upon increase of solvent's polarity, indicating a weak molecular dipole moment in its ground state (Fig. 2a). The alteration of fluorescence properties is more pronounced, yet not extreme. Fluorescence spectra become structureless and tend to slightly red shift (~20 nm). Fluorescence quantum yields (QYs) decrease from 61% to 49% upon changing the solvent from CyHex to MeCN. The fluorescence lifetimes remain relatively long – 9 ns (CyHex) to 12.4 ns (MeCN), indicating quite low cross section for the vertical S_1-S_0 transition. In addition, as it is obvious from fluorescence efficiency values, there is a close competition between radiative and non-radiative excitation decay channels. Furthermore, it is worth noting that already slow non-radiative decay is even more slacken in viscous DMSO solvent (τ_{nonrad} increase from 24.3 ns in MeCN to 56.1 ns in DMSO), resulting in the significant fluorescence quantum yield increase of up to 72%. This may indicate that photoexcitation in non-viscous environment is somewhat "lost" through molecular motions.

The newly synthesized water-soluble compounds **PTPa** and **PTPb** possess almost identical excited-state properties to each other in water that resemble those obtained for **PTP** in more polar surroundings (Fig. 2b). The fluorescence spectra peaking at 460 nm is red-shifted by 25 nm (in comparison to **PTP** in MeCN) and the fluorescence QY values drop to 17 %. The quenching of fluorescence in water is expected due to high-energy vibrations of OH groups[48], however, the obtained QY values are considered to be sufficient for further sensing applications in water.

To gain insights into potential application of the presented molecules as chemical metal ions sensors, the titration experiments with metal ion salts in MeCN and water and the discussion on the sensing mechanism will be presented in the upcoming sections.

Metal ion recognition by PTP in acetonitrile

Steady-state absorption and fluorescence titration experiments were performed using alkali (Na^+ and K^+), alkaline earth (Mg^{2+}, Ca^{2+}), transition (Fe^{2+}, Cu^{2+}, Zn^{2+}, Hg^{2+}) and other

(Pb^{2+}) metal ions. The C-C-linked triazole to the purine core enabled triazole complexation with metal ions at its N3 and purine complexation at its N7 (see ^{1}H-NMR titration experiments with metal salts, Fig. S15-S21 in the ESI).

Upon the addition of mercury salts into **PTP**- MeCN solution, the gradual absorption spectrum red-shift and the formation of a new absorption band peaking at 382 nm is observed. The complexation of metal ions with triazole N3 and purine N7 enhances their electron acceptor properties, thus the absorption energy is decreased until the ligand-metal complex is completely formed with its own characteristic absorption band. The changes of fluorescence spectra in the presence of metal ions are dramatic: the fluorescence spectra are gradually quenched until an almost non-emissive state with spectrum of low intensity peaking at 494 nm is observed (Fig. 3a and Fig. 3a inset).

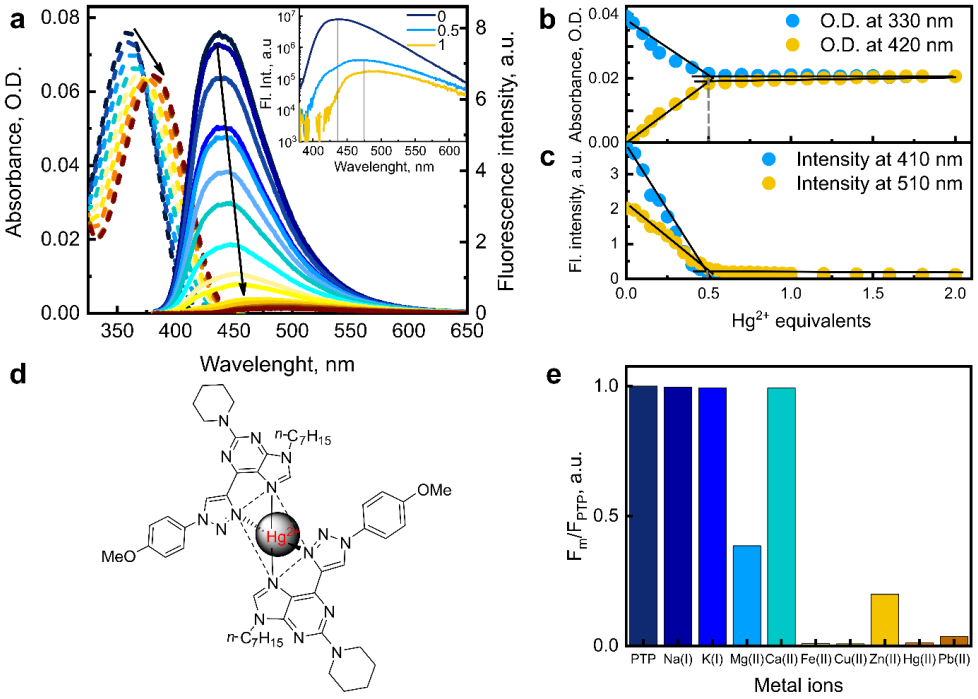

Figure 3. The absorption and fluorescence spectra response of compound **PTP** to added Hg^{2+} ions in MeCN (a). The black curves represent **PTP** absorption (dotted) and fluorescence spectra (solid) with 0 equivalents of Hg^{2+}; the initial titration step for absorption spectra is 0.1 eq, for fluorescence spectra is 0.05 eq. Final titration curves are obtained for **PTP** and 2 equivalents

of Hg^{2+} in MeCN. The inset in (a) represents fluorescence spectra with 0 eq, 0.5 eq and 1 eq of Hg^{2+} in a logarithmic scale. The absorbance (b) and fluorescence intensity (c) dependence on Hg^{2+} equivalents. Possible complexation mode of 2 **PTP** ligands and 1 mercury ion (d). The fluorescence intensity response diagram to different metal ions (e).

The absorption and fluorescence spectra amplitude dependence on mercury ion equivalents (Fig. 3b and 3c, respectively) indicates identical trends of complexation mode: coordination occurs between two ligands (L) and one metal (M) ion (2L : 1M) (Fig. 3d). The precise complexation pattern was further supported by ^{1}H NMR titration experiments of **PTP** in MeCN-d_3, using benzene as a standard and $Hg(ClO_4)_2 \cdot 3H_2O$ as a Hg^{2+} source and observing the shifts of CH(5) position of triazole and CH(8) position of purine. ^{1}H-NMR spectrum was taken after each addition of the solution containing 0.1 eq. of Hg^{2+} ions to the **PTP** solution in MeCN-d_3. The traces of **PTP** were seen after the addition of 0.5 eq. of Hg^{2+} ions and it fully disappeared after the addition of 0.6 eq. of Hg^{2+} ions, that supports our previous assumption about the coordination pattern (2 L:1 M) (Fig. S15 – S16). Indeed, as already shown by us earlier, the triazolyl-purine compounds can be considered as a general choice for coordination with metal ions[45].

As it is evident from additional fluorescence and absorption titration experiments (Fig. S28-S29 in the ESI), the **PTP** compound showed similar response to other transition metal ions, including Fe^{2+}, Cu^{2+}, Zn^{2+} as well as Pb^{2+}: the absorption spectra upon complexation tend to red-shift that results in new absorption bands, while fluorescence intensity is quenched (Fig. 3e). A more appealing complexation case is observed for Zn^{2+} that deserves a separate explanation. Both the absorption and titration experiments revealed a dual complexation mode of **PTP** that depends on the concentration of zinc ions in the system. Initially, when the concentration of Zn^{2+} ions is 0.5 equivalents and above in respect to the ligand, a complex with general formula [$\mathbf{PTP}_2$•Zn^{2+}] is formed. Next, as the zinc ion concentration increases (up to 1 equivalent of Zn^{2+} and above), the initial coordination compound equilibrates with the complex [**PTP**•Zn^{2+}] (see Fig. S17-S21, Table S7 and Fig. S30-S31 in the ESI). As it is seen from the fluorescence titration experiments, the fluorescence of single **PTP** molecules is quenched, nevertheless, the new red-shifted fluorescence band arises, with intensity peak value at 480 nm. Thus, the complex [**PTP**•Zn^{2+}] is fluorescent, contrary to what was observed for other metal ions.

Even though the coordination behavior with Zn^{2+} appeared to be interesting and well distinguishable from other metal ions, the titration experiments with water-soluble **PTPa** and **PTPb** compounds showed the absence of coordination with zinc ions in water (*vide infra*). Thus, we continue to attain deeper understanding into the complexation mechanism with mercury ions by performing transient absorption measurements and quantum chemical modelling.

Femtosecond transient absorption studies

The femtosecond transient absorption (TA) measurements were performed for **PTP** and **PTP** with 0.5 equivalent of Hg^{2+} in MeCN. The excited state absorption (ESA) spectra at 3 ps delay after excitation are shown in Fig. 4 (the spectrum-time resolved maps of ESA and TA signal decay are presented in Fig. S32-S33, ESI). The ESA spectra show narrow and intense absorption bands in the region of 400-430 nm and large non-structured absorption bands in the range of 500-850 nm for both samples. Though the ESA spectra are similar for both samples, one will notice that the narrow absorption band at 400-430 nm is red shifted for **PTP**:0.5 Hg^{2+} with the respect to the spectral position of corresponding absorption band of **PTP** by c.a. 16 nm.

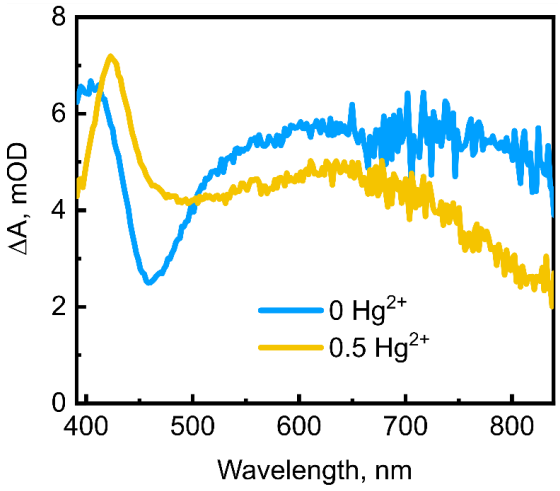

Figure 4. TA spectra for **PTP** and **PTP** with 0.5 eq. of Hg^{2+} observed at 3 ps delay after excitation.

We assign the blue absorption band to the transition of the remaining electron in HOMO towards a free place in LUMO already singly occupied. This absorption should be somewhat similar to that of cation radical of compound or complex. The absorption band in the visible spectral region is the electronic transition from singly occupied LUMO towards higher electronic states. This absorption should be similar to that of anion radical of compound or complex. The stimulated emission is not explicitly seen at fluorescence wavelengths, yet the valley in **PTP** spectrum centered at 460 nm may indicate the influence of stimulated emission on the overall spectrum shape. Moreover, the displacement of previously mentioned valley to the red at first 0.5 ps for **PTP** (see Fig. S32 in the ESI) confirms previous suggestion since this is a typical behaviour of dynamic solvation observed for stimulated emission of excited molecular compounds in MeCN.

HOMO – HOMO-1 switching, revealed by quantum chemistry modelling

To gain further insights into the photophysical properties of **PTP** molecule, density functional theory (DFT) and time-dependent (TD) – DFT calculations were performed at the B3LYP/6-31G(d) level employing polarized continuum model (PCM). According to the electron distribution in the highest occupied molecular orbital (HOMO) and the lowest unoccupied molecular orbital (LUMO) in the optimized ground state geometry (Fig. 5a and Fig. S38 in the ESI), both piperidine and purine moieties serve as electron donors, while upon photoexcitation charge is redistributed towards purine-triazole and slightly on 4-methoxyphenyl fragments. Optimized S_1 geometry and polar acetonitrile environment determined only negligible HOMO-LUMO charge distribution changes in comparison to optimized S_0 geometry in vacuum (Fig. S38, ESI). The calculated electronic absorption spectrum involves only HOMO→LUMO transition and estimated transition energy 3.56 eV (Table S14, ESI) well corresponds to the maximum of the lowest energy steady state absorption band at 360-365 nm. The next optically active electronic transition occurs at 4.74 eV (290 nm) and corresponds to HOMO-1→LUMO transition.

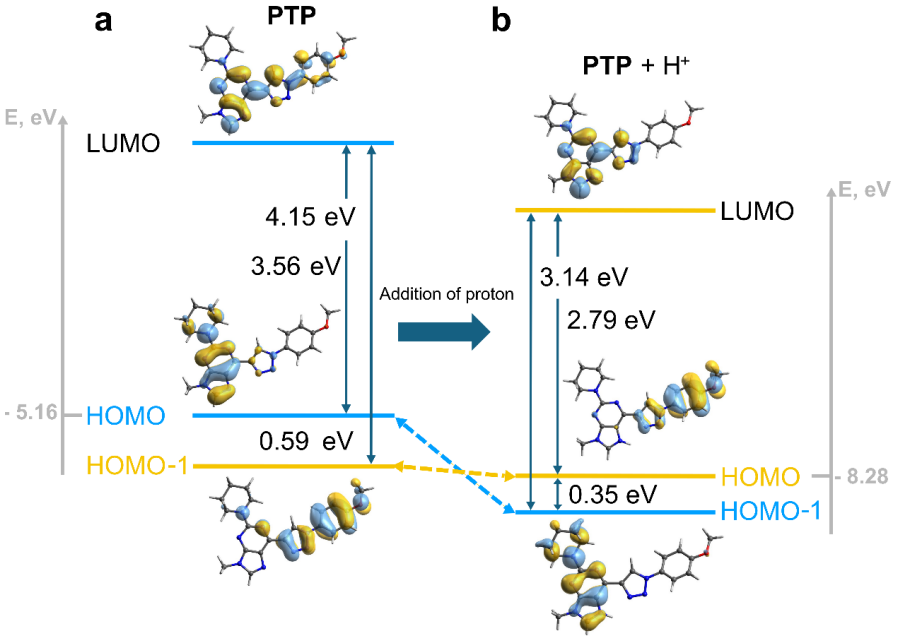

Figure 5. The HOMO-1, HOMO and LUMO orbital distribution and energy diagrams of **PTP** compound (a) and of **PTP** with added proton (**PTP** + H^+) (b), calculated with optimized ground state geometry in vacuum. Calculated ionization potentials are -5.15 eV for **PTP** and -8.28 eV for **PTP** + H^+.

In order to estimate the photophysical properties of the complexed compound, thought, maintaining the simplicity of the modelled system, the geometry of protonated compound (**PTP** + H^+) was optimized in its ground state. Interestingly, the localization of HOMO and HOMO-1 molecular orbitals are inversed in a complex as compared with the neutral compound. The HOMO is now located on methoxyphenyl-triazole and HOMO-1 on purine-piperidine fragment (Fig. 5b). This inversion may be easily understood since the positive proton charge cancels the excess negative charge of piperidine nitrogen due to H^+ incorporation into aromatic electronic system of purine, while the remaining part of compound is much less affected. The optical excitation creates a charge transfer state with negative charge shift from methoxyphenyl towards protonated purine.

The exchange of HOMO and HOMO-1 electronic levels upon complexation with cations can also explain the observed differences in TA spectra for **PTP** and **PTP** with 0.5 eq.

of Hg^{2+} shown in Fig. 4. Indeed, the electron donating and the electron accepting parts in two samples are different, so the optical absorption of cationic fragments changes from 400 nm for piperidine-purine to 415 nm for methoxybenzene, the usual absorption wavelength already observed for this donor (as an example see Fig. 5a in a reference[49]). Similarly, the absorption of anionic fragment is also different showing spectral shifts and intensity changes.

The absence of fluorescence in **PTP** with mercury ions suggests also that after excitation at 360 nm, we observe an entire electron charge shift from methoxybenzene to purine-triazole complex with mercury ion in sub-picosecond time range leading to a formation of radical pair. Yet, the relaxation of optical transient absorption spectral bands with the time constant of 1.7 ns shows a quite long charge recombination time (Fig. S33, ESI).

Metal ion recognition by PTPa and PTPb in water

The promising metal ion coordination results of **PTP** in organic aprotic solvents and its fluorescent water-soluble derivatives encouraged to extend this study by performing titration experiments in water. As presented in Fig.6a and 6b, both molecules **PTPa** and **PTPb** form complexes with mercury ions in water. The coordination determines the red shift of absorption spectra and results in new absorption bands peaking at 377 nm (**PTPa**) and 381 nm (**PTPb**). The fluorescence spectra is obviously quenched, though, not completely and without spectral shifts. These experiments highly resemble those obtained for **PTP** in MeCN with the presence of Hg^{2+}. However, the complexation occurs at a ligand : Hg^{2+} ratio 1 : 1 for both molecules as seen from Fig. 6c and 6d, as a consequence of reduced binding constant in water.

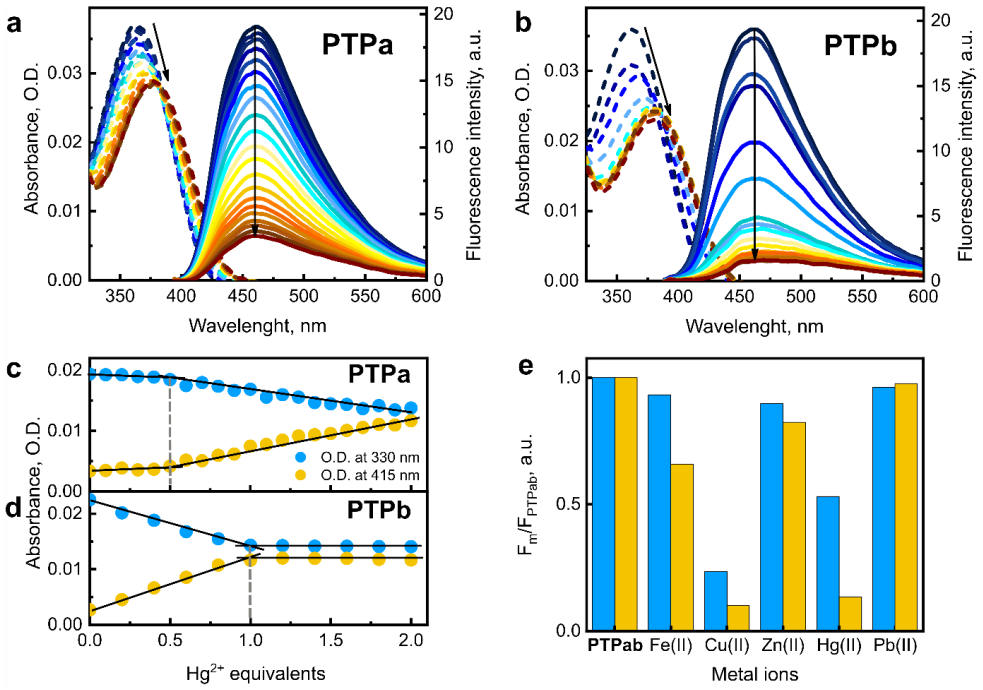

Figure 6. Absorption and fluorescence spectra response of compounds **PTPa** (a) and **PTPb** (b) upon addition of Hg^{2+} ions in water. The absorbance intensity dependence on Hg^{2+} equivalents at different wavelengths for **PTPa** (c) and **PTPb** (d). The fluorescence spectra intensity response to the added different metal ions of **PTPa** (blue columns) and **PTPb** (yellow columns) (e).

The titration experiments with **PTPa** and **PTPb** in water with other metal ions (Fe^{2+}, Cu^{2+}, Zn^{2+} and Pb^{2+}) revealed that besides mercury ions, molecules coordinate only with Cu^{2+} (Fig. 6e and Fig. S34-37). In general, it is well known that coordination of molecular probes with metal ions is less likely to occur in water than in an aprotic environment. This is mainly determined by solvation effects: water molecules may form hydration shells around metal ions and molecular probes, impeding the approach towards each other. Additionally, it is known that Cu^{2+} ion as Lewis acid is more azaphilic than oxophilic[50,51], therefore it still prefers to complex nitrogen ligands in aqueous solutions. Mercury salts, even if they are easy to hydrolyze, do not possess any noticeable oxophilicity and thus also can be complexed by nitrogen ligands[52] in the presence of water. On the other hand, Zn^{2+} and Fe^{2+} are rather oxophilic and therefore in aqueous medium as solvent outperforms nitrogen-based ligands[52]. However, in the present

case, the interference of water molecules to form complexes with metal ions for studied **PTPa** and **PTPb** derivatives may turn out to be a major advantage, as selectivity towards mercury ions increases.

Mercury ion imaging in living cells by PTPa

The reasonably good sensitivity of our studied **PTPa** and **PTPb** derivatives towards mercury ions in water and the low toxicity of some **PTP** derivatives studied in our previous work[40], encourage the further experiments of presented materials in living cells. Both **PTPa** and **PTPb** were used to treat living cells. However, the **PTPb** material with COOH in its aliphatic chain appeared to be too reactive as it strongly adheres the cultural plate. Thus, we continued the experiments with **PTPa** derivative.

To evaluate the capability of **PTPa** for use of Hg^{2+} imaging in living cells, MDA MB 231 cells were incubated in the presence and absence of $HgCl_2$ (10 μM) for 30 min to facilitate cellular uptake of Hg^{2+} ions. After this preincubation, the cells were treated with **PTPa** (50 μg/mL) for 30 min. Bright field and fluorescence microscopy was employed to assess the behaviour of **PTPa** within the cells (Fig. 7). The images clearly demonstrate that **PTPa** can be efficiently internalized by the cells, as indicated by its fluorescent signal. Furthermore, the material exhibits a fluorescence quenching effect in the mercury enriched environment, which suggests that the quenching of **PTPa** is directly correlated with the intracellular mercury concentration. This observation confirms the material's potential sensitivity to Hg^{2+} ions and its viability for imaging in biological systems where mercury's concentration plays a critical role.

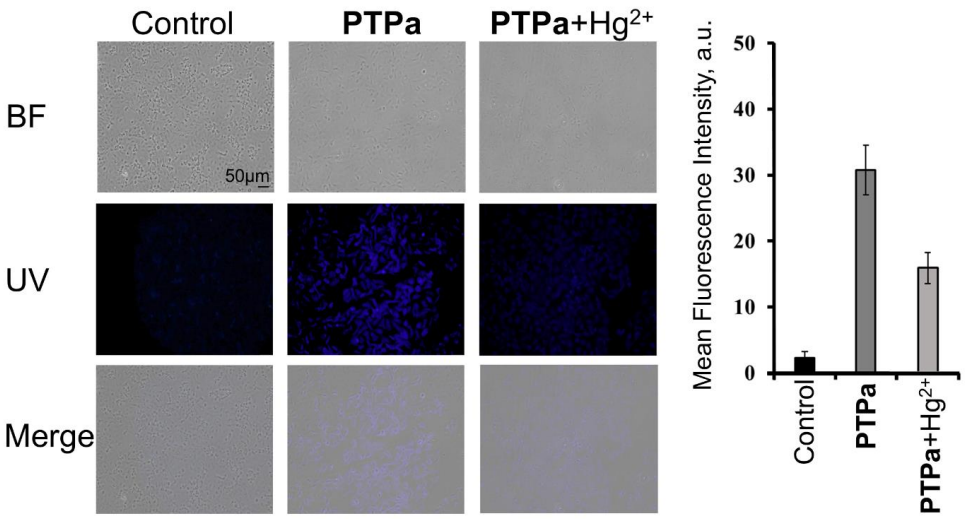

Figure 7. Bright-field and fluorescence microscopy images of MDA-MB-231 cells stained with **PTPa** (50 μg/mL) and treated with $HgCl_2$ (10 μM). The top row displays bright-field images showing the general cell morphology, while the middle and bottom rows depict fluorescence images illustrating **PTPa** fluorescence and its quenching in the presence of mercury ions.

Conclusions

The photophysical behaviour as well as spectroscopic titration response to different metal ions were studied for 2-piperidinyl-6-triazolylpurine **PTP** compound and further expanded to newly synthesized water soluble **PTPa** and **PTPb** derivatives. The piperidine unit at C2 position of purine core and 4-methoxyphenyl at C4 position of triazolyl ring allowed to create charge transfer type molecules with D-A-D' structure. The obtained fluorescence quantum yields were reasonably high – 49% in MeCN for **PTP** and 17% in water for **PTPa** and **PTPb**. The triazolyl ring, connected to purine core at C6 position via stable C-C bond, allowed to introduce a metal ion complexing site between nitrogen atoms of the triazole N3 and the purine N7. Indeed, the studied molecules tend to form complexes with metal ions, including Hg^{2+}. The coordination with mercury ions determines the switching between donors and thus, electronically different HOMO-LUMO transitions occur. The absorption and fluorescence titration experiments of **PTPa** and **PTPb** in water revealed the pronounced

selectivity towards Hg^{2+}. The favourable properties of water-soluble compounds encouraged the successful application of **PTPa** as Hg^{2+} "turn-off" fluorescence probe in living cells.

Methods

Synthesis: general information

Commercially available reagents were used without further purification. The reactions and the purity of the synthesized compounds were monitored by HPLC and TLC analysis on silica gel 60 F_{254} aluminum plates (Merck). Visualization was achieved using UV light. Column chromatography was carried out on silica gel (60 Å, 40−63 μm, ROCC). The reported yields correspond to materials that were homogeneous according to chromatographic and spectroscopic analysis. Infrared spectra were recorded in hexachlorobutadiene (4000−2000 cm^{-1}) and paraffin oil (2000−450 cm^{-1}) using a Perkin-Elmer Spectrum 100 FTIR spectrometer and in KBr tablets using a Perkin-Elmer Spectrum BX FTIR spectrometer (4000−450 cm^{-1}). Wavelengths are reported in cm^{-1}. ^{1}H and ^{13}C NMR spectra were recorded with Bruker Avance 500 spectrometer in chloroform-d ($CDCl_3$). Chemical shifts (δ) are reported in ppm and coupling constants (*J*) in Hz. The proton ($CDCl_3$ δ = 7.26 ppm) and carbon signals ($CDCl_3$ δ = 77.16 ppm) for residual non-deuterated solvents were used as an internal reference for ^{1}H and ^{13}C NMR spectra, respectively. ^{1}H NMR spectra were recorded at 500 MHz and ^{13}C NMR spectra at 126 MHz. The multiplicity is assigned as follows: s – singlet, d – doublet, t – triplet, q – quartet, m – multiplet. HPLC analysis was performed using an Agilent Technologies 1200 Series system equipped with an XBridge C_{18} column, 4.6 × 150 mm, particle size 3.5 μm, with a flow rate of 1 mL/min, using eluent A–0.1% TFA/H_2O with 5 vol % acetonitrile (MeCN) and eluent B–MeCN as the mobile phase. The wavelength of detection was 264 nm. Gradient: 30–95% B 5 min, 95% B 5 min, 95–30% B 2 min. LC-MS spectra were recorded with a Waters Acquity UPLC system equipped with an Acquity UPLC BEH C18 1.7 μm, 2.1 × 50 mm column, using 0.1% TFA/H_2O and MeCN as the mobile phase. High-resolution mass spectra (ESI) were recorded with Thermo Fisher Scientific Orbitrap Exploris 120 mass spectrometer operating in the Full Scan mode at the 120000 resolutions.

Synthesis and characterization of products

2,6-Dichloro-9-(2-(2-(2-(2-((tetrahydro-2*H*-pyran-2-yl)oxy)ethoxy)ethoxy)ethoxy)ethyl)-9*H*-purine (4)

A solution of 2,6-dichloropurine (1.0 g, 5.29 mmol, 1.0 equiv.), 2-(2-(2-((tetrahydro-2*H*-pyran-2-yl)oxy)ethoxy)ethoxy)ethan-1-ol[47] (2.22 g, 7.98 mmol, 1.5 equiv.) and triphenylphosphine (Ph_3P) (1.46 g, 5.57 mmol, 1.1 equiv.) in anhydrous tetrahydrofuran (THF) (20 mL) was cooled to 0 °C. DIAD (1.10 mL, 5.60 mmol, 1.1 equiv.) was added dropwise, the mixture was stirred for 2 h at 20 °C, controlled by HPLC, and then evaporated to dryness. The crude product was purified by flash column chromatography (ethyl acetate (EtOAc)/methanol (MeOH), 0% → 5%). Yield 1.6 g, 69 %. Yellowish oil. IR, ν (cm^{-1}): 2983, 2866, 1594, 1553, 1438, 1347, 1304, 1232, 1202, 1143, 1118, 1074, 1032, 986. ^{1}H-NMR (500 MHz, $CDCl_3$) δ (ppm): 8.36 (s, 1H, H-C(8)), 4.61 (t, 1H, ^3J = 3.5 Hz, (-CH-)), 4.44 (t, 2H, ^3J = 4.8 Hz, (-CH_2-)), 3.89–3.81 (m, 4H, 2×(-CH_2-)), 3.69–3.57 (m, 11H, 5×(-CH_2-), H_a-CH), 3.51–3.46 (m, 1H, H_b-CH), 1.85–1.46 (m, 6H, 3×(-CH_2-)). ^{13}C-NMR (75.5 MHz, $CDCl_3$) δ (ppm): 153.3, 152.8, 151.7, 147.6, 130.8, 99.2, 70.79, 70.77, 70.74, 70.72, 70.65, 68.9, 66.8, 62.5, 44.4, 30.7, 25.6, 19.7. HRMS (ESI): calculated [$C_{18}H_{26}Cl_2N_4O_5$+H^+] 449.1353 found 449.1341 (2.67 ppm).

2-Chloro-9-(2-(2-(2-(2-((tetrahydro-2*H*-pyran-2-yl)oxy)ethoxy)ethoxy)ethoxy)ethyl)-6-((trimethylsilyl)ethynyl)-9*H*-purine (5)

To a solution of compound **4** (800 mg, 1.78 mmol, 1.0 equiv.), Ph_3P (93 mg, 0.04 mmol, 0.2 equiv.), CuI (34 mg, 0.39 mmol, 0.1 equiv.), $PdCl_2$ (32 mg, 0.02 mmol, 0.1 equiv.) in absolutized THF (25 mL), triethylamine (Et_3N) (1.23 mL, ρ = 0.73 g/cm^3, 8.9 mmol, 5.0 equiv.) was added and the reaction mixture was stirred at 20 °C for 5 min. Then, trimethylsilylacetylene (1.01 mL, ρ = 0.69 g /cm^3, 7.1 mmol, 4.0 equiv.) was added, and the reaction mixture was stirred for 30 min at 50 °C. After reaction completion (monitored by HPLC), the reaction mixture was evaporated, and dried in a vacuum, and the product was purified by flash column chromatography (dichloromethane (DCM)/MeCN, gradient 0% → 10%). Yield: 659 mg, 72%. Yellowish oil. IR, ν (cm^{-1}): 2927, 2919, 2854, 1570, 1497, 1453, 1381, 1345, 1313, 1250, 1207, 1121, 1074, 1032, 1019, 987. ^{1}H-NMR (500 MHz, $CDCl_3$) δ (ppm): 8.30 (s, 1H, H-C(8)), 4.56 (t, 1H, ^3J = 3.5 Hz, (-CH-)), 4.39 (t, 2H, ^3J = 4.8 Hz, (-CH_2-)), 3.83–3.75 (m, 4H, 2×(-CH_2-)), 3.63–3.53 (m, 11H, 5×(-CH_2-), H_a-CH), 3.46–3.41 (m, 1H, H_b-CH), 1.81–1.47 (m, 6H, 3×(-CH_2-)), 0.28 (s, 9H, 3×(-CH_3)). ^{13}C-NMR (75.5 MHz, $CDCl_3$) δ (ppm): 153.7, 153.5, 147.7, 142.2, 133.5, 107.4, 99.0, 97.6, 70.7, 70.61, 70.59, 70.5, 68.8, 66.7, 62.3, 43.9, 30.6, 25.4, 19.6, -0.4. HRMS (ESI): calculated [$C_{23}H_{35}ClN_4O_5Si$+H^+] 511.2138 found 511.2127 (2.15 ppm).

2-Chloro-6-(1-(4-methoxyphenyl)-1*H*-1,2,3-triazol-4-yl)-9-(2-(2-(2-(2-((tetrahydro-2*H*-pyran-2-yl)oxy)ethoxy)ethoxy)ethoxy)ethyl)-9*H*-purine (5*)

To a solution of compound **5** (600 mg, 1.17 mmol, 1.0 equiv.) in DCM (10 mL) CuI (33 mg, 0.02 mmol, 15 mol%), Et_3N (180 µL, ρ = 0.73 g/mL, 1.29 mmol, 1.1 equiv.), acetic acid (AcOH) (75 µL, ρ = 1.05 g/mL, 1.29 mmol, 2.2 equiv.) and 1-azido-4-methoxybenzene solution in DCM (2.20 mL, C = 0.8 M, 1.76 mmol, 1.5 equiv.) were added. The reaction mixture was stirred for 3 h at 25 ºC and controlled by HPLC. Then the reaction mixture was diluted with DCM (20 mL), washed with saturated Na-EDTA solution (2×5 mL) and saturated NaCl solution, dried over anhydrous Na_2SO_4, filtered, and evaporated under vacuum. The crude product was purified by flash column chromatography. (EtOAc/MeOH, gradient 0% → 7%). Yield 240 mg, 35%. Yellowish solid. IR, ν (cm^{-1}): 3065, 2937, 2861, 1585, 1519, 1454, 1333, 1247, 1156, 1092, 1076, 1030. ^{1}H-NMR (500 MHz, $CDCl_3$) δ (ppm): 9.07 (s, 1H, H-C(triazole)) 8.37 (s, 1H, H-C(8)), 7.77, 7.06 (2d, 4H, ^3J = 8.8 Hz, Ar), 4.60 (t, 1H, ^3J = 3.5 Hz, (-CH-)), 4.48 (t, 2H, ^3J = 4.8 Hz, (-CH_2-)), 3.89 (s, 3H, (-OCH_3)) 3.88–3.82 (m, 4H, 2×(-CH_2-)), 3.68–3.59, 3.49–3.45 (2m, 12H, 6×(-CH_2-)), 1.84–1.76, 1.72–1.66, 1.60–1.46 (3m, 6H, 3×(-CH_2-)). ^{13}C-NMR (75.5 MHz, $CDCl_3$) δ (ppm): 160.3, 154.5, 154.0, 148.8, 147.3, 143.6, 130.2, 128.8, 125.2, 122.6, 115.0, 99.1, 70.8 (2C), 70.72, 70.68, 70.65, 69.1, 66.8, 62.4, 55.8, 43.9, 30.7, 25.5, 19.6. HRMS (ESI): calculated [$C_{27}H_{34}ClN_7O_6$+H^+] 588.2332 found 588.2307 (4.25 ppm).

6-(1-(4-Methoxyphenyl)-1*H*-1,2,3-triazol-4-yl)-2-(piperidin-1-yl)-9-(2-(2-(2-(2-((tetrahydro-2*H*-pyran-2-yl)oxy)ethoxy)ethoxy)ethoxy)ethyl)-9*H*-purine (6)

To a solution of compound **5*** (200 mg, 0.34 mmol, 1.0 equiv.) in dimethylformamide (DMF) (10 mL), piperidine (100 µL, ρ = 0.86 g/mL, 1.02 mmol, 3.0 equiv.) was added and the reaction mixture was stirred for 60 min at 100 ºC. The reaction mixture was evaporated and dried in a vacuum and purified by flash column chromatography (EtOAc/MeOH, gradient 0% → 8%). Yield: 138 mg, 64%. Brown oil. IR, ν (cm^{-1}): 2930, 2852, 1671, 1606, 1588, 1517, 1444, 1254, 1122, 1075, 1031, 987. ^{1}H-NMR (500 MHz, $CDCl_3$) δ (ppm): 9.01 (s, 1H, H-C(triazole)) 7.93 (s, 1H, H-C(8)), 7.76, 7.04 (2d, 4H, ^3J = 8.8 Hz, Ar), 4.61 (t, 1H, ^3J = 3.5 Hz, (-CH-)), 4.32 (t, 2H, ^3J = 4.8 Hz, (-CH_2-)), 3.96–3.92 (m, 4H, 2×(-CH_2-)), 3.88 (s, 3H, (-OCH_3)), 3.87–3.82 (m, 4H, 2×(-CH_2-)), 3.67–3.46 (m, 12H, 6×(-CH_2-)), 1.83–1.47 (m, 12H, 6×(-CH_2-)). ^{13}C-NMR (75.5 MHz, $CDCl_3$) δ (ppm): 160.1, 159.5, 154.3, 147.28, 145.1, 142.8, 130.6, 124.6, 123.0, 122.7, 114.9, 99.1, 70.8 (2C), 70.75, 70.73, 70.69, 69.4, 66.8, 62.4, 55.8, 45.6, 43.0, 30.7, 26.1, 25.6, 25.1, 19.7. HRMS (ESI): calculated [$C_{32}H_{44}O_8N_6$+H^+] 637.3457 found 637.3434 (3.60 ppm).

2-(2-(2-(2-(6-(1-(4-Methoxyphenyl)-1*H*-1,2,3-triazol-4-yl)-2-(piperidin-1-yl)-9*H*-purin-9-yl)ethoxy)ethoxy)ethoxy)ethan-1-ol (PTPa)

To a solution of compound **6** (300 mg, 0.47 mmol, 1.0 equiv.) in MeOH (5 mL), TFA (90 µL, 1.18 mmol, 2.5 equiv.) was added. The reaction mixture was stirred at 60 °C for 1 h, then evaporated and purified by reverse phase flash chromatography (MeOH/H_2O). Yield: 204 mg, 78%. Beige solid. IR, ν (cm^{-1}): 2912, 2857, 1603, 1582, 1518, 1469, 1450, 1405, 1353, 1302, 1251, 1211, 1182, 1130, 1093, 1030, 987. ^{1}H-NMR (500 MHz, $CDCl_3$) δ (ppm): 9.28 (s, 1H, H-C(triazole)), 8.23 (s, 1H, H-C(8)), 7.86, 7.03 (2d, 4H, ^3J = 8.8 Hz, Ar), 4.32 (t, 2H, ^3J = 4.4 Hz, (-CH_2-)), 3.97–3.92 (m, 4H, 2×(-CH_2-)), 3.87 (s, 3H, (-OCH_3)), 3.83 (t, 2H, ^3J = 4.4 Hz, (-CH_2-)), 3.80 (t, 2H, ^3J = 4.3 Hz, (-CH_2-)), 3.70–3.62 (m, 10H, 5×(-CH_2-)), 1.69–1.62 (m, 6H, 3×(-CH_2-)). ^{13}C-NMR (75.5 MHz, $CDCl_3$) δ (ppm): 159.9, 159.5, 154.2, 147.3, 144.4, 143.5, 130.8, 124.9, 122.3, 122.2, 114.9, 73.5, 70.8, 70.7, 70.3, 70.25, 69.3, 61.6, 55.8, 45.6, 42.5, 26.1, 25.1. HRMS (ESI): calculated [$C_{27}H_{36}O_5N_8$+H^+] 553.2881 found 553.2862 (3.43 ppm).

***tert*-Butyl 14-(6-(1-(4-methoxyphenyl)-1*H*-1,2,3-triazol-4-yl)-2-(piperidin-1-yl)-9*H*-purin-9-yl)-3,6,9,12-tetraoxatetradecanoate (PTPa*)**

To a solution of compound **PTPa** (100 mg, 0.18 mmol, 1.0 equiv.) and NaH (22 mg, 0.54 mmol, 3.0 equiv.) in THF (4 mL) *tert*-butyl 2-bromoacetate (183 µL, 1.44 mmol, 8.0 equiv.) was added. The reaction mixture was stirred at 20 °C for 18 h, and then 10 % acetic acid solution (1 mL) was added, and the reaction mixture evaporated under vacuum. The crude product was purified by flash column chromatography (EtOAc/MeOH, gradient 0% → 5%). Yield: 85 mg, 71%. Yellow oil. IR, ν (cm^{-1}): 2927, 2919, 2854, 1745, 1606, 1588, 1517, 1461, 1445, 1368, 1304, 1254, 1126, 1032, 988. ^{1}H-NMR (500 MHz, $CDCl_3$) δ (ppm): 9.01 (s, 1H, H-C(triazole)), 7.94 (s, 1H, H-C(8)), 7.76 (d, 2H, ^3J = 8.9 Hz, Ar), 7.04 (d, 2H, ^3J = 8.9 Hz, Ar), 4.32 (t, 2H, ^3J = 5.2 Hz, (-CH_2-)), 4.00 (s, 2H, (-CH_2-)), 3.96–3.92 (m, 4H, 2×(-CH_2-), 3.88 (s, 3H, (-CH_3)), 3.84 (t, 2H, ^3J = 5.2 Hz, (-CH_2-)), 3.71–3.66 (m, 4H, 2×(-CH_2-)), 3.65–3.60 (m, 8H, 4×(-CH_2-)), 1.69–1.64 (m, 6H, 3×(-CH_2-), 1.45 (s, 9H, 3×(-CH_3)). ^{13}C-NMR (75.5 MHz, $CDCl_3$) δ (ppm): 169.8, 160.1, 159.5, 154.3, 147.2, 145.1, 142.8, 130.6, 124.6, 123.0, 122.6, 114.9, 81.7, 70.80, 70.76, 70.72, 70.70, 70.68, 70.66, 69.4, 69.1, 55.8, 45.6, 43.0, 28.2, 26.0, 25.1. HRMS (ESI): calculated [$C_{33}H_{46}N_8O_7$+H^+] 667.3562 found 667.3542 (2.99 ppm).

14-(6-(1-(4-Methoxyphenyl)-1*H*-1,2,3-triazol-4-yl)-2-(piperidin-1-yl)-9*H*-purin-9-yl)-3,6,9,12-tetraoxatetradecanoic acid (PTPb)

To a solution of compound **PTPa*** (60 mg, 0.09 mmol, 1.0 equiv.) in THF (0.5 mL), aqueous phosphoric acid (0.5 mL, 85 *wt %*) was added. The reaction mixture was stirred at 20 °C for 48 h and then evaporated under vacuum. The crude product was purified by reverse phase flash column chromatography (H_2O/MeOH, gradient 10% → 95%). Yield: 45 mg, 82%. Light yellow solid. IR, ν (cm^{-1}): 2921, 2853, 1732, 1607, 1591, 1517, 1461, 1445, 1350, 1305, 1254, 1108, 1027, 988. ^{1}H-NMR (500 MHz, $CDCl_3$) δ (ppm): 8.90 (s, 1H, H-C(triazole)) 8.11 (s, 1H, H-C(8)), 7.74 (d, 2H, ^3J = 8.4 Hz, Ar), 7.00 (d, 2H, ^3J = 8.4 Hz, Ar), 4.34 (t, 2H, ^3J = 4.5 Hz, (-CH_2-)), 4.12 (s, 2H, (-CH_2-)), 3.94–3.91 (m, 4H, 4×(-CH_2-), 3.88 (s, 3H,(-CH_3)), 3.84 (t, 2H, ^3J = 4.5 Hz, (-CH_2-)), 3.74–3.70 (m, 2H, (-CH_2-)), 3.68–3.60 (m, 10H, 5×(-CH_2-)), 1.70–1.56 (m, 6H, 3×(-CH_2-). ^{13}C-NMR (75.5 MHz, $CDCl_3$) δ (ppm): 174.2, 160.0, 159.3, 154.2, 147.0, 145.2, 143.6, 130.4, 124.0, 122.4, 122.1, 114.8, 70.6, 70.4 (2C), 70.35 (2C), 70.3, 69.7, 69.1, 55.7, 45.5, 42.9, 25.9, 25.0. HRMS (ESI): calculated [$C_{29}H_{38}N_8O_7$+H^+] 611.2936 found 611.2912 (3.92 ppm).

Materials and methods for photophysical characterization

Spectroscopic measurements of **PTP** compound were performed in aprotic solvents of different polarities: cyclohexane (CyHex), diethyl ether (Et_2O), ethyl acetate (EtOAc), dimethoxyethane (DME), acetonitrile (MeCN) and dimethyl sulfoxide (DMSO). All solvents were purchased from Sigma Aldrich and were of spectroscopic or HPLC grade. The following salts for the UV and NMR titration experiments were also purchased from Sigma Aldrich: $NaClO_4$, $KClO_4$, $Mg(ClO_4)_2$, $Ca(ClO_4)_2$•$4H_2O$, $FeCl_2O_8$•H_2O, $CuCl_2O_8$•$6H_2O$, $ZnCl_2O_6$•$6H_2O$, $Hg(ClO_4)_2$•$3H_2O$, $Pb(ClO_4)_2$. Purified grade 2 water (Compact Pure, Adrona) was used for spectroscopic measurements of **PTPa** and **PTPb**.

The concentrations for fluorescence quantum yield measurements were selected so the absorbance at excitation wavelength would be in a range 0.03-0.08. For absorption and fluorescence measurements (including titration experiments) the initial concentration of compounds was 10^{-5} M. Quartz cells of 1 cm were used.

Absorption spectra were measured on a UV−vis−near infrared spectrophotometer Lambda 950 (PerkinElmer); fluorescence spectra were measured using a back-thinned CCD spectrometer PMA-11 (Hamamatsu) and a xenon lamp coupled to a monochromator (full width at half-maximum < 10 meV) as an excitation source. All steady-state fluorescence spectra were obtained by exiting samples to maxima of the lowest-energy absorption bands. Fluorescence quantum yields were determined by comparative method. The concentration of studied

compounds in solvents and relative standard quinine sulfate in 0.5M sulfuric acid (H_2SO_4) were selected so that OD would be around 0.05. Time-resolved fluorescence experiments were conducted by using time-correlated single photon counting system (PicoQuant PicoHarp 300). Femtosecond transient absorption measurements were carried out using commercial spectrometer (Harpia, Light Conversion) pumped with wavelength-tunable optical parametric amplifier (Orpheus, Light Conversion) coupled to 190 fs, 10 kHz pulsed laser (Pharos-SP, Light Conversion). Probe source was white light continuum (WLC) pulses generated by focusing the fundamental 1030 nm harmonic in purified water flowing inside quartz cuvette coupled to home-built flow system. The angle between linearly polarized pump and probe pulses was set to approximately 54 degrees. Samples were excited at 360 nm.

NMR titration experiments with metal salts

NMR titration was done in MeCN-d_3, using benzene as a standard and $Hg(ClO_4)_2 \cdot 3H_2O$ as a Hg^{2+} source or $Zn(ClO_4)_2 \cdot 6H_2O$ as a Zn^{2+} source. In the NMR tube, compound (**PTP**, **PTPa**, or **PTPb**) was dissolved in MeCN-d_3 (0.5 mL), and benzene (1.2 µL) was added to it as an internal standard. The amount of substance was calculated (Tables S1, S4, S8, S11, see Electronic Supplementary Information (ESI)). A solution of $Hg(ClO_4)_2 \cdot 6H_2O$ or $Zn(ClO_4)_2 \cdot 6H_2O$ in MeCN-d_3 with known concentration was prepared (Table S2, S5, S9, S12 in the ESI). Then ^{1}H-NMR spectra were taken (for 0 eq.). After that, the calculated amount of the titrant (0.10, 0.20, 0.30 equiv. etc., Tables S3, S6, S10, S13 in the ESI) was added to the NMR tube, which was shaken vigorously before taking the next ^{1}H-NMR spectrum. This procedure was repeated by adding the desired amount of titrant and taking ^{1}H-NMR spectra. All spectra were calibrated using a benzene signal at 7.37 ppm, then stacked, and their signal shift was analyzed.

DFT modelling

Density functional theory (DFT) calculations for **PTP** molecule were performed at the B3LYP/6-31G(d) level employing polarized continuum model (PCM). Excitation energy calculations and excited state optimization were performed using time-dependent (TD) - DFT with the same basis set. The theoretical evaluation of complexed **PTP** compound was carried out by introducing a proton (H^+) between nitrogen atoms of the triazole N3 and the purine N7 and using the same calculation conditions as previously described.

Acknowledgments

Authors thank the Latvia-Lithuania-Taiwan joint grant “Molecular Electronics in functionalized Purines: fundamental Study and applications (MEPS)” for the financial support. Funding received from the Research Council of Lithuania (LMT), project no. S-LLT-22-3.

Authors contribution

K.B data acquisition and analysis, design of the work; J.J. original draft preparation; J.J., G.J., S.J., I.N., M.T, H.T.C. idea & conceptualization, analysis, data interpretation, revise & editing; S. J., M.T. and H.T.C. supervision; G.K. software and simulation; A.B., Z.K., L.E.H., H.W.C. data acquisition and analysis.

Competing interest

The authors declare no competing interests.

Data availability

Data associated with this work and presented here (including Electronic Supplementary Information) will be made available on request. Correspondence and requests for materials should be addressed to J.J.

References

1. Rosemeyer, H. The Chemodiversity of Purine as a Constituent of Natural Products. *Chem. Biodivers.* **1**, 361–401. https://doi.org/10.1002/cbdv.200490033 (2004).

2. Parker, W. B. Enzymology of purine and pyrimidine antimetabolites used in the treatment of cancer. *Chem. Rev.* **109**, 2880–2893. https://doi.org/10.1021/cr900028p (2009).

3. Gogineni, V., Schinazi, R. F. & Hamann, M. T. Role of Marine Natural Products in the Genesis of Antiviral Agents. *Chem. Rev.* **115**, 9655–9706. https://doi.org/10.1021/cr4006318 (2015).

4. Seley-Radtke, K. L. & Yates, M. K. The evolution of nucleoside analogue antivirals: A review for chemists and non-chemists. Part 1: Early structural modifications to the nucleoside scaffold. *Antiviral Res.* **154**, 66–86. https://doi.org/10.1016/j.antiviral.2018.04.004 (2018).

5. Hu, Y. *et al.* Potential antibacterial ethanol-bridged purine azole hybrids as dual-targeting inhibitors of MRSA. *Bioorg. Chem.* **114**, 105096. https://doi.org/10.1016/j.bioorg.2021.105096 (2021).

6. Swennen, E. L. R., Dagnelie, P. C. & Bast, A. ATP inhibits hydroxyl radical formation and the inflammatory response of stimulated whole blood even under circumstances of severe oxidative stress. *Free Radic. Res.* **40**, 53–58. https://doi.org/10.1080/10715760500364298 (2006).

7. Berdis, A. Nucleobase-modified nucleosides and nucleotides: Applications in biochemistry, synthetic biology, and drug discovery. *Front. Chem.* **10**, 1051525. https://doi.org/10.3389/fchem.2022.1051525 (2022).

8. Wong, X. K. & Yeong, K. Y. From Nucleic Acids to Drug Discovery: Nucleobases as Emerging Templates for Drug Candidates. *Curr. Med. Chem.* **28**, 7076–7121. https://doi.org/10.2174/0929867328666210215113828 (2021).

9. Butler, R. S., Cohn, P., Tenzel, P., Abboud, K. A. & Castellano, R. K. Synthesis, Photophysical Behavior, and Electronic Structure of Push−Pull Purines. *J. Am. Chem. Soc.* **131**, 623–633. https://doi.org/10.1021/ja806348z (2009).

10. Matarazzo, A. & Hudson, R. H. E. Fluorescent adenosine analogs: a comprehensive

survey. *Tetrahedron* **71**, 1627–1657. https://doi.org/10.1016/j.tet.2014.12.066 (2015).

11. Saito, Y. & Hudson, R. H. E. Base-modified fluorescent purine nucleosides and nucleotides for use in oligonucleotide probes. *J. Photochem. Photobiol. C Photochem. Rev.* **36**, 48–73. https://doi.org/10.1016/j.jphotochemrev.2018.07.001 (2018).

12. Pu, F., Ren, J. & Qu, X. Nucleobases, nucleosides, and nucleotides: versatile biomolecules for generating functional nanomaterials. *Chem. Soc. Rev.* **47**, 1285–1306. https://doi.org/10.1039/C7CS00673J (2018).

13. Collier, G. S. *et al.* Linking design and properties of purine-based donor-acceptor chromophores as optoelectronic materials. *J. Mater. Chem. C* **5**, 6891–6898. https://doi.org/10.1039/C7TC01835E (2017).

14. Sebris, A. *et al.* Homoleptic purine-based NHC iridium(iii) complexes for blue OLED application: impact of isomerism on photophysical properties. *J. Mater. Chem. C* **11**, 14608–14620. https://doi.org/10.1039/D3TC02681G (2023).

15. Traskovskis, K. *et al.* All-organic fast intersystem crossing assisted exciplexes exhibiting sub-microsecond thermally activated delayed fluorescence. *J. Mater. Chem. C* **9**, 4532–4543. https://doi.org/10.1039/D0TC05099G (2021).

16. Yang, Y. *et al.* Ultraviolet-violet electroluminescence from highly fluorescent purines. *J. Mater. Chem. C* **1**, 2867–2874. https://doi.org/10.1039/C3TC00734K (2013).

17. Yang, Y. *et al.* Blue-violet electroluminescence from a highly fluorescent purine. *Chem. Mater.* **22**, 3580–3582. https://doi.org/10.1021/cm100407n (2010).

18. Wang, H. Y. *et al.* Three-in-one: information encryption, anti-counterfeiting and LD-tracking of multifunctional purine derivatives. *J. Mater. Chem. C* **9**, 2864–2872. https://doi.org/10.1039/D0TC05221C (2021).

19. Wang, A. *et al.* A purine-based fluorescent probe for H2S detection and imaging of cells. *Spectrochim. Acta Part A Mol. Biomol. Spectrosc.* **308**, 123674. https://doi.org/10.1016/j.saa.2023.123674 (2024).

20. Li, J. *et al.* Nucleoside-Based Ultrasensitive Fluorescent Probe for the Dual-Mode Imaging of Microviscosity in Living Cells. *Anal. Chem.* **88**, 5554–5560. https://doi.org/10.1021/acs.analchem.6b01395 (2016).

21. Xu, H.-Y., Chen, W., Zhang, W., Ju, L. & Lu, H. A selective Purine-based fluorescent chemosensor for the “naked-eye” detection of Zinc ion (Zn2+): applications in live cell imaging and test strips. *New J. Chem.* **44**, 15195–15201. https://doi.org/10.3390/molecules26237347 (2020).

22. Chen, X. *et al.* Synthesis and application of purine-based fluorescence probe for continuous recognition of Cu2+ and glyphosate. *Spectrochim. Acta Part A Mol. Biomol. Spectrosc.* **304**, 123291. https://doi.org/10.1016/j.saa.2023.123291 (2024).

23. Chen, W., Xu, H., Ju, L. & Lu, H. A highly sensitive fluorogenic “turn-on” chemosensor for the recognition of Cd2+ based on a hybrid purine-quinoline Schiff base. *Tetrahedron* **88**, 132123. https://doi.org/10.1016/j.tet.2021.132123 (2021).

24. Wu, G. *et al.* A novel rhodamine B and purine derivative-based fluorescent chemosensor for detection of palladium (II) ion. *Inorg. Chem. Commun.* **102**, 233–239. https://doi.org/10.1016/j.inoche.2019.02.038 (2019).

25. Hong, Y. S., Kim, Y. M. & Lee, K. E. Methylmercury Exposure and Health Effects. *J. Prev. Med. Public Heal.* **45**, 353–363. https://doi.org/10.3961/jpmph.2012.45.6.353 (2012).

26. Mercury in Food | FDA. https://www.fda.gov/food/environmental-contaminants-food/mercury-food .

27. Mercury. https://www.who.int/news-room/fact-sheets/detail/mercury-and-health .

28. Health Effects of Exposures to Mercury | US EPA. https://www.epa.gov/mercury/health-effects-exposures-mercury .

29. Wang, Y. *et al.* Fluorescent probe for mercury ion imaging analysis: Strategies and applications. *Chem. Eng. J.* **406**, 127166. https://doi.org/10.1016/j.cej.2020.127166 (2021).

30. Zhang, Y., Gao, Y., Liu, Q. S., Zhou, Q. & Jiang, G. Chemical contaminants in blood and their implications in chronic diseases. *J. Hazard. Mater.* **466**, 133511. https://doi.org/10.1016/j.jhazmat.2024.133511 (2024).

31. Briffa, J., Sinagra, E. & Blundell, R. Heavy metal pollution in the environment and their toxicological effects on humans. *Heliyon* **6**, e04691. https://doi.org/10.1016/j.heliyon.2020.e04691 (2020).

32. Duan, N. *et al.* The research progress of organic fluorescent probe applied in food and drinking water detection. *Coord. Chem. Rev.* **427**, 213557 https://doi.org/10.1016/j.ccr.2020.213557 (2021).

33. Saleem, M. & Lee, K. H. Optical sensor: a promising strategy for environmental and biomedical monitoring of ionic species. *RSC Adv.* **5**, 72150–72287. https://doi.org/10.1039/C5RA11388A (2015).

34. Chen, S. Y., Li, Z., Li, K. & Yu, X. Q. Small molecular fluorescent probes for the detection of lead, cadmium and mercury ions. *Coord. Chem. Rev.* **429**, 213691. https://doi.org/10.1016/j.ccr.2020.213691 (2021).

35. Fukuhara, G. Analytical supramolecular chemistry: Colorimetric and fluorimetric chemosensors. *J. Photochem. Photobiol. C Photochem. Rev.* **42**, 100340. https://doi.org/10.1016/j.jphotochemrev.2020.100340 (2020).

36. Yin, J., Hu, Y. & Yoon, J. Fluorescent probes and bioimaging: alkali metals, alkaline earth metals and pH. *Chem. Soc. Rev.* **44**, 4619–4644. https://doi.org/10.1039/C4CS00275J (2015).

37. Udhayakumari, D., Ramasundaram, S., Jerome, P. & Oh, T. H. A Review on Small Molecule Based Fluorescence Chemosensors for Bioimaging Applications. *J. Fluoresc.* https://doi.org/10.1007/s10895-024-03826-2 (2024).

38. Sebris, A. *et al.* Photophysical and Electrical Properties of Highly Luminescent 2/6-Triazolyl-Substituted Push-Pull Purines. *ACS Omega* **7**, 5242–5253. https://doi.org/10.1021/acsomega.1c06359 (2022).

39. Šišuļins, A. *et al.* Synthesis and fluorescent properties of N(9)-alkylated 2-amino-6-triazolylpurines and 7-deazapurines. *Beilstein J. Org. Chem.* **15**, 474–489. https://doi.org/10.3762/bjoc.15.41 (2019).

40. Burcevs, A. *et al.* Synthesis of Fluorescent C–C Bonded Triazole-Purine Conjugates. *J. Fluoresc.* **34**, 1091–1097. https://doi.org/10.1007/s10895-023-03337-6 (2024).

41. Kovaļovs, A. *et al.* 1,2,3-Triazoles as leaving groups in purine chemistry: A three-step synthesis of N6-substituted-2-triazolyl-adenine nucleosides and photophysical properties thereof. *Tetrahedron Lett.* **54**, 850–853. https://doi.org/10.1016/j.tetlet.2012.11.095 (2013).

42. Novosjolova, I., Bizděna, E. & Turks, M. Application of 2,6-diazidopurine derivatives in the synthesis of thiopurine nucleosides. *Tetrahedron Lett.* **54**, 6557–6561. https://doi.org/10.1016/j.tetlet.2013.09.095 (2013).

43. Krikis, K. E., Novosjolova, I., Mishnev, A. & Turks, M. 1,2,3-Triazoles as leaving groups in SNAr-Arbuzov reactions: Synthesis of C6-phosphonated purine derivatives. *Beilstein J. Org. Chem.* **17**, 193–202. https://doi.org/10.3762/bjoc.17.19 (2021).

44. Cīrule, D., Novosjolova, I., Bizdēna, Ē. & Turks, M. 1,2,3-Triazoles as leaving groups: SNAr reactions of 2,6-bistriazolylpurines with O- And C-nucleophiles. *Beilstein J. Org. Chem.* **17**, 410–419. https://doi.org/10.3762/bjoc.17.37 (2021).

45. Jovaisaite, J. *et al.* Proof of principle of a purine D-A-D′ ligand based ratiometric chemical sensor harnessing complexation induced intermolecular PET. *Phys. Chem. Chem. Phys.* **22**, 26502–26508. https://doi.org/10.1039/D0CP04091F (2020).

46. Gao, S. H. *et al.* Highly selective detection of Hg2+ ion by push-pull-type purine nucleoside-based fluorescent sensor. *Tetrahedron* **70**, 4929–4933. https://doi.org/10.1002/ejoc.201301897 (2014).

47. Ansell, S. M. Polyamide oligomers. US6320017B1 (2001).

48. Maillard, J. *et al.* Universal quenching of common fluorescent probes by water and alcohols. *Chem. Sci.* **12**, 1352–1362. https://doi.org/10.1039/D0SC05431C (2021).

49. Panchenko, P. A., Fedorov, Y. V., Fedorova, O. A. & Jonusauskas, G. FRET versus PET: ratiometric chemosensors assembled from naphthalimide dyes and crown ethers. *Phys. Chem. Chem. Phys.* **17**, 22749–22757. https://doi.org/10.1039/C5CP03510D (2015).

50. Yamamoto, Y. From σ- to π-electrophilic Lewis acids. Application to selective organic transformations. *J. Org. Chem.* **72**, 7817–7831. https://doi.org/10.1021/jo070579k (2007).

51. Å Kobayashi, S., Busujima, T. & Nagayama, S. A Novel Classification of Lewis Acids on the Basis of Activity and Selectivity. *Chem. A Eur. J.* **6**, 3491–3494. https://doi.org/10.1002/1521-3765(20001002)6:19<3491::aid-chem3491>3.3.co;2-g (2000).

52. Kobayashi, S., Nagayama, S. & Busujima, T. Lewis acid catalysts stable in water.

Correlation between catalytic activity in water and hydrolysis constants and exchange rate constants for substitution of inner-sphere water ligands. *J. Am. Chem. Soc.* **120**, 8287–8288. https://doi.org/10.1021/ja980715q (1998).

Pielikums V
Appendix V

Novosjolova, I.; Burcevs, A.; Tulaite, K.; Kapilinskis, Z.; Jovasaite, J.; Jursenas, S.; Turks, M.

2-Amino-6-triazolilpurīna atvasinājumu izmantošanas paņēmiens par metālu jonu sensoriem.
A method of application of 2-amino-6-triazolyl purine derivatives as metal ion sensors.

Iesniegts patents / Submitted patent

LVP2024000072, 29.11.2024.

Latvijas Republikas Patentu valde

Citadeles iela 7/70, Rīga, LV-1010, tālr. 67099600, fakss 67099650, e-pasts lietvediba@lrpv.gov.lv, www.lrpv.gov.lv

Adresāts:

Irīna BOIKO
RĪGAS TEHNISKĀ UNIVERSITĀTE
Ķīpsalas iela 6B - 406
Rīga, LV-1048
patenti@rtu.lv

PAZIŅOJUMS (R2)
Par pieteikuma dokumentu saņemšanu

Jūsu šifrs	Saņemšanas datums	Mūsu šifrs	Mūsu datums
	29.11.2024.	LVP2024000072	29.11.2024.

Patentu valde informē, ka ir saņemts patenta pieteikums:

(21) Patenta pieteikuma Nr.	LVP2024000072
(22) Pieteikuma datums	29.11.2024
(72) Izgudrotāji	Irina NOVOSJOLOVA, Anniņmuižas bulvāris 21 - 16, Rīga, LV-1067, LV Aleksejs BURCEVS, Dārziņu 26. līnija 3, Rīga, LV-1063, LV Kamilė TULAITĖ, V. Vaitkaus g. 1 - 24 , Vilnius, LT-04332, LT Zigfrīds KAPILINSKIS, Tapešu iela 20 - 8, Rīga, LV-1083, LV Justina JOVAŠAITĖ, Santariškių g. 73/10, Vilnius, LT-08457, LT Saulius Antanas JURŠĖNAS, A. Juozapavičiaus 9A - 119, Vilnius, LT-09311, LT Māris TURKS, Nometņu iela 32 - 28, Rīga, LV-1002, LV
(71) Pieteicēji	RĪGAS TEHNISKĀ UNIVERSITĀTE, Ķīpsalas iela 6A, Rīga, LV-1048, LV VILNIUS UNIVERSITY, 3 Universiteto St., LT-01513 Vilnius, LT
(54) Izgudrojuma nosaukums	2-AMINO-6-TRIAZOLILPURĪNA ATVASINĀJUMU IZMANTOŠANAS PAŅĒMIENS PAR METĀLU JONU SENSORIEM

(lūdzam informēt Patentu valdi par pamanītajām kļūdām)

Saistībā ar minēto pieteikumu ir saņemti sekojoši materiāli:

□ Iesniegums patenta piešķiršanai (2.pielikums MK Not.Nr.224)	2 gab. (e-doc; papīra)
□ Izgudrojuma apraksts latviešu valodā	1 eks.
□ Viena vai vairākas izgudrojuma pretenzijas	1 eks.
□ Izgudrojuma zīmējums(-i)	1 eks.
□ Kopsavilkums	1 eks.
□ Kopsavilkuma tulkojums angļu valodā	1 eks.

Pielikums VI
Appendix VI

Kapilinskis, Z.; Burcevs, A.; Novosjolova, I.; Turks, M.

Ūdenī šķīstoši 2-amino-6-triazolilpurīni un to sintēzes paņēmiens.
Water soluble 2-amino-6-triazolyl purines and their synthesis approach.

Iesniegts patents / Submitted patent

LV15925A, 20.03.2025.

B sekcija

(51) **B23K 26/03** (11) **15923 A**
(21) LVP2023000085 (22) 11.09.2023
(43) 20.03.2025
(71) LATVIJAS UNIVERSITĀTE; Raiņa bulvāris 19, Rīga, LV-1050, LV
(72) Vyacheslav KIM (LV)
(74) Jevgeņijs FORTŪNA, FORAL Intelektuālā īpašuma aģentūra, SIA; Kalēju iela 14 - 7, Rīga, LV-1050, LV
(54) **IERĪCE LĀZERLOKA METINĀŠANAI AR REGULĒJAMU METINĀŠANAS KVALITĀTI**
A DEVICE FOR LASER-ARC WELDING WITH ADJUSTABLE QUALITY OF WELDING

(57) Izgudrojums attiecas uz hibrīda lāzerloka metināšanu, precīzāk, uz ierīci lāzerloka metināšanai ar regulējamu metināšanas kvalitāti, kas ietver lāzera avotu ar fokusēšanas sistēmu, loka degli, kurš atrodas blakus lāzera avotam leņķī a=25°−35° no lāzera optiskās ass, analogo-digitālo pārveidotāju, lāzera vadības bloku, loka strāvas avota vadības bloku, strāvas vadības sensora loka izlādes ķēdi, kas ir uzstādīta loka izlādes ķēdē, stieples elektrodu barošanas sistēmu, spektrālo sensoru lāzera loka izlādes zonas uzraudzībai, kas ir uzstādīts attālumā L=8−15 cm no lāzera loka izlādes zonas no sāniem leņķī b=45°−55° no lāzera optiskās ass, regulējamu diafragmu un traucējumu slāpētājfiltrus, kas ir uzstādīti spektrālā sensora priekšā lāzera loka izlādes zonas kontrolei un datora reģistrēšanai. Kombinācijā ar nepārtrauktu lāzera jaudas un loka strāvas vadību, stieples padeves ātrumu un hibrīda lāzera loka degļa kustības regulēšanu piedāvātā ierīce ļauj uzlabot lāzera loka metināšanas kvalitāti.

The invention relates to hybrid laser-arc welding, more specifically, to a device for laser-arc welding with adjustable quality of welding, comprising a laser source with a focusing system, an arc torch located next to the laser source at an angle a=25°−35° from the optical axis of the laser, an analog-to-digital converter, a laser control unit, an arc current source control unit, a current control sensor arc discharge circuit installed in the arc discharge circuit, wire electrode power supply system, spectral sensor for monitoring the laser-arc discharge zone, installed at a distance L=8−15 cm from the laser-arc discharge zone on the side at an angle b=45°−55° from the optical axis of the laser, adjustable diaphragm and interference filters installed in front of the spectral sensor to control the zone of the laser-arc discharge and register the computer. In combination with continuous laser power and arc current control, wire feed speed and hybrid laser-arc torch motion tuning the proposed device allows improvements in quality of laser-arc welding.

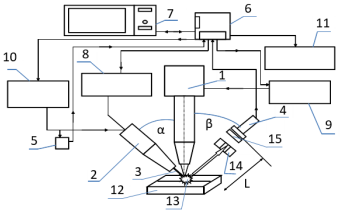

(51) **B60L 1/00** (11) **15924 A**
(21) LVP2023000078 (22) 22.08.2023
(41) 20.03.2025
(71) Vitālijs ENTINS; Kastrānes iela 1 k-1 - 40, Rīga, LV-1039, LV
(72) Vitālijs ENTINS (LV)
(54) **IERĪCE UN PĀRVIETOŠANĀS METODE ELEKTRISKAJIEM TRANSPORTLĪDZEKĻIEM BEZ DEGVIELAS UZPILDES**
DEVICE AND TRANSFERING METHOD FOR ELECTRIC VEHICLES WITHOUT FUEL REFILL

(57) Tiek piedāvāta metode un ierīce elektriska transportlīdzekļa pārvietošanai bez uzlādēšanas, kas sastāv no riteņpāra un virsbūves, ko darbina pāris elektromotoru, kas griežas ar paātrinājumu un nodod vienmērīgi paātrinātu kustību virsbūvei un riteņpārim. Elektromotorus uzlādē uz aizmugurējiem riteņiem uzstādīti ģeneratori, un apstājoties, aizmugurējie riteņi, kas uzstādīti uz rotējošajiem cilindriem.

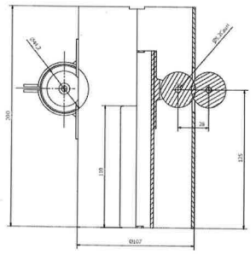

C sekcija

(51) **C07D 249/00** (11) **15925 A**
(21) LVP2024000059 (22) 16.09.2024
(41) 20.03.2025
(71) RĪGAS TEHNISKĀ UNIVERSITĀTE; Ķīpsalas iela 6A, Rīga, LV-1048, LV
(72) Zigfrīds KAPILINSKIS (LV),
Aleksejs BURCEVS (LV),
Irina NOVOSJOLOVA (LV),
Māris TURKS (LV)
(54) **ŪDENĪ ŠĶĪSTOŠI 2-AMINO-6-TRIAZOLILPURĪNI UN TO SINTĒZES PAŅĒMIENS**
WATER SOLUBLE 2-AMINO-6-TRIAZOLYL PURINES AND THEIR SYNTHESIS METHOD

(57) Izgudrojums attiecas uz organiskās ķīmijas un materiālzinātnes nozarēm, konkrēti, jaunu 6-(1-(4-metoksifenil)-1H-1,2,3-triazol-4-il)-2-(piperidin-1-il)-9H-purin-9-ilatvasinājumu sintēzi, ievietojot šķīdību ūdenī veicinošas grupas purīna 9. pozīcijā.

The invention relates to the field of organic and materials chemistry, in particular to the synthesis of new 6-(1-(4-methoxyphenyl)-1H-1,2,3-triazol-4-yl)-2-(piperidin-1-yl)-9H-purin-9-yl derivatives by inserting water-solubility enhancing groups at purine N9 position.

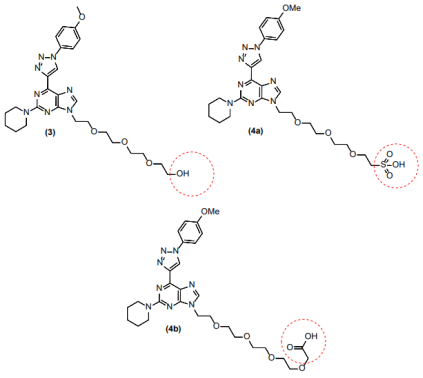

C07K 14/20	**15922**
C12N 7/00	**15922**

Pielikums VII
Appendix VII

Burcevs, A.; Jonusauskas, G.; Turks, M.; Novosjolova, I.

Synthesis of purine-1,4,7,10-tetraazacyclododecane conjugate and its complexation modes with copper(II)

Molecules **2025**, 30, 1612.

doi.org/10.3390/molecules30071612

molecules

MDPI

Article

Synthesis of Purine-1,4,7,10-Tetraazacyclododecane Conjugate and Its Complexation Modes with Copper(II)

Aleksejs Burcevs [1], Gediminas Jonusauskas [2], Irina Novosjolova [1,*] and Māris Turks [1,*]

[1] Institute of Chemistry and Chemical Technology, Faculty of Natural Sciences and Technology, Riga Technical University, P. Valdena Str. 3, LV-1048 Riga, Latvia
[2] Laboratoire Ondes et Matière d'Aquitaine, Bordeaux University, UMR CNRS 5798, 351 Cours de la Libération, 33405 Talence, France
* Correspondence: irina.novosjolova@rtu.lv (I.N.); maris.turks@rtu.lv (M.T.)

Abstract: Purine-1,4,7,10-tetraazacyclododecane (cyclen) conjugate was designed to study its Cu^{2+} ions complexation capability. Several synthetic approaches were tested to achieve the target compound. The optimal approach involved stepwise modifications of purine *N*9, *C*8, and *C*6 positions that, in nine consecutive steps, provided purine–cyclen conjugate. The synthetic sequence involved Mitsunobu-type alkylation at *N*9 and iodination at *C*8, followed by Stille, S_NAr, CuAAC, and alkylation reactions. The designed purine–cyclen conjugate is able to complex Cu^{2+} ions in both the cyclen part and between the purine *N*7 and triazole *N*2 positions. The complexation pattern and equilibrium were studied using the NMR titration technique in MeCN-d_3 and absorption spectra.

Keywords: purines; fluorescence; metal ion complexation; synthesis; cyclen

check for updates

Academic Editor: Gianfranco Favi

Received: 3 March 2025
Revised: 21 March 2025
Accepted: 2 April 2025
Published: 4 April 2025

Citation: Burcevs, A.; Jonusauskas, G.; Novosjolova, I.; Turks, M. Synthesis of Purine-1,4,7,10-Tetraazacyclododecane Conjugate and Its Complexation Modes with Copper(II). *Molecules* **2025**, *30*, 1612. https://doi.org/10.3390/molecules30071612

1. Introduction

Purines have a broad range of applications in medicine and materials science due to their wide biological [1–4] and photophysical [5–12] properties. Therefore, the importance of the development of new synthetic approaches towards intended substitution into purine is high.

In this study, we designed purine–cyclen conjugate **1** as a potential photocatalyst (Figure 1). The incorporation of redox-active transition metals into organic light-absorbing molecular structures makes it possible to use light to change the oxidation state of metal ions. Cyclen derivative is an attractive moiety for derivatization due to its great ability to complex such metal ions as Cu^{2+}, Ni^{2+}, Pd^{2+}, and Zn^{2+} [13–18]. The photoinitiated electron transfer may be easily controlled and directed toward a site containing metal ions. Moreover, the use of available molecular building blocks using well-developed synthetic methods makes the molecular construction easily adapted for specific metal ions and targeted chemical reactions. The ON/OFF switching possibility of the catalytically active state largely increases the flexibility in the control of the reaction.

Our previous work [19] inspired us to create a new structural design of the photocatalyst based on the purine core. Instead of using benzophenone with its complicated excited state behavior, including unwanted side reactions, the ground state association between dimethylaniline electron donor and strongly absorbing antenna, bearing purine, will ensure efficient light absorption and electron transfer between them without wasting the absorbed energy. The oxidation potentials of all molecular fragments are known to be optimal for an electron transfer until copper(II) is bound by cyclen. The formed copper(I) may be used for a wealth of chemical reactions, including the generation of H_2O_2, which possesses

high reactivity towards biological structures and may also be employed for wastewater treatment using only sunlight.

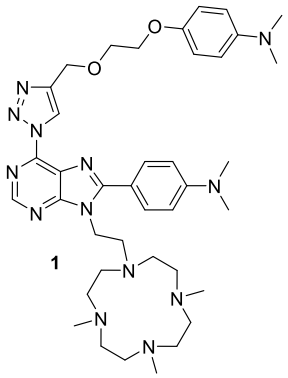

Figure 1. The structure of purine–cyclen conjugate **1** as a potential photocatalyst.

Over the years, a wide range of methods for the derivatization of purines have been developed. Four positions in the purine core can be modified: *C*2, *C*6, *C*8, and *N*7 or *N*9. Derivatization of the C positions of the purine cycle is usually done in metal-catalyzed cross-coupling or S_NAr reactions (Scheme 1). In S_NAr reactions, halogens are the most common leaving groups in the purine, but there are reports about sulfonyl groups [20], azides [21], and C-N bonded 1,2,3-triazoles [22] acting as leaving groups as well. Various *O*- [23,24], *N*- [25–27], and *S*- [20,23,28] nucleophiles have been introduced to the purine ring via S_NAr reactions. On the other hand, the most widespread cross-coupling reactions within the purine core are Suzuki-Miyaura [29–31], Negishi [32,33], Stille [34,35], and Sonogashira [36–38] reactions. In cases of di- or trihalogenated purines, reactions occur chemo- and regioselectively [39,40], with the purine *C*6 position being the most reactive. By choosing different halogens at the purine core, it is possible to control reaction occurrence at less reactive positions with the introduction of the iodine there. It is worth noting that the proton at the purine *C*8 position is the most acidic, making it the primary target of deprotonation and C-H activation reactions [41–43].

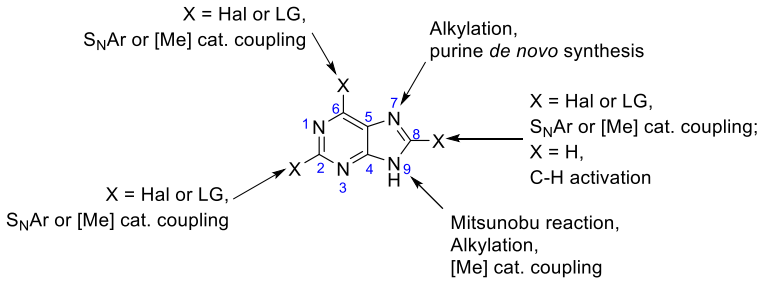

Scheme 1. Most used approaches for derivatization of purine at *C*2, *C*6, *C*8, *N*7, and *N*9 positions.

In derivatizations of the *N*9 position of purine, a mixture of products is frequently formed due to the purine imidazole ring *N*7/*N*9 position tautomerism. The most used reactions for the introduction of the substituents to the *N*9 position are alkylation, Mitsunobu, and copper-catalyzed cross-coupling reactions [41,42,44]. Alkylation reactions with the formation of *N*7 product as a major product are challenging, requiring specific substrates and

additives, like alkyl halides in the presence of Grignard reagents [45], glycosyl donors or *tert*-butyl halides with bis(trimethylsilyl)acetamide, $TiCl_4$ or $SnCl_4$ [46,47]. The most certain way of acquiring *N*7 purine derivatives is purine de novo synthesis from the corresponding pyrimidines [48] or imidazoles [49].

In addition, purine derivatives can complex metal ions and be used in medicine and as metal ion sensors. Cisplatin (*cis*-diamminedichloroplatinum(II)) is a known anticancer drug where the metal binds with the *N*7-positions of guanine bases and thus activates signal transduction pathways and apoptosis [50]. In 1971, 6-amino-, 6-chloro-, 6-hydroxy- and 6-mercaptopurines were studied for such metals as Mn^{2+}, Ca^{2+}, Mg^{2+}, Zn^{2+}, Ni^{2+}, Co^{2+}, and Cu^{2+} complexation in water, and it was proposed that the 1:1 complexes formed and metal coordinated to *N*7 of purine and to substituent at *C*6 position [51].

Purine–metal complexes are often studied by fluorescence because, due to the formation of complexes, fluorescence changes. Known purine-based derivatives are used as sensors for Hg^{2+} and Pd^{2+} ion detection in aqueous media [52,53] and for Cu^{2+} in cells [54,55]; upon complexation, they quench the fluorescence. Recently, there were published reports about purine nucleoside complexes for Cu^{2+} ions [56,57]. On the other hand, purine Schiff base conjugate forms complexes with Al^{3+} and increases the fluorescence [58]. 1,2,3-Triazolyl pyridine, isoquinoline, and ferrocene derivatives form complexes with Pd^{2+}, Cu^{2+}, Ni^{2+}, Ru^{2+}, Au^{+}, and Ag^{+}, but there is only one example in the literature of 2,6-bistriazolylpurine derivatives, which can serve as ratiometric fluorescence cation sensors, especially for the Zn^{2+} and Ca^{2+} ions [59].

The formation constant for tetramethylated cyclen and Cu^{2+} complex reaches logK 18.4 [60]. For triazole–pyridine–triazole conjugate with tridentate coordination of Cu^{2+} ions complex with logK 19.69 forms, and the complex is protonated ($\log\beta[CuHL_2]^{3+}$ [61]. On the other hand, 6-aminopurine forms a complex with Cu^{2+} ions with coordination to the *N*7 position and amino group at the *C*6 position and a formation constant logK 8.94 [62]. 3-Methyl-5-pyridin-2-yl-1,2,4-triazole forms complexes with Cu^{2+} ions in metal-to-ligand ratios 1:1 and 1:3, and their complex formation logK are 10.35 and 17.82, respectively [63]. Based on this information, the competitive complexation between cyclen moiety Cu^{2+} ions and between the *N*7 position of purine and the *N*2 position of triazole and Cu^{2+} ions may take place. In addition, the most structurally related compounds to the target compound **1** reported in the literature are purine–copper–cyclen complexes, where purine and cyclen moieties are separate ligands and are not linked within a single molecule. In these complexes, copper ions coordinate with the nitrogen atoms of the cyclen and purine *N*7, *N*9, or *N*3 positions. However, binding constants for these interactions have not been reported. Notably, these studies are focused on the chelating properties of the complexes rather than their potential photocatalytic applications [64,65].

Hence, we report here the design and synthesis of the purine derivative, which contains all the foreseen necessary substituents for metal complexation along with light absorption and electron transfer from the organic ligand to the metal center.

2. Results and Discussion

The proposed structure consists of a purine core and three main moieties A, B, and C, which may be added in various order. The retrosynthetic analysis of the proposed structure **1** offers possible approaches toward the introduction of target building blocks (Scheme 2). Moiety A makes it possible to construct via copper-catalyzed azide–alkyne cycloaddition reaction (CuAAC) between the azido group containing purine derivative **2** and alkyne **3**. Thus, the azidation of 6-chloropurines is well-known and results in high to quantitative yields [66,67], while corresponding alkyne **3** requires a separate synthetic approach. Derivatization of the purine *C*8 position is possible to achieve via a palladium-

catalyzed cross-coupling reaction. We decided to use the Stille reaction conditions due to the easy, one-step synthesis of the stannane **5** from commercially available 4-bromo-*N*,*N*-dimethylaniline [68]. The introduction of moiety C is proposed to be achieved in two ways—either via the Mitsunobu reaction between 9*H*-purine **6** and cyclen derivative **7** or using the S_N2 reaction between substituted 9-(2-iodoethyl)-9*H*-purine **8** and cyclen derivative **9**.

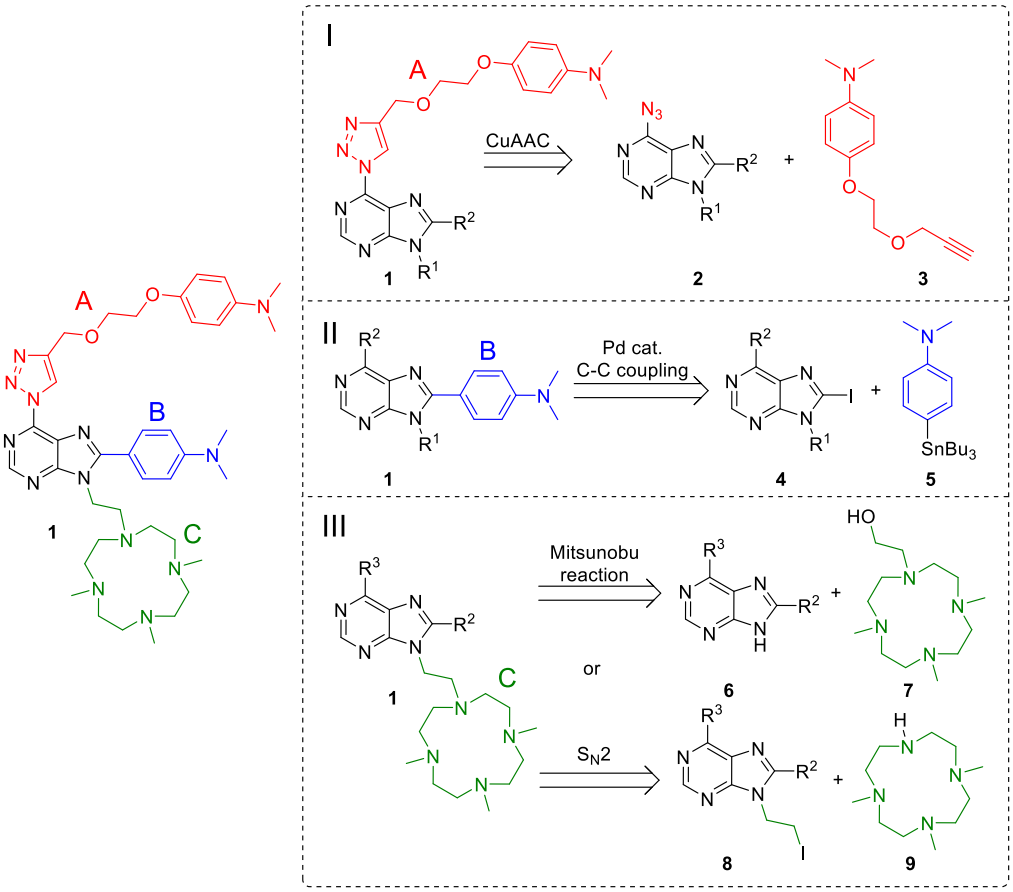

Scheme 2. Retrosynthetic analysis toward purine–cyclen conjugate **1**.

In general, we have explored several synthetic routes toward target compound **1**. The first synthetic route started with S_NAr reaction between 6-chloro-9-tetrahydropyranyl purine **10** [69] and sodium azide, resulting in 6-azidopurine derivative **11** in a 70% yield (Scheme 3). Next, we envisioned two approaches for the construction of moiety A at the C6 position of purine. The first approach included the CuAAC reaction of compound **11** with 2-(prop-2-yn-1-yloxy)ethan-1-ol (**12**) [70], followed by the derivatization of the free hydroxyl group of an obtained product **13**. While the CuAAC reaction successfully provided triazole derivative **13** in a 63% yield, the further derivatizations with 4-bromo-*N*,*N*-dimethylaniline (**14**) via copper-catalyzed Ullmann-type reactions were unsuccessful [71–73]. For this transformation, we applied previously reported reagent systems of KOH/CuI/1,10-phenanthroline/*n*-Bu_4NI at 100 °C [71], CuI/3,4,7,8-tetramethyl-1,10-

phenanthroline/Cs_2CO_3 at 110 °C [72] and CuI/K_3PO_4/8-hydroxyquinoline at 110 °C [73], but did not achieve any conversion. For the second approach, building block **3** was obtained in 4 steps from 1-bromo-4-nitrobenzene (**16**) and used in CuAAC reaction with compound **11**, resulting in a 56% yield of desired product **15**. While deprotection of the tetrahydropyranyl group at the purine *N*9 position of compound **15** was easily achieved in AcOH/H_2O/THF mixture at 50 °C temperature overnight, further attempts to derivatize *N*9 position of this compound using the Mitsunobu (DIAD/PPh_3/2-bromoethanol or 2-chloroethanol at 0 → 60 °C) or alkylation (NaH/1,2-dibromoethane at 0 → 100 °C) reaction procedures were not fruitful. The explanation involves the electron-poor nature of the purine system and the reduced reactivity of the *N*9 position after the introduction of the triazolyl moiety A. This encouraged us to design the second approach toward the desired compound **1**.

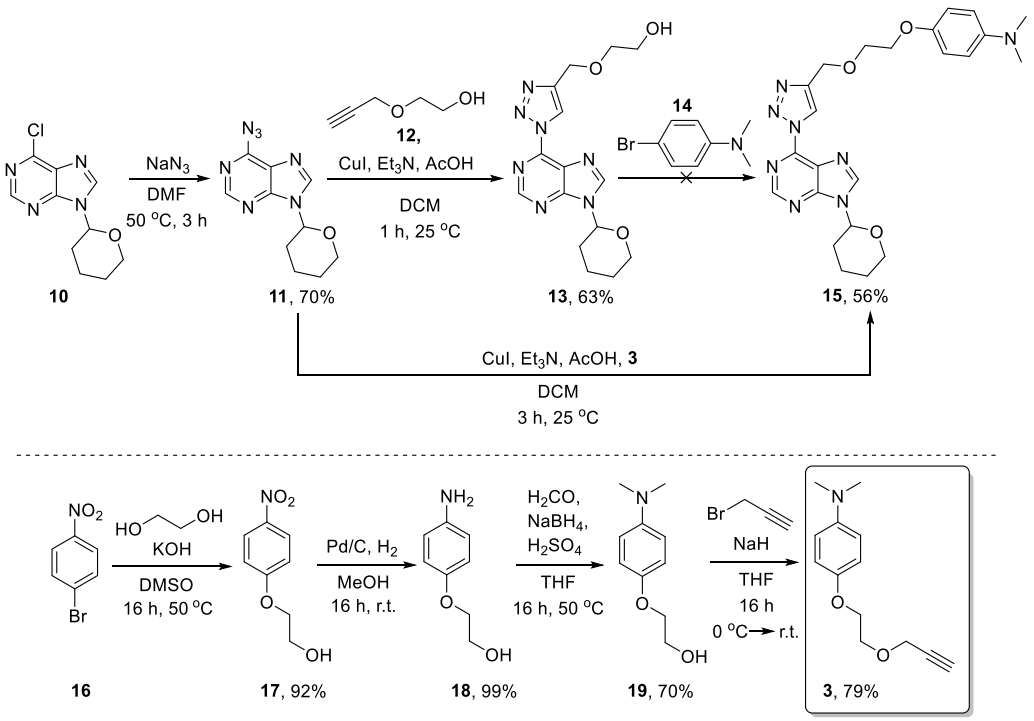

Scheme 3. Attempts to introduce moiety A to the 6-chloro-9-tetrahydropyranyl purine **10**.

Next, we decided to introduce the THP-protected oxyethyl linker at the *N*9 position prior to derivatization of the *C*6 position with moiety A, keeping in mind that the cyclen part should be introduced later due to the excellent complexation ability of cyclen with transition metals [16], which would make CuAAC and cross-coupling reactions impossible. Thereby, the second synthetic route started with a Mitsunobu reaction between 6-chloropurine (**20**) and 2-(cyclohexyloxy)ethan-1-ol (**21**) [74], yielding product **22** in a 60% yield (Scheme 4). Next, the sequence of S_NAr and CuAAC reactions was used toward compound **24**. The following bromination attempt of the *C*8 purine position with NBS resulted in phenyl ring bromination instead, providing product **25** with a 59% yield. The use of LDA and other deprotonation reagents (NaH and *n*-BuLi) led to the deprotonation of triazole instead of

the purine *C*8 position, so we concluded that the introduction of halogen to the *C*8 position and moiety B should be done prior to the derivatization of the *C*6 position.

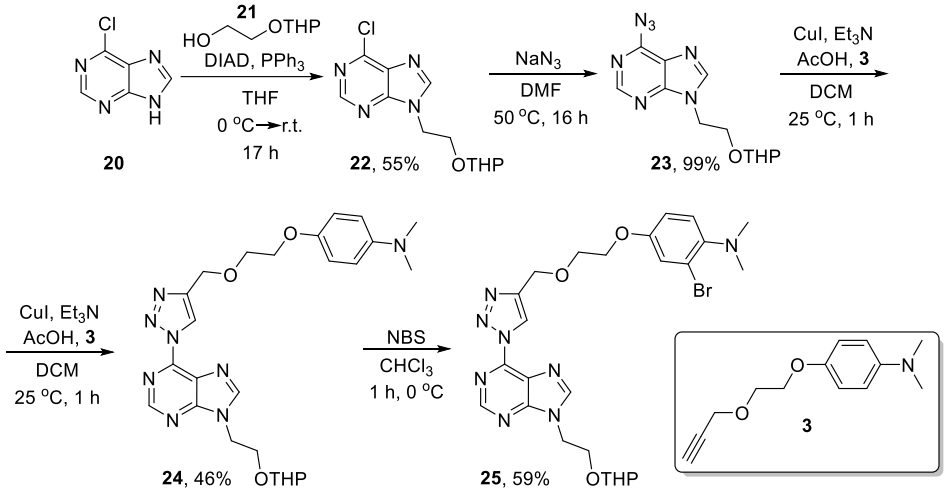

Scheme 4. Introduction of THP-protected oxyethyl linker to 6-chloropurine (**20**), followed by a moiety A and attempts to modify the *C*8 purine position.

The final synthetic route started with the iodination of previously obtained compound **22** using the LDA and I_2 reagent system (Scheme 5). After that, a Stille cross-coupling reaction between *N*,*N*-dimethyl-4-(tributylstannyl)aniline (**5**) and purine derivative **26** resulted in *C*8 derivatized product **27** in a 52% yield. Next, the S_NAr and CuAAC reaction sequence was performed to achieve compound **29**. Further, THP group cleavage with the following mesylation step resulted in almost quantitative yields in both transformations. In the first attempts, cyclen derivative **9**, which was previously obtained in three steps using literature methods [75], did not react with acquired mesylate **31** in the S_N2 reaction. Thus, we decided to substitute the mesylate group with bromide and then perform an alkylation reaction with cyclen derivative **9**. The best conversion toward target product **1** in this reaction was 20%, with a 6% isolated yield due to the difficulties with purification stemming from the similar polarity of by-products. In addition, this transformation preferred the E2 mechanism, forming elimination product **32** as a main by-product with 57% isolated yield.

With target product **1** in hand, we did preliminary studies using ^{1}H NMR titration experiments (in the Supplementary Materials) to determine the complexation ability of purine–cyclen conjugate toward metal ions. Purine-cyclen conjugate **1** was titrated in MeCN-d_3 with Cu^{2+} ions using $Cu(ClO_4)_2 \cdot 6H_2O$ as a Cu^{2+} source and benzene as an internal standard. The corresponding spectra were taken after each 0.1 eq. addition of Cu^{2+} ions (Figure 2).

The shifts of the signals correspond to protons from triazole at the *C*6 position of purine, phenyl ring at the *C*8 position of purine, and cyclen at the *N*9 position of purine. The ^{1}H NMR spectra show relatively complex behavior of the Cu^{2+} binding process by compound **1**. The most important feature representing an expected Cu^{2+} binding in cyclen is shown by a thick arrow at the values 2.0–2.5 ppm. Starting from approximately 0.7 equivalents of metal ion, all ^{1}H NMR signals of cyclen assemble into a single peak at approximately 2.2 ppm, which does not shift at higher concentrations of Cu^{2+}. This fact indicates that metal ion is coordinated inside the cyclen ring in a unique configuration, and all four

cyclen nitrogens are equally involved in metal ion binding. An additional metal binding site between triazole and purine nitrogens is also occupied by $Cu^{2+,}$ as is seen by triazole proton shift at approximately 9.0–9.2 ppm. The proton shifts of the other aromatic fragments of compound **1** indicate the rearrangements of electron density over the molecule during the complexation process. Based on NMR titration experiments, the possible equivalence points were determined at 0.35 and 0.50 equivalents, which corresponded to M1:L3 and M1:L2 complexes, respectively (Figures 3 and 4). The competitive complexation happened between the cyclen part and the triazole *N*2 and purine *N*7 positions.

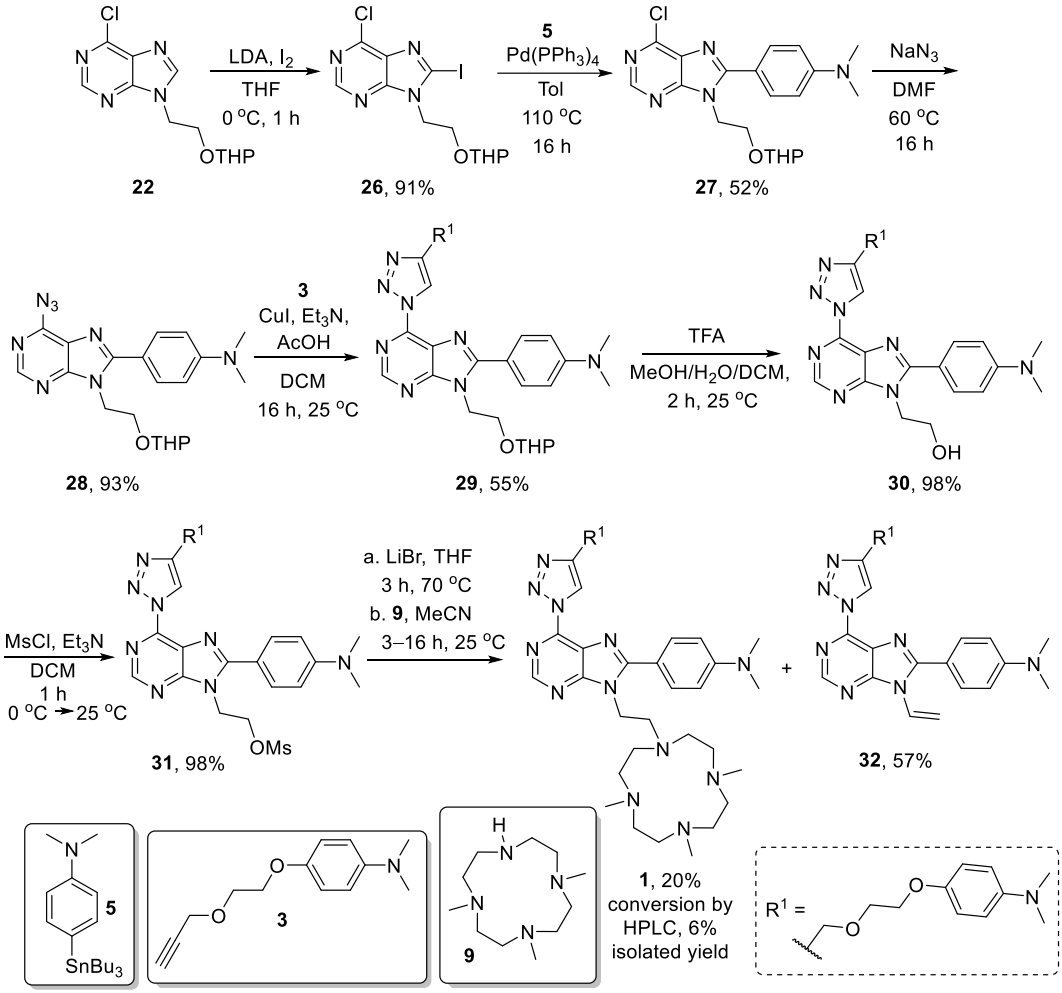

Scheme 5. The final synthetic route toward target purine–cyclen conjugate **1**.

Due to the paramagnetic nature of the copper, the performance and analysis of NMR experiments and obtaining spectra at higher metal ion concentrations turn out to be difficult. Thus, the complex formation of compound **1** with Cu^{2+} and the UV–spectrophotometric titration was performed in acetonitrile (ACN) at room temperature, and it confirmed the result obtained by ^{1}H NMR titration. The initial concentration of **1** was 5×10^{-5} mol/L.

The ratio of compound **1** to Cu^{2+} was varied by adding aliquots of a solution of copper(II) perchlorate with 0.125×10^{-6} mol/L concentration.

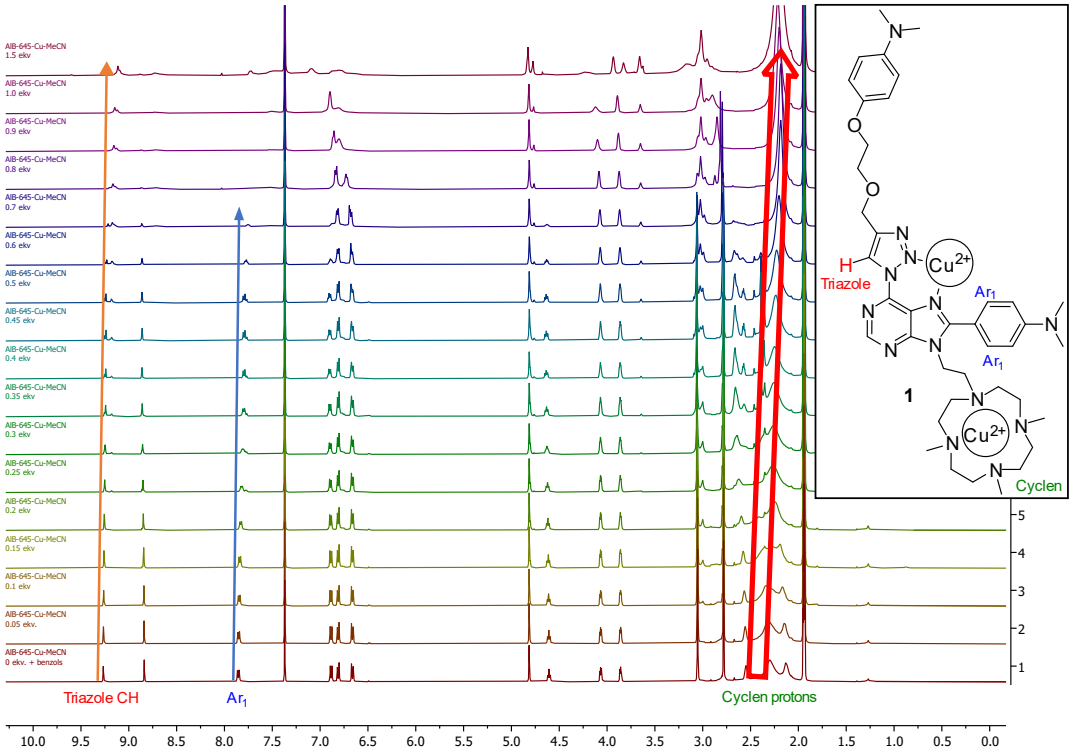

Figure 2. ^{1}H NMR titration spectra of compound **1** with Cu^{2+} ions in MeCN-d_3.

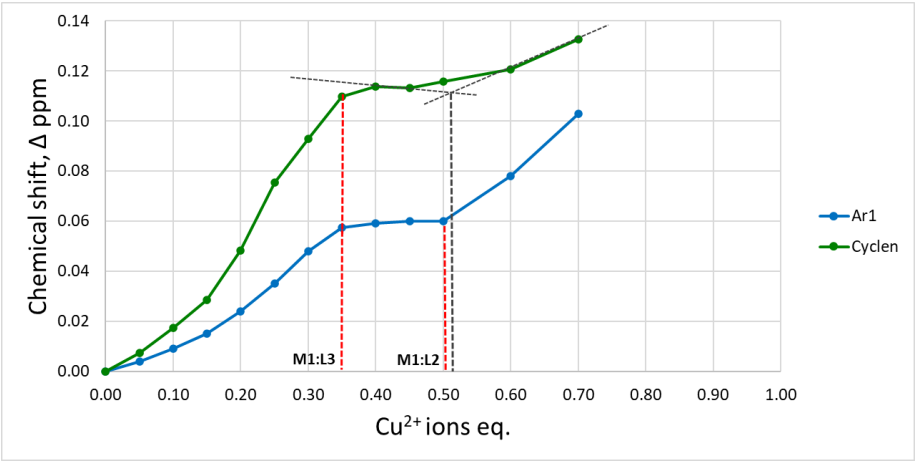

Figure 3. The change of the chemical shifts of Ar_1 and cyclen proton signals in ^{1}H NMR titration experiments for compound **1** with Cu^{2+} ions in MeCN-d_3.

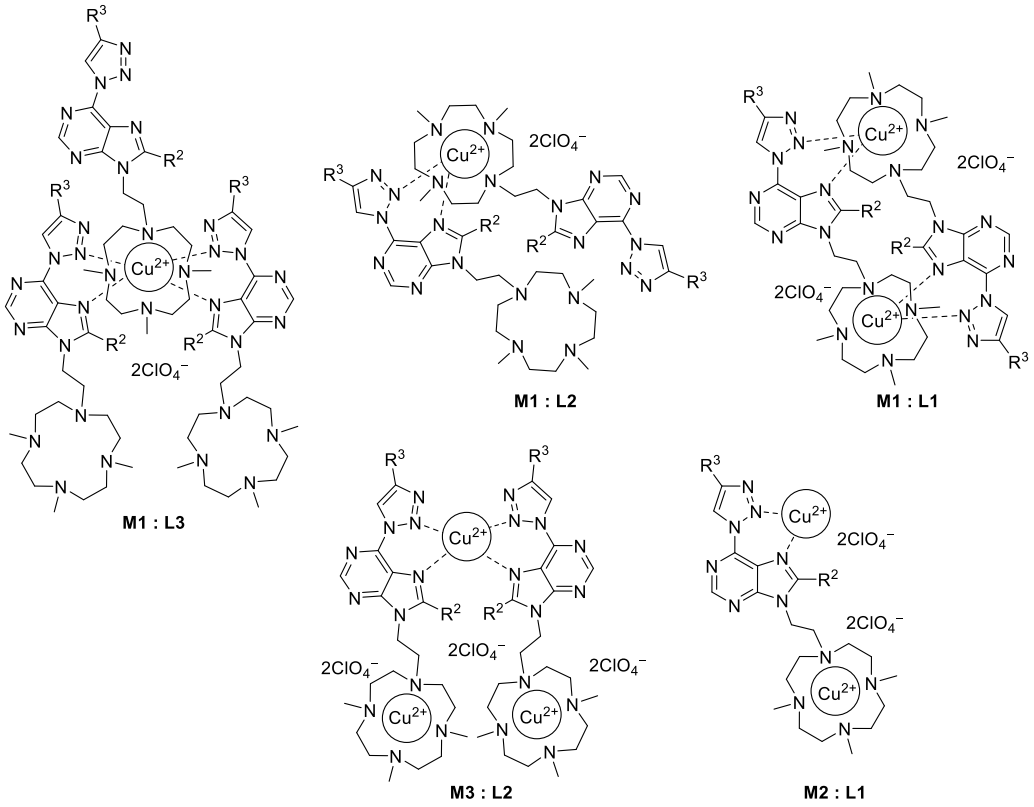

Figure 4. Possible Cu^{2+} complexes with purine–cyclen conjugate.

The variation of absorption spectra upon adding Cu^{2+} into the solution of **1** is quite complex, yet the step-by-step analysis of absorption spectra crossed with the data of NMR titration provides a realistic picture of the composition and geometry of the formed complexes (Figures 4–6). The increase of the intensity of spectral feature at approximately 290 nm indicates the increase of the concentration of Cu^{2+} ions in the ACN solution. According to the literature [76], this absorption band may be attributed to the ligand-to-metal charge transfer (LMCT) transition between ACN and copper ion. At the concentrations corresponding to metal–ligand ratio below 1:1, the main spectral changes occur at the 450–800 nm spectral range (Figure 5a). The absorption bands observed may be attributed to the d-d transition of Cu^{2+} ions coordinated by cyclen nitrogens [15].

It is important to note that the main absorption band (including the vibronic replicas) located at 370 nm remains at the same position; only the intensity varies within 30% (Figure 5b). Such behavior may suggest that the π-conjugated electronic system of *N*,*N*-dimethylaniline-purine fragment is not affected by a metal ion. The main coordination site for Cu^{2+} is located inside cyclen until the metal–ligand ratio reaches 1:1; the ligands in excess are most probably oriented with triazole-purine fragment pointing towards Cu^{2+} inside cyclen and forming a lossy 1:3 and 1:2 complexes. After the metal–ligand ratio exceeds 1:1, the 370 nm absorption band starts to decay, causing a simultaneous rise of a new absorption band at 410 nm, which reaches its maximum at a metal–ligand ratio equal to 2:1. The formation of a new red-shifted absorption band is a typical spectroscopic signature of coordination of metal ion by an acceptor in donor-acceptor compounds; in

our situation, it corresponds to the coordination of the second Cu^{2+} by triazole-purine fragment. Additionally, selected absorption spectra, together with complex compositions and supposed geometries, as well as types of vertical transitions involved [76], are presented in Figure 6.

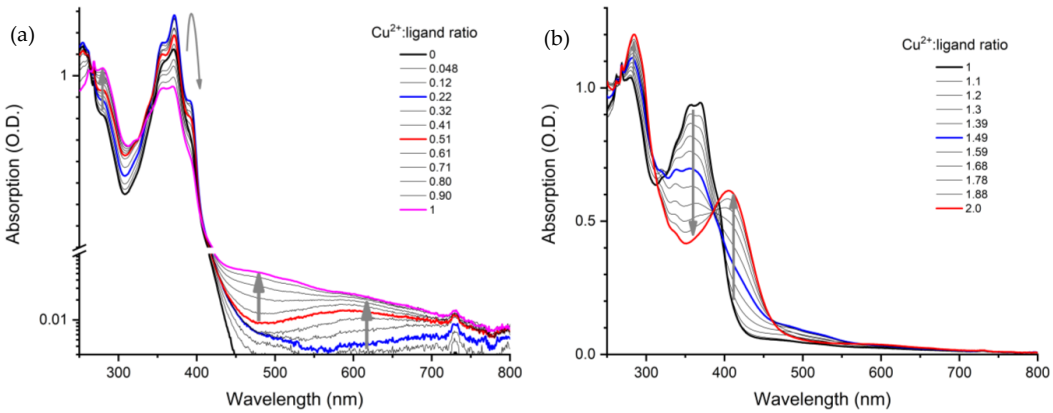

Figure 5. (**a**) The variation of the absorption spectra of complexes going from pure compound **1** until a 1:1 metal–ligand ratio; (**b**) the absorption spectra of complexes with compositions going from 1:1 until a 2:1 metal–ligand ratio.

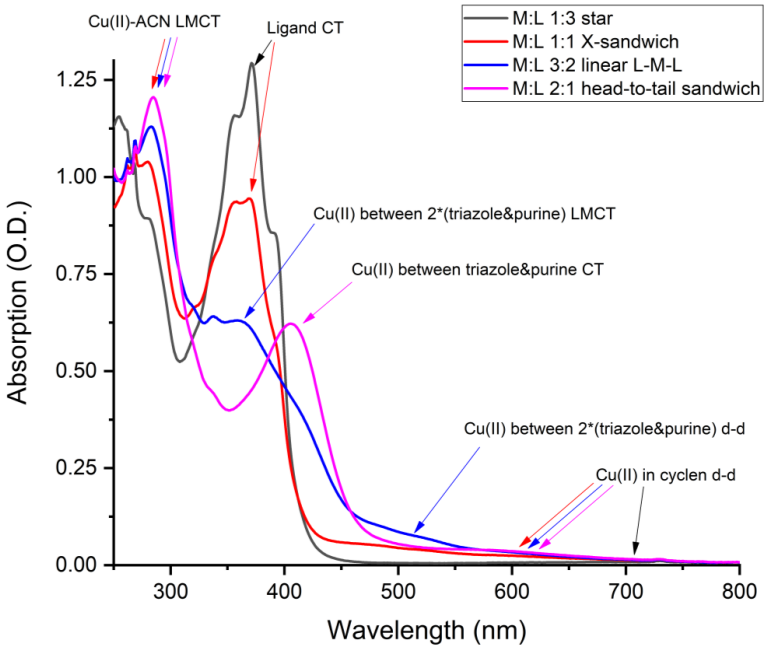

Figure 6. Characteristic absorption spectra extracted from spectrophotometric titration experiment indicating types of vertical transitions, compound **1**: Cu^{2+} complex compositions, and supposed geometries.

3. Materials and Methods

3.1. General Information

Compounds **5**, **9**, **10**, **12**, and **21** were prepared according to the procedures outlined in the literature [68–70,74,75]. Compounds **17**–**19** were prepared using synthetic procedures described in this work, and their ^{1}H spectra match the literature [77–79].

Commercial grade reagents and solvents were purchased from Sigma-Aldrich (Burlington, MA, USA), Fluorochem (Hadfield, UK) or BLD Pharm (Reinbek, Germany) at the highest commercial quality and used without further purification.

The absorption spectra were recorded using the UV-VIS-NIR absorption spectrometer Varian Cary 5000 (Agilent Technologies, Santa Clara, CA, USA). Overall, more than 200 titration steps were provided to obtain the full picture of the complexation process.

3.2. Characterization Data for Products

3.2.1. 2-(4-Nitrophenoxy)ethan-1-ol (**17**)

KOH (26.7 g, 0.48 mol, 4.0 eq.) was added in portions to abs. ethylene glycol (200 mL) at 0 °C, and the solution was stirred for 30 min at 0 °C. Then, the reaction mixture was warmed up to 25 °C and stirred until KOH was fully dissolved. Meanwhile, 1-bromo-4-nitrobenzene (**16**) (24.0 g, 0.12 mol, 1.0 eq.) was dissolved in abs. DMSO (200 mL) was then added to the KOH solution and stirred at 50 °C for 30 min. An additional abs. DMSO (40 mL) was added until everything was dissolved, and the reaction was stirred overnight at 50 °C for 16 h. The final reaction mixture was poured into cold water (1.5 L), and the formed precipitate was filtered (13.53 g of **17**). Filtrate was extracted with DCM (3 × 100 mL). The organic phase was washed with brine (100 mL), dried over anhydrous Na_2SO_4, filtered, evaporated in a vacuum, and then lyophilized from the remaining DMSO. After lyophilization, the solid was dissolved in a minimum amount of DCM, added to the cold hexane (100 mL), and the resulting precipitate was filtered (6.4 g of **17**). Beige amorphous solid, yield: 19.93 g, 92%. ^{1}H-NMR spectrum is consistent with the literature [77].

3.2.2. 2-(4-Aminophenoxy)ethan-1-ol (**18**)

Compound **17** (13.5 g, 73.77 mmol, 1.0 eq.) and 10% palladium on carbon (1.35 g) were suspended in MeOH (300 mL) and H_2 gas was bubbled through for 6 h at 25 °C. The reaction was controlled with HPLC. The reaction mixture was filtered through a celite pad and evaporated, providing product **18** (yield: 11.12 g, 99%) as a brown oil. HPLC: t_R = 1.47 min, eluent E_1. ^{1}H-NMR spectrum is consistent with the literature [78].

3.2.3. 2-(4-(Dimethylamino)phenoxy)ethan-1-ol (**19**)

Compound **18** (11.12 g, 72.7 mmol, 1.0 eq.) and $NaBH_4$ (16.5 g, 436.2 mmol, 6.0 eq.) were suspended in abs. THF (250 mL) and then slowly added to the mixture of H_2SO_4 (3M, 28.8 mL) and H_2CO (37%, 21.6 mL) at 0 °C. The resulting mixture was left to stir for 2 h at 25 °C, then 4 h at 50 °C. The reaction mixture was basified with 2M KOH solution till pH = 11 and extracted with DCM (2 × 100 mL). The organic phase was washed with brine (2 × 100 mL), dried over anhydrous Na_2SO_4, filtered and evaporated. Silica gel column chromatography (EtOH/Tol, gradient 0% → 7%) provided product **19** (yield: 9.16 g, 70%) as a brown amorphous solid. R_f = 0.73 (Tol/EtOH = 5:1). ^{1}H-NMR spectrum is consistent with the literature [79].

3.2.4. *N*,*N*-Dimethyl-4-(2-(prop-2-yn-1-yloxy)ethoxy)aniline (**3**)

To the solution of compound **19** (9.16 g, 50.5 mmol, 1.0 eq.) in abs. THF (100 mL) at 0 °C, 60% NaH (3.03 g, 75.8 mmol, 1.5 eq.) was added in small portions over 30 min, then warmed until 25 °C. 80 wt% propargyl bromide in toluene (8.18 mL, ρ = 1.38 g/cm^3,

75.9 mmol, 1.5 eq.) was added, and the reaction was left to stir for 16 h at 25 °C. The reaction mixture was quenched with water (50 mL) and extracted with DCM (2 × 100 mL); the organic phase was washed with brine (100 mL), dried over anhydrous Na_2SO_4, filtered, and evaporated. Silica gel column chromatography (EtOH/Tol, gradient 0% → 20%) provided product **3** (yield: 8.73 g, 79%) as a brown amorphous solid. R_f = 0.67 (EtOH/Tol = 5:1). HPLC: t_R = 1.52 min, eluent E_1. IR (KBr) ν (cm^{-1}): 2923, 2852, 1513, 1455, 1352, 1242, 1104, 1035, 947, 817, 704. ^{1}H-NMR (500 MHz, $CDCl_3$) δ (ppm): 6.87 (d, 2H, ^3J = 9.0 Hz, 2 × H-Ar), 6.73 (d, 2H, ^3J = 9.0 Hz, 2 × H-Ar), 4.27 (s, 2H, (-CH_2-)), 4.10 (t, 2H, ^3J = 4.4 Hz, (-CH_2-)), 3.87 (t, 2H, ^3J = 4.4 Hz, (-CH_2-)), 2.87 (s, 6H, 2 × (-CH_3)), 2.45 (s, 1H, CH(alkynyl)). ^{13}C NMR (126 MHz, $CDCl_3$) δ (ppm): 151.1, 146.2, 115.9, 114.8, 79.7, 74.8, 68.6, 68.1, 58.7, 41.8. HRMS (ESI) m/z: $[M + H]^+$ Calculated for $C_{13}H_{18}NO_2$ 220.1332; Found 220.1330 (0.91 ppm).

3.2.5. 6-Azido-9-(Tetrahydro-2*H*-pyran-2-yl)-9*H*-purine (**11**)

To a solution of 10 [69] (7.0 g, 29.33 mmol, 1.0 eq.) in DMF (240 mL) NaN_3 (3.81 g, 58.66 mmol, 2 eq.) was added, and the reaction mixture was stirred at 50 °C for 3 h. Then, it was evaporated and dried in a vacuum. The resulting solid was suspended in DCM (100 mL) and washed with 5% aqueous LiCl solution (2 × 100 mL), water (2 × 200 mL), and brine (100 mL). The organic phase was dried over anhydrous Na_2SO_4, filtered, and evaporated, providing compound 11 (yield: 5.06 g, 70%) as a beige amorphous solid. HPLC: t_R = 3.00 min, eluent E_1. IR (KBr) ν (cm^{-1}): 2917, 2852, 2134, 1640, 1374, 1345, 1228, 1083, 1043, 967, 915. ^{1}H-NMR (500 MHz, DMSO-d_6) δ (ppm): 10.12 (s, 1H, H-C(2)), 8.87 (s, 1H, H-C(8)), 5.90 (d, 1H, ^3J = 11.2 Hz, H_a-C), 4.05 (d, 1H, ^3J = 11.2 Hz, H_e-C), 3.77 (td, 1H, ^2J = ^3J = 11.2 Hz, ^3J = 4.1 Hz, H_e-C), 2.42–2.35 (qd, 1H, ^2J = ^3J = 11.2 Hz, ^3J = 4.1 Hz, H_b-C), 2.09–1.98 (m, 2H, H_b-C, H_c-C), 1.87–1.74 (m, 1H, H_c-C), 1.68–1.58 (m, 2H, (-CH_2-)). ^{13}C-NMR (126 MHz, DMSO-d_6) δ (ppm): 145.4, 142.5, 141.5, 136.0, 119.9, 82.0, 67.8, 30.0, 24.4, 22.2. HRMS (ESI) m/z: $[M + H]^+$ Calculated for $C_{10}H_{12}N_7O$ 246.1098; Found 246.1093 (2.03 ppm).

3.2.6. 2-({1-[9-(Tetrahydro-2*H*-pyran-2-yl)-9*H*-purin-6-yl]-1*H*-1,2,3-triazol-4-yl}methoxy)ethan-1-ol (**13**)

General method A for CuAAC reactions: To a solution of **11** (1.0 g, 4.08 mmol, 1.0 eq.), CuI (0.14 g, 0.73 mmol, 0.18 eq.), AcOH (0.26 mL, ρ = 1.05 g/cm^3, 4.49 mmol, 1.1 eq.) and Et_3N (0.63 mL, ρ = 0.73 g/cm^3, 8.16 mmol, 2 eq.) in DCM (40 mL) 2-(prop-2-yn-1-yloxy)ethanol (0.82 g, 0.90 mmol, 1.5 eq.) (**12**) [70] was added and the reaction mixture was stirred isolated from the daylight for 1 h at 25 °C. Then, the reaction mixture was poured into water (50 mL) and extracted with DCM (3 × 50 mL). The combined organic phase was washed with aqueous NaHS (2 × 30 mL) and brine (50 mL), dried over anhydrous Na_2SO_4, filtered, and evaporated. Silica gel column chromatography (DCM/EtOH, gradient 0% → 15%) provided product **13** (yield: 881 mg, 63%) as a white amorphous solid. R_f = (0.48 DCM/EtOH = 10:1). HPLC: t_R = 2.16 min, eluent E_1. IR (KBr) ν (cm^{-1}): 3370, 3111, 2924, 2862, 1616, 1574, 1462, 1335, 1212, 1082, 1014, 908, 822. ^{1}H-NMR (500 MHz, $CDCl_3$) δ 9.07 (s, 1H, H-C(triazole)), 8.92 (s, 1H, H-C(2)), 8.42 (s, 1H, H-C(8)), 5.86 (dd, 1H, ^2J = 10.5 Hz, ^3J = 2.5 Hz, H_a-C), 4.84 (s, 2H, (-CH_2-)), 4.23–4.18 (m, 1H, H_e-C), 3.84–3.75 (m, 3H, H_e-C, (-CH_2-)), 3.74–3.70 (m, 2H, (-CH_2-)), 2.45 (s, 1H, (-OH)), 2.26–2.17 (m, 1H, H_b-C), 2.14–2.01 (m, 2H, H_b-C, H_c-C), 1.87–1.73 (m, 2H, H_c-C, H_d-C), 1.73–1.64 (m, 1H, H_d-C). ^{13}C-NMR (126 MHz, $CDCl_3$) δ (ppm): 153.8, 152.3, 145.8, 144.9, 144.1, 123.2, 122.9, 82.6, 72.1, 69.1, 64.5, 62.0, 32.1, 24.9, 22.8. HRMS (ESI) m/z: $[M + H]^+$ Calculated for $C_{15}H_{20}N_7O_3$ 346.1622; Found 346.1613 (2.6 ppm).

3.2.7. *N*,*N*-Dimethyl-4-[2-({1-[9-(tetrahydro-2*H*-pyran-2-yl)-9*H*-purin-6-yl]-1*H*-1,2,3-triazol-4-yl}methoxy)ethoxy]aniline (**15**)

Prepared according to general method A: Compound **11** (85 mg, 0.35 mmol, 1.0 eq.), CuI (12 mg, 0.06 mmol, 0.18 eq.), AcOH (23 µL, ρ = 1.05 g/cm^3, 0.39 mmol, 1.1 eq.), Et_3N (54 µL, ρ = 0.73 g/cm^3, 0.39 mmol, 1.1 eq.) and *N*,*N*-dimethyl-4-(2-(prop-2-yn-1-yloxy)ethoxy)aniline (115 mg, 0.52 mmol, 1.5 eq.), DCM (4 mL), 25 °C, 3 h. Silica gel column chromatography (Tol/EtOH, gradient 0% → 8%) provided product **15** (yield: 90 mg, 56%) as a gray amorphous solid. R_f = 0.49 (Tol/EtOH = 5:1). HPLC: t_R = 1.93 min, eluent E_1. IR (KBr) ν (cm^{-1}): 2939, 2869, 2801, 1614, 1523, 1456, 1231, 1209, 1083, 1032, 910, 803. ^{1}H-NMR (500 MHz, $CDCl_3$) δ 9.11 (s, 1H, H-C(triazole)), 8.92 (s, 1H, H-C(2)), 8.42 (s, 1H, H-C(8)), 6.85 (d, 2H, ^3J = 6.5 Hz, 2 × H-C(Ar)), 6.68 (d, 2H, ^3J = 6.5 Hz, 2 × H-C(Ar)), 5.85 (d, 1H, ^3J = 10.5 Hz, H_a-C), 4.90 (s, 2H, (-CH_2-)), 4.20 (d, 1H, ^3J = 10.5 Hz, H_e-C), 4.14–4.05 (m, 2H, (-CH_2-)), 3.95–3.88 (m, 2H, (-CH_2-)), 3.80 (t, 1H, ^3J = 10.5 Hz, H_e-C), 2.83 (s, 6H, 2 × (-CH_3)), 2.23–2.16 (m, 1H, H_b-C), 2.13–2.01 (m, 2H, H_b-C, H_c-C), 1.87–1.72 (m, 2H, H_c-C, H_d-C), 1.71–1.64 (m, 1H, H_d-C). ^{13}C-NMR (126 MHz, $CDCl_3$) δ (ppm): 153.8, 152.3, 151.0, 146.0, 145.9, 144.8, 144.0, 123.3, 122.8, 115.8, 114.7, 82.6, 69.4, 69.0, 68.2, 64.7, 41.8, 31.9, 24.9, 22.7. HRMS (ESI) m/z: [M + H]$^+$ Calculated for $C_{23}H_{29}N_8O_3$ 465.2357; Found 465.2355 (0.43 ppm).

3.2.8. 6-Chloro-9-{2-[(Tetrahydro-2*H*-pyran-2-yl)oxy]ethyl}-9*H*-purine (**22**)

To a suspension of 6-chloropurine (**20**) (4.8 g, 31.15 mmol, 1.1 eq.), PPh_3 (9.65 g, 36.82 mmol, 1.3 eq.) and 2-((tetrahydro-2*H*-pyran-2-yl)oxy)ethanol (**21**) [74] (4.14 g, 28.32 mmol, 1.0 eq.) in dry THF (200 mL) at 0 °C DIAD (6.12 mL, ρ = 1.03 g/cm^3, 31.15 mmol, 1.1 eq.) was added slowly over 1 h. Then, the reaction mixture was left to stir for 16 h at 25 °C and then filtered. The filtrate was evaporated. Reverse phase silica gel column chromatography (MeOH/H_2O, gradient 0% → 70%) provided product **22** (yield: 4.82 g, 55%) as a pale yellow oil. R_f = 0.84 (DCM/EtOH = 10:1). HPLC: t_R = 2.15 min, eluent E_1. IR (KBr) ν (cm^{-1}): 2941, 2867, 1593, 1560, 1334, 1197, 1123, 1034, 933, 856. ^{1}H-NMR (500 MHz, $CDCl_3$) δ (ppm): 8.73 (s, 1H, H-C(2)), 8.28 (s, 1H, H-C(8)), 4.56–4.45 (m, 3H, H_a-C, (-CH_2-)), 4.11–4.05 (m, 1H, H_f-C), 3.77–3.71 (m, 1H, H_f-C), 3.61–3.54 (m, 1H, H_e-C), 3.44–3.38 (m, 1H, H_e-C), 1.77–1.62 (m, 2H, H_b-C, H_c-C), 1.57–1.45 (m, 4H, H_b-C, H_c-C, (-CH_2-)). ^{13}C-NMR (126 MHz, $CDCl_3$) δ (ppm): 152.0, 151.9, 151.0, 146.5, 131.6, 99.3, 65.2, 62.6, 44.4, 30.5, 25.3, 19.5. HRMS (ESI) m/z: [M + H]$^+$ Calculated for $C_{12}H_{16}ClN_4O_2$ 283.0956; Found 283.0950 (2.12 ppm).

3.2.9. 6-Azido-9-{2-[(Tetrahydro-2*H*-pyran-2-yl)oxy]ethyl}-9*H*-purine (**23**)

To a solution of **22** (0.72 g, 2.54 mmol, 1.0 eq.) in DMF (14 mL) NaN_3 (0.33 g, 5.08 mmol, 2 eq.) was added and the reaction mixture was stirred at 50 °C for 16 h. Then, it was evaporated and dried in a vacuum. The resulting solid was suspended in DCM (20 mL) and washed with 5% aqueous LiCl solution (2 × 20 mL), water (2 × 20 mL), and brine (20 mL). The organic phase was dried over anhydrous Na_2SO_4, filtered, and evaporated, providing compound **23** (yield: 0.73 g, 99%) as a white amorphous solid. HPLC: t_R = 2.94 min, eluent E_1. IR (KBr) ν (cm^{-1}): 2985, 2938, 2185, 1636, 1376, 1345, 1256, 1125, 1071, 981, 872. ^{1}H-NMR (500 MHz, DMSO-d_6) δ (ppm): 10.11 (s, 1H, H-C(2)), 8.63 (s, 1H, H-C(8)), 4.68–4.55 (m, 3H, H_a-C, (-CH_2-)), 4.02 (ddd, 1H, ^2J = 10.9 Hz, ^3J = 6.5, 4.1 Hz, H_f-C), 3.84 (ddd, 1H, ^2J = 10.9 Hz, ^3J = 6.5, 4.1 Hz, H_f-C), 3.44 (ddd, 1H, ^2J = 11.2 Hz, ^3J = 8.4, 3.0 Hz, H_e-C), 3.32–3.29 (m, 1H, H_e-C), 1.64–1.48 (m, 2H, H_b-C, H_c-C), 1.45–1.31 (m, 4H, H_b-C, H_c-C, (-CH_2-)). ^{13}C NMR (126 MHz, DMSO-d_6) δ (ppm): 145.4, 144.7, 142.3, 135.7, 119.6, 97.6, 64.6, 61.1, 44.3, 29.9, 24.8, 18.8. HRMS (ESI) m/z: [M + H]$^+$ Calculated for $C_{12}H_{16}N_7O_2$ 290.1360; Found 290.1350 (3.45 ppm).

3.2.10. *N*,*N*-Dimethyl-4-(2-{[1-(9-{2-[(Tetrahydro-2*H*-pyran-2-yl)oxy]ethyl}-9*H*-purin-6-yl)-1*H*-1,2,3-triazol-4-yl]methoxy}ethoxy)aniline (**24**)

Prepared according to general method A: Compound **23** (100 mg, 0.35 mmol, 1.0 eq.), CuI (12 mg, 0.06 mmol, 0.16 eq.), AcOH (21 µL, ρ = 1.05 g/cm^3, 0.38 mmol, 1.1 eq.), Et_3N (53 µL, ρ = 0.73 g/cm^3, 0.38 mmol, 1.1 eq.) and *N*,*N*-dimethyl-4-(2-(prop-2-yn-1-yloxy)ethoxy)aniline (151 mg, 0.69 mmol, 2.0 eq.), DCM (3 mL), 25 °C, 1 h. Silica gel column chromatography (DCM/EtOH, gradient 0% → 5%) provided product **24** (yield: 81 mg, 46%) as a pale brown amorphous solid. R_f = 0.53 (DCM/EtOH = 20:1). HPLC: t_R = 5.03 min, eluent E_2. IR (KBr) ν (cm^{-1}): 2919, 2868, 1605, 1513, 1331, 1234, 1111, 1032, 845, 823. ^{1}H-NMR (500 MHz, $CDCl_3$) δ (ppm): 9.11 (s, 1H, H-C(triazole)), 8.91 (s, 1H, H-C(2)), 8.39 (s, 1H, H-C(8)), 6.86 (d, 2H, ^3J = 9.2 Hz, 2 × H-C(Ar)), 6.70 (d, 2H, ^3J = 9.2 Hz, 2 × H-C(Ar)), 4.90 (s, 2H, (-CH_2-)), 4.64–4.51 (m, 3H, H_a-C, (-CH_2-)), 4.17–4.12 (m, 1H, H_f-C), 4.11 (dd, 2H, ^3J = 6.0, 4.0 Hz, (-CH_2-)), 3.92 (dd, 2H, ^3J = 6.0, 4.0 Hz, (-CH_2-)), 3.78 (ddd, 1H, ^2J = 10.7 Hz, ^3J = 7.1, 3.4 Hz, H_f-C), 3.62–3.56 (m, 1H, H_e-C), 3.46–3.39 (m, 1H, H_e-C), 2.83 (s, 6H, 2 × (-CH_3)), 1.80–1.64 (m, 2H, H_b-C, H_c-C), 1.59–1.45 (m, 4H, H_b-C, H_c-C, (-CH_2-)). ^{13}C-NMR (126 MHz, $CDCl_3$) δ (ppm): 154.6, 152.1, 151.1, 147.3, 146.0, 145.9, 144.7, 123.3, 122.6, 115.8, 114.8, 99.3, 69.4, 68.2, 65.2, 64.8, 62.6, 44.4, 41.8, 30.5, 25.2, 19.4. HRMS (ESI) m/z: $[M + H]^+$ Calculated for $C_{25}H_{33}N_8O_4$ 509.2619; Found 509.2624 (0.98 ppm).

3.2.11. 2-Bromo-*N*,*N*-Dimethyl-4-{2-[(1-(9-{2-[(Tetrahydro-2*H*-pyran-2-yl)oxy]ethyl}-9*H*-purin-6-yl)-1*H*-1,2,3-triazol-4-yl)methoxy]ethoxy}aniline (**25**)

To a solution of **24** (100 mg, 0.2 mmol, 1.0 eq.) in $CHCl_3$ (3 mL) at 0 °C NBS (37 mg, 0.21 mmol, 1.05 eq.) was slowly added. The reaction mixture was left to stir for 1 h at 0 °C, then diluted with $CHCl_3$ to 20 mL in total, washed with water (3 × 50 mL) and brine (20 mL), then evaporated and dried in a vacuum. Silica gel column chromatography (DCM/EtOH, gradient 0% → 10%) provided product **25** (yield: 68 mg, 59%) as a brown oil. R_f = 0.85 (DCM/EtOH = 10:1). HPLC: t_R = 5.37 min, eluent E_2. IR (KBr) ν (cm^{-1}): 2940, 2867, 1604, 1575, 1331, 1223, 1122, 1031, 991, 850. ^{1}H-NMR (500 MHz, $CDCl_3$) δ (ppm): 9.14 (s, 1H, H-C(triazole)), 8.94 (s, 1H, H-C(2)), 8.42 (s, 1H, H-C(8)), 7.20 (d, 1H, ^4J = 2.8 Hz, H-C(Ar)), 7.02 (d, 1H, ^3J = 8.9 Hz, H-C(Ar)), 6.85 (dd, 1H, ^3J = 8.9 Hz, ^4J = 2.8 Hz, H-C(Ar)), 4.91 (s, 2H, (-CH_2-)), 4.66–4.51 (m, 3H, H_a-C, (-CH_2-)), 4.17–4.13 (m, 1H, H_f-C), 4.12 (dd, 2H, ^3J = 5.7, 3.6 Hz, (-CH_2-)), 3.94 (dd, 2H, ^3J = 5.7, 3.6 Hz, (-CH_2-)), 3.79 (ddd, 1H, ^2J = 10.7 Hz, ^3J = 7.1, 3.3 Hz, H_f-C), 3.65–3.58 (m, 1H, H_e-C), 3.47–3.40 (m, 1H, H_e-C), 2.71 (s, 6H, 2 × (-CH_3)), 1.81–1.69 (m, 2H, H_b-C, H_c-C), 1.59–1.44 (m, 4H, H_b-C, H_c-C, (-CH_2-)). ^{13}C-NMR (126 MHz, $CDCl_3$) δ (ppm): 155.1, 154.6, 152.2, 147.4, 145.9, 145.7, 144.8, 123.3, 122.6, 121.1, 120.2, 115.9, 114.3, 99.4, 69.1, 68.1, 65.3, 64.8, 62.7, 44.9, 44.4, 30.5, 25.3, 19.5. HRMS (ESI) m/z: $[M + H]^+$ Calculated for $C_{25}H_{32}BrN_8O_4$ 587.1724; Found 587.1707 (2.90 ppm).

3.2.12. 6-Chloro-8-iodo-9-{2-[(Tetrahydro-2*H*-pyran-2-yl)oxy]ethyl}-9*H*-purine (**26**)

To dry, degassed THF (96 mL) at −78 °C DIPEA (3.71 mL, ρ = 0.72 g/cm^3, 26.31 mmol, 1.55 eq.) and *n*-BuLi (10.38 mL, 2.29 M, 23.77 mmol, 1.4 eq.) were added and left to stir for 30 min at −78 °C. Compound **22** (4.8 g, 16.98 mmol, 1.0 eq.) was dissolved in dry, degassed THF (48 mL), slowly added to the solution of LDA at −78 °C, and left to stir for 1 h at that temperature. I_2 (21.5 g, 84.89 mmol, 5.0 eq.) was dissolved in dry, degassed THF (20 mL) and slowly added to the reaction mixture until it became solid. Then, the reaction was warmed up to room temperature, and saturated aqueous $Na_2S_2O_3{\cdot}5H_2O$ solution was added until the aqueous phase became colorless. The reaction mixture was washed with EtOAc (3 × 150 mL), and the combined organic phase was washed with brine (100 mL) and dried over anhydrous Na_2SO_4, filtered, and evaporated. Silica gel column chromatography (DCM/EtOH, gradient 0% → 5%) provided product **26** (yield: 6.34 g, 91%) as a pale brown amorphous solid. R_f = 0.65 (DCM/EtOH = 20:1). HPLC: t_R = 4.66 min, eluent E_1. IR (KBr)

ν (cm^{-1}): 2940, 2865, 1587, 1558, 1454, 1321, 1150, 1123, 1068, 1037, 948, 866. ^{1}H-NMR (500 MHz, $CDCl_3$) δ (ppm): 8.65 (s, 1H, H-C(2)), 4.58–4.41 (m, 3H, H_a-C, (-CH_2-)), 4.10 (ddd, 1H, ^2J = 11.1 Hz, ^3J = 6.8, 4.5 Hz, H_f-C), 3.81 (ddd, 1H, ^2J = 11.1 Hz, ^3J = 6.8, 4.5 Hz, H_f-C), 3.48 (td, 1H, ^2J = 11.4 Hz, ^3J = 3.3 Hz, H_e-C), 3.41–3.34 (m, 1H, H_e-C), 1.73–1.57 (m, 2H, H_b-C, H_c-C), 1.54–1.40 (m, 4H, H_b-C, H_c-C, (-CH_2-)). ^{13}C-NMR (126 MHz, $CDCl_3$) δ (ppm): 153.1, 151.9, 149.3, 134.0, 109.1, 98.5, 64.3, 62.0, 46.6, 30.2, 25.3, 19.0. HRMS (ESI) m/z: [M + H]$^+$ Calculated for $C_{12}H_{15}ClIN_4O_2$ 408.9923; Found 408.9913 (2.45 ppm).

3.2.13. 4-(6-Chloro-9-{2-[(Tetrahydro-2*H*-pyran-2-yl)oxy]ethyl}-9*H*-purin-8-yl)-*N*,*N*-Dimethylaniline (**27**)

In the pressure flask a solution of compound **26** (825 mg, 2.02 mmol, 1.0 eq.), *N*,*N*-dimethyl-4-(tributylstannyl)aniline [68] (911 mg, 2.22 mmol, 1.1 eq.) and $Pd(PPh_3)_4$ (116 mg, 0.1 mmol, 0.05 eq.) in dry toluene (25 mL) was stirred at 110 °C for 16 h. Then, it was evaporated and dried in a vacuum. Silica gel column chromatography (DCM/EtOH, gradient 0% → 25%) provided product **27** (yield: 420 mg, 52%) as a pale orange amorphous solid. R_f = 0.60 (DCM/EtOH = 20:1). HPLC: t_R = 5.89 min, eluent E_1. IR (KBr) ν (cm^{-1}): 2930, 2863, 1609, 1479, 1365, 1343, 1125, 1037, 978, 948, 819. ^{1}H-NMR (500 MHz, $CDCl_3$) δ (ppm): 8.67 (s, 1H, H-C(2)), 7.91 (d, 2H, ^3J = 8.6 Hz, 2 × H-C(Ar)), 6.78 (d, 2H, ^3J = 8.6 Hz, 2 × H-C(Ar)), 4.65–4.55 (m, 2H, (-CH_2-)), 4.53–4.48 (m, 1H, H_a-C), 4.26–4.16 (m, 1H, H_f-C), 4.00–3.90 (m, 1H, H_f-C), 3.56–3.47 (m, 1H, H_e-C), 3.43–3.35 (m, 1H, H_e-C), 3.07 (s, 6H, 2 × (-CH_3)), 1.75–1.59 (m, 2H, H_b-C, H_c-C), 1.55–1.40 (m, 4H, H_b-C, H_c-C, (-CH_2-)). ^{13}C-NMR (126 MHz, $CDCl_3$) δ (ppm): 157.8, 154.3, 152.0, 150.8, 148.7, 131.8, 131.2, 115.6, 111.8, 98.8, 64.7, 62.0, 44.7, 40.3, 30.3, 25.3, 19.2. HRMS (ESI) m/z: [M + H]$^+$ Calculated for $C_{20}H_{25}ClN_5O_2$ 402.1691; Found 402.1685 (1.49 ppm).

3.2.14. 4-(6-Azido-9-{2-[(Tetrahydro-2*H*-pyran-2-yl)oxy]ethyl}-9*H*-purin-8-yl)-*N*,*N*-Dimethylaniline (**28**)

To a solution of **27** (2.84 g, 7.07 mmol, 1.0 eq.) in DMF (140 mL) NaN_3 (1.40 g, 21.22 mmol, 3.0 eq.) was added and the reaction mixture was stirred at 60 °C for 16 h. Then, the reaction mixture was poured into cold water (1 L), and the precipitate was filtered and washed with water (0.5 L), providing compound **28** (yield: 2.69 g, 93%) as a pale pink amorphous solid. HPLC: t_R = 4.66 min, eluent E_1. IR (KBr) ν (cm^{-1}): 2939, 2886, 2025, 1608, 1478, 1344, 1202, 1126, 1073, 977, 874, 821. ^{1}H-NMR (500 MHz, DMSO-d_6) δ (ppm): 10.08 (s, 1H, H-C(2)), 7.86 (d, 2H, ^3J = 8.7 Hz, 2 × H-C(Ar)), 6.86 (d, 2H, ^3J = 8.7 Hz, 2 × H-C(Ar)), 4.48–4.45 (m, 2H, (-CH_2-)), 4.48–4.43 (m, 1H, H_a-C), 4.06 (ddd, 1H, ^2J = 11.2 Hz, ^3J = 6.7, 4.7 Hz, H_f-C), 3.86 (ddd, 1H, ^2J = 11.2 Hz, ^3J = 6.7, 4.7 Hz, H_f-C), 3.35–3.30 (m, 1H, H_e-C), 3.26–3.22 (m, 1H, H_e-C), 3.02 (s, 6H, 2 × (-CH_3)), 1.47–1.40 (m, 2H, H_b-C, H_c-C), 1.37–1.24 (m, 4H, H_b-C, H_c-C, (-CH_2-)). ^{13}C-NMR (126 MHz, DMSO-d_6) δ (ppm): 154.6, 151.4, 144.9, 144.0, 134.4, 130.3, 119.6, 115.6, 111.6, 97.5, 64.2, 60.8, 44.7, 39.72, 29.7, 24.7, 18.6. HRMS (ESI) m/z: [M + H]$^+$ Calculated for $C_{20}H_{25}N_8O_2$ 409.2095; Found 409.2097 (0.49 ppm).

3.2.15. 4-[6-(4-({2-[4-(Dimethylamino)phenoxy]ethoxy)methyl}-1*H*-1,2,3-triazol-1-yl)-9-{2-[(Tetrahydro-2*H*-pyran-2-yl)oxy]ethyl}-9*H*-purin-8-yl]-*N*,*N*-Dimethylaniline (**29**)

Prepared according to general method A: Compound **28** (500 mg, 1.22 mmol, 1.0 eq.), CuI (40 mg, 0.20 mmol, 0.16 eq.), AcOH (77 µL, ρ = 1.05 g/cm^3, 1.35 mmol, 1.1 eq.), Et_3N (187 µL, ρ = 0.73 g/cm^3, 1.35 mmol, 1.1 eq.) and *N*,*N*-dimethyl-4-(2-(prop-2-yn-1-yloxy)ethoxy)aniline (540 mg, 2.45 mmol, 2.0 eq.), DCM (20 mL), 25 °C, 16 h. Silica gel column chromatography (DCM/EtOH, gradient 0% → 3%) provided product **29** (yield: 420 mg, 55%) as a brown amorphous solid. R_f = 0.43 (DCM/EtOH = 20:1). HPLC: t_R = 4.15 min, eluent E_1. IR (KBr) ν (cm^{-1}): 2923, 2855, 1606, 1512, 1457, 1338, 1243, 1118, 1032, 816, 797. ^{1}H-NMR (500 MHz, $CDCl_3$) δ (ppm): 9.40 (s, 1H, H-C(triazole)), 8.88 (s,

1H, H-C(2)), 7.96 (d, 2H, ^3J = 8.6 Hz, 2 × H-C(Ar)), 6.85 (d, 2H, ^3J = 8.6 Hz, 2 × H-C(Ar)), 6.78 (d, 2H, ^3J = 8.6 Hz, 2 × H-C(Ar)), 6.67 (d, 2H, ^3J = 8.6 Hz, 2 × H-C(Ar)), 4.91 (s, 2H, (-CH_2-)), 4.72–4.62 (m, 2H, (-CH_2-)), 4.54–4.49 (m, 1H, H_a-C), 4.25 (ddd, 1H, ^2J = 11.0 Hz, ^3J = 5.6, 5.2 Hz, H_f-C), 4.10 (t, 2H, ^3J = 4.7 Hz, (-CH_2-)), 3.98 (ddd, 1H, ^2J = 11.0 Hz, ^3J = 5.6, 5.2 Hz, H_f-C), 3.92(t, 2H, ^3J = 4.7 Hz, (-CH_2-)), 3.55–3.48 (m, 1H, H_e-C), 3.40–3.34 (m, 1H, H_e-C), 3.07 (s, 6H, 2 × (-CH_3)), 2.82 (s, 6H, 2 × (-CH_3)), 1.64–1.54 (m, 2H, H_b-C, H_c-C), 1.51–1.36 (m, 4H, H_b-C, H_c-C, (-CH_2-)). ^{13}C NMR (126 MHz, $CDCl_3$) δ 158.4, 157.0, 152.1, 151.1, 151.0, 146.0, 145.8, 142.9, 131.2, 124.5, 122.8, 115.8, 115.5, 114.8, 111.7, 98.8, 69.1, 68.2, 64.68, 64.67, 62.0, 44.7, 41.8, 40.2, 30.3, 25.3, 19.1. HRMS (ESI) m/z: $[M + H]^+$ Calculated for $C_{33}H_{42}N_9O_4$ 628.3354; Found 628.3383 (4.62 ppm).

3.2.16. 2-{6-[4-({2-[4-(Dimethylamino)phenoxy]ethoxy}methyl)-1*H*-1,2,3-triazol-1-yl]-8-[4-(Dimethylamino)phenyl]-9*H*-purin-9-yl}ethan-1-ol (**30**)

To the mixture of compound **29** (815 mg, 1.30 mmol, 1.0 eq.) in 52 mL of MeOH/H_2O/DCM mixture (10:2:1) TFA (0.99 mL, ρ = 1.49 g/cm^3, 13.0 mmol, 10.0 eq.) was added at 25 °C. Then, the reaction was left stirring for 2 h, evaporated, dissolved in DCM (10 mL), and washed with aqueous $NaHCO_3$ solution (10 mL) and brine (10 mL). The organic phase was dried over anhydrous Na_2SO_4, filtered, and evaporated, providing product **30** (yield: 689 mg, 98%) as a dark yellow amorphous solid. R_f = 0.68 (DCM/EtOH = 10:1). HPLC: t_R = 6.32 min, eluent E_2. IR (KBr) ν (cm^{-1}): 3339, 2873, 1606, 1513, 1483, 1338, 1229, 1200, 1033, 950, 819. ^{1}H-NMR (500 MHz, $CDCl_3$) δ (ppm): 9.28 (s, 1H, H-C(triazole)), 8.78 (s, 1H, H-C(2)), 7.81 (d, 2H, ^3J = 8.8 Hz, 2 × H-C(Ar)), 6.85 (d, 2H, ^3J = 8.6 Hz, 2 × H-C(Ar)), 6.75 (d, 2H, ^3J = 8.8 Hz, 2 × H-C(Ar)), 6.68 (d, 2H, ^3J = 8.6 Hz, 2 × H-C(Ar)), 4.89 (s, 2H, (-CH_2-)), 4.55 (t, 2H, ^3J = 5.0 Hz, (-CH_2-)), 4.22 (t, 2H, ^3J = 5.0 Hz, (-CH_2-)), 4.10 (t, 2H, ^3J = 4.7 Hz, (-CH_2-)), 3.92 (t, 2H, ^3J = 4.7 Hz, (-CH_2-)), 3.06 (s, 6H, 2 × (-CH_3)), 2.82 (s, 6H, 2 × (-CH_3)). ^{13}C-NMR (126 MHz, $CDCl_3$) δ (ppm): 158.6, 156.8, 152.1, 151.3, 150.6, 146.0, 145.9, 142.7, 131.4, 124.2, 122.7, 115.8, 115.0, 114.9, 111.8, 69.3, 68.2, 64.7, 61.2, 48.2, 42.0, 40.2. HRMS (ESI) m/z: $[M + H]^+$ Calculated for $C_{28}H_{34}N_9O_3$ 544.2779; Found 544.2805 (4.78 ppm).

3.2.17. 2-{6-[4-({2-[4-(Dimethylamino)phenoxy]ethoxy}methyl)-1*H*-1,2,3-triazol-1-yl]-8-[4-(Dimethylamino)phenyl]-9*H*-purin-9-yl}ethyl Methanesulfonate (**31**)

To a solution of compound **30** (689 mg, 1.27 mmol, 1.0 eq.) in DCM (5 mL), Et_3N (176 μL, ρ = 0.73 g/cm^3, 1.27 mmol, 1.0 eq.) was added. The reaction mixture was cooled to 0 °C. MsCl (0.11 mL, ρ = 1.48 g/cm^3, 1.46 mmol, 1.15 eq.) was slowly added dropwise to the reaction mixture, and it was left to stir for 1 h at 25 °C. Then, the reaction mixture was washed with H_2O (2 × 10 mL) and brine (10 mL). The organic phase was dried over anhydrous Na_2SO_4, filtered, and poured in cold hexane (200 mL). The resulting precipitate was filtered, providing product **31** (yield: 772 mg, 98%) as a dark orange amorphous solid. HPLC: t_R = 5.34 min, eluent E_2. IR (KBr) ν (cm^{-1}): 2929, 2868, 1608, 1514, 1477, 1339, 1221, 1170, 1038, 898, 810. ^{1}H-NMR (500 MHz, $CDCl_3$) δ (ppm): 9.34 (s, 1H, H-C(triazole)), 8.86 (s, 1H, H-C(2)), 7.76 (d, 2H, ^3J = 8.4 Hz, 2 × H-C(Ar)), 6.86 (d, 2H, ^3J = 8.8 Hz, 2 × H-C(Ar)), 6.82 (d, 2H, ^3J = 8.8 Hz, 2 × H-C(Ar)), 6.77 (d, 2H, ^3J = 8.4 Hz, 2 × H-C(Ar)), 4.89 (s, 2H, (-CH_2-)), 4.84–4.77 (m, 2H, (-CH_2-)), 4.74–4.68 (m, 2H, (-CH_2-)), 4.15–4.07 (m, 2H, (-CH_2-)), 3.95–4.89 (m, 2H, (-CH_2-)), 3.06 (s, 6H, 2 × (-CH_3)), 2.87 (s, 6H, 2 × (-CH_3)), 2.84 (s, 3H, (-CH_3)). ^{13}C NMR (126 MHz, $CDCl_3$) δ (ppm): 157.9, 156.8, 152.7, 152.2, 151.2, 145.8, 144.1, 143.1, 130.8, 124.4, 122.8, 116.1, 115.9, 114.6, 111.9, 69.1, 68.1, 65.6, 64.6, 43.8, 42.8, 40.2, 37.6. HRMS (ESI) m/z: $[M + H]^+$ Calculated for $C_{29}H_{36}N_9O_5S$ 622.2555; Found 625.2549 (0.94 ppm).

3.2.18. 4-(6-(4-((2-(4-(Dimethylamino)phenoxy)ethoxy)methyl)-1*H*-1,2,3-triazol-1-yl)-9-(2-(4,7,10-trimethyl-1,4,7,10-tetraazacyclododecan-1-yl)ethyl)-9*H*-purin-8-yl)-*N*,*N*-Dimethylaniline (**1**)

A suspension of compound **31** (770 mg, 1.24 mmol, 1.0 eq.) and LiBr (215 mg, 2.48 mmol, 2.0 eq.) in THF (16 mL) was stirred in a pressure flask at 70 °C for 3 h. Then, the reaction mixture was evaporated, suspended in DCM (10 mL), and washed with water (2 × 10 mL) and brine (10 mL). The organic phase was dried over anhydrous Na_2SO_4, filtered, and evaporated. 1,4,7-Trimethyl-1,4,7,10-tetraazacyclododecane [75] (2.66 g, 12.4 mmol, 10 eq.) was added to the precipitate, and this mixture was dissolved in abs. MeCN (60 mL) and left to stir for 72 h at 25 °C. Silica gel column chromatography (DCM/EtOH, gradient 0% → 5%) provided by-product **32** (yield: 370 mg, 57%) as a yellow amorphous solid. Reverse phase silica gel column chromatography ($MeOH/H_2O$, gradient 0% → 70%) with the following preparative HPLC column chromatography (that used TFA as an additive) was used to separate impurities from the product. Then, it was dissolved in DCM (10 mL), washed with sat. aqueous $NaHCO_3$ solution (10 mL) and brine (10 mL), and evaporated. Next, it was dissolved in water (10 mL), filtered, and lyophilized, providing product **1** (yield: 56 mg, 6%) as a yellow amorphous solid. R_f = 0.1 (DCM/EtOH = 20:1). HPLC: t_R = 4.38 min, eluent E_2. IR (KBr) ν(cm^{-1}): 2924, 2852, 1667, 1607, 1585, 1464, 1338, 1259, 1066, 1033, 796. ^{1}H-NMR (500 MHz, $CDCl_3$) δ 9.41 (ppm) (s, 1H, H-C(triazole)), 8.89 (s, 1H, H-C(2)), 7.83 (d, 2H, ^3J = 8.8 Hz, 2 × H-C(Ar)), 6.86 (d, 2H, ^3J = 9.0 Hz, 2 × H-C(Ar)), 6.80 (d, 2H, ^3J = 8.8 Hz, 2 × H-C(Ar)), 6.67 (d, 2H, ^3J = 9.0 Hz, 2 × H-C(Ar)), 4.92 (s, 2H, (-CH_2-)), 4.59 (t, 2H, ^3J = 6.8 Hz, (-CH_2-)), 4.11 (t, 2H, ^3J = 4.8 Hz, (-CH_2-)), 3.92 (t, 2H, ^3J = 4.8 Hz, (-CH_2-)), 3.07 (s, 6H, 2 × (CH_3)), 2.82 (s, 6H, 2 × (CH_3)), 2.77 (t, 2H, ^3J = 6.8 Hz, (-CH_2-)), 2.65–2.61 (m, 4H, 2 × (-CH_2-)), 2.32–2.26 (m, 12H, 6 × (-CH_2-)), 2.16 (s, 3H, (-CH_3)), 2.11 (s, 6H, 2 × (-CH_3)). ^{1}H-NMR (500 MHz, MeCN-d_3) δ 9.27 (ppm) (s, 1H, H(1)), 8.84 (s, 1H, H(2)), 7.85 (d, 2H, ^3J = 8.6 Hz, 2 × H(3)), 6.88 (d, 2H, ^3J = 8.6 Hz, 2 × H(4)), 6.81 (d, 2H, ^3J = 9.1 Hz, 2 × H(5)), 6.66 (d, 2H, ^3J = 9.1 Hz, 2 × H(6)), 4.81 (s, 2H, 2 × H(7)), 4.61 (t, 2H, ^3J = 6.6 Hz, 2 × H(8)), 4.07 (t, 2H, ^3J = 4.6 Hz, 2 × H(9)), 3.86 (t, 2H, ^3J = 4.6 Hz, 2 × H(10)), 3.05 (s, 6H, 6 × H(11)), 2.86–2.74 (m, 8H, 6 × H(12), 2 × H(13)), 2.58 – 2.51 (m, 4H, 4 × H(14)), 2.46 – 2.17 (m, 21H, 12 × H(15), 9 × H(16)). ^{13}C NMR (126 MHz, $CDCl_3$) δ (ppm): 157.8, 157.2, 152.1, 151.13, 151.03, 146.0, 145.8, 142.9, 130.7, 124.6, 122.7, 115.9, 115.8, 114.8, 111.9, 69.1, 68.2, 64.7, 56.4, 55.79, 55.75, 54.6, 53.4, 45.0, 44.4, 42.9, 41.8, 40.2. HRMS (ESI) m/z: $[M + H]^+$ Calculated for $C_{39}H_{58}N_{13}O_2$ 740.4831; Found 740.4846 (2.03 ppm).

3.2.19. 4-(6-(4-((2-(4-(Dimethylamino)phenoxy)ethoxy)methyl)-1*H*-1,2,3-triazol-1-yl)-9-vinyl-9*H*-purin-8-yl)-*N*,*N*-Dimethylaniline (**32**)

R_f = 0.61 (DCM/EtOH = 20:1). HPLC: t_R = 6.21 min, eluent E_2. IR (KBr) ν (cm^{-1}): 2925, 2865, 1606, 1480, 1342, 1199, 1124, 1036, 1023, 946, 819. ^{1}H NMR (500 MHz, $CDCl_3$) δ 9.39 (s, 1H, H-C(triazole)), 8.95 (s, 1H, H-C(2)), 7.84 (d, 2H, ^3J = 8.6 Hz, 2 × H-C(Ar)), 7.07 (dd, 1H, ^3J = 15.8, 8.9 Hz, (-CH_a)), 6.86 (d, 2H, ^3J = 8.6 Hz, 2 × H-C(Ar)), 6.81 (d, 2H, ^3J = 8.6 Hz, 2 × H-C(Ar)), 6.68 (d, 2H, ^3J = 8.6 Hz, 2 × H-C(Ar)), 6.43 (d, 1H, ^2J = 15.8 Hz, (-CH_b)), 5.51 (d, 1H, ^3J = 8.9 Hz, (-CH_c)), 4.93 (s, 2H, (-CH_2-)), 4.12 (t, 2H, ^3J = 4.8 Hz, (-CH_2-)), 3.94 (t, 2H, ^3J = 4.8 Hz, (-CH_2-)), 3.09 (s, 6H, 2 × (-CH_3)), 2.83 (s, 6H, 2 × (-CH_3)). ^{13}C NMR (126 MHz, $CDCl_3$) δ (ppm): 156.8, 156.2, 152.3, 151.5, 151.1, 146.0, 145.9, 143.2, 131.6, 128.4, 124.5, 123.4, 115.9, 114.8, 114.7, 111.7, 110.9, 69.2, 68.3, 64.7, 41.8, 40.2. HRMS (ESI) m/z: $[M + H]^+$ Calculated for $C_{28}H_{32}N_9O_2$ 526.2673; Found 526.2688 (2.85 ppm).

4. Conclusions

We have developed a new synthetic approach toward the proposed purine–cyclen conjugate using the sequence of modifications, which includes Mitsunobu, iodination, Stille, S_NAr, CuAAC, and alkylation reactions as main transformations. The optimal sequence

of derivatization (positions: *N*9 → *C*8 → *C*6 → *N*9) was found as the result of several less successful attempts toward the target compound. Purine–cyclen conjugate was obtained in nine steps, starting from commercially available 6-chloropurine. As the main by-product, the *N*9-vinyl group containing purine–triazole conjugate was obtained, which was formed via the E2 type reaction mechanism between purine alkyl bromide derivative and modified cyclen moiety. Preliminary NMR and UV titration experiments revealed that target purine–cyclen conjugate easily complexes copper(II) ions in the cyclen ring and between triazole *N*2 and purine *N*7 positions. Photophysical and photocatalytic properties of the developed purine–cyclen derivatives will be studied in the future and will be reported elsewhere.

Supplementary Materials: The following supporting information can be downloaded at: https://www.mdpi.com/article/10.3390/molecules30071612/s1, ^{1}H- and ^{13}C-NMR spectra of compounds **1**, **3**, **11**, **13**, **15**, **22**–**32**; NMR titration procedure and stacked spectra for the titration experiments of compound **1**.

Author Contributions: Synthetic experiments, investigation, methodology, and manuscript draft, A.B.; conceptualization, the idea of the purine–cyclen conjugate, spectrophotometric analysis, and manuscript review, G.J.; conceptualization, supervision, and manuscript review, I.N. and M.T. All authors have read and agreed to the published version of the manuscript.

Funding: The authors acknowledge the financial support provided by the Latvia–Lithuania–Taiwan joint grant #LV-LT-TW/2022/9 "Molecular Electronics in Functionalized Purines: Fundamental Study and Applications (MEPS)" from the Latvian Council of Science. I.N. and G.J. acknowledge the PHC Osmosis program project (#50602NB for France, #LV-FR/2024/5 for Latvia) "Purine-based carbenes: synthesis, photophysical and optical studies (PBC)" for financial support of scientific exchanges.

Institutional Review Board Statement: Not applicable.

Informed Consent Statement: Not applicable.

Data Availability Statement: The original contributions presented in this study are included in the article/Supplementary Materials. Further inquiries can be directed to the corresponding authors.

Conflicts of Interest: The authors declare no conflicts of interest.

References

1. Müller, C.E.; Thorand, M.; Qurishi, R.; Diekmann, M.; Jacobson, K.A.; Padgett, W.L.; Daly, J.W. Imidazo[2,1-*i*]Purin-5-Ones and Related Tricyclic Water-Soluble Purine Derivatives: Potent A_{2A}- and A_3-Adenosine Receptor Antagoniststs. *J. Med. Chem.* **2002**, *45*, 3440–3450. [CrossRef] [PubMed]
2. Al Jaroudi, W.; Iskandrian, A.E. Regadenoson: A New Myocardial Stress Agent. *J. Am. Coll. Cardiol.* **2009**, *54*, 1123–1130. [CrossRef] [PubMed]
3. Shelton, J.; Lu, X.; Hollenbaugh, J.A.; Cho, J.H.; Amblard, F.; Schinazi, R.F. Metabolism, Biochemical Actions, and Chemical Synthesis of Anticancer Nucleosides, Nucleotides, and Base Analogs. *Chem. Rev.* **2016**, *116*, 14379–14455. [CrossRef] [PubMed]
4. Parker, W.B. Enzymology of Purine and Pyrimidine Antimetabolites Used in the Treatment of Cancer. *Chem. Rev.* **2009**, *109*, 2880–2893. [CrossRef]
5. Xu, W.; Chan, K.M.; Kool, E.T. Fluorescent Nucleobases as Tools for Studying DNA and RNA. *Nat. Chem.* **2017**, *9*, 1043–1055. [CrossRef]
6. Sinkeldam, R.W.; Greco, N.J.; Tor, Y. Fluorescent Analogs of Biomolecular Building Blocks: Design, Properties, and Applications. *Chem. Rev.* **2010**, *110*, 2579–2619. [CrossRef]
7. Dumas, A.; Luedtke, N.W. Site-Specific Control of *N*7-Metal Coordination in DNA by a Fluorescent Purine Derivative. *Chem.-A Eur. J.* **2012**, *18*, 245–254. [CrossRef]
8. Omumi, A.; McLaughlin, C.K.; Ben-Israel, D.; Manderville, R.A. Application of a Fluorescent C-Linked Phenolic Purine Adduct for Selective N7-Metalation of DNA. *J. Phys. Chem. B* **2012**, *116*, 6158–6165. [CrossRef]
9. Sun, K.M.; McLaughlin, C.K.; Lantero, D.R.; Manderville, R.A. Biomarkers for Phenol Carcinogen Exposure Act as pH-Sensing Fluorescent Probes. *J. Am. Chem. Soc.* **2007**, *129*, 1894–1895. [CrossRef]
10. Venkatesh, V.; Shukla, A.; Sivakumar, S.; Verma, S. Purine-Stabilized Green Fluorescent Gold Nanoclusters for Cell Nuclei Imaging Applications. *ACS Appl. Mater. Interfaces* **2014**, *6*, 2185–2191. [CrossRef]

11. Li, J.; Zhang, Y.; Zhang, H.; Xuan, X.; Xie, M.; Xia, S.; Qu, G.; Guo, H. Nucleoside-Based Ultrasensitive Fluorescent Probe for the Dual-Mode Imaging of Microviscosity in Living Cells. *Anal. Chem.* **2016**, *88*, 5554–5560. [CrossRef] [PubMed]
12. Wang, Z.; Yao, J.; Zhan, L.; Gong, S.; Ma, D.; Yang, C. Purine-Based Thermally Activated Delayed Fluorescence Emitters for Efficient Organic Light-Emitting Diodes. *Dye. Pigment.* **2020**, *180*, 108437. [CrossRef]
13. Kong, B.; Joshi, T.; Belousoff, M.J.; Tor, Y.; Graham, B.; Spiccia, L. Neomycin B-Cyclen Conjugates and Their Zn(II) Complexes as RNA-Binding Agents. *J. Inorg. Biochem.* **2016**, *162*, 334–342. [CrossRef]
14. Abdollahi, M.; Hosseini, A. Hydrogen Sulfide. In *Encyclopedia of Toxicology*, 3rd ed.; Wexler, P., Ed.; Elsevier: Amsterdam, The Netherlands, 2014; pp. 971–974, ISBN 9780123864550.
15. Lima, L.M.P.; Esteban-Gómez, D.; Delgado, R.; Platas-Iglesias, C.; Tripier, R. Monopicolinate Cyclen and Cyclam Derivatives for Stable Copper(II) Complexation. *Inorg. Chem.* **2012**, *51*, 6916–6927. [CrossRef]
16. Delgado, R.; Félix, V.; Lima, L.M.P.; Price, D.W. Metal Complexes of Cyclen and Cyclam Derivatives Useful for Medical Applications: A Discussion Based on Thermodynamic Stability Constants and Structural Data. *Dalt. Trans.* **2007**, 2734–2745. [CrossRef]
17. Paderni, D.; Voccia, M.; Macedi, E.; Formica, M.; Giorgi, L.; Caporaso, L.; Fusi, V. A Combined Solid State, Solution and DFT Study of a Dimethyl-Cyclen-Pd(II) Complex. *Dalt. Trans.* **2024**, *53*, 14300–14314. [CrossRef]
18. Verma, A.; Bhuvanesh, N.; Reibenspies, J.; Tayade, S.B.; Kumbhar, A.S.; Bretosh, K.; Sutter, J.P.; Sunkari, S.S. Structurally Characterised New Twisted Conformer for Cyclen, Controlled by Metal Ion Complexation as Seen in Ni^{II} and Cu^{II} complexes with Halides and Pseudohalides. *CrystEngComm* **2022**, *24*, 119–131. [CrossRef]
19. Harmand, L.; Cadet, S.; Kauffmann, B.; Scarpantonio, L.; Batat, P.; Jonusauskas, G.; McClenaghan, N.D.; Lastécouères, D.; Vincent, J.M. Copper Catalyst Activation Driven by Photoinduced Electron Transfer: A Prototype Photolatent Click Catalyst. *Angew. Chemie-Int. Ed.* **2012**, *51*, 7137–7141. [CrossRef]
20. Zaķis, J.M.; Ozols, K.; Novosjolova, I.; Vilšķērsts, R.; Mishnev, A.; Turks, M. Sulfonyl Group Dance: A Tool for the Synthesis of 6-Azido-2-Sulfonylpurine Derivatives. *J. Org. Chem.* **2020**, *85*, 4753–4771. [CrossRef]
21. Frieden, M.; Aviñó, A.; Eritja, R. Convenient Synthesis of 8-Amino-2′-Deoxyadenosine. *Nucleosides Nucleotides Nucleic Acids* **2003**, *22*, 193–202. [CrossRef]
22. Cīrule, D.; Novosjolova, I.; Bizdēna, Ē.; Turks, M. 1,2,3-Triazoles as Leaving Groups: S_NAr Reactions of 2,6-Bistriazolylpurines with O- And C-Nucleophiles. *Beilstein J. Org. Chem.* **2021**, *17*, 410–419. [CrossRef] [PubMed]
23. Guo, H.M.; Xin, P.Y.; Niu, H.Y.; Wang, D.C.; Jiang, Y.; Qu, G.R. Microwave Irradiated C6-Functionalization of 6-Chloropurine Nucleosides with Various Mild Nucleophiles under Solvent-Free Conditions. *Green Chem.* **2010**, *12*, 2131–2134. [CrossRef]
24. Borrmann, T.; Abdelrahman, A.; Volpini, R.; Lambertucci, C.; Alksnis, E.; Gorzalka, S.; Knospe, M.; Schiedel, A.C.; Cristalli, G.; Müller, C.E. Structure-Activity Relationships of Adenine and Deazaadenine Derivatives as Ligands for Adenine Receptors, a New Purinergic Receptor Family. *J. Med. Chem.* **2009**, *52*, 5974–5989. [CrossRef]
25. Singh, B.; Diaz-Gonzalez, R.; Ceballos-Perez, G.; Rojas-Barros, D.I.; Gunaganti, N.; Gillingwater, K.; Martinez-Martinez, M.S.; Manzano, P.; Navarro, M.; Pollastri, M.P. Medicinal Chemistry Optimization of a Diaminopurine Chemotype: Toward a Lead for Trypanosoma Brucei Inhibitors. *J. Med. Chem.* **2020**, *63*, 9912–9927. [CrossRef]
26. Malínková, V.; Řezníčková, E.; Jorda, R.; Gucký, T.; Kryštof, V. Trisubstituted Purine Inhibitors of PDGFRα and Their Antileukemic Activity in the Human Eosinophilic Cell Line EOL-1. *Bioorg. Med. Chem.* **2017**, *25*, 6523–6535. [CrossRef]
27. Novosjolova, I.; Bizdēna, Ē.; Turks, M. Synthesis and Applications of Azolylpurine and Azolylpurine Nucleoside Derivatives. *Eur. J. Org. Chem.* **2015**, *2015*, 3629–3649. [CrossRef]
28. Kurimoto, A.; Ogino, T.; Ichii, S.; Isobe, Y.; Tobe, M.; Ogita, H.; Takaku, H.; Sajiki, H.; Hirota, K.; Kawakami, H. Synthesis and Evaluation of 2-Substituted 8-Hydroxyadenines as Potent Interferon Inducers with Improved Oral Bioavailabilities. *Bioorg. Med. Chem.* **2004**, *12*, 1091–1099. [CrossRef]
29. Buchanan, H.S.; Pauff, S.M.; Kosmidis, T.D.; Taladriz-Sender, A.; Rutherford, O.I.; Hatit, M.Z.C.; Fenner, S.; Watson, A.J.B.; Burley, G.A. Modular, Step-Efficient Palladium-Catalyzed Cross-Coupling Strategy to Access C6-Heteroaryl 2-Aminopurine Ribonucleosides. *Org. Lett.* **2017**, *19*, 3759–3762. [CrossRef]
30. Havelková, M.; Dvořák, D.; Hocek, M. The Suzuki-Miyaura Cross-Coupling Reactions of 2-, 6- or 8-Halopurines with Boronic Acids Leading to 2-, 6- or 8-Aryl- and -Alkenylpurine Derivatives. *Synthesis* **2001**, *11*, 1704–1710. [CrossRef]
31. Strouse, J.J.; Ješelnik, M.; Arterburn, J.B. Applications of Boronic Acids in Selective C-C and C-N Arylation of Purines. *Acta Chim. Slov.* **2005**, *52*, 187–199. [CrossRef]
32. Wang, D.C.; Niu, H.Y.; Qu, G.R.; Liang, L.; Wei, X.J.; Zhang, Y.; Guo, H.M. Nickel-Catalyzed Negishi Cross-Couplings of 6-Chloropurines with Organozinc Halides at Room Temperature. *Org. Biomol. Chem.* **2011**, *9*, 7663–7666. [CrossRef] [PubMed]
33. Prasad, A.S.B.; Stevenson, T.M.; Citineni, J.R.; Nyzam, V.; Knochel, P. Preparation and Reactions of New Zincated Nitrogen-Containing Heterocycles. *Tetrahedron* **1997**, *53*, 7237–7254. [CrossRef]
34. Nolsøe, J.M.J.; Gundersen, L.L.; Rise, F. Regiochemistry in the Pd-Mediated Coupling between 6,8-Dihalopurines and Organometallic Reagents. *Acta Chem. Scand.* **1999**, *53*, 366–372.

35. Gundersen, L.L.; Langli, G.; Rise, F. Regioselective Pd-Mediated Coupling between 2,6-Dichloropurines and Organometallic Reagents. *Tetrahedron Lett.* **1995**, *36*, 1945–1948. [CrossRef]
36. Bag, S.S.; Jana, S.; Kasula, M. Sonogashira Cross-Coupling: Alkyne-Modified Nucleosides and Their Applications. In *Palladium-Catalyzed Modification of Nucleosides, Nucleotides and Oligonucleotides*; Kapdi, A.R., Maiti, D., Sanghvi, Y.S., Eds.; Elsevier: Amsterdam, The Netherlands, 2018; pp. 75–146, ISBN 9780128112922.
37. Ibrahim, N.; Chevot, F.; Legraverend, M. Regioselective Sonogashira Cross-Coupling Reactions of 6-Chloro-2,8-diiodo-9-THP-9*H*-purine with Alkyne Derivatives. *Tetrahedron Lett.* **2011**, *52*, 305–307.
38. Bilbao, N.; Vázquez-González, V.; Aranda, M.T.; González-Rodríguez, D. Synthesis of 5-/8-Halogenated or Ethynylated Lipophilic Nucleobases as Potential Synthetic Intermediates for Supramolecular Chemistry. *Eur. J. Org. Chem.* **2015**, *2015*, 7160–7175. [CrossRef]
39. Hocek, M.; Pohl, R. Regioselectivity in Cross-Coupling Reactions of 2,6,8-Trichloro-9-(Tetrahydropyran-2-Yl)Purine: Synthesis of 2,6,8-Trisubstituted Purine Bases. *Synthesis* **2004**, *36*, 2869–2876. [CrossRef]
40. Hocek, M.; Hocková, D.; Dvořáková, H. Dichotomy in Regioselective Cross-Coupling Reactions of 6,8-Dichloropurines with Phenylboronic Acid and Methylmagnesium Chloride: Synthesis of 6,8-Di-Substituted Purines. *Synthesis* **2004**, *6*, 889–894. [CrossRef]
41. Mahajan, T.R.; Ytre-Arne, M.E.; Strøm-Andersen, P.; Dalhus, B.; Gundersen, L.L. Synthetic Routes to *N*-9 Alkylated 8-Oxoguanines; Weak Inhibitors of the Human DNA Glycosylase OGG1. *Molecules* **2015**, *20*, 15944–15965. [CrossRef]
42. Abdoli, M.; Mirjafary, Z.; Saeidian, H.; Kakanejadifard, A. New Developments in Direct Functionalization of C-H and N-H Bonds of Purine Bases via Metal Catalyzed Cross-Coupling Reactions. *RSC Adv.* **2015**, *5*, 44371–44389. [CrossRef]
43. Mooney, D.T.; Moore, P.R.; Lee, A.L. Direct Minisci-Type C-H Amidation of Purine Bases. *Org. Lett.* **2022**, *24*, 8008–8013. [CrossRef] [PubMed]
44. Larsen, A.F.; Ulven, T. Direct *N*9-Arylation of Purines with Aryl Halide. *Chem. Commun.* **2014**, *50*, 4997–4999. [CrossRef]
45. Chen, S.; Graceffa, R.F.; Boezio, A.A. Direct, Regioselective N-Alkylation of 1,3-Azoles. *Org. Lett.* **2016**, *18*, 16–19. [CrossRef]
46. Tranová, L.; Stýskala, J. Study of the *N*7 Regioselective Glycosylation of 6-Chloropurine and 2,6-Dichloropurine with Tin and Titanium Tetrachloride. *J. Org. Chem.* **2021**, *86*, 13265–13275. [CrossRef]
47. Nevrlka, F.; Bědroň, A.; Valenta, M.; Tranová, L.; Stýskala, J. Study of Direct N^7 Regioselective Tert-Alkylation of 6-Substituted Purines and Their Modification at Position C6 through O, S, N, and C Substituents. *ACS Omega* **2024**, *9*, 17368–17378. [CrossRef]
48. Sebris, A.; Novosjolova, I.; Turks, M. Synthesis of 7-Arylpurines from Substituted Pyrimidines. *Synthesis* **2022**, *54*, 5529–5539. [CrossRef]
49. Bollier, M.; Klupsch, F.; Six, P.; Dubuquoy, L.; Azaroual, N.; Millet, R.; Leleu-Chavain, N. One- or Two-Step Synthesis of *C*-8 and *N*-9 Substituted Purines. *J. Org. Chem.* **2018**, *83*, 422–430. [CrossRef]
50. Dasari, S.; Bernard Tchounwou, P. Cisplatin in Cancer Therapy: Molecular Mechanisms of Action. *Eur. J. Pharmacol.* **2014**, *740*, 364–378. [CrossRef]
51. Taqui Khan, M.; Krishnamoorthy, C.R. Interaction of Metal Ions with Monosubstittuted Purines. *J. Inorg. Nucl. Chem.* **1971**, *33*, 1417–1425. [CrossRef]
52. Gao, S.H.; Xie, M.S.; Wang, H.X.; Niu, H.Y.; Qu, G.R.; Guo, H.M. Highly Selective Detection of Hg^{2+} Ion by Push-Pull-Type Purine Nucleoside-Based Fluorescent Sensor. *Tetrahedron* **2014**, *70*, 4929–4933. [CrossRef]
53. Li, J.P.; Wang, H.X.; Wang, H.X.; Xie, M.S.; Qu, G.R.; Niu, H.Y.; Guo, H.M. Push-Pull-Type Purine Nucleoside-Based Fluorescent Sensors for the Selective Detection of Pd^{2+} in Aqueous Buffer. *Eur. J. Org. Chem.* **2014**, *2014*, 2225–2230. [CrossRef]
54. Chen, X.; Mao, Y.; Wang, A.; Lu, L.; Shao, Q.; Jiang, C.; Lu, H. Synthesis and Application of Purine-Based Fluorescence Probe for Continuous Recognition of Cu^{2+} and Glyphosate. *Spectrochim. Acta-Part A Mol. Biomol. Spectrosc.* **2024**, *304*, 123291. [CrossRef]
55. Tao, X.; Mao, Y.; Alam, S.; Wang, A.; Qi, X.; Zheng, S.; Jiang, C.; Chen, S.Y.; Lu, H. Sensitive Fluorescence Detection of Glyphosate and Glufosinate Ammonium Pesticides by Purine-Hydrazone-Cu^{2+} Complex. *Spectrochim. Acta-Part A Mol. Biomol. Spectrosc.* **2024**, *314*, 124226. [CrossRef]
56. Sadowska, P.; Jankowski, W.; Bregier-Jarzębowska, R.; Pietrzyk, P.; Jastrząb, R. Deciphering the Impact of Nucleosides and Nucleotides on Copper Ion and Dopamine Coordination Dynamics. *Int. J. Mol. Sci.* **2024**, *25*, 9137. [CrossRef]
57. Schino, I.; Cantore, M.; de Candia, M.; Altomare, C.D.; Maria, C.; Barros, J.; Cachatra, V.; Calado, P.; Shimizu, K.; Freitas, A.A.; et al. Exploring Mannosylpurines as Copper Chelators and Cholinesterase Inhibitors with Potential for Alzheimer's Disease. *Pharmaceuticals* **2023**, *16*, 54. [CrossRef]
58. Xu, H.; Chen, W.; Ju, L.; Lu, H. A Purine Based Fluorescent Chemosensor for the Selective and Sole Detection of Al^{3+} and Its Practical Applications in Test Strips and Bio-Imaging. *Spectrochim. Acta-Part A Mol. Biomol. Spectrosc.* **2021**, *247*, 119074. [CrossRef]
59. Jovaisaite, J.; Cīrule, D.; Jeminejs, A.; Novosjolova, I.; Turks, M.; Baronas, P.; Komskis, R.; Tumkevicius, S.; Jonusauskas, G.; Jursenas, S. Proof of Principle of a Purine D-A-D′ Ligand Based Ratiometric Chemical Sensor Harnessing Complexation Induced Intermolecular PET. *Phys. Chem. Chem. Phys.* **2020**, *22*, 26502–26508. [CrossRef]

60. Tomczyk, M.D.; Kuźnik, N.; Walczak, K. Cyclen-Based Artificial Nucleases: Three Decades of Development (1989–2022). Part a–Hydrolysis of Phosphate Esters. *Coord. Chem. Rev.* **2023**, *481*, 215047. [CrossRef]
61. Gałęzowska, J.; Boratyński, P.J.; Kowalczyk, R.; Lipke, K.; Czapor-Irzabek, H. Copper(II) Complexes of Chiral 1,2,3-Triazole Biheterocyclic 'Click' Ligands Equipped in Cinchona Alkaloid Moiety. *Polyhedron* **2017**, *121*, 1–8. [CrossRef]
62. Cheney, G.E.; Freiser, H.; Fernando, Q.; Freiser, H. Metal Complexes of Purine and Some of Its Derivatives. *J. Am. Chem. Soc.* **1959**, *81*, 2611–2615. [CrossRef]
63. Petrenko, Y.P.; Piasta, K.; Khomenko, D.M.; Doroshchuk, R.O.; Shova, S.; Novitchi, G.; Toporivska, Y.; Gumienna-Kontecka, E.; Martins, L.M.D.R.S.; Lampeka, R.D. An Investigation of Two Copper(II) Complexes with a Triazole Derivative as a Ligand: Magnetic and Catalytic Properties. *RSC Adv.* **2021**, *11*, 23442–23449. [CrossRef] [PubMed]
64. Pérez-Toro, I.; Domínguez-Martín, A.; Choquesillo-Lazarte, D.; Vílchez-Rodríguez, E.; González-Pérez, J.M.; Castiñeiras, A.; Niclós-Gutiérrez, J. Lights and Shadows in the Challenge of Binding Acyclovir, a Synthetic Purine-like Nucleoside with Antiviral Activity, at an Apical-Distal Coordination Site in Copper(II)-Polyamine Chelates. *J. Inorg. Biochem.* **2015**, *148*, 84–92. [CrossRef] [PubMed]
65. Rahman, M.S.; Yuan, H.Q.; Kikuchi, T.; Fujisawa, I.; Aoki, K. Metal Ion Interactions with Nucleobases in the Tetradentate 1,4,7,10-Tetraazacyclododecane (Cyclen)-Ligand System: Crystal Structures of [Cu(Cyclen)(Adeninato)]·ClO_4·$2H_2O$, [{Cu(Cyclen)}$_2$(Hypoxanthinato)]·$(ClO_4)_3$, [Cu(Cyclen)(Theophyllinato)]$_3$·$(ClO_4)_3$·$2H_2O$, and [Cu(cyclen)(theophyllinato)]$_3$·$(ClO_4)_3$·$2H_2O$, and [Cu(cyclen)(xanthinato)]·$(0.7ClO_4)_3$·$(0.3ClO_4)_3$·$3H_2O$·$(0.5H_2O)_3$. *J. Mol. Struct.* **2010**, *966*, 92–101. [CrossRef]
66. Šišuļins, A.; Bucevičius, J.; Tseng, Y.T.; Novosjolova, I.; Traskovskis, K.; Bizdēna, Ē.; Chang, H.T.; Tumkevičius, S.; Turks, M. Synthesis and Fluorescent Properties of N(9)-Alkylated 2-Amino-6-Triazolylpurines and 7-Deazapurines. *Beilstein J. Org. Chem.* **2019**, *15*, 474–489. [CrossRef]
67. Sebris, A.; Traskovskis, K.; Novosjolova, I.; Turks, M. Synthesis and Photophysical Properties of 2-Azolyl-6-Piperidinylpurines. *Chem. Heterocycl. Compd.* **2021**, *57*, 560–567. [CrossRef]
68. Sessler, J.L.; Sathiosatham, M.; Doerr, K.; Lynch, V.V.; Abboud, K.A. A G-Quartet Formed in the Absence of a Templating Metal Cation: A New 8-(*N*,*N*-Dimethylaniline)Guanosine Derivative. *Angew. Chem. Int. Ed. Engl.* **2000**, *39*, 1300–1303. [CrossRef]
69. Liu, T.; Zhan, W.; Wang, Y.; Zhang, L.; Yang, B.; Dong, X.; Hu, Y. Structure-Based Design, Synthesis and Biological Evaluation of Diphenylmethylamine Derivatives as Novel Akt1 Inhibitors. *Eur. J. Med. Chem.* **2014**, *73*, 167–176. [CrossRef]
70. Selmani, A.; Serpier, F.; Darses, S. From Tetrahydrofurans to Tetrahydrobenzo[d]Oxepines via a Regioselective Control of Alkyne Insertion in Rhodium-Catalyzed Arylative Cyclization. *J. Org. Chem.* **2019**, *84*, 4566–4574. [CrossRef]
71. Zhao, D.; Wu, N.; Zhang, S.; Xi, P.; Su, X.; Lan, J.; You, J. Synthesis of Phenol, Aromatic Ether, and Benzofuran Derivatives by Copper-Catalyzed Hydroxylation of Aryl Halides. *Angew. Chemie-Int. Ed.* **2009**, *48*, 8729–8732. [CrossRef]
72. Altman, R.A.; Shafir, A.; Choi, A.; Lichtor, P.A.; Buchwald, S.L. An Improved Cu-Based Catalyst System for the Reactions of Alcohols with Aryl Halides. *J. Org. Chem.* **2008**, *73*, 284–286. [CrossRef]
73. Niu, J.; Guo, P.; Kang, J.; Li, Z.; Xu, J.; Hu, S. Copper(I)-Catalyzed Aryl Bromides to Form Intermolecular and Intramolecular Carbon-Oxygen Bonds. *J. Org. Chem.* **2009**, *74*, 5075–5078. [CrossRef] [PubMed]
74. Kreibich, M.; Petrović, D.; Brückner, R. Mechanistic Studies of the Deslongchamps Annulation. *J. Org. Chem.* **2018**, *83*, 1116–1133. [CrossRef] [PubMed]
75. Ohashi, M.; Konkol, M.; Del Rosal, I.; Poteau, R.; Maron, L.; Okuda, J. Rare-Earth Metal Alkyl and Hydride Complexes Stabilized by a Cyclen-Derived [NNNN] Macrocyclic Ancillary Ligand. *J. Am. Chem. Soc.* **2008**, *130*, 6920–6921. [CrossRef]
76. Mereshchenko, A.S.; Olshin, P.K.; Karimov, A.M.; Skripkin, M.Y.; Burkov, K.A.; Tveryanovich, Y.S.; Tarnovsky, A.N. Photochemistry of Copper(II) Chlorocomplexes in Acetonitrile: Trapping the Ligand-to-Metal Charge Transfer Excited Staterelaxations Pathways. *Chem. Phys. Lett.* **2014**, *615*, 105–110. [CrossRef]
77. Ding, H.W.; Wang, S.; Qin, X.C.; Wang, J.; Song, H.R.; Zhao, Q.C.; Song, S.J. Design, Synthesis, and Biological Evaluation of Some Novel 4-Aminoquinazolines as Pan-PI3K Inhibitors. *Bioorg. Med. Chem.* **2019**, *27*, 2729–2740. [CrossRef]
78. Qiu, X.P.; Korchagina, E.V.; Rolland, J.; Winnik, F.M. Synthesis of a Poly(*N*-Isopropylacrylamide) Charm Bracelet Decorated with a Photomobile α-Cyclodextrin Charm. *Polym. Chem.* **2014**, *5*, 3656–3665. [CrossRef]
79. Mazaki, Y.; Mutai, K. Charge-Transfer Interaction and Molecular Arrangement in the Crystals of 2-(*p*-Nitrophenoxy)Ethyl Ethers and Amines. *Bull. Chem. Soc. Jpn.* **1995**, *68*, 3247–3254. [CrossRef]

Pielikums VIII
Appendix VIII

Burcevs, A.; Sebris, A.; Novosjolova, I.; Mishnev, A.; Turks, M.

Synthesis of Indole Derivatives via Aryl Triazole Ring-Opening and Subsequent Cyclization

Molecules **2025**, 30, 337.

doi.org/10.3390/molecules30020337

molecules

MDPI

Article

Synthesis of Indole Derivatives via Aryl Triazole Ring-Opening and Subsequent Cyclization

Aleksejs Burcevs [1], Armands Sebris [1], Irina Novosjolova [1,*], Anatoly Mishnev [2] and Māris Turks [1,*]

[1] Institute of Chemistry and Chemical Technology, Faculty of Natural Sciences and Technology, Riga Technical University, P. Valdena Str. 3, LV-1048 Riga, Latvia
[2] Latvian Institute of Organic Synthesis, Aizkraukles Str. 21, LV-1006 Riga, Latvia
* Correspondence: irina.novosjolova@rtu.lv (I.N.); maris.turks@rtu.lv (M.T.)

Abstract: A metal-free two-step synthetic approach for obtaining indole derivatives from aryl triazole fragment-containing compounds has been developed. In the first step, the Dimroth equilibrium, followed by nitrogen extrusion, Wolff rearrangement, and amine nucleophile addition, leads to the formation of *N*-aryl ethene-1,1-diamines. In the second step, the latter intermediates are cyclized into the target 1*H*-indoles in the presence of iodine. The developed method ensures the synthesis of indoles that possess *N*-substituents at the indole *C*2 position. Depending on the applied *N*-nucleophile, the indolization step provides a selectivity either towards 1*H*-indoles or 1-aryl-1*H*-indoles.

Keywords: indoles; purines; triazole ring-opening; indole synthesis; metal-free approach

1. Introduction

Both purine and indole are heterocycles that are abundant in nature and have a wide array of biological activities and thus, are important to be studied for their applications in medicinal chemistry [1–4]. Since many compounds in these substance classes possess fluorescent properties, they are also used as probes for studying many biological processes in cells [5–8]. A logic junction of both structural motifs has led to the synthesis of purine–indole conjugates to test their combined properties. There have been multiple reports from different research groups on purine–indole conjugates as fluorescent probes for various processes in organism, such as the NarI recognition sequence [9], the protein-mediated duplex to G-quadruplex exchange [10], and Hoogsteen base pairing [11]. Purine–indole conjugates possessing antitumor properties [12] or regulating lipid metabolism [13] have also been reported.

Purine–indole conjugates can be synthesized using multiple methods, with the most common method being Pd catalysed cross-coupling between selected fragments of indole and purine [9,11,13,14]. There have also been reports of the transition metal free synthesis of purine–indole conjugates by the direct arylation of purine *C*6 position using $AlCl_3$ [15] or a TfOH and HFIP combination [16]. Nevertheless, the latter methods are limited to a specific purine position and substituents at the aromatic ring, which is being attached to the purine core.

On the other hand, chemistry leading to purine–triazole conjugates has been well developed. Among others [17–26], we have also contributed to both C–C and C–N linked triazolyl purines and have demonstrated their further synthetic applications in S_NAr reactions [27–30], as well as their use as metal ion sensors [31] and fluorescent materials [32–34]. We have envisaged that the triazole ring-opening in a C–C-linked triazolyl purine via the sequential Dimroth equilibrium and Wolff rearrangement should provide a ketenimine

check for updates

Academic Editor: Gianfranco Favi

Received: 21 December 2024
Revised: 13 January 2025
Accepted: 13 January 2025
Published: 16 January 2025

Citation: Burcevs, A.; Sebris, A.; Novosjolova, I.; Mishnev, A.; Turks, M. Synthesis of Indole Derivatives via Aryl Triazole Ring-Opening and Subsequent Cyclization. *Molecules* **2025**, *30*, 337. https://doi.org/10.3390/molecules30020337

intermediate, which upon amine addition, will result in ethene-1,1-diamine. The latter, in turn, can be cyclized to indole if an *N*-aryl substituent is available (Scheme 1).

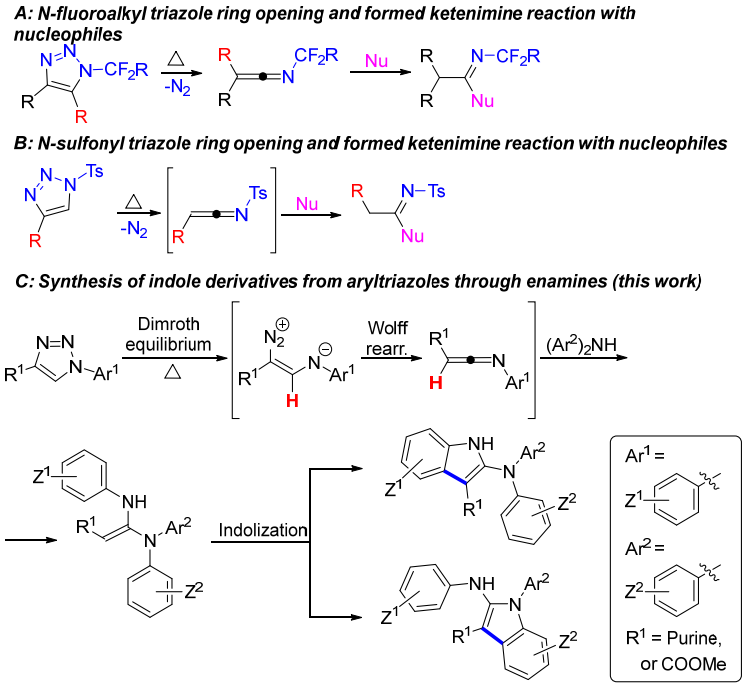

Scheme 1. (**A**) *N*-fluoroalkyl triazole ring-opening and subsequent reactions. (**B**) *N*-sulfonyl triazole ring-opening and subsequent reactions. (**C**) Synthesis of indole derivatives from aryl triazoles (this work).

The triazole ring-opening reactions that are required for our planned sequence are known in the literature. At high temperatures using flash vacuum pyrolysis conditions (400−800 °C), the triazole ring opens with the formation of carbene species that further rearrange into various products [35–38]. Other examples involve the use of transition metal catalysis at more ordinary temperatures, yet most of these methods are developed for triazoles bearing a *N*-tosyl group or other similar electron-withdrawing substituents. These methods are mostly developed for rhodium catalysis [39], and the formed metal-stabilized carbene can be used to form new five- or six-membered heterocycles [40,41]. Other metals, such as Ag [42,43], Cu [44], and Ni [45], have also been used in triazole ring-opening.

Nevertheless, evidence for triazole ring-opening at ordinary temperatures and in the absence of transition metals is present in the literature. By using 1-fluoroalkyl-1*H*-triazole, the ring-opening and formation of ketenimine occurs under metal-free conditions at 130−160 °C [46] (Scheme 1A). Next, the formed intermediate can react with *N*-, *S*-, or *O*-nucleophiles with the formation of amidines, thioimidates, or iminoesters. Also, *N*-sulfonyltriazoles can be opened similarly [42] (Scheme 1B).

Hence, we report a synthetic sequence which involves a metal-free triazole ring-opening of C–C-linked purine triazole conjugates, an amine addition to the intermediate ketenimine, and an oxidative cyclization of the resulting ethene-1,1-diamines to indoles. (Scheme 1C).

2. Results and Discussion

We started our research with attempts to open model aryl triazoles **1** [47–51] with carbazole. Carbazole nucleophile was chosen due to its extensive use in fluorescent materials [52] and its presence in both biologically active natural alkaloids [53] and numerous drugs [54]. We found that such transformation was possible by using *t*-BuOK and DMF at 100 °C (Scheme 2), and only in the case of starting material **1a**, we observed the formation of ethene-1,1-diamine **2a**, which could be isolated. With the model ethene-1,1-diamine **2a** in hand, we proceeded to its cyclization into indole. There are several examples of similar known transformations that use Pd, Cu, and Fe catalysts [55–59]. We have unsuccessfully explored combinations of $Pd(OAc)_2/Bu_4NBr/O_2$ [55], CuI/Li_2CO_3/phen [56], and $CuCl_2/K_3PO_4$ [58] as the reagent systems for the substrate **2a** cyclization. Then, we switched to the screening of metal-free methods that involved the use of CBr_4/K_2CO_3 [60], PIDA [61], and I_2/K_2CO_3 [62]. To our delight, we have found that the I_2/K_2CO_3 reagent system led to the formation of envisaged indole **3a**. For the given sequence, a step-wise process provided better yield than the tested one-pot approach.

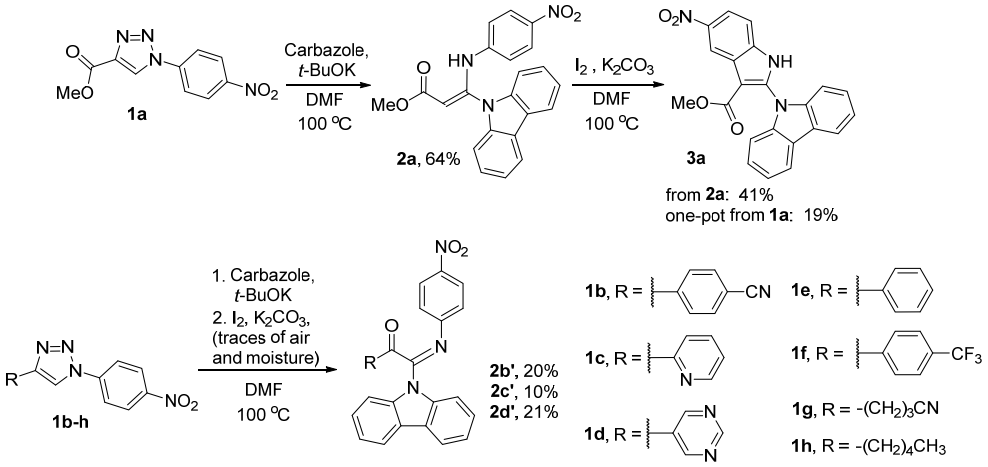

Scheme 2. Model studies for 1*H*-indole synthesis from triazoles **1a**–**h**.

On the other hand, triazoles **1b–d**, which contained weaker electron-withdrawing substituents such as cyanophenyl, pyridyl, or pyrimidinyl groups, provided ethene-1,1-diamine intermediates **2b–d,** which appeared to be incompatible with standard isolation and purification approaches. Therefore, the one-pot approach was applied, which implied the direct addition of I_2/K_2CO_3 to the reaction mixture after the first triazole ring-opening/carbazole addition step. In this case, we observed only the formation of acyclic oxidation products of type **2b′–d′**, whose structures were elucidated by standard spectroscopic methods and unambiguously proved by single crystal X-ray analysis, in the case of product **2c′** (Figure 1). Compounds **1e–h**, bearing other sidechains, including aliphatic substituents, underwent rapid degradation of their starting material into various unidentifiable mixtures of products upon attempted triazole ring-opening reactions.

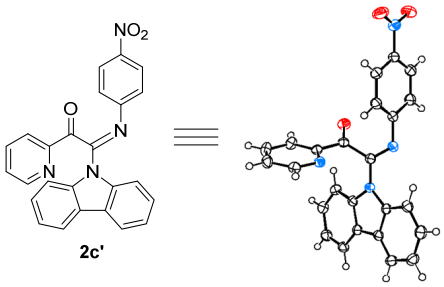

Figure 1. X-ray crystallographic analysis of compound **2c′**.

Next, we applied the developed synthetic sequence to triazolyl purines **4**, creating aromatic ethene-1,1-diamines **5** that we subsequently cyclized into 1*H*-indole derivatives **6**. Both a stepwise sequence and a one-pot approach were tested (Scheme 3 and Table 1). In the reaction, we used triazolyl purines **4**, with or without a chlorine substituent at the purine *C*2 position. In the case of the dimethylamino group containing derivative **4e**, it was only possible to obtain ethene-1,1-diamine **5e** by lowering the temperature, yet this did not provide indole in the next step. In all cases, ethene-1,1-diamines **5** were formed as the only products. The total yields of the final products **6** are either significantly higher (Table 1, Entries 1, 4) or just slightly lower (Table 1, Entries 2, 3) in the case of one-pot reactions when compared to those obtained using the stepwise approach. After that, we decided to derivatize the starting material further and introduced another phenyl triazole moiety at the purine C2 position. Thus, we synthesized starting material **4h** and applied standard triazole ring-opening conditions using carbazole as a nucleophile. The resulting product was compound **5h**, with only one triazole being opened at the purine C6 position (Table 1, Entry 8).

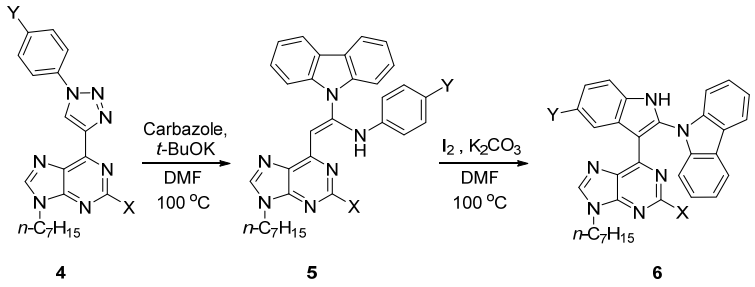

Scheme 3. Synthesis of purine–indole–carbazole conjugates **6**.

We can conclude that triazole ring-opening—carbazole addition proceeds with purine–triazole conjugates containing aryl groups with either electron-donating or electron-withdrawing substituents. On the other hand, further cyclization to indole is not possible with the dimethylaminophenyl substituent under the given reaction conditions (Entry 5). Also, it is evident that at least one sufficiently strong electron-withdrawing substituent (e.g., purine or a COOMe group) should be present at the triazole ring.

In transformations from **4** to **5**, another side reaction is theoretically possible. In the presence of a base, carbazole could provide the S_NAr product with the used 2-chloropurine starting materials (Entries 1–5). However, the observed results prove that the Dimroth–Wolff cascade, followed by *N*-nucleophile addition, is proceeding at a higher rate than the S_NAr process. It is worth mentioning that 5-nitro-indole derivative **6b** was successfully

synthesized using our approach, while such a substitution pattern may provide synthetic difficulties for other methodologies [16].

Table 1. Synthesis of purine–indole–carbazole conjugates **6** from triazolyl purines **4**.

Entry	Starting Material 4a–h	Substituents		Yield of Comp. 5, % for the Transformation 4→5	Yield of Comp. 6, % for the Transformation 5→6	Yield of Comp. 6, % for the One-Pot Process 4→[5]→6
		X	Y			
1	**4a**	Cl	H	**5a**, 63	**6a**, 84	**6a**, 63
2	**4b**	Cl	NO_2	**5b**, 84	**6b**, 60	**6b**, 48
3	**4c**	Cl	OMe	**5c**, 69	**6c**, 75	**6c**, 48
4	**4d**	Cl	CN	**5d**, 88	**6d**, 57	**6d**, 70
5	**4e**	Cl	NMe_2	**5e**, 68 *	-	-
6	**4f**	H	H	-	-	**6f**, 35
7	**4g**	H	NO_2	-	-	**6g**, 55
8	**4h**	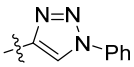	H	**5h**, 33	-	-

* the reaction performed at 25 °C.

In order to prove the double bond configuration of the formed ethene-1,1-diamines and to verify the molecular structure of the target purine–indole conjugate, single crystal X-ray crystallographic analysis was performed for compounds **5b** and **6b** (Figure 2). On the other hand, X-ray analysis of the mono triazole ring-opened product **5h** proved the reaction selectivity for the triazole ring at the purine C6 position (Figure 3).

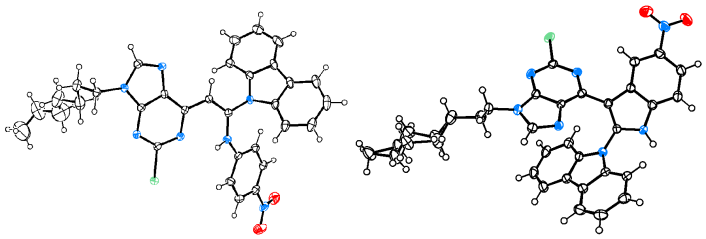

5b **6b**

Figure 2. X-ray crystallographic analyses of compounds **5b** and **6b**.

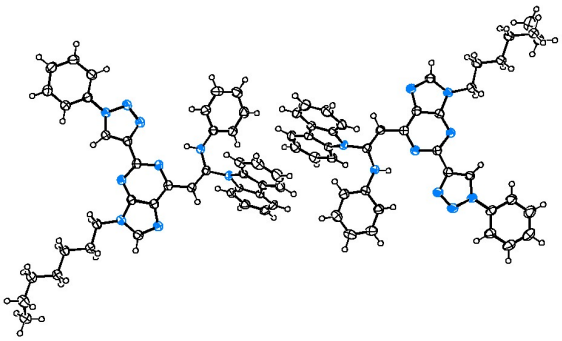

Figure 3. X-ray crystallographic analysis of compound **5h**.

Next, we have explored our methodology through the use of diphenylamine, applying the previously developed conditions to starting materials **4a** and **4b**. The expected ethene-1,1-diamines **7a**,**b** were obtained in 70% and 45% yields, respectively. Interestingly, products **7a**,**b** underwent the cyclization at the phenyl group of the incoming diphenylamine nucleophile. Thus, the formation of *N*-phenyl indole products **8** was observed (Scheme 4). As with previous reactions, the total yields of one-pot synthesis were proven to be higher than those obtained using the same reactions in a stepwise approach.

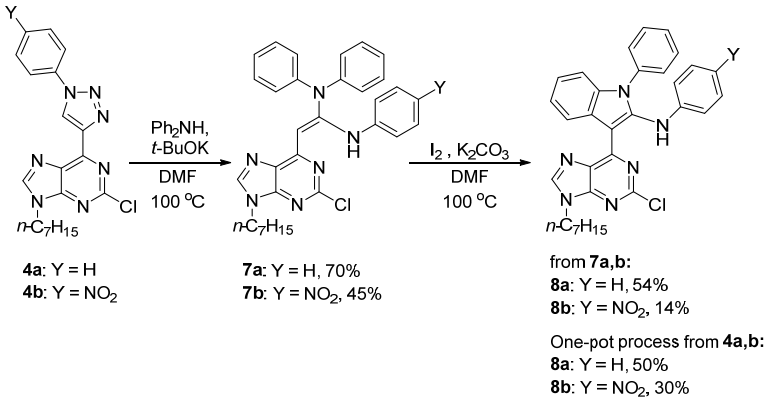

Scheme 4. Synthesis of *N*-phenyl-containing indole derivatives **8** from triazolyl purines **4**.

The chemical structure of products **8a**,**b**, which featured changed cyclization regioselectivity, were established by standard spectroscopic techniques and were additionally proved by crystallographic analysis, in the case of compound **8b** (Figure 4).

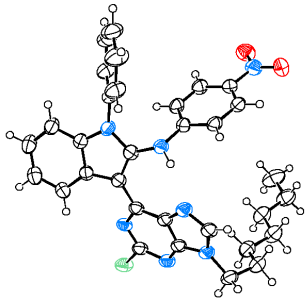

Figure 4. X-ray crystallographic analysis of compound **8b**.

Cyclization of compound **7a**, which contained three phenyl rings, without any substituents, and formed selectively product **8a**, proves that steric hindrance or linker flexibility plays a more important role than do the electronic effects (Scheme 5). Thus, in the cyclization **5**→**6**, which is featured by conformation **5**$^{\#}$ (Scheme 5) arylamine moiety, with a flexible NH-linker, ensures cyclization, even of such electron-deficient substituents as the nitrophenyl or cyanophenyl groups (formation of compounds **6b**, **6d**, **6g**, Table 1). On the other hand, when both *N*-linkers are equally flexible, which is featured by conformation **7**$^{\#}$ (Scheme 5) and cyclization **7**→**8**, both the statistical accessibility of the aryl group and their electronic density determined the reaction outcome, i.e., cyclization occurred at the phenyl ring instead of the nitrophenyl ring (formation of product **8b**, Scheme 4).

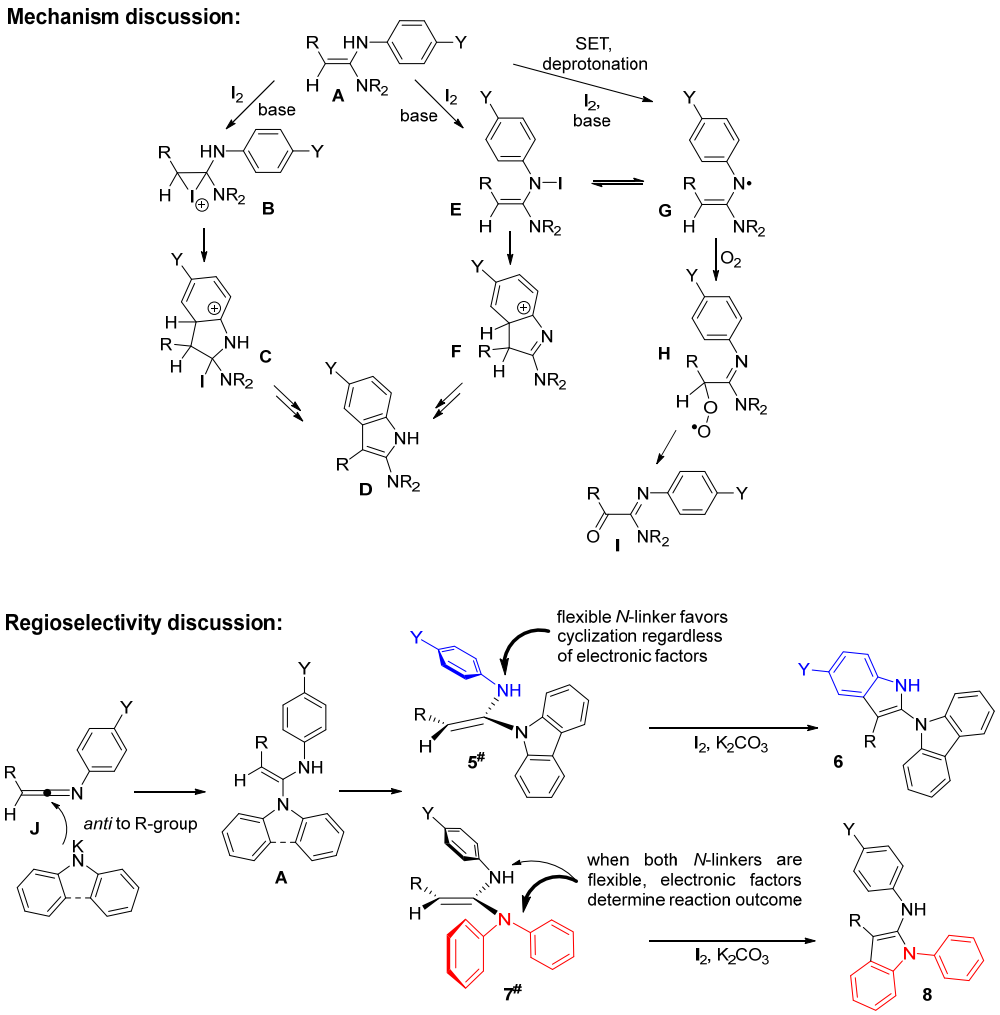

Scheme 5. Proposed reaction mechanism and regioselectivity model for indolization of ethene-1,1-diamines **A**.

Based on the observed product and byproduct formation, we propose reaction mechanisms for both indole **3**, **6**, and **8,** as well as acyclic compound **2′** formation. For the indole formation, two distinct pathways are plausible: (1) **A**→**B**→**C**→**D** [62], and (2) **A**→**E**→**F**→**D**, which differ regarding the electrophilic iodine attachment site. However, the pathway **A**→**E**→**F**→**D** better explains the observed reaction outcomes, depending on the electronic nature of the substituents, and permits the coupling of the proposed early intermediate **E** with the side product formation pathway **E**→**G**→**H**→**I**. Thus, iodoamine **E** formation can occur either via a nucleophilic attack of arylamine moiety or via a SET process [63–65]. The rate and efficiency of the cyclization of **E**→**F** most probably depends on electron density in the ethene-1,1-diamine system, for which the electron-withdrawing substituents R (-COOMe or purine) favor the attack of the aromatic ring as π-nucleophile. On the other hand, the electron-richer ethene-1,1-diamine systems meet with difficulties in accepting the incoming π-nucleophile. Therefore, intermediate **E** can engage in homolytic

N-I bond cleavage and form acyclic oxidation products of type **I** in the presence of oxygen traces [66].

3. Materials and Methods

3.1. General Information

Compounds **1a–c, 1e–f,** and **1h** were prepared according to the procedures outlined in the literature [47–51,67]. Compounds **1d** and **1g** were synthesized in a similar way as was **1a–c**, and their characterization is found in the Supplementary Materials. Compounds **4d–h** were synthesized using known procedures [32], and their descriptions and characterization are found in the Supplementary Materials.

Crystallographic data for **2c′**, **5b**, **5h**, **6b**, and **8b** have been deposited with the Cambridge Crystallographic Data Center as supplementary publications No. CCDC-2391861, CCDC-2391852, CCDC-2391858, CCDC-2391859, and CCDC-2392586, respectively.

3.2. General Methods

General method **A** for triazole ring-opening: in an inert atmosphere, to a mixture of triazole derivative (1.0 eq.) in dry DMF (1 mL/0.15 mmol of triazole derivative), KO*t*Bu (1.1 eq.) and nucleophile (1.1 eq.) were added, and the reaction mixture was stirred at a temperature of 100 °C for 1 h. Then, it was evaporated and dried in a vacuum. The resulting solid was suspended in DCM (20 mL) and washed with 5% aqueous LiCl solution (2 × 20 mL) and brine (20 mL). The organic phase was dried over anhydrous Na_2SO_4, filtered, and evaporated, followed by silica gel column chromatography.

General method **B** for cyclization into indole: in an inert atmosphere, to a mixture of enamine derivative (1.0 eq.) in dry DMF (1 mL/0.05 mmol of enamine derivative), K_2CO_3 (1.1 eq.) and I_2 (1.2 eq.) were added, and the reaction mixture was stirred at a temperature of 100 °C for 1 h. Then, it was evaporated and dried in a vacuum. The resulting solid was suspended in DCM (20 mL) and washed with 5% aqueous LiCl solution (2 × 20 mL), 20% aqueous $Na_2S_2O_3 \cdot 5H_2O$ solution (20 mL), and brine (20 mL). The organic phase was dried over anhydrous Na_2SO_4, filtered, and evaporated, followed by silica gel column chromatography.

General method **C** for one-pot reactions: in an inert atmosphere, to a mixture of triazole derivative (1.0 eq.) in dry DMF (1 mL/0.10 mmol of triazole derivative), KO*t*Bu (1.1 eq.) and nucleophile (1.1 eq.) were added, and the reaction mixture was stirred at a temperature 100 °C for 1 h. Then, K_2CO_3 (1.2 eq.) and I_2 (1.2 eq.) were quickly added, and the reaction mixture was stirred at a temperature of 100 °C for 1 h. Then, it was evaporated and dried in a vacuum. The resulting solid was suspended in DCM (20 mL) and washed with 5% aqueous LiCl solution (2 × 20 mL), 20% aqueous $Na_2S_2O_3 \cdot 5H_2O$ solution (20 mL), and brine (20 mL). The organic phase was dried over anhydrous Na_2SO_4, filtered, and evaporated, followed by silica gel column chromatography.

3.3. Characterization Data for Products

Methyl (*E*)-3-(9*H*-carbazol-9-yl)-3-[(4-nitrophenyl)amino]acrylate (**2a**)

Method **A**, 250 mg of **1a**, with carbazole as the nucleophile. Silica gel column chromatography (Hex/DCM, gradient 0%→100%) provided product **2a** (yield: 252 mg, 64%) as an orange amorphous solid. R_f = 0.67 (DCM = 100%). HPLC: t_R = 7.23 min, eluent E_2. IR (neat) ν (cm^{-1}): 1659, 1635, 1588, 1479, 1327, 1253, 1205, 1159, 1109, 1046, 844, 741. ^{1}H-NMR (500 MHz, $CDCl_3$) δ (ppm): 10.53 (s, 1H, (-NH)), 8.03 (d, 2H, ^3J = 7.9 Hz, 2 × H-C(carbazole)), 7.77 (d, 2H, ^3J = 9.1 Hz, 2 × H-C(Ar)), 7.57 (d, 2H, ^3J = 7.9 Hz, 2 × H-C(carbazole)), 7.38 (t, 2H, ^3J = 7.9 Hz, 2 × H-C(carbazole)), 7.29 (t, 2H, ^3J = 7.9 Hz, 2 × H-C(carbazole)), 6.54 (d, 2H, ^3J = 9.1 Hz, 2 × H-C(Ar)), 5.39 (s, 1H, H-C(vinyl)), 3.83 (s,

3H, (-OMe)). ^{13}C-NMR (126 MHz, $CDCl_3$) δ (ppm): 170.5, 147.7, 144.8, 142.8, 138.3, 126.9, 125.3, 124.5, 121.9, 120.6, 118.4, 111.5, 90.1, 51.5. HRMS (ESI) m/z: $[M - H]^-$ Calcd for $C_{22}H_{16}N_3O_4$ 386.1146; Found 386.1149 (0.78 ppm).

(*E*)-4-(2-(9*H*-Carbazol-9-yl)-2-((4-nitrophenyl)imino)acetyl)benzonitrile (**2b′**)

Method **C**, 150 mg of **1b**, with carbazole as the nucleophile. Silica gel column chromatography (DCM = 100%) provided product **2b′** (yield: 46 mg, 20%) as an orange amorphous solid. R_f = 0.70 (DCM = 100%). HPLC: t_R = 7.34 min, eluent E_2. IR (neat) ν (cm^{-1}): 2227, 1679, 1610, 1582, 1508, 1445, 1381, 1332, 1222, 1206, 1163, 1103, 854, 751, 721. ^{1}H-NMR (500 MHz, $CDCl_3$) δ (ppm): 8.09–8.04 (m, 4H, 2 × H-C(Ar-NO_2), 2 × H-C(carbazole)), 7.93–7.86 (m, 4H, 2 × H-C(Ar-CN), 2 × H-C(carbazole)), 7.68 (d, 2H, ^3J = 8.2 Hz, 2 × H-C(Ar-CN)), 7.41 (t, 2H, ^3J = 7.7 Hz, 2 × H-C(carbazole)), 7.37 (t, 2H, ^3J = 7.7 Hz, 2 × H-C(carbazole)), 6.95 (d, 2H, ^3J = 8.7 Hz, 2 × H-C(Ar-NO_2). ^{13}C-NMR (126 MHz, $CDCl_3$) δ (ppm): 188.3, 152.0, 144.3, 138.1, 137.0, 133.4, 129.6, 127.6, 127.5, 126.4, 124.9, 124.2, 121.6, 120.6, 118.7, 117.2, 114.9. HRMS (ESI) m/z: $[M + H]^+$ Calcd for $C_{27}H_{17}N_4O_3$ 445.1295; Found 445.1297 (0.45 ppm).

(*E*)-2-(9*H*-Carbazol-9-yl)-2-((4-nitrophenyl)imino)-1-(pyridin-2-yl)ethan-1-one (**2c′**)

Method **C**, 200 mg of **1c**, with carbazole as the nucleophile. Silica gel column chromatography (DCM/EtOH, gradient 0%→2%) provided product **2c′** (yield: 31 mg, 10%) as an orange solid. m_p = 201–202 °C (crystallized from DCM:Hex = 1:40). R_f = 0.70 (DCM/MeCN = 20:1). HPLC: t_R = 7.32 min, eluent E_2. IR (neat) ν (cm^{-1}): 1698, 1581, 1505, 1443, 1380, 1328, 1221, 1204, 1166, 1104, 1007, 939. ^{1}H-NMR (500 MHz, $CDCl_3$) δ (ppm): 8.58–8.54 (m, 1H, H-C(Pyr)), 8.06–8.02 (m, 2H, 2 × H-C(carbazole)), 7.99 (d, 2H, ^3J = 8.4 Hz, 2 × H-C(Ar)), 7.94–7.90 (m, 3H, H-C(Pyr), 2 × H-C(carbazole)), 7.82–7.75 (m, 1H, H-C(Pyr)), 7.44–7.40 (m, 1H, H-C(Pyr)), 7.38–7.32 (m, 4H, 4 × H-C(carbazole)), 6.96 (d, 2H, ^3J = 8.4 Hz, 2 × H-C(Ar)). ^{13}C-NMR (126 MHz, $CDCl_3$) δ (ppm): 190.4, 153.1, 152.2, 151.7, 150.1, 143.9, 138.7, 137.7, 128.6, 127.1, 126.2, 124.5, 123.5, 123.4, 121.5, 120.2, 114.8. HRMS (ESI) m/z: $[M + H]^+$ Calcd for $C_{25}H_{17}N_4O_3$ 421.1295; Found 421.1291 (0.95 ppm).

(*E*)-2-(9*H*-Carbazol-9-yl)-2-((4-nitrophenyl)imino)-1-(pyrimidin-5-yl)ethan-1-one (**2d′**)

Method **C**, 150 mg of **1d**, with carbazole as the nucleophile. Silica gel column chromatography (Hex/EtOAc, gradient 0%→50%) provided product **2d′** (yield: 49 mg, 21%) as a yellow amorphous solid. R_f = 0.80 (Hex/EtOAc = 1:1). HPLC: t_R = 6.84 min, eluent E_2. IR (neat) ν (cm^{-1}): 1683, 1624, 1583, 1574, 1510, 1445, 1332, 1310, 1223, 1100, 932, 873, 751, 723, 677. ^{1}H-NMR (500 MHz, $CDCl_3$) δ (ppm): 9.31 (s, 1H, H-C(pyrimidine)), 9.05 (s, 2H, 2 × H-C(pyrimidine)), 8.09 (d, 2H, ^3J = 8.4 Hz, 2 × H-C(Ar)), 8.07–8.03 (m, 2H, 2 × H-C(carbazole)), 7.95–7.83 (m, 2H, 2 × H-C(carbazole)), 7.49–7.34 (m, 4H, 4 × H-C(carbazole)), 6.96 (d, 2H, ^3J = 8.4 Hz, 2 × H-C(Ar)). ^{13}C-NMR (126 MHz, $CDCl_3$) δ (ppm): 187.0, 162.7, 157.6, 151.7, 149.4, 144.5, 137.9, 127.7, 127.6, 126.4, 125.1, 124.4, 121.5, 120.7, 114.6. HRMS (ESI) m/z: $[M + H]^+$ Calcd for $C_{24}H_{16}N_5O_3$ 422.1248; Found 422.1246 (0.47 ppm).

Methyl 2-(9*H*-carbazol-9-yl)-5-nitro-1*H*-indole-3-carboxylate (**3a**)

Method **B**, 75 mg of **2a**; silica gel column chromatography (DCM = 100%) provided product **3a** (yield: 31 mg, 41%) as an orange amorphous solid. R_f = 0.39 (DCM = 100%). HPLC: t_R = 6.45 min, eluent E_2. IR (neat) ν (cm^{-1}): 3203, 1670, 1520, 1471, 1340, 1227, 1200, 1096, 787, 740, 720. ^{1}H-NMR (500 MHz, $CDCl_3$) δ (ppm): 13.52 (s, 1H, (-NH)), 9.01 (d, 1H, ^4J = 2.4 Hz, H-C(indole)), 8.28 (d, 2H, ^3J = 7.7 Hz, 2 × H-C(carbazole)), 8.24 (dd, 1H, ^3J = 9.0 Hz, ^4J = 2.4 Hz, H-C(indole)), 7.71 (d, 1H, ^3J = 9.0 Hz, H-C(indole)), 7.46 (t, 2H, ^3J = 7.7 Hz, 2 × H-C(carbazole)), 7.38–7.31 (m, 4H, 4 × H-C(carbazole)), 3.56 (s, 3H, (-OMe)). ^{13}C-NMR (126 MHz, $CDCl_3$) δ (ppm): 162.6, 142.7, 140.2, 138.6, 136.9, 126.6, 125.2,

123.3, 121.2, 120.6, 118.8, 117.6, 113.2, 110.8, 102.7, 51.1. HRMS (ESI) m/z: $[M - H]^-$ Calcd for $C_{22}H_{14}N_3O_4$ 384.0990; Found 384.0990.

Method **C**, 100 mg of **1a**, with carbazole as the nucleophile. Silica gel column chromatography (DCM = 100%) provided product **3a** (yield: 30 mg, 19%) as an orange amorphous solid.

(*E*)-*N*-[1-(9*H*-Carbazol-9-yl)-2-(2-chloro-9-heptyl-9*H*-purin-6-yl)vinyl]aniline (**5a**)

Method **A**, 300 mg of **4a** [32], with carbazole as the nucleophile. Silica gel column chromatography (DCM = 100%) provided product **5a** (yield: 254 mg, 63%) as a yellow amorphous solid. R_f = 0.52 (DCM = 100%). HPLC: t_R = 10.36 min, eluent E_1. IR (neat) ν (cm^{-1}): 2925, 2854, 1632, 1575, 1553, 1440, 1309, 1250, 1224, 981, 746, 722. ^{1}H-NMR (500 MHz, $CDCl_3$) δ (ppm): 12.03 (s, 1H, -NH), 8.05 (d, 2H, ^3J = 8.3 Hz, 2 × H-C(carbazole)), 7.87 (s, 1H, H-C(purine)), 7.68 (d, 2H, ^3J = 8.3 Hz, 2 × H-C(carbazole)), 7.38 (t, 2H, ^3J = 8.3 Hz, 2 × H-C(carbazole)), 7.27 (t, 2H, ^3J = 8.3 Hz, 2 × H-C(carbazole)), 6.98 (t, 2H, ^3J = 7.8 Hz, 2 × H-C(Ar)), 6.82 (t, 1H, ^3J = 7.8 Hz, H-C(Ar)), 6.69 (d, 2H, ^3J = 7.8 Hz, 2 × H-C(Ar)), 6.35 (s, 1H, H-C(vinyl)), 4.19 (t, 2H, ^3J = 6.8 Hz, (-CH_2-)), 1.94–1.87 (m, 2H, (-CH_2-)), 1.36–1.20 (m, 8H, 4 × (-CH_2-)), 0.89 (t, 3H, ^3J = 6.8 Hz, (-CH_3)). ^{13}C-NMR (126 MHz, $CDCl_3$) δ (ppm): 157.2, 152.9, 151.2, 146.1, 142.6, 139.2 (2C), 129.3, 128.0, 126.7, 124.4, 123.8, 121.3, 120.3, 119.8, 112.0, 90.0, 44.1, 31.7, 30.1, 28.8, 26.7, 22.7, 14.2. HRMS (ESI) m/z: $[M + H]^+$ Calcd for $C_{32}H_{32}ClN_6$ 535.2371; Found 535.2369 (0.37 ppm).

(*E*)-*N*-[1-(9*H*-Carbazol-9-yl)-2-(2-chloro-9-heptyl-9*H*-purin-6-yl)vinyl]-4-nitroaniline (**5b**)

Method **A**, 750 mg of **4b** [32], with carbazole as the nucleophile. Silica gel column chromatography (DCM = 100%) provided product **5b** (yield: 831 mg, 84%) as an orange solid. m_p = 230–231 °C (crystallized from DCM:Hex = 1:40). R_f = 0.48 (DCM = 100%). HPLC: t_R = 8.12 min, eluent E_1. IR (neat) ν (cm^{-1}): 2925, 2857, 1640, 1557, 1448, 1304, 1260, 1110, 983, 851, 748, 721. ^{1}H-NMR (500 MHz, $CDCl_3$) δ (ppm): 12.36 (s, 1H, -NH), 8.08 (d, 2H, ^3J = 7.6 Hz, 2 × H-C(carbazole)), 7.92 (s, 1H, H-C(purine)), 7.83 (d, 2H, ^3J = 9.2 Hz, 2 × H-C(Ar)), 7.65 (d, 2H, ^3J = 7.6 Hz, 2 × H-C(carbazole)), 7.39 (t, 2H, ^3J = 7.6 Hz, 2 × H-C(carbazole)), 7.31 (t, 2H, ^3J = 7.6 Hz, 2 × H-C(carbazole)), 6.57 (d, 2H, ^3J = 9.2 Hz, 2 × H-C(Ar)), 6.55 (s, 1H, H-C(vinyl)), 4.22 (t, 2H, ^3J = 7.3 Hz, (-CH_2-)), 1.93–1.86 (m, 2H, (-CH_2-)), 1.36–1.23 (m, 8H, 4 × (-CH_2-)), 0.88 (t, 3H, ^3J = 7.3 Hz, (-CH_3)). ^{13}C-NMR (126 MHz, $CDCl_3$) δ (ppm): 156.1, 152.7, 151.8, 145.2, 143.7, 143.5, 142.5, 138.7, 128.5, 127.0, 125.6, 124.5, 121.9, 120.6, 118.0, 111.6, 93.5, 44.2, 31.7, 30.0, 28.8, 26.6, 22.6, 14.1. HRMS (ESI) m/z: $[M - H]^-$ Calcd for $C_{32}H_{29}ClN_7O_2$ 578.2077; Found 578.2088 (1.9 ppm).

(*E*)-*N*-[1-(9*H*-Carbazol-9-yl)-2-(2-chloro-9-heptyl-9*H*-purin-6-yl)vinyl]-4-methoxyaniline (**5c**)

Method **A**, 300 mg of **4c** [32], with carbazole as the nucleophile. Silica gel column chromatography (DCM/MeCN, gradient 0%→4%) provided product **=** (yield: 275 mg, 69%) as an orange amorphous solid. R_f = (DCM/MeCN = 20:1). HPLC: t_R = 8.60 min, eluent E_1. IR (neat) ν (cm^{-1}): 2927, 2855, 1631, 1575, 1556, 1507, 1446, 1293, 1224, 1030, 984, 748, 722. ^{1}H-NMR (500 MHz, $CDCl_3$) δ (ppm): 11.93 (s, 1H, -NH), 8.03 (d, 2H, ^3J = 7.8 Hz, 2 × H-C(carbazole)), 7.84 (s, 1H, H-C(purine)), 7.68 (d, 2H, ^3J = 7.8 Hz, 2 × H-C(carbazole)), 7.38 (t, 2H, ^3J = 7.8 Hz, 2 × H-C(carbazole)), 7.26 (t, 2H, ^3J = 7.8 Hz, 2 × H-C(carbazole)), 6.67 (d, 2H, ^3J = 8.9 Hz, 2 × H-C(Ar)), 6.49 (d, 2H, ^3J = 8.9 Hz, 2 × H-C(Ar)), 6.29 (s, 1H, H-C(vinyl)), 4.18 (t, 2H, ^3J = 7.3 Hz, (-CH_2-)), 3.56 (s, 3H, -OMe), 1.88 (quintet, 2H, ^3J = 7.3 Hz, (-CH_2-)), 1.38–1.24 (m, 8H, 4 × (-CH_2-)), 0.89 (t, 3H, ^3J = 7.3 Hz, (-CH_3)). ^{13}C-NMR (126 MHz, $CDCl_3$) δ (ppm): 157.2, 156.2, 152.8, 150.9, 146.6, 142.3, 139.2, 132.2, 127.7, 126.6, 124.2, 121.6, 121.2, 120.2, 114.5, 111.9, 89.1, 55.3, 44.0, 31.7, 30.1, 28.8, 26.6, 22.6, 14.1. HRMS (ESI) m/z: $[M - H]^-$ Calcd for $C_{33}H_{32}ClN_6O$ 563.2332; Found 563.2345 (2.31 ppm).

(*E*)-*N*-{[1-(9*H*-Carbazol-9-yl)-2-(2-chloro-9-heptyl-9*H*-purin-6-yl)vinyl]amino}benzonitrile (**5d**)

Method **A**, 500 mg of **4d**, with carbazole as the nucleophile. Silica gel column chromatography (DCM/MeCN, gradient 0%→4%) provided product **5d** (yield: 588 mg, 88%) as a yellow amorphous solid. R_f = 0.82 (DCM/MeCN = 20:1). HPLC: t_R = 8.12 min, eluent E_2. IR (neat) ν (cm^{-1}): 2926, 2855, 2222, 1637, 1580, 1556, 1509, 1445, 1309, 1256, 1223, 982, 831, 748, 722. ^{1}H-NMR (500 MHz, $CDCl_3$) δ (ppm): 12.27 (s, 1H, (-NH)), 8.09 (d, 2H, ^3J = 7.6 Hz, 2 × H-C(carbazole)), 7.94 (s, 1H, H-C(purine)), 7.64 (d, 2H, ^3J = 8.7 Hz, 2 × H-C(Ar)), 7.40 (t, 2H, ^3J = 7.6 Hz, 2 × H-C(carbazole)), 7.32 (t, 2H, ^3J = 7.6 Hz, 2 × H-C(carbazole)), 7.24 (d, 2H, ^3J = 7.6 Hz, 2 × H-C(carbazole)), 6.60 (d, 2H, ^3J = 8.7 Hz, 2 × H-C(Ar)), 6.50 (s, 1H, H-C(vinyl)), 4.24 (t, 2H, ^3J = 7.3 Hz, (-CH_2-)), 1.96–1.86 (m, 2H, (-CH_2-)), 1.38–1.22 (m, 8H, 4 × (-CH_2-)), 0.88 (t, 3H, ^3J = 7.3 Hz, (-CH_3)). ^{13}C-NMR (126 MHz, $CDCl_3$) δ (ppm): 156.4, 152.8, 151.8, 144.2, 143.40, 143.36, 138.8, 133.7, 128.5, 127.0, 124.6, 121.9, 120.7, 119.0, 118.8, 111.8, 105.8, 92.8, 44.2, 31.8, 30.1, 28.8, 26.7, 22.7, 14.2. HRMS (ESI) *m*/*z*: $[M - H]^-$ Calcd for $C_{33}H_{29}ClN_7$ 558.2178; Found 558.2189 (1.97 ppm).

(*E*)-N^1-[1-(9*H*-Carbazol-9-yl)-2-(2-chloro-9-heptyl-9*H*-purin-6-yl)vinyl]-N^4,N^4-dimethylbenzene-1,4-diamine (**5e**)

Method **A**, 405 mg of **4e**, with carbazole as the nucleophile. Silica gel column chromatography (DCM/MeCN, gradient 0%→5%) provided product **5e** (yield: 409 mg, 68%) as a red amorphous solid. R_f = 0.73 (DCM/MeCN = 20:1). HPLC: t_R = 5.34 min, eluent E_1. IR (neat) ν (cm^{-1}): 2925, 2854, 1631, 1573, 1553, 1516, 1445, 1292, 1224, 984, 807, 748, 722. ^{1}H-NMR (500 MHz, $CDCl_3$) δ (ppm): 11.93 (s, 1H, (-NH)), 8.03 (d, 2H, ^3J = 7.9 Hz, 2 × H-C(carbazole)), 7.83 (s, 1H, H-C(purine)), 7.66 (d, 2H, ^3J = 7.9 Hz, 2 × H-C(carbazole)), 7.38 (t, 2H, ^3J = 7.9 Hz, 2×H-C(carbazole)), 7.25 (t, 2H, ^3J = 7.8 Hz, 2 × H-C(carbazole)), 6.65 (d, 2H, ^3J = 8.8 Hz, 2 × H-C(Ar)), 6.35 (d, 2H, ^3J = 8.8 Hz, 2 × H-C(Ar)), 6.20 (s, 1H, H-C(vinyl)), 4.20 (t, 2H, ^3J = 7.3 Hz, (-CH_2-)), 2.74 (s, 6H, (-NMe_2)), 1.89 (quintet, 2H, ^3J = 7.3 Hz, (-CH_2-)), 1.35–1.26 (m, 8H, 4 × (-CH_2-)), 0.88 (t, 3H, ^3J = 7.3 Hz, (-CH_3)). ^{13}C-NMR (126 MHz, $CDCl_3$) δ (ppm): 157.4, 153.0, 150.8, 147.6, 146.9, 142.1, 139.3, 128.7, 127.6, 126.6, 124.3, 121.6, 121.0, 120.2, 113.2, 112.0, 88.4, 44.0, 40.7, 31.8, 30.2, 28.9, 26.7, 22.7, 14.2. HRMS (ESI) *m*/*z*: $[M - H]^-$ Calcd for $C_{34}H_{35}ClN_7$ 576.2648; Found 576.2664 (2.78 ppm).

(*E*)-*N*-(1-(9*H*-Carbazol-9-yl)-2-(9-heptyl-2-(1-phenyl-1*H*-1,2,3-triazol-4-yl)-9*H*-purin-6-yl)-vinyl)aniline (**5h**)

Method **A**, 303 mg of **4h**, with carbazole as a nucleophile. Silica gel column chromatography (DCM/EtOH, gradient 0%→2%) provided product **5h** (yield: 130 mg, 33%) as a yellow solid. m_p = 185–186 °C (crystallized from DCM:Hex = 1:40). R_f = 0.7 (DCM/EtOH = 20:1). IR (neat) ν (cm^{-1}): 3056, 2919, 2853, 1646, 1587, 1560, 1499, 1439, 1316, 1255, 1028, 746. ^{1}H-NMR (500 MHz, $CDCl_3$) δ (ppm): 13.19 (s, 1H, -NH), 8.70 (s, 1H, H-C(triazole)), 8.08 (d, 2H, ^3J = 7.7 Hz, 2 × H-C(carbazole)), 7.94 (s, 1H, H-C(purine)), 7.87 (d, 2H, ^3J = 7.7 Hz, 2 × H-C(carbazole)), 7.77 (d, 2H, ^3J = 8.2 Hz, H-C(Ph)), 7.58 (t, 2H, ^3J = 7.7 Hz, 2 × H-C(carbazole)), 7.49 (t, 1H, ^3J = 8.2 Hz, H-C(Ph)), 7.39 (t, 2H, ^3J = 7.7 Hz, 2 × H-C(carbazole)), 7.28 (t, 2H, ^3J = 8.2 Hz, H-C(Ph)), 7.00 (t, 2H, ^3J = 7.8 Hz, H-C(Ph)), 6.89 (d, 2H, ^3J = 7.8 Hz, H-C(Ph)), 6.80 (t, 1H, ^3J = 7.8 Hz, H-C(Ph)), 6.46 (s, 1H, H-C(vinyl)), 4.31 (t, 2H, ^3J = 6.9 Hz, (-CH_2-)), 2.04–1.92 (m, 2H, (-CH_2-)), 1.44–1.34 (m, 4H, 2 × (-CH_2-)), 1.34–1.24 (m, 4H, 2 × (-CH_2-)), 0.88 (t, 3H, ^3J = 6.9 Hz, (-CH_3)). ^{13}C-NMR (126 MHz, $CDCl_3$) δ (ppm): 155.8, 151.4, 150.6, 148.9, 145.4, 142.7, 139.9, 139.4, 137.2, 130.0, 129.3, 129.1, 128.4, 126.6, 124.3, 123.1, 122.2, 121.1, 120.8, 120.3, 119.5, 112.1, 90.4, 43.9, 31.8, 30.2, 28.9, 26.8, 22.7, 14.2. HRMS (ESI) *m*/*z*: $[M + H]^+$ Calcd for $C_{40}H_{38}N_9$ 644.3245; Found 644.3234 (1.70 ppm).

9-[3-(2-Chloro-9-heptyl-9*H*-purin-6-yl)-1*H*-indol-2-yl]-9*H*-carbazole (**6a**)

Method **B**, 100 mg of **5a**. Silica gel column chromatography (DCM/EtOH, gradient 0%→0.5%) provided product **6a** (yield: 84 mg, 84%) as an orange amorphous solid. R_f = 0.79 (DCM/EtOH = 20:1). HPLC: t_R = 5.96 min, eluent E_1. IR (neat) ν (cm^{-1}): 3365, 2926, 2855, 1567, 1444, 1313, 1227, 1153, 845, 745, 721. ^{1}H-NMR (500 MHz, $CDCl_3$) δ (ppm): 9.38 (s, 1H, (-NH)), 8.52 (d, 1H, ^3J = 8.0 Hz, H-C(indole)), 7.87 (d, 2H, ^3J = 7.7 Hz, 2 × H-C(carbazole)), 7.34 (t, 1H, ^3J = 8.0 Hz, H-C(indole)), 7.22 (t, 1H, ^3J = 8.0 Hz, H-C(indole)), 7.09–7.00 (m, 5H, 1 × H-C(indole), 4 × H-C(carbazole)), 6.94 (d, 2H, ^3J = 7.7 Hz, 2 × H-C(carbazole)), 6.86 (s, 1H, H-C(purine)), 3.72 (t, 2H, ^3J = 7.2 Hz, (-CH_2-)), 1.50 (quintet, 2H, ^3J = 7.2 Hz, (-CH_2-)), 1.28–1.20 (m, 2H, (-CH_2-)), 1.20–1.12 (m, 4H, 2×(-CH_2-)), 1.01–0.93 (m, 2H, (-CH_2-)), 0.87 (t, 3H, ^3J = 7.2 Hz, (-CH_3)). ^{13}C-NMR (126 MHz, $CDCl_3$) δ (ppm): 153.8, 153.5, 152.9, 143.3, 140.7, 134.1, 133.2, 129.4, 126.4, 126.0, 123.8, 123.7, 122.10, 122.07, 120.4, 119.9, 111.4, 110.2, 106.2, 43.5, 31.6, 29.4, 28.6, 26.3, 22.6, 14.1. HRMS (ESI) m/z: $[M - H]^-$ Calcd for $C_{32}H_{28}ClN_5$ 531.2069; Found 531.2078 (1.69 ppm).

Method **C**, 200 mg of **4a**, with carbazole as the nucleophile. Silica gel column chromatography (DCM/EtOH, gradient 0%→0.5%) provided product **6a** (yield: 169 mg, 63%) as an orange amorphous solid.

9-[3-(2-Chloro-9-heptyl-9*H*-purin-6-yl)-5-nitro-1*H*-indol-2-yl]-9*H*-carbazole (**6b**)

Method **B**, 200 mg of **5b**. Silica gel column chromatography (DCM/MeCN, gradient 0%→3%) provided product **6b** (yield: 120 mg, 60%) as a red solid. m_p = 242–243 °C (crystallized from acetone: MeCN = 1:40). R_f = 0.59 (DCM/EtOH = 20:1). HPLC: t_R = 5.47 min, eluent E_1. IR (neat) ν (cm^{-1}): 2925, 2855, 1568, 1446, 1314, 1216, 1152, 838, 741, 722. ^{1}H-NMR (500 MHz, $CDCl_3$) δ (ppm): 9.56 (s, 1H, (-NH)), 9.38 (d, 1H, ^4J = 2.3 Hz, H-C(indole)), 8.16 (dd, 1H, ^3J = 8.9 Hz, ^4J = 2.3 Hz, H-C(indole)), 7.97–7.91 (m, 2H, 2 × H-C(carbazole)), 7.46 (s, 1H, H-C(purine)), 7.22 (d, 1H, ^3J = 8.9 Hz, H-C(indole)), 7.15–7.07 (m, 4H, 4 × H-C(carbazole)), 7.06–7.00 (m, 2H, 2 × H-C(carbazole)), 4.03 (t, 2H, ^3J = 7.0 Hz, (-CH_2-)), 1.73 (quintet, 2H, ^3J = 7.0 Hz, (-CH_2-)), 1.28–1.20 (m, 6H, 3 × (-CH_2-)), 1.13 (quintet, 2H, ^3J = 7.0 Hz, (-CH_2-)), 0.87 (t, 3H, ^3J = 7.0 Hz, (-CH_3)). ^{13}C-NMR (126 MHz, $CDCl_3$) δ (ppm): 153.9, 153.6, 152.3, 144.3, 143.5, 140.1, 136.9, 135.6, 129.7, 126.2, 125.9, 124.3, 121.1, 120.4, 119.7, 119.4, 111.3, 109.8, 107.4, 44.0, 31.7, 29.7, 28.7, 26.5, 22.7, 14.2. HRMS (ESI) m/z: $[M - H]^-$ Calcd for $C_{32}H_{27}ClN_7O_2$ 576.1920; Found 576.1930 (1.74 ppm).

Method **C**, 220 mg of **4b**, with carbazole as the nucleophile. Silica gel column chromatography (DCM/MeCN, gradient 0%→3%) provided product **6b** (yield: 139 mg, 48%) as a red amorphous solid.

9-[3-(2-Chloro-9-heptyl-9*H*-purin-6-yl)-5-methoxy-1*H*-indol-2-yl]-9*H*-carbazole (**6c**)

Method **B**, 200 mg of **5c**. Silica gel column chromatography (DCM/MeCN, gradient 0%→5%) provided product **6c** (yield: 149 mg, 75%) as a red amorphous solid. R_f = 0.88 (DCM/MeCN = 20:1). HPLC: t_R = 5.74 min, eluent E_1. IR (neat) ν (cm^{-1}): 3362, 2927, 2855, 1568, 1450, 1313, 1215, 1143, 1029, 858, 800, 747, 721. ^{1}H-NMR (500 MHz, $CDCl_3$) δ (ppm): 9.44 (s, 1H, (-NH)), 8.09 (d, 1H, ^4J = 2.3 Hz, H-C(indole)), 7.83 (d, 2H, ^3J = 7.4 Hz, 2 × H-C(carbazole)), 7.02 (t, 2H, ^3J = 7.4 Hz, 2 × H-C(carbazole)), 6.99 (t, 2H, ^3J = 7.4 Hz, 2 × H-C(carbazole)), 6.91 (d, 2H, ^3J = 7.4 Hz, 2 × H-C(carbazole)), 6.90 (d, 1H, ^3J = 8.8 Hz, H-C(indole)), 6.85 (dd, 1H, ^3J = 8.8 Hz, ^4J = 2.3 Hz, H-C(indole)), 6.80 (s, 1H, H-C(purine)), 3.94 (s, 3H, (-OMe)), 3.70 (t, 2H, ^3J = 7.2 Hz, (-CH_2-)), 1.48 (quintet, 2H, ^3J = 7.2 Hz, (-CH_2-)), 1.27–1.20 (m, 2H, (-CH_2-)), 1.20–1.13 (m, 4H, 2 × (-CH_2-)), 0.94 (quintet, 2H, ^3J = 7.2 Hz, (-CH_2-)), 0.87 (t, 3H, ^3J = 7.0 Hz, (-CH_3)). ^{13}C-NMR (126 MHz, $CDCl_3$) δ (ppm): 155.7, 153.9, 153.5, 152.8, 143.1, 140.6, 133.6, 129.1, 129.0, 127.0, 125.9, 123.6, 120.3, 119.8, 113.8, 112.3, 110.1, 105.9, 103.9, 55.8, 43.4, 31.5, 29.3, 28.5, 26.2, 22.5, 14.1. HRMS (ESI) m/z: $[M - H]^-$ Calcd for $C_{33}H_{30}ClN_6O$ 561.2175; Found 561.2184 (1.6 ppm).

Method **C**, 212 mg of **4c**, with carbazole as the nucleophile. Silica gel column chromatography (DCM/MeCN, gradient 0%→5%) provided product **6c** (yield: 133 mg, 48%) as a red amorphous solid.

2-(9*H*-Carbazol-9-yl)-3-(2-chloro-9-heptyl-9*H*-purin-6-yl)-1*H*-indole-5-carbonitrile (**6d**)

Method **B**, 100 mg of **5d**. After workup, the resulting solid was suspended in EtOAc (4 mL) and filtered, providing product **6d** (yield: 57 mg, 57%) as a beige amorphous solid. IR (neat) ν (cm^{-1}): 2927, 2856, 2217, 1571, 1479, 1452, 1314, 1214, 1160, 933, 795, 802, 747, 723. ^{1}H-NMR (500 MHz, DMSO-d_6) δ (ppm): 13.37 (s, 1H, (-NH)), 8.91 (s, 1H, H-C(indole)), 8.20 (d, 2H, ^3J = 7.7 Hz, 2 × H-C(carbazole)), 8.14 (s, 1H, H-C(purine)), 7.75–7.70 (m, 2H, 2 × H-C(indole)), 7.28 (t, 2H, ^3J = 7.7 Hz, 2 × H-C(carbazole)), 7.24 (t, 2H, ^3J = 7.7 Hz, 2 × H-C(carbazole)), 7.19 (d, 2H, ^3J = 7.7 Hz, 2 × H-C(carbazole)), 4.04 (t, 2H, ^3J = 6.9 Hz, (-CH_2-)), 1.66 (quintet, 2H, ^3J = 6.9 Hz, (-CH_2-)), 1.25–1.12 (m, 6H, 3 × (-CH_2-)), 0.99 (quintet, 2H, ^3J = 6.9 Hz, (-CH_2-)), 0.82 (t, 3H, ^3J = 6.9 Hz, (-CH_3)). ^{13}C-NMR (126 MHz, DMSO-d_6) δ (ppm): 153.3, 152.13, 152.10, 146.1, 139.9, 136.5, 135.8, 129.2, 127.2, 126.1, 125.9, 125.8, 123.6, 120.7, 120.5, 120.4, 113.5, 110.2, 104.7, 103.3, 43.1, 31.1, 28.7, 28.0, 25.6, 22.0, 13.9. HRMS (ESI) m/z: $[M - H]^-$ Calcd for $C_{33}H_{27}ClN_7$ 556.2022; Found 556.2029 (1.26 ppm).

Method **C**, 210 mg of **4d**, with carbazole as the nucleophile. Silica gel column chromatography (DCM/EtOH, gradient 0%→1%) provided product **6d** (yield: 194 mg, 70%) as a red amorphous solid.

9-[3-(9-Heptyl-9*H*-purin-6-yl)-1*H*-indol-2-yl]-9*H*-carbazole (**6f**)

Method **C**, 100 mg of **4f**, with carbazole as the nucleophile. Silica gel column chromatography (DCM/MeCN, gradient 0%→8%) provided product **6f** (yield: 48 mg, 35%) as a brown amorphous solid. R_f = 0.45 (DCM/MeCN = 20:1). HPLC: t_R = 3.49 min, eluent E_1. IR (neat) ν (cm^{-1}): 3365, 2927, 2855, 1579, 1448, 1322, 1228, 841, 745, 722. ^{1}H-NMR (500 MHz, $CDCl_3$) δ (ppm): 9.26 (s, 1H, (-NH)), 8.78 (s, 1H, H-C(purine)), 8.40 (d, 1H, ^3J = 7.9 Hz, H-C(indole)), 7.98–7.93 (m, 2H, 2 × H-C(carbazole)), 7.34–7.29 (m, 1H, H-C(indole)), 7.28–7.22 (m, 2H, 2 × H-C(indole)), 7.17 (s, 1H, H-C(purine)), 7.16–7.10 (m, 6H, 6 × H-C(carbazole)), 3.92 (t, 2H, ^3J = 7.1 Hz, (-CH_2-)), 1.63 (quintet, 2H, ^3J = 7.1 Hz, (-CH_2-)), 1.27–1.13 (m, 6H, 3 × (-CH_2-)), 1.04 (quintet, 2H, ^3J = 7.1 Hz, (-CH_2-)), 0.86 (t, 3H, ^3J = 7.1 Hz, (-CH_3)). ^{13}C-NMR (126 MHz, $CDCl_3$) δ (ppm): 152.5, 152.2, 151.4, 143.2, 140.7, 134.2, 132.4, 131.1, 126.8, 126.1, 123.8, 123.6, 121.9, 121.8, 120.5, 120.0, 111.3, 110.3, 107.1, 43.6, 31.7, 29.7, 28.7, 26.4, 22.6, 14.2. HRMS (ESI) m/z: $[M - H]^-$ Calcd for $C_{32}H_{29}N_6$ 497.2459; Found 497.2466 (1.41 ppm).

9-[3-(9-Heptyl-9*H*-purin-6-yl)-5-nitro-1*H*-indol-2-yl]-9*H*-carbazole (**6g**)

Method **C**, 100 mg of **4g**, with carbazole as the nucleophile. Silica gel column chromatography (DCM/MeCN, gradient 0%→8%) provided product **6g** (yield: 74 mg, 55%) as a brown amorphous solid. R_f = 0.60 (DCM/MeCN = 20:1). HPLC: t_R = 4.19 min, eluent E_1. IR (neat) ν (cm^{-1}): 2924, 2857, 1580, 1449, 1322, 1225, 1003, 838, 747, 723. ^{1}H-NMR (500 MHz, DMSO-d_6) δ (ppm): 13.34 (s, 1H, (-NH)), 9.34 (d, 1H, ^4J = 2.3 Hz, H-C(indole)), 8.72 (s, 1H, H-C(purine)), 8.23 (dd, 1H, ^3J = 9.0 Hz, ^4J = 2.3 Hz, H-C(indole)), 8.19 (d, 2H, ^3J = 7.5 Hz, 2 × H-C(carbazole)), 8.12 (s, 1H, H-C(purine)), 7.72 (d, 1H, ^3J = 9.0 Hz, H-C(indole)), 7.29–7.15 (m, 6H, 6 × H-C(carbazole)), 4.10 (t, 2H, ^3J = 6.9 Hz, (-CH_2-)), 1.69 (quintet, 2H, ^3J = 6.9 Hz, (-CH_2-)), 1.25–1.12 (m, 6H, 3 × (-CH_2-)), 0.99 (quintet, 2H, ^3J = 6.9 Hz, (-CH_2-)), 0.82 (t, 3H, ^3J = 6.9 Hz, (-CH_3)). ^{13}C-NMR (126 MHz, DMSO-d_6) δ (ppm): 151.6, 151.5, 150.3, 145.4, 141.9, 139.8, 137.9, 135.4, 130.3, 126.1, 125.7, 123.5, 120.6, 120.4, 118.6, 118.1, 112.6, 110.2, 106.9, 42.9, 31.1, 28.9, 28.0, 25.7, 22.0, 13.9. HRMS (ESI) m/z: $[M - H]^-$ Calcd for $C_{32}H_{28}N_7O_2$ 542.2310; Found 542.2318 (1.48 ppm).

(*E*)-2-(2-Chloro-9-heptyl-9*H*-purin-6-yl)-*N*,*N*,*N*′-triphenylethene-1,1-diamine (**7a**)

Method **A**, 200 mg of **4a** [32], with diphenylamine as the nucleophile. Silica gel column chromatography (DCM/EtOH, gradient 0%→2%) provided product **7a** (yield: 215 mg, 70%) as a yellow amorphous solid. R_f = 0.71 (DCM/EtOH = 20:1). HPLC: t_R = 6.72 min, eluent E_2. IR (neat) ν (cm^{-1}): 2926, 2855, 1619, 1545, 1489, 1366, 1241, 976, 748, 691. ^{1}H-NMR (500 MHz, $CDCl_3$) δ (ppm): 11.68 (s, 1H, (-NH)), 7.73 (s, 1H, H-C(purine)), 7.18 (t, 4H, ^3J = 7.8 Hz, 4 × H-C(Ph)), 7.13–7.06 (m, 8H, 8 × H-C(Ph)), 7.00 (t, 2H, ^3J = 7.8 Hz, 2 × H-C(Ph)), 6.90 (t, 1H, ^3J = 6.6 Hz, H-C(Ph)), 5.73 (s, 1H, H-C(vinyl)), 4.14 (t, 2H, ^3J = 7.0 Hz, ($-CH_2$-)), 1.85 (quintet, 2H, ^3J = 7.0 Hz, ($-CH_2$-)), 1.37–1.20 (m, 8H, 4 × ($-CH_2$-)), 0.87 (t, 3H, ^3J = 7.0 Hz, ($-CH_3$)). ^{13}C-NMR (126 MHz, $CDCl_3$) δ (ppm): 157.8, 156.6, 152.8, 150.2, 145.1, 141.2, 139.0, 129.2, 128.7, 126.7, 124.9, 124.5, 123.9, 122.2, 86.6, 43.9, 31.8, 30.2, 28.9, 26.7, 22.7, 14.2. HRMS (ESI) m/z: $[M - H]^-$ Calcd for $C_{32}H_{32}ClN_6$ 535.2382; Found 535.2396 (2.62 ppm).

(*E*)-2-(2-Chloro-9-heptyl-9*H*-purin-6-yl)-*N*-(4-nitrophenyl)-*N*′,*N*′-diphenylethene-1,1-diamine (**7b**)

Method **A**, 200 mg of **4b** [32], with diphenylamine as the nucleophile. Silica gel column chromatography (DCM/MeCN, gradient 0%→3%) provided product **7b** (yield: 120 mg, 45%) as a brown amorphous solid. R_f = 0.63 (DCM/MeCN = 20:1). HPLC: t_R = 8.63 min, eluent E_2. IR (neat) ν (cm^{-1}): 2923, 2855, 1629, 1550, 1454, 1303, 1245, 1107, 977, 844, 754, 693. ^{1}H-NMR (500 MHz, $CDCl_3$) δ (ppm): 12.10 (s, 1H, (-NH)), 8.00 (d, 2H, ^3J = 9.0 Hz, 2 × H-C(Ar-NO_2)), 7.80 (s, 1H, H-C(purine)), 7.28–7.23 (m, 6H, 2 × H-C(Ar-NO_2), 4 × H-C(Ph)), 7.17 (d, 4H, ^3J = 8.4 Hz, 4 × H-C(Ph)), 7.08 (t, 2H, ^3J = 8.4 Hz, 2 × H-C(Ph)), 5.87 (s, 1H, H-C(vinyl)), 4.16 (t, 2H, ^3J = 7.3 Hz, ($-CH_2$-)), 1.86 (quintet, 2H, ^3J = 7.3 Hz, ($-CH_2$-)), 1.33–1.19 (m, 8H, 4 × ($-CH_2$-)), 0.87 (t, 3H, ^3J = 7.3 Hz, ($-CH_3$)). ^{13}C-NMR (126 MHz, $CDCl_3$) δ (ppm): 157.0, 154.0, 152.6, 151.0, 145.2, 144.6, 142.4, 142.2, 129.6, 127.4, 125.2, 125.1, 124.8, 119.1, 89.9, 44.1, 31.7, 30.1, 28.8, 26.7, 22.7, 14.2. HRMS (ESI) m/z: $[M - H]^-$ Calcd for $C_{32}H_{31}ClN_7O_2$ 580.2233; Found 580.2245 (2.07 ppm).

3-(2-Chloro-9-heptyl-9*H*-purin-6-yl)-*N*,1-diphenyl-1*H*-indol-2-amine (**8a**)

Method **B**, 100 mg of **7a**. Silica gel column chromatography (DCM/EtOH, gradient 0%→1%) provided product **8a** (yield: 54 mg, 54%) as a yellow amorphous solid. R_f = 0.92 (DCM/EtOH = 20:1). HPLC: t_R = 9.35 min, eluent E_1. IR (neat) ν (cm^{-1}): 2926, 2859, 1633, 1559, 1466, 1435, 1310, 1225, 1074, 1029, 883, 744, 691. ^{1}H-NMR (500 MHz, $CDCl_3$) δ (ppm): 11.30 (s, 1H, (-NH)), 8.90 (d, 1H, ^3J = 8.0 Hz, H-C(indole)), 7.95 (s, 1H, H-C(purine)), 7.45 (d, 2H, ^3J = 7.6 Hz, 2 × H-C(Ph)), 7.35 (t, 1H, ^3J = 8.0 Hz, H-C(indole)), 7.30 (t, 2H, ^3J = 7.6 Hz, 2 × H-C(Ph)), 7.23–7.16 (m, 3H, H-C(Ph), 2 × H-C(indole)), 6.95 (d, 2H, ^3J = 7.7 Hz, 2 × H-C(Ph)), 6.75 (d, 2H, ^3J = 7.7 Hz, 2 × H-C(Ph)), 6.71 (t, 1H, ^3J = 7.7 Hz, 2 × H-C(Ph)), 4.21 (t, 2H, ^3J = 7.2 Hz, ($-CH_2$-)), 1.95–1.86 (m, 2H, ($-CH_2$-)), 1.40–1.22 (m, 8H, 4 × ($-CH_2$-)), 0.88 (t, 3H, ^3J = 7.2 Hz, ($-CH_3$)). ^{13}C-NMR (126 MHz, $CDCl_3$) δ (ppm): 155.4, 154.3, 152.3, 146.2, 142.2, 140.6, 136.8, 136.6, 129.1, 128.6, 127.7, 127.4, 127.1, 126.7, 122.7, 122.4, 122.1, 121.7, 119.3, 109.8, 100.9, 44.1, 31.7, 30.0, 28.8, 26.7, 22.6, 14.1. HRMS (ESI) m/z: $[M + H]^+$ Calcd for $C_{32}H_{32}ClN_6$ 535.2371; Found 535.2366 (0.93 ppm).

Method **C**, 200 mg of **4a**, with diphenylamine as the nucleophile. Silica gel column chromatography (DCM/EtOH, gradient 0%→1%) provided product **8a** (yield: 136 mg, 50%) as a yellow amorphous solid.

3-(2-Chloro-9-heptyl-9*H*-purin-6-yl)-*N*-(4-nitrophenyl)-1-phenyl-1*H*-indol-2-amine (**8b**)

Method **B**, 84 mg of **7b**. Silica gel column chromatography (DCM/EtOH, gradient 0%→2%) provided product **8b** (yield: 12 mg, 14%) as a yellow solid. m_p = 135–136 °C (crystallized from DCM:Hex = 1:40). R_f = 0.91 (DCM/EtOH = 20:1). HPLC: t_R = 8.52 min,

eluent E_1. IR (neat) ν (cm^{-1}): 2924, 2851, 1567, 1488, 1327, 1248, 1111, 1027, 935, 849, 745, 683. ^{1}H-NMR (500 MHz, $CDCl_3$) δ (ppm): 11.45 (s, 1H, (-NH)), 8.81, (d, 1H, ^3J = 8.0 Hz, H-C(indole)), 8.09 (s, 1H, H-C(purine)), 7.82 (d, 2H, ^3J = 8.9 Hz, 2 × H-C(Ar-NO_2)), 7.52, (d, 2H, ^3J = 7.9 Hz, 2 × H-C(Ph)), 7.42–7.36 (m, 3H, 2 × H-C(Ph), H-C(indole)), 7.33 (d, 1H, ^3J = 8.0 Hz, H-C(indole)), 7.30–7.26 (m, 2H, 1×H-C(Ph), 1 × H-C(indole)), 6.68 (d, 2H, ^3J = 8.9 Hz, 2 × H-C(Ar-NO_2)), 4.27 (t, 2H, ^3J = 7.0 Hz, (-CH_2-)), 1.97–1.89 (m, 2H, (-CH_2-)), 1.40–1.31 (m, 4H, 2 × (-CH_2-)), 1.30–1.23 (m, 4H, 2 × (-CH_2-)), 0.87 (t, 3H, ^3J = 7.0 Hz, (-CH_3)). ^{13}C-NMR (126 MHz, $CDCl_3$) δ (ppm): 154.8, 154.7, 152.6, 148.9, 141.5, 141.3, 140.9, 136.3, 136.2, 129.6, 128.3, 127.6, 127.0, 126.1, 125.2, 123.6, 123.3, 122.4, 115.8, 110.3, 103.6, 44.4, 31.7, 30.0, 28.8, 26.8, 22.7, 14.2. HRMS (ESI) m/z: $[M - H]^-$ Calcd for $C_{32}H_{29}ClN_7O_2$ 578.2077; Found 578.2088 (1.9 ppm).

Method **C**, 220 mg of **4b**, with diphenylamine as the nucleophile. Silica gel column chromatography (DCM/EtOH, gradient 0%→1%) provided product **8b** (yield: 88 mg, 30%) as a yellow amorphous solid.

4. Conclusions

We have developed a new metal-free synthetic approach to convert 1-aryl-1*H*-1,2,3-triazoles into indoles by transforming triazole carbon atoms C4 and C5 into indole C2 and C3 atoms. The reaction sequence in the first step involves triazole ring-opening and nitrogen extrusion, followed by Wolff rearrangement. The formed ketenimine intermediate is susceptible to *N*-nucleophile attack and forms ethene-1,1-diamines in a 33–88% yield. The highest yields for this step are observed for the substrates bearing aryl groups with electron-withdrawing substituents such as -NO_2 (84%) and -CN (88%) groups. Purine, as an electron deficient entity at the C4 position of the triazole ring, facilitates this transformation better than does the -COOMe moiety. In the second step, the oxidative cyclization in the presence of the I_2/K_2CO_3 system provided indoles. Depending on the conformational flexibility of the *N*-substituents at the ethene-1,1-diamines, cyclization occurs in two distinct ways: (1) substrates containing a conformationally non-flexible carbazole ring undergo indolization with the initial triazole's aryl group in 57–84% yields; (2) substrates containing flexible aryl substituents arising from diarylamine nucleophile undergo indolization with the latter substituent in 14–54% yields. The developed synthetic sequence may also be performed in a one-pot fashion, reaching an indole yield of up to 70%, in some cases. Our findings demonstrate that the purinyl group activates the triazole ring in a similar fashion as that previously reported for electron-withdrawing substituents, such as the -Ts, -CF_2CF_3, and -COOMe groups. Moreover, during the indole-forming oxidative cyclization step, the steric factors play a more important role than does the electronic nature of the substituents, as indoles **6b** and **6d** bearing the -NO_2 and -CN groups were obtained in good yields. Given that the synthesis of 1,2,3-triazoles is well developed, and indoles are important structural motifs in medicinal chemistry, the further expansion of this methodology is expected.

Supplementary Materials: The following supporting information can be downloaded at: https://www.mdpi.com/article/10.3390/molecules30020337/s1, synthesis procedures, ^{1}H- and ^{13}C-NMR spectra of starting materials **1d, 1g**, **4d–h**; ^{1}H- and ^{13}C-NMR spectra of compounds **2a**, **2b′–d′**, **3a**, **5a–e**,**h**, **6a–d**, **6f–g**, **7a–b**, and **8a–b**. X-ray crystallography data of compounds **2c′**, **5b**, **5h**, **6b**, and **8b**. Checkcif and Cif files for compounds **2c′**, **5b**, **5h**, **6b**, and **8b**. Starting materials in the Supplementary Materials part were prepared according to the procedures outlined in the literature [32,47,68,69].

Author Contributions: Synthetic experiments, investigation, methodology, and manuscript draft, A.B. and A.S.; X-ray analysis, A.M.; conceptualization, supervision, and manuscript review, I.N. and M.T. All authors have read and agreed to the published version of the manuscript.

Funding: A.B. thanks the 2024 Riga Technical University's Doctoral Grant program for their financial support. A.B., I.N., and M.T. acknowledge the financial support provided by the Latvia–Lithuania–Taiwan joint grant "Molecular Electronics in Functionalized Purines: Fundamental Study and Applications (MEPS)" from the Latvian Council of Science.

Institutional Review Board Statement: Not applicable.

Informed Consent Statement: Not applicable.

Data Availability Statement: The original contributions presented in this study are included in the article/Supplementary Materials. Further inquiries can be directed to the corresponding authors.

Acknowledgments: The authors thank Ričards Kārkliņš, Emma Galiņa, and Khadija Khaldoune for the synthesis of the starting materials, as well as Kristīne Lazdoviča for providing FTIR analysis.

Conflicts of Interest: The authors declare no conflicts of interest.

References

1. Shaw, G. 4.09-Purines. In *Comprehensive Heterocyclic Chemistry*; Katritzky, A.R., Rees, C.W., Eds.; Elsevier: Pergamon, Turkey, 1984; Volume 5, pp. 499–605.
2. Legraverend, M.; Grierson, D.S. The Purines: Potent and Versatile Small Molecule Inhibitors and Modulators of Key Biological Targets. *Bioorg. Med. Chem.* **2006**, *14*, 3987–4006. [CrossRef]
3. Inman, M.; Moody, C.J. Indole Synthesis-Something Old, Something New. *Chem. Sci.* **2013**, *4*, 29–41. [CrossRef]
4. Dorababu, A. Indole—A Promising Pharmacophore in Recent Antiviral Drug Discovery. *RSC Med. Chem.* **2020**, *11*, 1335–1353. [CrossRef]
5. Venkatesham, A.; Pillalamarri, S.R.; De Wit, F.; Lescrinier, E.; Debyser, Z.; Van Aerschot, A. Propargylated Purine Deoxynucleosides: New Tools for Fluorescence Imaging Strategies. *Molecules* **2019**, *24*, 468. [CrossRef] [PubMed]
6. Saito, Y.; Hudson, R.H.E. Base-Modified Fluorescent Purine Nucleosides and Nucleotides for Use in Oligonucleotide Probes. *J. Photochem. Photobiol. C Photochem. Rev.* **2018**, *36*, 48–73. [CrossRef]
7. Nan, M.; Niu, W.; Fan, L.; Lu, W.; Shuang, S.; Li, C.; Dong, C. Indole-Based pH Probe with Ratiometric Fluorescence Behavior for Intracellular Imaging. *RSC Adv.* **2015**, *5*, 99739–99744. [CrossRef]
8. Wang, Q.; Li, D.; Rao, N.; Zhang, Y.; Le, Y.; Liu, L.; Huang, L.; Yan, L. Development of Indole-Based Fluorescent Probe for Detection of Fluoride and Cell Imaging of HepG2. *Dye. Pigment.* **2021**, *188*, 109166. [CrossRef]
9. Rankin, K.M.; Sproviero, M.; Rankin, K.; Sharma, P.; Wetmore, S.D.; Manderville, R.A. C^8-Heteroaryl-2′-Deoxyguanosine Adducts as Conformational Fluorescent Probes in the *Nar*I Recognition Sequence. *J. Org. Chem.* **2012**, *77*, 10498–10508. [CrossRef]
10. Fadock, K.L.; Manderville, R.A.; Sharma, P.; Wetmore, S.D. Optimization of Fluorescent 8-Heteroaryl-Guanine Probes for Monitoring Protein-Mediated Duplex → G-Quadruplex Exchange. *Org. Biomol. Chem.* **2016**, *14*, 4409–4419. [CrossRef] [PubMed]
11. Schlitt, K.M.; Millen, A.L.; Wetmore, S.D.; Manderville, R.A. An Indole-Linked C8-Deoxyguanosine Nucleoside Acts as a Fluorescent Reporter of Watson-Crick versus Hoogsteen Base Pairing. *Org. Biomol. Chem.* **2011**, *9*, 1565–1571. [CrossRef] [PubMed]
12. Ye, F.; Chen, L.; Hu, L.; Xiao, T.; Yu, S.; Chen, D.; Wang, Y.; Liang, G.; Liu, Z.; Wang, S. Design, Synthesis and Preliminary Biological Evaluation of C-8 Substituted Guanine Derivatives as Small Molecular Inhibitors of FGFRs. *Bioorg. Med. Chem. Lett.* **2015**, *25*, 1556–1560. [CrossRef]
13. Guo, S.Y.; Wei, L.Y.; Song, B.B.; Hu, Y.T.; Jiang, Z.; Zhao, D.D.; Xu, Y.H.; Lin, Y.W.; Xu, S.M.; Chen, S.B.; et al. Design, Synthesis and Evaluation of 2-Pyrimidinylindole Derivatives as Anti-Obesity Agents by Regulating Lipid Metabolism. *Eur. J. Med. Chem.* **2023**, *260*, 115729. [CrossRef]
14. Wang, Z.; Li, K.; Zhao, D.; Lan, J.; You, J. Palladium-Catalyzed Oxidative C-H/C-H Cross-Coupling of Indoles and Pyrroles with Heteroarenes. *Angew. Chem.-Int. Ed.* **2011**, *50*, 5365–5369. [CrossRef]
15. Guo, H.M.; Li, P.; Niu, H.Y.; Wang, D.C.; Qu, G.R. Direct Synthesis of 6-Arylpurines by Reaction of 6-Chloropurines with Activated Aromatics. *J. Org. Chem.* **2010**, *75*, 6016–6018. [CrossRef] [PubMed]
16. Takenaga, N.; Shoji, T.; Menjo, T.; Hirai, A.; Ueda, S.; Kikushima, K.; Hanasaki, T.; Dohi, T. Nucleophilic Arylation of Halopurines Facilitated by Brønsted Acid in Fluoroalcohol. *Molecules* **2019**, *24*, 3812. [CrossRef] [PubMed]
17. Khandelwal, R.; Vasava, M.; Abhirami, R.B.; Karsharma, M. Recent Advances in Triazole Synthesis via Click Chemistry and Their Pharmacological Applications: A Review. *Bioorg. Med. Chem. Lett.* **2024**, *112*, 129927. [CrossRef]
18. Cosyn, L.; Palaniappan, K.K.; Kim, S.K.; Duong, H.T.; Gao, Z.G.; Jacobson, K.A.; Van Calenbergh, S. 2-Triazole-Substituted Adenosines: A New Class of Selective A_3 Adenosine Receptor Agonists, Partial Agonists, and Antagonists. *J. Med. Chem.* **2006**, *49*, 7373–7383. [CrossRef]

19. Neres, J.; Labello, N.P.; Somu, R.V.; Boshoff, H.I.; Wilson, D.J.; Vannada, J.; Chen, L.; Barry, C.E.; Bennett, E.M.; Aldrich, C.C. Inhibition of Siderophore Biosynthesis in *Mycobacterium tuberculosis* with Nucleoside Bisubstrate Analogues: Structure-Activity Relationships of the Nucleobase Domain of 5′-*O*-[*N*-(Salicyl)Sulfamoyl]Adenosine. *J. Med. Chem.* **2008**, *51*, 5349–5370. [CrossRef] [PubMed]
20. Lakshman, M.K.; Kumar, A.; Balachandran, R.; Day, B.W.; Andrei, G.; Snoeck, R.; Balzarini, J. Synthesis and Biological Properties of C-2 Triazolylinosine Derivatives. *J. Org. Chem.* **2012**, *77*, 5870–5883. [CrossRef]
21. Lakshman, M.K.; Singh, M.K.; Parrish, D.; Balachandran, R.; Day, B.W. Azide-Tetrazole Equilibrium of C-6 Azidopurine Nucleosides and Their Ligation Reactions with Alkynes. *J. Org. Chem.* **2010**, *75*, 2461–2473. [CrossRef] [PubMed]
22. Mathew, S.C.; By, Y.; Berthault, A.; Virolleaud, M.A.; Carrega, L.; Chouraqui, G.; Commeiras, L.; Condo, J.; Attolini, M.; Gaudel-Siri, A.; et al. Expeditious Synthesis and Biological Evaluation of New C-6 1,2,3-Triazole Adenosine Derivatives A1 Receptor Antagonists or Agonists. *Org. Biomol. Chem.* **2010**, *8*, 3874–3881. [CrossRef]
23. Dyrager, C.; Börjesson, K.; Dinér, P.; Elf, A.; Albinsson, B.; Wilhelmsson, L.M.; Grøtli, M. Synthesis and Photophysical Characterisation of Fluorescent 8-(1*H*-1,2,3-Triazol-4-yl)Adenosine Derivatives. *Eur. J. Org. Chem.* **2009**, *2009*, 1515–1521. [CrossRef]
24. Redwan, I.N.; Bliman, D.; Tokugawa, M.; Lawson, C.; Grøtli, M. Synthesis and Photophysical Characterization of 1- and 4-(Purinyl)Triazoles. *Tetrahedron* **2013**, *69*, 8857–8864. [CrossRef]
25. Creech, C.; Kanaujia, M.; Causey, C.P. Synthesis and Evaluation of 2-Ethynyl-Adenosine-5′-Triphosphate as a Chemical Reporter for Protein AMPylation. *Org. Biomol. Chem.* **2015**, *13*, 8550–8555. [CrossRef]
26. Buchanan, H.S.; Pauff, S.M.; Kosmidis, T.D.; Taladriz-Sender, A.; Rutherford, O.I.; Hatit, M.Z.C.; Fenner, S.; Watson, A.J.B.; Burley, G.A. Modular, Step-Efficient Palladium-Catalyzed Cross-Coupling Strategy to Access C6-Heteroaryl 2-Aminopurine Ribonucleosides. *Org. Lett.* **2017**, *19*, 3759–3762. [CrossRef]
27. Kriķis, K.E.; Novosjolova, I.; Mishnev, A.; Turks, M. 1,2,3-Triazoles as Leaving Groups in S_NAr-Arbuzov Reactions: Synthesis of C6-Phosphonated Purine Derivatives. *Beilstein J. Org. Chem.* **2021**, *17*, 193–202. [CrossRef] [PubMed]
28. Cīrule, D.; Novosjolova, I.; Bizdēna, Ē.; Turks, M. 1,2,3-Triazoles as Leaving Groups: S_NAr Reactions of 2,6-Bistriazolylpurines with O- And C-Nucleophiles. *Beilstein J. Org. Chem.* **2021**, *17*, 410–419. [CrossRef]
29. Kovaļovs, A.; Novosjolova, I.; Bizdēna, Ē.; Bižāne, I.; Skardziute, L.; Kazlauskas, K.; Jursenas, S.; Turks, M. 1,2,3-Triazoles as Leaving Groups in Purine Chemistry: A Three-Step Synthesis of N^6-Substituted-2-Triazolyl-Adenine Nucleosides and Photophysical Properties Thereof. *Tetrahedron Lett.* **2013**, *54*, 850–853. [CrossRef]
30. Novosjolova, I.; Bizdēna, Ē.; Turks, M. Application of 2,6-Diazidopurine Derivatives in the Synthesis of Thiopurine Nucleosides. *Tetrahedron Lett.* **2013**, *54*, 6557–6561. [CrossRef]
31. Jovaisaite, J.; Cīrule, D.; Jeminejs, A.; Novosjolova, I.; Turks, M.; Baronas, P.; Komskis, R.; Tumkevicius, S.; Jonusauskas, G.; Jursenas, S. Proof of Principle of a Purine D-A-D′ Ligand Based Ratiometric Chemical Sensor Harnessing Complexation Induced Intermolecular PET. *Phys. Chem. Chem. Phys.* **2020**, *22*, 26502–26508. [CrossRef]
32. Burcevs, A.; Sebris, A.; Traskovskis, K.; Chu, H.W.; Chang, H.T.; Jovaišaitė, J.; Juršėnas, S.; Turks, M.; Novosjolova, I. Synthesis of Fluorescent C–C Bonded Triazole-Purine Conjugates. *J. Fluoresc.* **2024**, *34*, 1091–1097. [CrossRef]
33. Šišuļins, A.; Bucevičius, J.; Tseng, Y.T.; Novosjolova, I.; Traskovskis, K.; Bizdēna, Ē.; Chang, H.T.; Tumkevičius, S.; Turks, M. Synthesis and Fluorescent Properties of N(9)-Alkylated 2-Amino-6-Triazolylpurines and 7-Deazapurines. *Beilstein J. Org. Chem.* **2019**, *15*, 474–489. [CrossRef]
34. Sebris, A.; Novosjolova, I.; Traskovskis, K.; Kokars, V.; Tetervenoka, N.; Vembris, A.; Turks, M. Photophysical and Electrical Properties of Highly Luminescent 2/6-Triazolyl-Substituted Push-Pull Purines. *ACS Omega* **2022**, *7*, 5242–5253. [CrossRef] [PubMed]
35. Fulloon, B.E.; Wentrup, C. Imidoylketene-Oxoketenimine Interconversion. Rearrangement of a Carbomethoxyketenimine to a Methoxyimidoylketene and 2-Methoxy-4-Quinolone. *J. Org. Chem.* **1996**, *61*, 1363–1367. [CrossRef]
36. Clarke, D.; Mares, W.; McNab, H. Preparation and pyrolysis of 1-(pyrazol-5-yl)-1,2,3-triazoles and related compounds. *J. Chem. Soc. Perkin Trans. 1* **1997**, *12*, 1799–1804. [CrossRef]
37. Rao, V.V.R.; Wentrup, C. Synthesis of Aminoquinolones from Triazoles via Carboxamidoketenimine and Amidinoketene Intermediates. *J. Chem. Soc. Perkin Trans. 1* **1998**, *16*, 2583–2586. [CrossRef]
38. Fulloon, B.E.; Wentrup, C. Fluoroquinolones from Imidoylketenes and Iminopropadienones, R-N=C=C=C=O. *Aust. J. Chem.* **2009**, *62*, 115–120. [CrossRef]
39. Davies, H.M.L.; Alford, J.S. Reactions of Metallocarbenes Derived from *N*-Sulfonyl-1,2,3-Triazoles. *Chem. Soc. Rev.* **2014**, *43*, 5151–5162. [CrossRef]
40. Zhao, Y.Z.; Yang, H.B.; Tang, X.Y.; Shi, M. Rh^{II}-Catalyzed [3+2] Cycloaddition of 2 *H*-Azirines with *N*-Sulfonyl-1,2,3-Triazoles. *Chem.—A Eur. J.* **2015**, *21*, 3562–3566. [CrossRef] [PubMed]
41. Horneff, T.; Chuprakov, S.; Chernyak, N.; Gevorgyan, V.; Fokin, V.V. Rhodium-Catalyzed Transannulation of 1,2,3-Triazoles with Nitriles. *J. Am. Chem. Soc.* **2008**, *130*, 14972–14974. [CrossRef]

42. Feng, Y.; Zhou, W.; Sun, G.; Liao, P.; Bi, X.; Li, X. Highly Efficient Synthesis of *N*-Sulfonylamidines via Silver-Catalyzed or Metal-Free Thermally Promoted Denitrogenative Amination of *N*-Sulfonyl-1,2,3-Triazoles. *Synthesis* **2017**, *49*, 1371–1379. [CrossRef]
43. Wang, Y.; Wu, Y.; Li, Y.; Tang, Y. Denitrogenative Suzuki and Carbonylative Suzuki Coupling Reactions of Benzotriazoles with Boronic Acids. *Chem. Sci.* **2017**, *8*, 3852–3857. [CrossRef]
44. Yoo, E.J.; Bae, I.; Sharpless, K.B.; Fokin, V.V.; Chang, S. Mechanistic Studien on the Cu-catalyzed Three-Component Reactions of Sulfonyl Azides, 1-Alkynes and Amines, Alcohols, or Water: Dichotomy via a Common Pathway. *J. Org. Chem.* **2008**, *73*, 5520–5528. [CrossRef]
45. Liu, Y.; Xie, P.; Li, J.; Bai, W.J.; Jiang, J. Nickel-Catalyzed Coupling of *N*-Sulfonyl-1,2,3-Triazole with *H*-Phosphine Oxides: Stereoselective and Site-Selective Synthesis of α-Aminovinylphosphoryl Derivatives. *Org. Lett.* **2019**, *21*, 4944–4949. [CrossRef]
46. Kubíčková, A.; Markos, A.; Voltrová, S.; Marková, A.; Filgas, J.; Klepetářová, B.; Slavíček, P.; Beier, P. Aza-Wolff Rearrangement of *N*-Fluoroalkyl Triazoles to Ketenimines. *Org. Chem. Front.* **2023**, *10*, 3201–3206. [CrossRef]
47. Barral, K.; Moorhouse, A.D.; Moses, J.E. Efficient Conversion of Aromatic Amines into Azides: A One-Pot Synthesis of Triazole Linkages. *Org. Lett.* **2007**, *9*, 1809–1811. [CrossRef]
48. Bag, S.S.; Kundu, R. Installation/Modulation of the Emission Response via Click Reaction. *J. Org. Chem.* **2011**, *76*, 3348–3356. [CrossRef]
49. Alonso, F.; Moglie, Y.; Radivoy, G.; Yus, M. Click Chemistry from Organic Halides, Diazonium Salts and Anilines in Water Catalysed by Copper Nanoparticles on Activated Carbon. *Org. Biomol. Chem.* **2011**, *9*, 6385–6395. [CrossRef] [PubMed]
50. Kim, T.Y.; Elliott, A.B.S.; Shaffer, K.J.; John McAdam, C.; Gordon, K.C.; Crowley, J.D. Rhenium(I) Complexes of Readily Functionalized Bidentate Pyridyl-1,2,3-Triazole "Click" Ligands: A Systematic Synthetic, Spectroscopic and Computational Study. *Polyhedron* **2013**, *52*, 1391–1398. [CrossRef]
51. Molteni, G.; Ponti, A. Arylazide Cycloaddition to Methyl Propiolate: DFT-Based Quantitative Prediction of Regioselectivity. *Chem. A Eur. J.* **2003**, *9*, 2770–2774. [CrossRef] [PubMed]
52. Wex, B.; Kaafarani, B.R. Perspective on Carbazole-Based Organic Compounds as Emitters and Hosts in TADF Applications. *J. Mater. Chem. C* **2017**, *5*, 8622–8653. [CrossRef]
53. Greger, H. Phytocarbazoles: Alkaloids with Great Structural Diversity and Pronounced Biological Activities. *Phytochem. Rev.* **2017**, *16*, 1095–1153. [CrossRef]
54. Patil, S.A.; Patil, S.A.; Ble-González, E.A.; Isbel, S.R.; Hampton, S.M.; Bugarin, A. Carbazole Derivatives as Potential Antimicrobial Agents. *Molecules* **2022**, *27*, 6575. [CrossRef]
55. Shi, Z.; Glorius, F. Efficient and Versatile Synthesis of Indoles from Enamines and Imines by Cross-Dehydrogenative Coupling. *Angew. Chem.-Int. Ed.* **2012**, *51*, 9220–9222. [CrossRef]
56. Bernini, R.; Fabrizi, G.; Sferrazza, A.; Cacchi, S. Copper-Catalyzed C-C Bond Formation through C-H Functionalization: Synthesis of Multisubstituted Indoles from *N*-Aryl Enaminones. *Angew. Chem.-Int. Ed.* **2009**, *48*, 8078–8081. [CrossRef]
57. Drouhin, P.; Taylor, R.J.K. A Copper-Mediated Oxidative Coupling Route to 3*H*- and 1*H*-Indoles from *N*-Aryl-Enamines. *Eur. J. Org. Chem.* **2015**, *11*, 2333–2336. [CrossRef]
58. Huang, F.; Wu, P.; Wang, L.; Chen, J.; Sun, C.; Yu, Z. Copper-Mediated Intramolecular Oxidative C-H/C-H Cross-Coupling of α-Oxo Ketene N, S -Acetals for Indole Synthesis. *J. Org. Chem.* **2014**, *79*, 10553–10560. [CrossRef]
59. Guan, Z.H.; Yan, Z.Y.; Ren, Z.H.; Liu, X.Y.; Liang, Y.M. Preparation of Indoles via Iron Catalyzed Direct Oxidative Coupling. *Chem. Commun.* **2010**, *46*, 2823–2825. [CrossRef]
60. Zhao, L.; Qiu, C.; Zhao, L.; Yin, G.; Li, F.; Wang, C.; Li, Z. Base-Promoted, CBr_4-Mediated Tandem Bromination/Intramolecular Friedel-Crafts Alkylation of *N*-Aryl Enamines: A Facile Access to 1*H*- And 3*H*-Indoles. *Org. Biomol. Chem.* **2021**, *19*, 5377–5382. [CrossRef] [PubMed]
61. Yu, W.; Du, Y.; Zhao, K. PIDA-Mediated Oxidative C-C Bond Formation: Novel Synthesis of Indoles from *N*-Aryl Enamines. *Org. Lett.* **2009**, *11*, 2417–2420. [CrossRef]
62. He, Z.; Li, H.; Li, Z. Iodine-Mediated Synthesis of 3*H* -Indoles via Intramolecular Cyclization of Enamines. *J. Org. Chem.* **2010**, *75*, 4636–4639. [CrossRef] [PubMed]
63. Wang, M.; Yu, W.; Chang, J. I_2-Mediated Oxidation of Amines in Water toward Imines and Amides. *Asian J. Org. Chem.* **2023**, *12*, e202300159. [CrossRef]
64. He, Z.; Liu, W.; Li, Z. I_2-Catalyzed Indole Formation via Oxidative Cyclization of *N*-Aryl Enamines. *Chem. Asian J.* **2011**, *6*, 1340–1343. [CrossRef] [PubMed]
65. Le, P.Q.; Dinh, V.M.; Nguyen, D.D.T.; Ha, H.Q.; Truong, T.V. Iodine-promoted amide formation via oxidative cleavage of indoles: Novel quinazoline-4(3*H*)-one and tryptanthrin syntheses. *RSC Adv.* **2024**, *14*, 15597–15603. [CrossRef] [PubMed]
66. Choi, W.; Kim, J.; Ryu, T.; Kim, K.-B.; Lee, P.H. Synthesis of *N*-Imidoyl and *N*-Oxoimidoyl Sulfoximines from 1-Alkynes, *N*-Sulfonyl Azides, and Sulfoximines. *Org. Lett.* **2015**, *17*, 3330–3333. [CrossRef]

67. Ramachary, D.B.; Shashank, A.B.; Karthik, S. An Organocatalytic Azide–Aldehyde [3+2] Cycloaddition: High-Yielding Regioselective Synthesis of 1,4-Disubstituted 1,2,3-Triazoles. *Angew. Chem. Int. Ed.* **2014**, *53*, 10420–10424. [CrossRef]
68. Das, J.; Patil, S.N.; Awasthi, R.; Narasimhulu, C.P.; Trehan, S. An Easy Access to Aryl Azides from Aryl Amines under Neutral Conditions. *Synthesis* **2005**, 1801–1806. [CrossRef]
69. Westrip, S.P. *publCIF*: software for editing, validating and formatting crystallographic information files. *J. Appl. Cryst.* **2010**, *43*, 920–925. [CrossRef]

Aleksejs Burcevs dzimis 1996. gadā Rīgā. Rīgas Tehniskajā universitātē (RTU) ieguvis bakalaura (2019) un maģistra (2021) grādu ķīmijas tehnoloģijā. Patlaban ir RTU Dabaszinātņu un tehnoloģiju fakultātes Ķīmijas un ķīmijas tehnoloģijas institūta pētnieks. Zinātniskās intereses saistītas ar jaunu purīna atvasinājumu sintēzi.

Aleksejs Burcevs was born in 1996 in Riga. He obtained a Bachelor's degree (2019) and a Master's degree (2021) in Chemical Technology from Riga Technical University. Currently, he is a researcher at the Institute of Chemistry and Chemical Technology at the Faculty of Natural Sciences and Technologies of RTU. His research interests are related to the synthesis of new purine derivatives.